In presenting this thesis in partial fulfillment of the requirements for an advanced degree at Idaho State University, I agree that the Library shall make it freely available for inspection. I further state that permission for extensive copying of my thesis for scholarly purposes may be granted by the Dean of the Graduate School, Dean of my academic division, or by the University Librarian. It is understood that any copying or publication of this thesis for financial gain shall not be allowed without my written permission.

Signature ___________________________________

Date _____________________________________

Geologic Mapping and Detrital Zircon Provenance of the Bayhorse Anticline, Custer County, Idaho: Revised Neoproterozoic to Lower Paleozoic Stratigraphy

by

Daniel T. Brennan

A thesis

submitted in partial fulfillment

of the requirements for the degree of

Master of Science in the Department of Geosciences

Idaho State University

Spring 2018

To the Graduate Faculty:

The members of the committee appointed to examine the thesis of Daniel T. Brennan find it satisfactory and recommend that it be accepted.

David M. Pearson

Major Advisor

Paul K. Link

Committee Member

Tracy Payne

Graduate Faculty Representative

DEDICATION

This thesis is dedicated to the three men I was named after: Dad, for inspiring me to take risks while I have youth on my side, and even more for always being there to reassure me that I am not the failure I sometimes fear I am; Papa, I am sorry to say you were right (for at least the next 4 years) when you warned everyone that if I moved out west, I won't move back; and lastly, in memory of my Grandpa. Thank you for passing down your love for mountains, camping, and a good beer.

ACKNOWLEDGMENTS

I must first express my sincere gratitude to Dave Pearson and Paul Link. Thank you both for your insight, guidance, and willingness to share your time and knowledge to make me a better scientist. Conversations and lessons that diverged from geology to other facets of life are remembered and appreciated as well. You both gave me much to aspire to be.

I would also like to thank Phil Ihinger and J. Brian Mahoney, for taking a chance on me and igniting my passion for geology.

This work benefited from discussions, assistance, and support from many people including Tracy Payne, Mike McCurry, Glenn Thackray, Bruce Finney, Reed Lewis, Dave Stewart, Matt Ashton, Diana Boyack, Breane Burkhalter, Kate Zajanc, fluorite pod-mates, and others.

I must also acknowledgement and extends thanks to Braedon Warner for your hard work and for treating my research with the same level of intensity as if it were your own. I would also like to thank Kyle Miller for keeping me motivated this past summer, driving, DJing and sharing your cooking skills.

Lastly, I need to extend thanks to my family and friends from Idaho to Wisconsin and everywhere in between. Without you, none of this would have been possible, nor would it have mattered. I would especially like to thank my Mom, Dad, and sisters. I appreciate your unwavering love and support more than I can express.

The funding to support this project was from EdMap grant RGEO2F, Geological Society of America student research grant, and the Idaho State Geoscience Geslin award. I also acknowledge NSF-EAR 1649254 for support of the Arizona LaserChron Center and extend a thank you to Mark Pecha, Kojo Kelty, and Chelsi White.

TABLE OF CONTENTS

LIST OF FIGURES

Geologic Mapping and Detrital Zircon Provenance of the Bayhorse Anticline, Custer County, Idaho: Revised Neoproterozoic to Lower Paleozoic Stratigraphy

Thesis Abstract—Idaho State University (2018)

Geologic mapping and detrital zircon analysis of rocks exposed within the Bayhorse and Bayhorse Lake quadrangles in central Idaho has identified a slightly metamorphosed yet intact ~1.5 km thick stratigraphic section of Neoproterozoic argillaceous and dolomitic rocks, which overlie in stratigraphic continuum a 667 Ma tuff in a borehole and correlate to the upper Pocatello Formation, Blackrock Canyon Limestone, and Papoose Creek Formation of southeast Idaho. This fine-grained succession is overlain by a gradational contact with a ~1 km thick coarse-grained, Neoproterozoic and Cambrian siliciclastic unit which correlates to the thick Neoproterozoic/Cambrian quartzites of the Caddy Canyon through Camelback Mountain formations of southeast Idaho and northern Utah suggesting correlative Cryogenian and Ediacaran strata are present west of the Lemhi arch from Edwardsburg to Bayhorse to Pocatello. However, at Bayhorse much of the Upper Cambrian and Lower Ordovician section is missing with Middle Ordovician rocks unconformably overlying Middle Cambrian rocks. About 50 km northeast of Bayhorse, Middle Ordovician Kinnikinic Quartzite lies in angular unconformity above Mesoproterozoic Belt Supergroup rocks, defining the Lemhi arch unconformity. This Late Cambrian unconformity possibly correlates with the newly documented unconformity in the Bayhorse region.

Key Words: Rodinia, Neoproterozoic, Lemhi arch, Bayhorse, Rifting, Windermere Supergroup

CHAPTER 1: INTRODUCTION

Amalgamation and breakup of the supercontinent Rodinia dominates much of Earth's Meso- and Neoproterozoic geologic history (Li et al., 2008). During Cryogenian time (see timescale of Walker et al., 2013 used here and henceforth), the western Laurentian margin began to develop from the initial breakup of this supercontinent. Recent research has shown that along much of the western margin of Laurentia, Neoproterozoic to early Paleozoic syn-rift and passive margin strata contain a consistent and recognized facies and detrital zircon progression (Yonkee et al., 2014). This is in stark contrast with multidisciplinary investigations that have demonstrated major along-strike complexity in Neoproterozoic Laurentian continental rifting and passive margin development (Lund, 2010; Thomas, 2011; Link et al., 2017b). The disagreement among these recent studies exposes a substantial gap between our understanding of rift processes along modern continental margins, and our ability to reconstruct continental margin evolution in the ancient record. Reconstruction of the tectonic evolution of ancient continental margins and evaluation of these conflicting paradigms requires a synthesis of the spatial and temporal variations in exhumation and subsidence patterns, sediment dispersal, crustal deformation, and rift-related magmatism within each proposed structural domain. Additionally, the pre-existing stratigraphic geometry of the Neoproterozoic to early Paleozoic miogeocline is known to strongly influence the geometry and style of subsequent Sevier and Laramide orogenesis (DeCelles, 2004).

North of the Snake River Plain, within a proposed "upper-plate" domain (Lund, 2008; Lund et al., 2010; Link et al., 2017b), Ordovician rocks lie unconformably upon Mesoproterozoic rocks, forming the Lemhi arch (Sloss, 1954; Scholten 1957; Ruppel, 1986). Bayhorse is located west of the Lemhi arch, ~10 km southwest of Challis, Idaho (Fig. 1.1). This area contains exposures of poorly dated lower Paleozoic and possibly Neoproterozoic rift-related sedimentary rocks intruded and overlain by Cretaceous and Eocene volcanic and plutonic rocks.

Study Area

This project involved 1:24,000-scale geologic mapping and structural analysis of a region within the Bayhorse and Bayhorse Lake 7.5-minute quadrangles southwest of Challis in central Idaho (Fig. 1.1). Within the study area, existing mapping of lower Paleozoic rocks (Hobbs et al., 1991; Fisher et al., 1992; Krohe, 2016) suggests an unusually thick Ordovician stratigraphic section (~5,000 m) compared to correlative deposits in southeastern Idaho (<1,000 m) (Oriel and Platt, 1980). Existing mapping also suggests this Ordovician section contains ~1.5 km of coarse quartz sandstones and quartz pebble conglomerates which would be anomalous in Cordilleran Ordovician strata, Generally; an extensive carbonate platform is found in both southeast and north Idaho during Late Cambrian and Early Ordovician time (Bush et al., 2012). A mineral exploration borehole drilled in the northeastern corner of the study area encountered a subsurface tuff that yielded a Neoproterozoic U/Pb zircon age of 667 Ma, suggesting that the overlying strata within the borehole are Neoproterozoic in age (Lund et al., 2010; Isakson, 2017). It has been hypothesized that a major fault exists that offsets the borehole from the allegedly lower Paleozoic strata exposed at the surface (Lund et al., 2010). Existing 1:62,500 scale mapping (Hobbs et al., 1991) shows only minor faulting between the location of the borehole and the Bayhorse anticline. However, this has not been tested by detailed mapping. Thus, an integrated structural, stratigraphic, and geochronologic study of this region was undertaken.

Field work focused on mapping a region within the Bayhorse and Bayhorse Lake quadrangles and then (1) constraining the structural context of the Daugherty Gulch borehole (Jacob, 1990) containing the 667 Ma (Isakson, 2017) subsurface tuff, therefore testing Lund et al.'s (2010) hypothesis that structural deformation offsets the borehole from the adjacent outcrops considered Ordovician in age (Hobbs et al., 1991); and (2) evaluating the critical contact between the Clayton Mine Quartzite and Ramshorn Slate in detail, as significant inconsistency exists as to whether it is a thrust (Hobbs and Hays, 1990; Hobbs et al., 1991) or a stratigraphic contact (Krohe, 2016). Additionally, several detrital zircon samples were analyzed from key stratigraphic intervals and compared to previous detrital zircon results from southeast and central Idaho (Yonkee et al., 2014; Link et al., 2017b; and references therein).

This study of the Bayhorse region offers an opportunity to evaluate the timing and geometry of Laurentian rifting, the rift-drift transition, as well as to speculate on the role of crustal heterogeneity in influencing the geometry of rift and subsequent passive margin development. Proper understanding of the Neoproterozoic and early Paleozoic tectonostratigraphic architecture west of the Lemhi arch in central Idaho fills a gap in our understanding of the stratigraphic architecture, sediment thickness, facies distribution, and subsidence patterns along the Neoproterozoic to Cambrian Laurentian margin. Additionally, a thorough understanding of the tectonostratigraphic architecture of central Idaho is required for evaluation of controls on subsequent Sevier and Laramide deformation through central Idaho and southwest Montana.

Figure 1.1- Regional map of the U.S. and Canadian Cordillera showing exposure belts for Neoproterozoic rocks and shelf and slope facies belts for Paleozoic sedimentary Rocks (Lund, 2008). The Bayhorse region and its location west of the Lemhi arch in central Idaho is shown with existing 1:250,000-scale mapping from Fisher et al. (1992). Recent (1:24,000-scale) mapping areas from this study (Plate 1) and Krohe (2016) are outlined. Locations of Challis and Leaton Gulch are shown for reference. Correlation and description of map units are in Fisher et al. (1992).

Figure 1.1

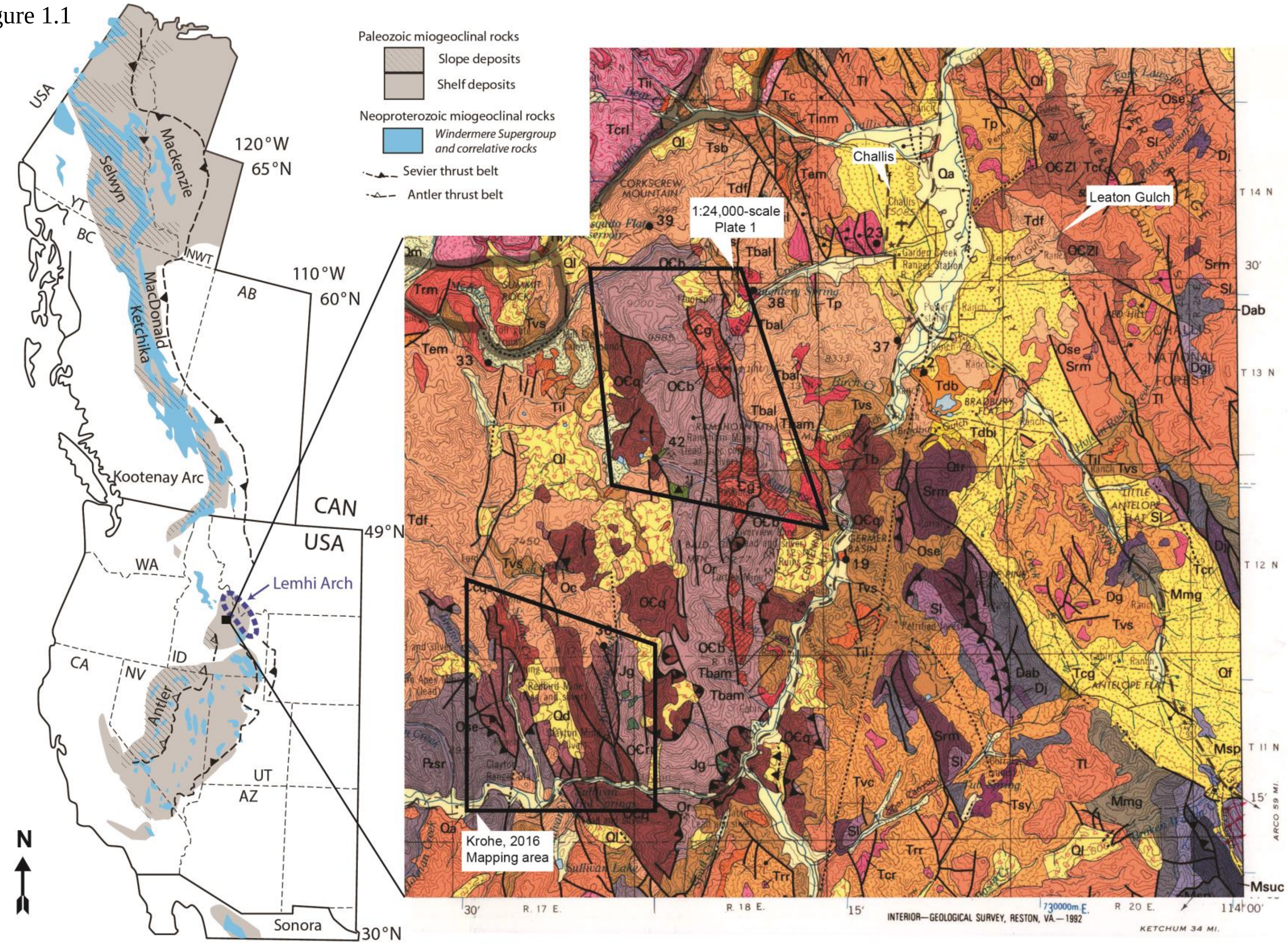

Paleozoic miogeoclinal rocks
Slope deposits
Shelf deposits
Neoproterozoic miogeoclinal rocks
Windermere Supergroup and correlative rocks
Sevier thrust belt
Antler thrust belt
USA
Selwyn
Mackenzie
120°W
65°N
YT
BC
NWT
110°W
60°N
AB
MacDonald
Ketchika
Kootenay Arc
CAN
USA
49°N
WA
Lemhi Arch
ID
CA
NV
Antler
UT
AZ
Sonora
30°N
N
Challis
Leaton Gulch
1:24,000-scale
Plate 1
Krohe, 2016
Mapping area
INTERIOR—GEOLOGICAL SURVEY, RESTON, VA—1992

CHAPTER 2: GEOLOGIC BACKGROUND

In the mountains of central Idaho, several younger orogenic, magmatic, and extensional events obscure the record of Neoproterozoic and early Paleozoic continental rifting. This study focuses on deciphering this older record through field and provenance examination of the Ordovician and older stratigraphy of the Bayhorse region. An overview of the main geologic events of central Idaho presents a basis from which the Bayhorse region will be scrutinized in depth. Idaho's geologic history can be broadly separated into the following intervals that include: (1) Paleoproterozoic and Archean basement amalgamation; (2) Mesoproterozoic Belt-Purcell Basin deposition; (3) Mesoproterozoic to early Neoproterozoic construction of Rodinia; (4) Late Neoproterozoic to early Paleozoic rifting and formation of the miogeocline; (5) Mid- to Late Paleozoic orogenesis; (6) Mid Mesozoic to early Paleogene development of the N. American Cordillera, including intrusion of the Idaho batholith; (7) Eocene back-arc extension and Challis volcanism; and finally (8) Miocene and younger Basin and Range extension and development of the Yellowstone hotspot track.

Geologic History of Idaho

Basement Framework

Various workers have inferred and subdivided a mosaic of basement rocks that underlie the northwestern United States (Fig. 2.1). Exposures of Paleoproterozoic and older basement occur in the Wyoming Province, in addition to the Medicine Hat and Grouse Creek blocks (Vervoort et al., 2016). On the far western side of Idaho, the margin of Laurentia was truncated by Neoproterozoic rifting during the breakup of Rodinia and now abuts juvenile Paleozoic and Mesozoic provinces accreted in the Late Jurassic or Early Cretaceous (Armstrong et al., 1977).

In Idaho, basement exposures are limited to the Priest River and Clearwater core complexes in north-central Idaho, and at House Mountain as well as the Pioneer and Albion metamorphic core complexes in south-central Idaho. In the Albion Mountains, south of the Neogene Snake River Plain, the basement comprises the Neoarchean Grouse Creek block (2.5-2.6 Ga; Strickland et al., 2011). North of the Snake River Plain, in central Idaho, the Pioneer metamorphic core complex exposes a felsic orthogneiss that crystallized at 2.60-2.67 Ga; this orthogneiss overlaps in age and is interpreted to be part of the Grouse Creek block of the Albion Mountains to the south (Link et al., 2017a). In north-central Idaho, the Clearwater and Priest River complexes expose rocks with Neoarchean (2.67 to 2.65 Ga) zircon U-Pb ages and have been interpreted as part of the same crustal block, known as the Clearwater block (Vervoort et al., 2016).

The presence of Neoarchean inherited zircons in the southern Atlanta lobe of the Idaho batholith suggests that the Archean Grouse Creek block exists farther north than previously thought and may be separated from the Priest River Complex to the north by the Paleoproterozoic Great Falls tectonic zone (Gaschnig et al., 2013), a collapsed arc and collisional suture (Foster et al., 2006). A single sharp ca. 1.38 Ga zircon age peak from inherited zircons found near Elk City, suggests the presence of Mesoproterozoic lithosphere (Elk City domain of Gaschnig et al., 2013) exists under the southwestern portion of the Belt Basin. This has been interpreted to represent Mesoproterozoic transitional oceanic lithosphere that formed during late rifting of the Belt basin (Doughty and Chamberlain, 1996). Elsewhere, Hf isotopic data from inherited zircon cores in the Idaho batholith provide evidence for the existence of pre-3.5 Ga crust. The presence of >3.5 Ga grains is likely due to partial recycling of even older crust, indicating that the Grouse Creek block and Priest River terrane may have shared an early history

(Gaschnig et al., 2013). The Grouse Creek block is separated from the Archean Wyoming craton to the west by the obscure Farmington zone (Foster et al., 2006). The Farmington zone is interpreted to record early Paleoproterozoic (~2.45 Ga) rifting of the Wyoming craton, and juxtaposition of other western Laurentian terranes at ca. 1.7 Ga (Mueller et al., 2011).

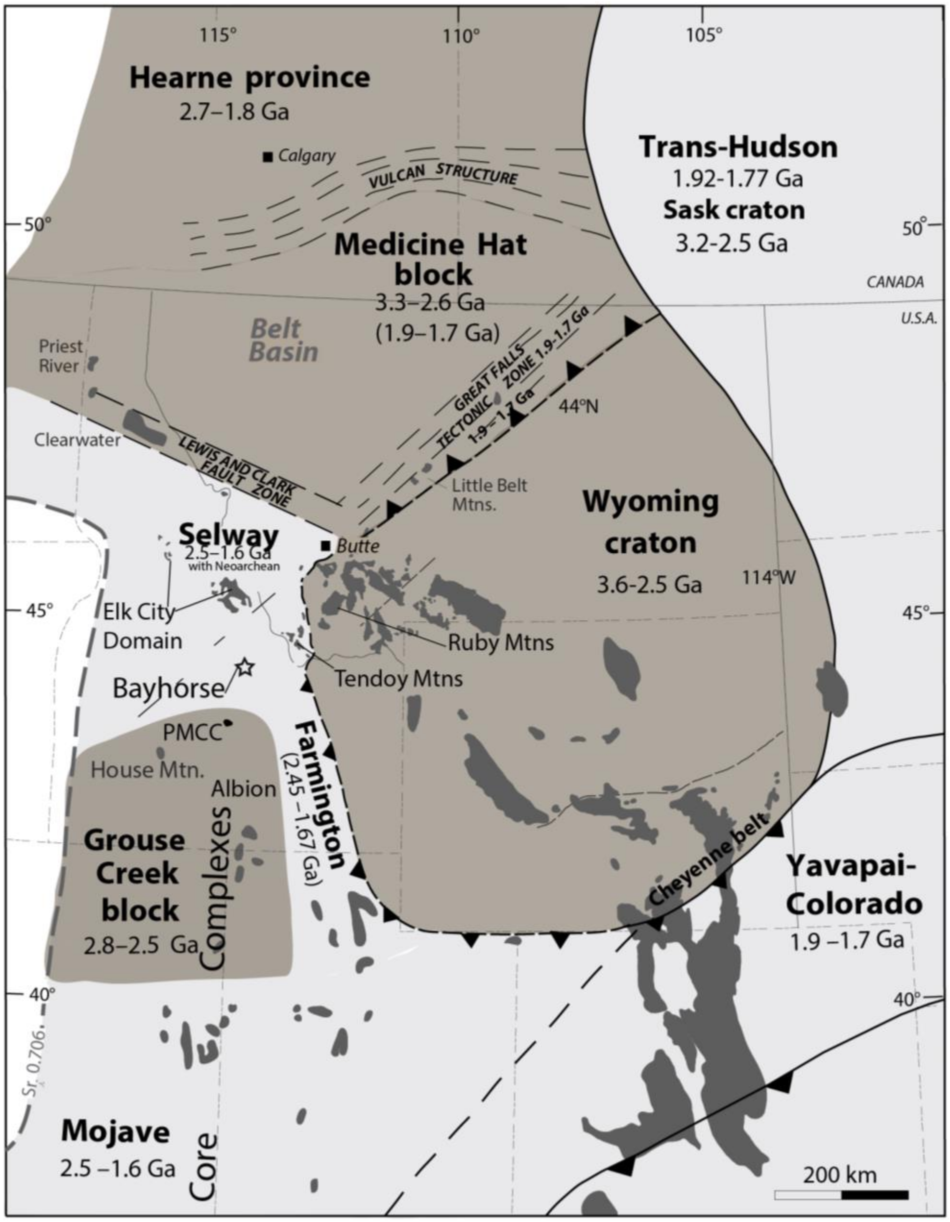

Figure 2.1- Map of basement provinces and related tectonic structures in the Idaho region of Laurentia modified from Link et al. (2017a). Bayhorse, Idaho is labeled and indicated by the star. PMCC: Pioneer Metamorphic Core Complex. Extent of Elk City Domain exposure from Lewis et al. (2010).

Mesoproterozoic Belt Supergroup

On top of the basement framework, Mesoproterozoic Belt Supergroup was deposited from 1.47-1.40 Ga in a huge (>200,000 km^2) intracratonic basin that extended across western Montana, northern Idaho, and into eastern Washington and Canada (Price, 1964; Winston 1986; Sears, 2007; Lewis et al., 2010). The occurrence of extensive 2.1-1.8 Ga collisional orogens and related cratonic blocks suggest the occurrence of a pre-Rodinia, Mesoproterozoic supercontinent termed Nuna (or Columbia) (Zhao et al., 2002; Rodgers and Santosh, 2002). Growing geologic evidence suggests a pervasive deformational event from 1.9-1.8 Ga (Wopmay Orogen) in northwest Canada. This event (known as the Barramundi Orogen in northeast Australia) is often interpreted to link Australia and Laurentia during the late Paleoproterozoic and early Mesoproterozoic as part of the supercontinent Nuna (Medig, 2016; Nordsvan et al., 2018). Pisarevsky et al. (2014) suggests that the Belt basin developed on a failed arm of a Nuna rift system. However, the tectonic setting of the Belt basin is debated (Winston and Link, 1993 and references therein).

It has also been proposed that these Mesoproterozoic and westward Neoproterozoic and Paleozoic passive margin rocks (of the Antler and Cassiar platforms) are part of a ribbon continent exotic to Laurentia and were accreted during Cretaceous westward subduction of North America beneath this continent (Johnston, 2008; Hildebrand, 2009). However, no suture zone or subduction-related metamorphism has been identified and a dominantly Laurentian provenance for supposedly exotic strata (Link et al., 2017b; Matthews et al., 2018) indicates that this model is improbable.

The Belt basin contains a thick (in the northern part of the basin, >15 km) succession of fine-grained clastic and carbonate strata. The southern part of the Belt basin is termed the Lemhi sub-basin. The boundary between rocks of the Lemhi sub-basin and the main Belt basin is non-distinct and gradational (Link et al., 2016). The Lemhi sub-basin shows a greater thickness of upper Belt, Missoula Group equivalents (Winston et al., 1999). However, the rocks of the Belt basin and Lemhi subbasin cannot be structurally separated (Winston et al., 1999; Link et al., 2007, 2016, 2017a; Stewart et al., 2010; Burmester et al., 2016). The southeastern extent of the Belt Supergroup is currently unknown (Link et al., 2017a). However, in the Albion-Raft River metamorphic core complex (Fig. 2.1), Neoproterozoic (Pocatello Formation equivalent) Elba Quartzite rests on Archean basement (Konstantinou et al., 2012; Yonkee et al., 2014) indicating a limit for the southwestern extent of the Belt Basin.

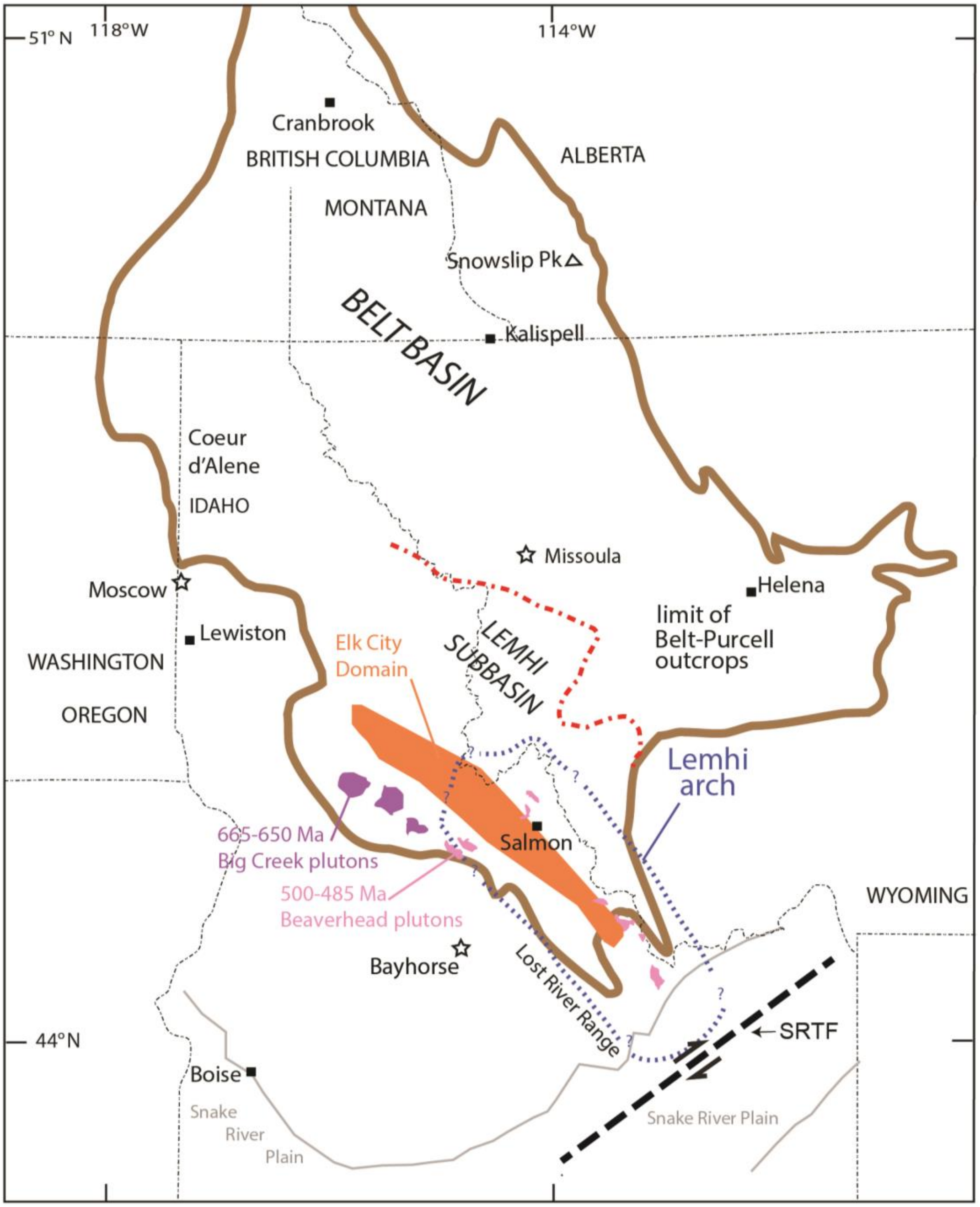

Figure 2.2- Location map showing areal limit of present outcrops of Belt-Purcell Supergroup (outlined in brown), boundary between the Belt basin and Lemhi subbasin deposits (red dot-dash line) and the relevant geologic features of east-central Idaho. These features included the Mesoproterozoic (~1.38 Ga) Elk City Domain (orange), ca. 665-650 Ma Big Creek plutons (purple), ca. 500-485 Ma Beaverhead plutons (pink), and extent of the Lemhi arch (blue dotted line). SRTF: Snake River transfer fault, hypothesized to bound the Lemhi arch to the south (Link et al., 2017b). Adapted from Lund et al. (2010); Lewis et al. (2012); Burmester et al. (2016) and Link et al. (2017b).

Rodinia Formation

Although the exact configuration and timing of Nuna supercontinent formation and rifting are poorly constrained, it is thought to have broken up during Mesoproterozoic time (~1.65 to 1.4 Ga) (Zhao et al., 2002; Medig, 2016; Nordsvan et al., 2018). Through a series of orogenic events, including the Grenville orogeny, the subsequent supercontinent, Rodinia, was assembled between 1300 Ma and 900 Ma (Moores, 1991; Dalziel, 1991; Hoffman, 1991; Li et al., 2008).

Evidence of geologic activity in western Laurentian from after the cessation of Belt deposition until the rifting of Rodinia and subsequent formation of the Cordilleran miogeocline is minimal. Because Laurentia was flanked by Neoproterozoic syn-rift margins, it is commonly regarded as being the center of the supercontinent Rodinia. The location of other continental blocks in Rodinia, particularly along the western margin of Laurentia, is still a topic of debate (Li et al., 2008). Multiple competing Rodinia reconstructions have been proposed, including: (1) "SWEAT" (Moores, 1991; Hoffman, 1991), (2) "Missing-Link" (Fig 2.3; Li et al., 1995), (3) "AUSWUS" (Karlstrom et al., 1999), (4) "AUSMES" (Wingate et al., 2002); and (5) "Siberian connection" (Sears and Price, 2000; Pisarevsky et al., 2008), with no consensus. There is also a growing body of evidence suggesting the possible presence of Grenville-aged low-magnitude crustal shortening and metamorphism along the western margin of Laurentia (Borg and DePaolo, 1994; Anderson and Davis, 1995; Berry et al., 2005; Fioretti et al., 2005; Vervoort et al., 2005; Doughty and Chamberlain, 2008; Zirakparvar et al., 2010; Nesheim et al., 2012); this brings into question the paleogeography and timing of several leading Rodinia models.

The supercontinent Rodinia lasted about 150 million years after complete assembly at ca. 1.0 Ga (Li et al., 2008). Sinking of stagnated slabs accumulated along the mantle transition zone (where spinel transitions to perovskite at ~670 km depth; for in-depth discussion of the mantle transition zone see Tackley et al., 1993), surrounding the supercontinent, may have led to eventual mantle "avalanches." Li et al. (2008) hypothesized that these mantle "avalanches," in addition to thermal insulation by the supercontinent, led to the formation of a mantle superswell (or superplume) beneath Rodinia, which resulted in Neoproterozoic rifting (Li et al., 2008).

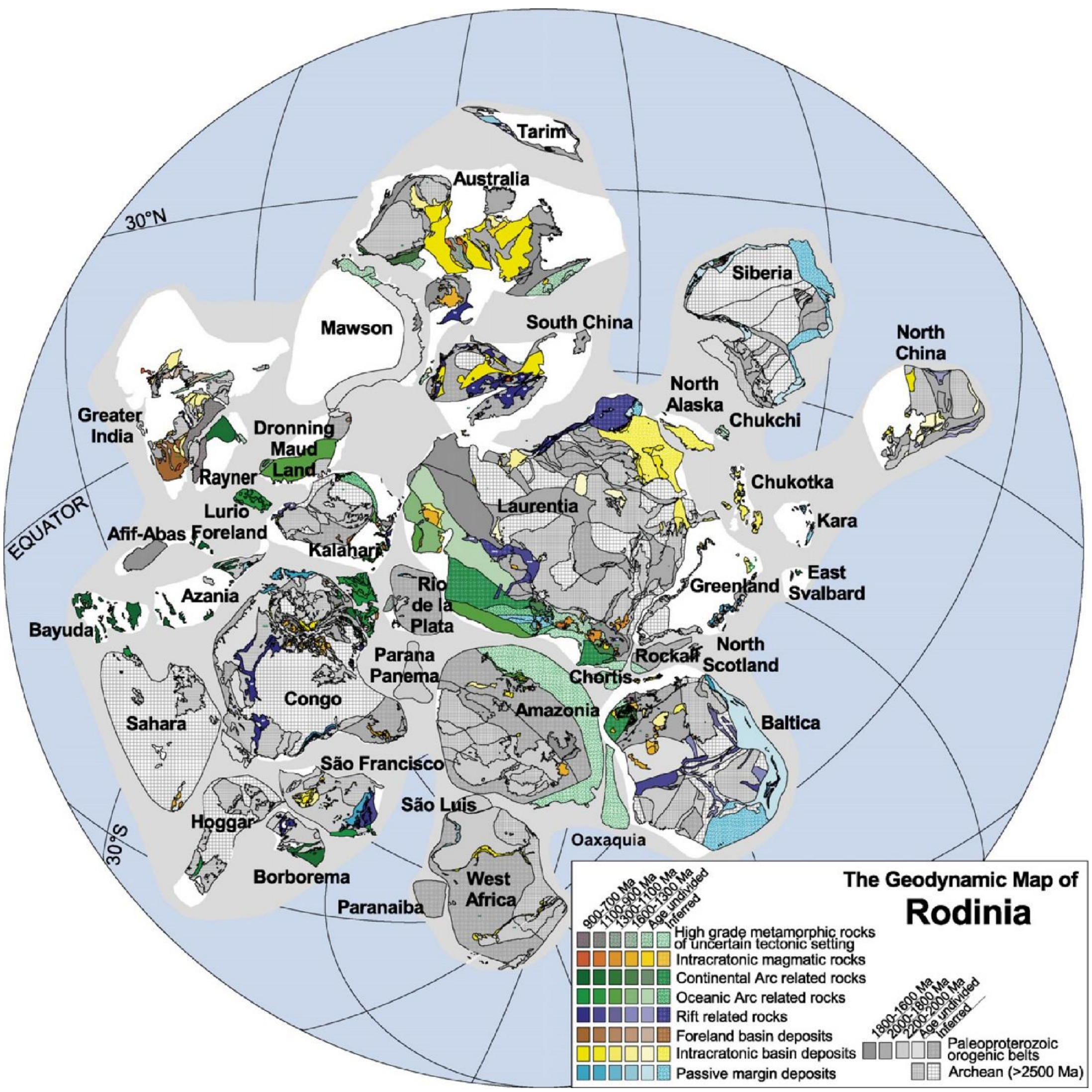

Figure 2.3- Simplified map of the most current Rodinia model from Li et al. (2008). The arrangement shown follows the "Missing-Link" configuration of Li et al. (1995) at ca. 900 Ma. Colored regions (see legend) represent areas of major crustal elements of the Precambrian continental blocks.

Neoproterozoic Rifting and Formation of the Passive Margin

As Rodinia rifted, the western Laurentian margin began to develop. Along the western margin of Laurentia, the first record of this breakup event started with the development of intracratonic basins and intrusion of the 780 Ma Gunbarrel dikes (Harlan et al., 2003; Yonkee et al., 2014). This western Laurentian margin has long served as a type example for a classic passive margin or miogeocline (Sloss, 1950; Stewart, 1972; Bush et al., 2012). However, issues remain with the duration and proposed structure of rifting prior to passive margin formation. Along much of the western margin of Laurentia, Neoproterozoic to early Paleozoic syn-rift and passive margin strata contain a consistent facies and detrital zircon progression, as seen in the Windermere Supergroup and its correlatives (Fig. 2.4). This well-documented stratigraphic pattern reveals a systematic depositional history. This pattern consists of: (1) siliciclastic strata deposited in intracratonic basins (Uinta Mountain and upper Crystal Springs) from ca. 770 to 740 Ma; (2) deposition of diamictite-bearing strata from 720 to 660 Ma during early rifting and volcanism; (3) deposition of mature siliciclastic strata associated with broad subsidence from 660 to 580 Ma; (4) deposition of variably immature siliciclastic strata associated with final rifting and transition to drift from 570 to 520 Ma; followed by (5) deposition of Middle Cambrian to Devonian carbonate-rich strata marking regional subsidence along a passive margin (Link et al., 1993; Dickinson, 2004; Mahon et al., 2014; Yonkee et al., 2014).

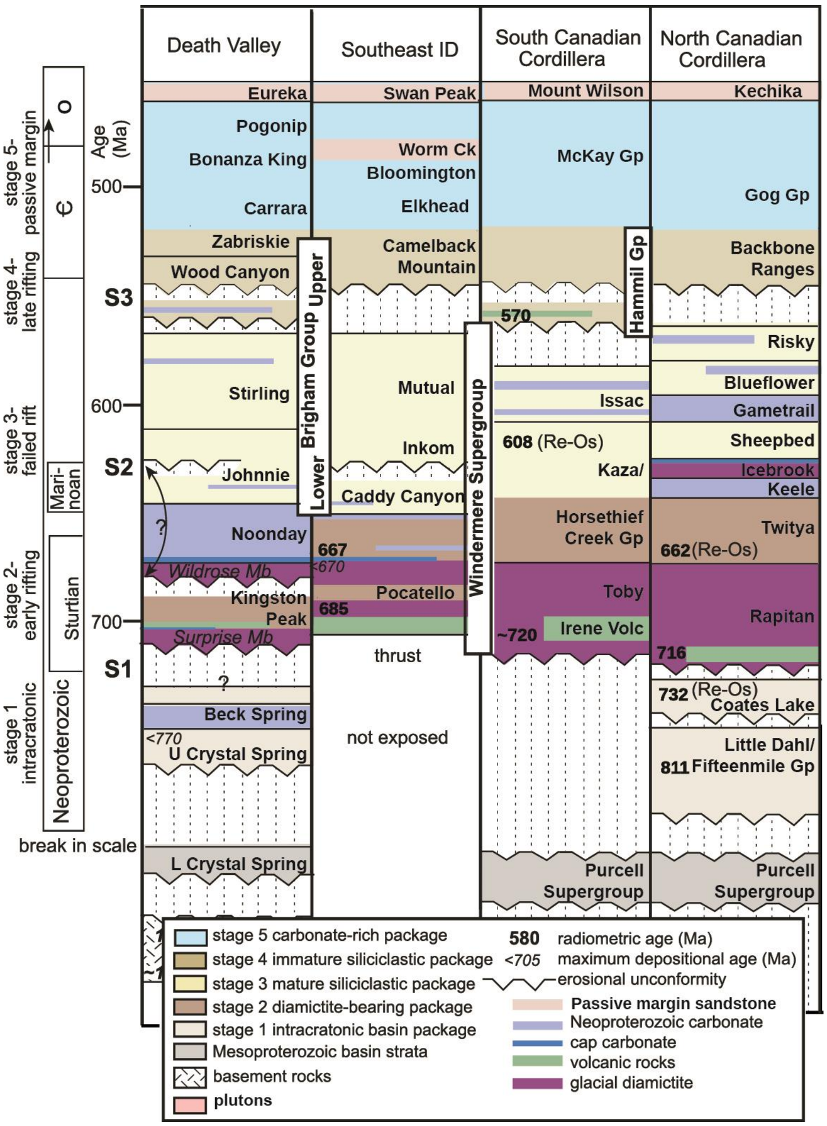

Figure 2.4- Reference stratigraphic sections and published age constraints for Neoproterozoic to Ordovician strata along the Cordilleran margin. Along the vertical axis, five stages of rifting from Yonkee et al. (2014) are indicated. Major sequence boundaries (S1 to S3) are also indicated (Link et al., 1987); in the southeast Idaho section, these boundaries occur above the Caddy Canyon Quartzite (S2) and above the Mutual Formation (S3). Modified from Yonkee et al., (2014).

South of the modern Snake River Plain, >6 km of Neoproterozoic and lower Paleozoic strata were deposited on the margin of Laurentia as part of the Sauk Megasequence (Sloss, 1963; Bush et al., 2012). North of the modern Snake River Plain, in east-central Idaho, there are no Neoproterozoic or Cambrian passive margin strata across an unconformity known as the Lemhi arch (Fig. 2.2; Sloss, 1954; Scholten, 1957; Ruppel 1986). The Lemhi arch is characterized by

Middle Ordovician Kinnikinic Quartzite unconformably overlying locally tilted Mesoproterozoic Belt Supergroup of the Lemhi sub-basin (Fig. 2.5; Sloss, 1950; Scholten, 1957; Link et al., 2017b).

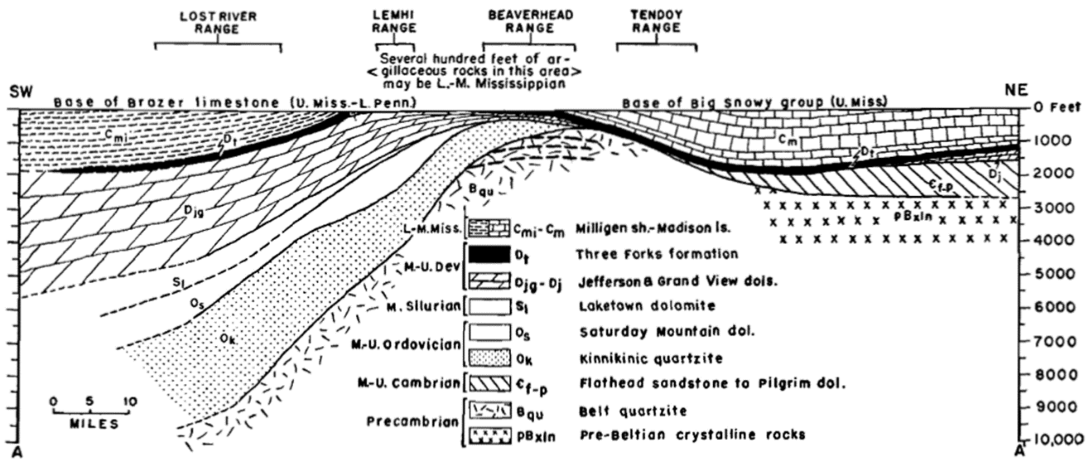

FIGURE 7.—STRATIGRAPHIC CROSS SECTION OF PRE-UPPER MISSISSIPPIAN ROCKS
Line of cross section is shown on Figure 2.

Figure 2.5- A schematic cross section across the Lemhi arch. The absence of Neoproterozoic and Cambrian rocks defines this feature (Scholten, 1957). The approximate extent of this feature can be seen in Fig. 2.2.

In southeast Idaho, a 500-490 Ma detrital zircon age peak dominates the Worm Creek Member of the Upper Cambrian St. Charles Formation. Intermediate εHf values from these zircon grains overlap with the isotopic composition of the Deep Creek and Beaverhead plutons, presenting a strong correlation. This requires active exhumation of the Lemhi arch during Late Cambrian time (Link et al., 2017b). Oblique normal faulting and subsidence along the hypothesized dextral Snake River transfer fault was proposed for the formation of the Worm Creek basin and juxtaposition of the active Cambrian magmatism and exhumation of the Lemhi arch with passive margin sedimentation to the south (Link et al., 2017b).

Rift Models

Various models have been proposed to explain the uncertain rift evolution of the Neoproterozoic Cordilleran margin that formed over a >300 m.y. period of episodic lithospheric extension, breakup, and syn- to post-breakup magmatism. Lund (2008) evokes a "detachment fault model;" Yonkee et al. (2014) applies a "depth-dependent extension model;" and Beranek (2017) notes similarities between the modern Newfoundland-Iberia "magma-poor margin" and the Cordilleran margin. However, none of these models address the issue that central Idaho took ~50 million years longer to transition to a passive margin (Link et al., 2017b) than the rest of the miogeocline. Additionally, these models do not easily explain the presence of "two-passive margin sequences" along the Cordillera margin (Johnston, 2008). These suggested "two-passive margin sequences" are composed of the western Antler platform (Cassiar platform in Canada and northern U.S.), which contains thick Mesoproterozoic and Neoproterozoic successions overlain by basal Cambrian sandstones, and an eastern North American platform, where basal Cambrian sandstones lie on thin Neoproterozoic deposits or directly on crystalline rocks of Laurentia (Matthews et al., 2018).

A detachment-fault model (Lister, 1986) was applied to the Cordilleran margin (Lund, 2008) to explain the geometry along with thickness and location of sedimentary rocks, volcanism, and mineralization along the rift margin. In this model, rifting is localized on a low-angle detachment fault that results in paired, asymmetric, upper (hanging wall), and lower-plate (footwall) margins, with along-strike transitions accommodated by transfer faults (Fig 2.6).

A depth-dependent extension model (Huismans and Beaumont, 2011) that emphasizes the influence of crustal rheology on rift timing and geometry, has also been applied to the Cordilleran margin of western North America (Yonkee et al., 2014). This model suggests that rifted margin heterogeneity is a result of depth-dependent extension due to decoupling (or lack of decoupling) between the upper and lower lithosphere due to lithospheric composition and strength.

Recent structural comparison of Atlantic rifted margins indicates that a set of spatial domains characterize both rifted margins. These consist of a: 1) proximal, 2) necking, 3) distal, 4) outer, and 5) oceanic domain. Collectively, these domains record the progressive localization of rifting toward the area of eventually breakup. Each of these entities formed during one specific phase of deformation within: 1) the stretching phase, 2) the thinning phase, 3) the hyperextension and exhumation phase(s), 4) the magmatic phase, or the 5) oceanization phase. These phases affect the margin successively, migrating and concentrating oceanward. They tend to overprint each other spatially and temporally, notably re-using former structural weaknesses to continue to accommodate extension (Peron-Pinvidic et al., 2013).

A magma-poor rift model of the Cordilleran margin shows some similarities to the Newfoundland-Iberia modern rift system (Fig 2.7c; Beranek, 2017). This new model applied to the western Laurentian margin suggests 30 Ma of Neoproterozoic mantle exhumation (Beranek, 2017). Neoproterozoic exhumed mantle is not observed along the Cordilleran margin, but it has been interpreted to underlie the accreted terranes that underlie western North America (Hayward, 2015).

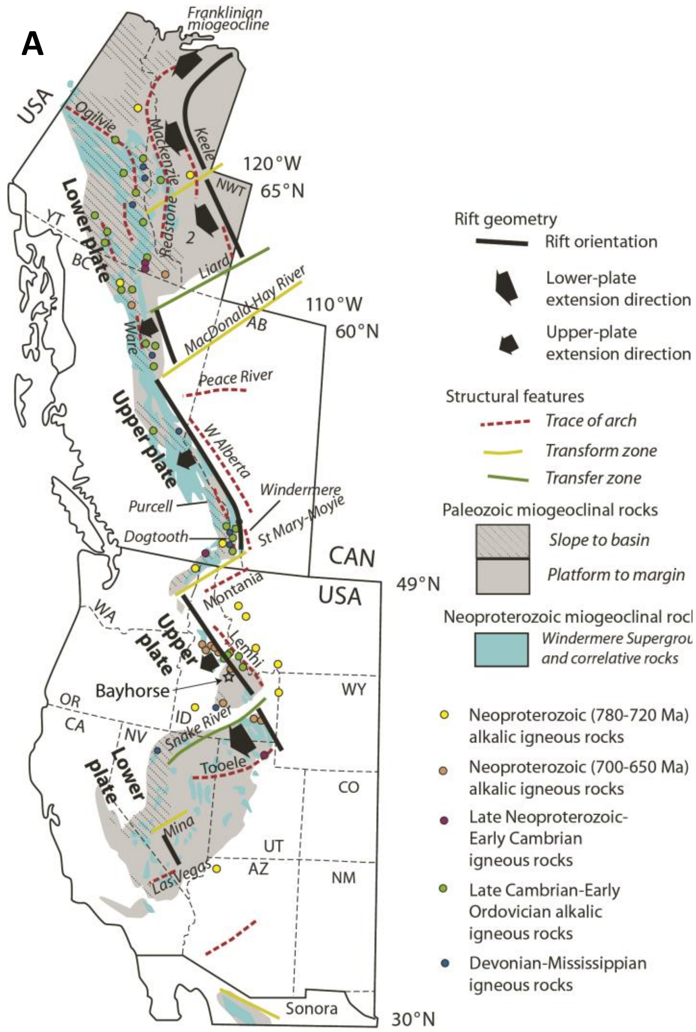

Figure 2.6- (A) Regional map showing sedimentary basins forming the miogeocline and schematic interpretation of rift segments, transfer and transform zones, and arches of the U.S. and Canadian Cordillera (adapted from Lund et al., 2010). (B) Schematic cross-section view of structures in asymmetric extension. Limited crustal thinning, manifested by relatively narrow continental shelf margins, development of proximal continental drainage divides (arches), alkalic magmatism, and down to the basin normal faults characterizes “upper-plate margins”. Marked thinning of continental crust, manifested by subsidence across a broad continental shelf margin, and rotated crust blocks characterizes “lower-plate margins” (Lister et al., 1986; Lund, 2010).

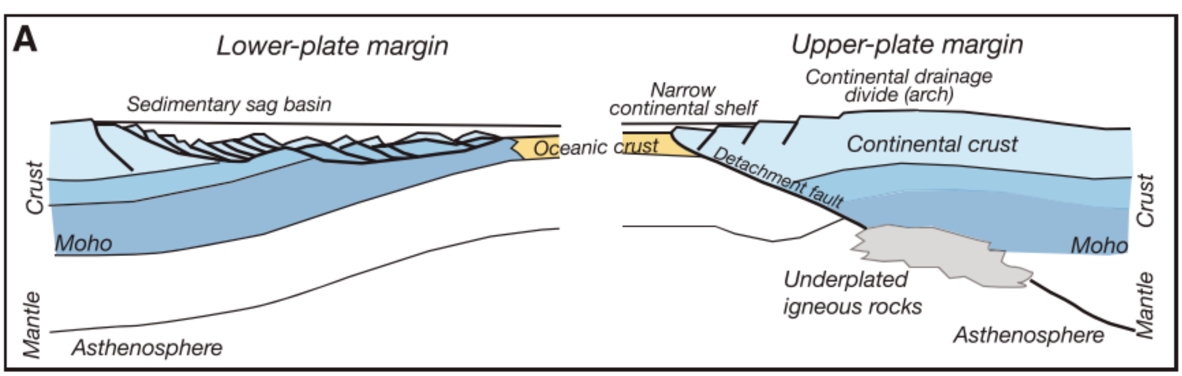

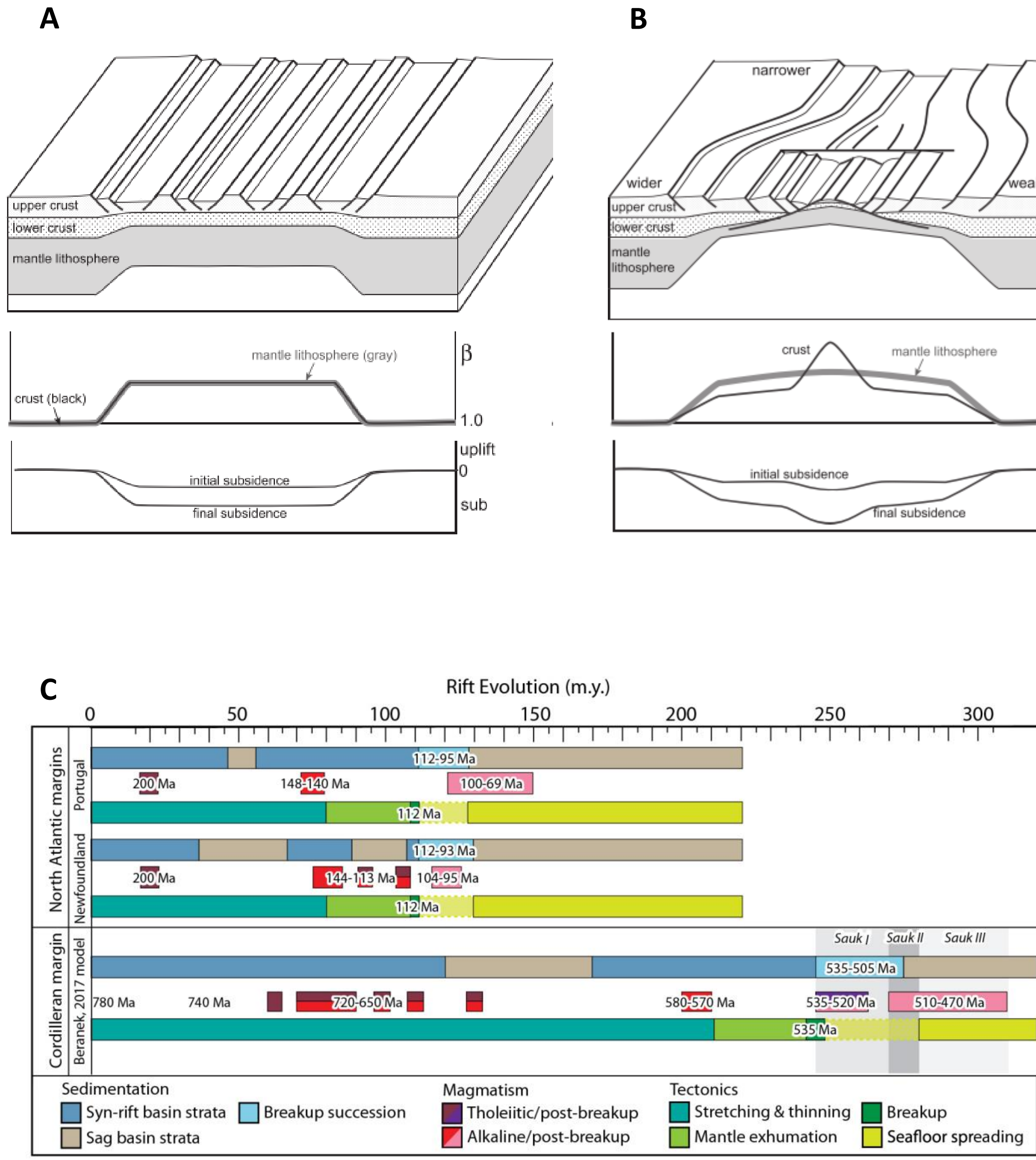

Figure 2.7- The Cordilleran two-stage rift model of Yonkee et al. (2014) consists of (A) uniform pure shear thinning of crust and mantle lithosphere during initial rifting, followed by (B) depth-dependent crust and mantle lithosphere thinning with localized necking during final rifting. (C) The observed rift evolution of the North Atlantic margin compared to a proposed Magma-poor rift model for the Cordilleran margin (Beranek, 2017 and references therein).

Middle to Late Paleozoic Orogenesis

Following rifting, the western margin of Laurentia was tectonically quiescent until the Late Devonian to Mississippian Antler orogeny. The Antler orogeny marks the transition from a Paleozoic passive margin to an active margin along the western edge of Laurentia (Beranek et al., 2016). Several tectonic scenarios have been presented for the occurrence of this puzzling orogenic event. Tectonic models include an arc-collisional (Speed and Sleep, 1982), a non-collisional (Burchfiel and Royden, 1991), and the current leading model: an oblique tectonic model (Beranek et al., 2016). The Copper Basin Group and the Salmon River assemblage in the Pioneer Mountains region of central Idaho were interpreted to have been deposited in an Antler pull apart basin (Wilson et al., 1994; Beranek et al., 2016).

During the Pennsylvanian to Permian, the south-eastern flank of Laurentia underwent a series of orogenic events (culminating with the Alleghenian orogeny), that resulted in closing of the Iapetus ocean and assembly of Pangea, the 3rd and most recent supercontinent (Dickinson, 2004). This orogeny also contributed detritus for aeolian transport into Pennsylvanian-Permian continental margin basins of central Idaho such as the Wood River Basin (Link et al., 2014). Rocks deposited in central Idaho during this middle and late Paleozoic interval have been transported on younger thrusts and are now juxtaposed against the early Paleozoic and older rocks of the Bayhorse region (Fig. 2.8).

Sevier Thrusting and Idaho Batholith Magmatism

The breakup of the supercontinent Pangea in the Triassic and subsequent Jurassic-Cretaceous accretion of intraoceanic island arcs, and the initiation of subduction along the western margin of Laurentia led to an ensuing 100 Myr of eastward propagating deformation (DeCelles, 2004; Dickinson, 2004). This also resulted in widespread Late Cretaceous and early

Tertiary magmatism throughout central Idaho (Gaschnig et al., 2010). The intrusive portion of this Cretaceous magmatic arc is present in central Idaho as the Idaho batholith. This Cordilleran orogenic system developed partly on Laurentian basement and sedimentary cover rocks, and partly on accreted terranes.

In the interior of the dissected orogen, the 39,000 km^2 Idaho batholith was intruded over a span of approximately 50 million years starting at ca. 110 Ma (Gaschnig et al., 2010). The Cretaceous-Paleocene Idaho batholith is divided into a larger southern Atlanta lobe and smaller northern Bitterroot lobe. The Atlanta lobe is composed primarily of hornblende granodiorites and tonalites ranging in age from 98 to 85 Ma and the voluminous Atlanta peraluminous suite with ages of 83 to 67 Ma. The Bitterroot lobe consists of biotite granodiorites and two-mica granite with ages of 83 to 60 M and a late metaluminous suite, with ages of 66 to 54 Ma (Gaschnig et al., 2013). A zone (formerly termed the Salmon River arch) of metamorphosed Belt Supergroup, Windermere Supergroup sedimentary rocks, and 1.38 Ga augen gneiss forms a general boundary between the two lobes (Armstrong, 1975a; Doughty and Chamberlain, 1996; Elk City Domain of Gaschnig et al., 2013).

Zircons from the southern part of the Atlanta lobe show inheritance from the Archean Grouse Creek block. The northern and central portion of the Atlanta lobe show a large population of Grenville-aged zircons, suggesting inheritance from Neoproterozoic Windermere Supergroup country rock. The Bitterroot lobe shows inherited zircons primarily ranging in age from ca. 1400 to 1900 Ma, suggesting inheritance from the Mesoproterozoic Belt Supergroup country rock (Gaschnig et al., 2013). The Idaho batholith may have also intruded a portion of the Neoproterozoic to Ordovician marginal succession (Ma et al., 2016) and obscures much of the Paleozoic and older strata of central Idaho. Within the Bayhorse area, the Juliette stock (U-Pb age of 96.9 ± 0.8 Ma; Krohe, 2016) is the eastern expression of the Idaho batholith.

To the east of the Idaho batholith, central Idaho is composed of several Cordilleran thrust sheets. The major thrusts in central Idaho consist of (from southwest to northeast): The Pioneer, Copper Basin, and Hawley Creek thrusts (Rodgers and Janecke, 1992; Beranek et al., 2016). Overall, these thin-skinned “Sevier” thrusts displaced primarily sedimentary strata and form an imbricate fan. Thrusts are inferred to young to the northeast. The Pioneer thrust carried primarily Permian to Devonian Sun Valley Group, Milligen Formation, and equivalents. The next major and structurally lower thrust to the east, the Copper Basin thrust, carried Mississippian Copper Basin Group, Devonian Jefferson Formation, Ordovician Kinnikinic Quartzite and Neoproterozoic (?) to Cambrian strata. The Hawley Creek thrust, exposed in the Beaverhead Mountains, carried age-equivalent but shallower facies Permian to Devonian strata as well as Ordovician Kinnikinic and Neoproterozoic (?) to Cambrian strata (Beranek et al., 2016).

Previous mapping attributes the contractional fabrics, thrusts, and folds within the Bayhorse region to this period of Cretaceous deformation (Hobbs and Hays, 1990). In a Cordilleran-scale perspective, central Idaho geology provides a long-term record of interrelations among upper crustal shortening, lower crustal thickening, metamorphism, and changing plate dynamics through a complete orogenic cycle. Rheology, strength, and associated heterogeneity of the North American basement and sedimentary cover are suggested to have partially controlled subsequent structural development of the Sevier and Laramide belts (DeCelles, 2004; Weil and Yonkee, 2012; Yonkee and Weil, 2015). Thus, improved understanding of the basement, the overlying stratigraphy (such as at Bayhorse), and the influence of the Lemhi arch is needed to evaluate the structural controls of the fold and thrust belt and the adjacent basement Laramide "uplifts" of southwest Montana.

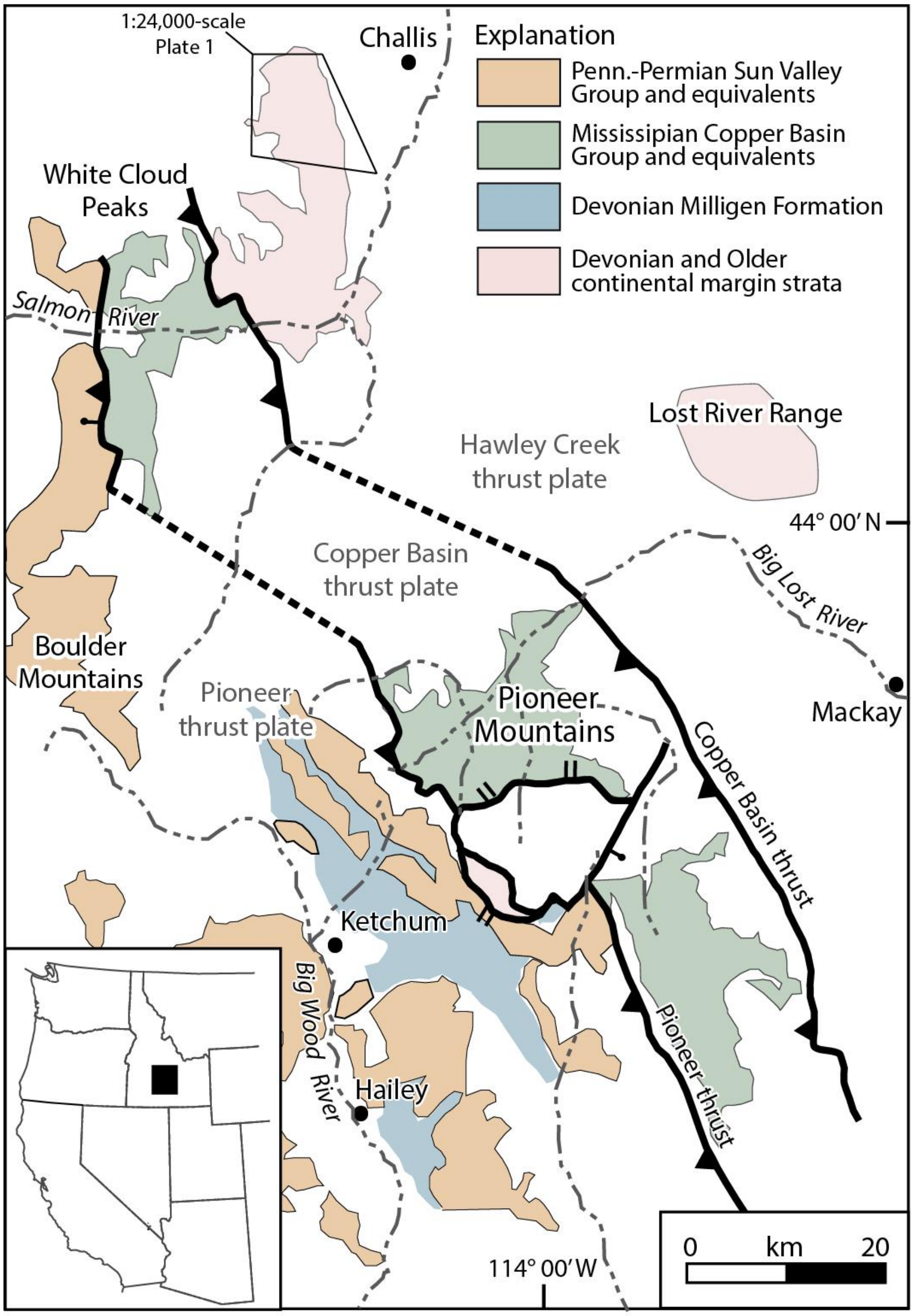

Figure 2.8- Simplified bedrock map of the Pioneer Mountains region, east-central Idaho, modified from Lewis et al., (2012) and Beranek et al., (2016). The Hawley Creek thrust is located off the map to the northeast (right). The mapping area of this study is shown on the hanging-wall of the Hawley Creek thrust.

Eocene Challis Group Volcanism

The Challis volcanic field is part an extensive Eocene (~51-40 Ma) magmatic belt that is exposed over an area of about 25,000 km^2 (Armstrong and Ward, 1991; Gaschnig et al., 2010). The Challis is part of a larger Eocene volcanic belt that extends 1,500 km from west to east and includes the British Columbia alkalic province, the Sanpoil field in northeastern Washington and southern British Columbia, the Absaroka field in Montana and Wyoming, the Montana alkalic province, and numerous smaller scattered outliers of Eocene volcanic rocks (Armstrong and Ward, 1991). Challis volcanic rocks are dominantly high-K andesites, high-K dacites and latites but range from basalt to alkali rhyolite in composition (Sandford, 2005). An equally complex assemblage of associated hypabyssal intrusive plutonic rocks is associated with Eocene Challis volcanism (McIntyre et al., 1982). These intrusive rocks have characteristics of A-type rocks that are generally associated with crustal extension (Bennett, 1986). The Challis Volcanic Group extrusive deposits blanketed irregular pre-volcanic terrane resulting in complex stratigraphic relations and variable thicknesses (McIntrye et al., 1982). The Challis often exhibits a basal "Smiley Creek" conglomerate that contains only clasts of Paleozoic sedimentary rocks with no volcanic component (Sanford, 2005). Challis Volcanic Group deposits obscure the rocks of the Bayhorse region to the north, south, and east.

The Trans-Challis fault system constitutes a network of northeast-southwest striking normal and associated strike-slip faults (McIntyre et al., 1982; Bennett, 1986; Sandford, 2005). Synchronicity between Trans-Challis faulting and Challis volcanism is observable in growth-faults, emplacement of intrusive rocks along Trans-Challis associated faults, and a consistently northeast-striking nature of Eocene dikes (Link and Janecke, 1999; Meyers, 2014). The initiation of Challis volcanism is often explained by a slowing of tectonic convergence rates, allowing the subducting Farallon plate to steepen beneath the North American plate. This is inferred to have resulted in back-arc extension and decompression melting of the thickened Precambrian lithospheric mantle (Armstrong, 1982; Coney and Harms, 1984; Janecke et al., 1997; Dostal et al., 2003; Meyers, 2014).

Yellowstone Hotspot and Basin and Range Extension

The eastern Snake River Plain of southern Idaho represents the 100-km wide track of the Yellowstone hotspot during the last ~16-17 m.y. (Pierce and Morgan, 1992; Parsons et al., 1998). The Yellowstone Snake River Plain (YSRP) system consists of a northeast-younging rhyolitic volcanic track, which is overlain by basalt flows. The migration of this track relative to North America matches the present-day velocity of the North American plate (Pierce and Morgan, 1992). Vigorous debate regarding the source of the YSRP system has continued for decades. The traditional model relies on a deep mantle plume (Pierce and Morgan, 2009), however several other models exist including: convective roll (Humphreys et al., 2000), a propagating rift (Christiansen et al., 2002), edge driven convection (King, 2007), lithospheric control (Tikoff et al., 2008), and subducted slab-controlled upwelling (Faccenna et al., 2010). Subsidence of the Eastern Snake River Plain (ESRP) has been attributed to densification of the middle crust compensated by density-driven lower crustal flow away from the ESRP (McQuarrie and Rodgers, 1998). Several North American Cordilleran tectonic models, most notably the detachment-fault model (Fig 2.6) of Lund (2008), suggest that the Yellowstone hotspot track overprints a major pre-existing structure.

Widespread extension across the Basin and Range province was contemporaneous with the initial impingement of this Yellowstone "mantle plume" (Camp et al., 2015). The Cenozoic extensional history of the Basin and Range Province has been explained through a variety of models. These include: (1) broadly distributed shear of the plate interior driven by dextral motion of the Pacific plate (Livaccari, 1979); (2) thickening of the crust sufficient to produce buoyancy-driven extensional strain (Jones et al., 1998); or (3) subslab upwelling and lateral spreading of asthenosphere, derived either from a “slab window” behind the trailing edge of the Farallon plate (Dickinson and Snyder, 1979) or from the adiabatic rise of the Yellowstone mantle plume (Pierce et al., 2002). It has also been suggested to be a combination of all three (Camp et al., 2015). Seismic data suggests that the Bayhorse region is experiencing active Basin and Range extension. However, recent investigations using remote sensing techniques were not able to identify a surface expression of an active fault (Shields, 2017).

GPS measurements indicate that the Basin and Range in central Idaho is extending at an order of magnitude greater rate than the ESRP (Payne et al., 2008). This suggests that a northeast trending zone of right-lateral shear, dubbed the “Centennial shear zone”, exists between these two provinces (Payne et al., 2008; Payne et al., 2012). However, concrete geologic evidence of this shear zone has not been recognized.

Geology of the Bayhorse Region

The region surrounding the town of Challis, the Salmon River Mountains, and Custer County Idaho, is at the nexus of several geologic provinces. Cretaceous Sevier thrusting, and Neogene to present extension of the Basin and Range in this region exposes lower Paleozoic and potentially older strata in central Idaho. It also adds significant structural complexity, which is obscured by Cretaceous Idaho batholith plutonism and extensive Eocene volcanism.

Previous Work

The first geologic study of the Bayhorse region, beyond early reconnaissance reports, produced a map at 1:125,000 scale and identified several stratigraphic problems that are still unresolved (Ross, 1937), thus the need for this study. The work of Ross (1937) was followed up by the work of Patton (1948), Hobbs et al. (1968), Hobbs et al. (1975), Hobbs (1985), McIntyre and Hobbs (1987), Hobbs and Hays (1990), Jacob (1990), Hobbs et al. (1991), and Fisher et al., (1992). Studies located approximately 20 km northeast of Bayhorse at Leaton Gulch (Carr and Link, 1999; Hargraves et al., 2007) and relatively recent studies incorporating new mapping along with geochronologic methods (Lund et al., 2010; Krohe, 2016; Brennan et al., 2017; Isakson, 2017, Link et al., 2017b) also have implications for the Neoproterozoic to early Paleozoic, tectonic, volcanic and sedimentary history of the Bayhorse region and central Idaho.

This study presents a new age assignment for several stratigraphic units within the Bayhorse region. This new correlation presents a solution to many of the existing stratigraphic problems. Problems such as: (1) Uncharacteristic thicknesses and lithologies compared to nearby correlative lower Paleozoic sections (Fig. 2.12; Hobbs et al., 1991; Krohe, 2016), (2) Detrital zircon signatures (Krohe, 2016), (3) Distinct lack of early Paleozoic fossils in fine-grained rocks with a high preservation potential (Hobbs et al., 1991), and (4) Complex structural interpretations including thrust faults interpreted to place younger on older rocks (Hobbs et al., 1991). Considering new observations and data, I argue that an older Neoproterozoic age assignment for a large section of the Bayhorse stratigraphy better matches the proposed geometry, timing, and progression of rifting through central Idaho, its relation to the Lemhi arch, and of the entirety of the Cordilleran margin.

Previous Stratigraphic Correlations

Ross (1937) identified and defined the Garden Greek Phyllite, Bayhorse Dolomite, and Ramshorn Slate (in ascending stratigraphic order) exposed in a regional anticline, ~10 km west of Challis in the Bayhorse and Bayhorse Lake quadrangles. No fossils were recovered from this section. However, fragmentary graptolites were recovered ~35 km to the south along Big Lake and Pine Creek in the Zeigler Basin quadrangle from a small (<1 km^2) shale outcrop surrounded by Eocene volcanic rocks. The fossil assemblage was dated from Lower Ordovician to Silurian in age (Ross, 1937). This shale was originally tentatively correlated to the Ramshorn Slate.

However, this shale along Big Lake and Pine Creek has since been considered correlative with the Middle and Upper Ordovician Saturday Mountain Formation, and probably the Phi Kappa Formation in the Pioneer Mountains, and not the Ramshorn Slate (Hobbs and Hays, 1990). This means that no fossil constraints exist for the Garden Creek Phyllite, Bayhorse Dolomite, and Ramshorn Slate section.

The formation that crops out along Kinnikinic Creek, just west of Clayton, Idaho, was originally named the Kinnikinic Quartzite (Ross, 1934; Patton, 1948). Initially, the Kinnikinic Quartzite was defined as an over 1,200 m thick quartzite with intercalated calcareous beds, with the lower quartzite being locally conglomeratic. No fossils were recovered from the Kinnikinic Quartzite, but it was tentatively correlated to the Swan Peak Quartzite of SE Idaho/Utah and thought to be Middle to Lower Ordovician due to its position under the Upper Ordovician Saturday Mountain Formation and above the Ramshorn Slate (whose Lower Ordovician to Silurian fossil constraints have since been shown to be incorrect). Subsequent study of the intercalated quartzites, dolomite, and argillaceous lithologies of Ross's (1937) and Patton's (1948) Kinnikinic Quartzite put them in several formations of distinctly different lithologies and ages (Hobbs et al., 1968).

Stratigraphic correlation between the Bayhorse region, the Wood River region, and southeastern Idaho

Bayhorse region				Wood River region [1]	Southeastern Idaho [2]	Age [3]
Age	Formation	Character	Thickness (feet)			
Upper Ordovician.	Saturday Mountain formation.	Dark massive dolomite interbedded with argillite and shaly dolomite, in part carbonaceous.	3,000±	Phi Kappa formation.	Fish Haven dolomite	Upper Ordovician.
Middle (?) Ordovician.	Kinnikinic quartzite.	Massive light-colored quartzite with local lenses of dolomite and dolomitic shale, separately mapped. Some conglomerate.	3,500±			
Lower Ordovician.	Ramshorn slate.	Dark thin-banded slate predominates in most places, with argillite and argillaceous quartzite locally, mainly in the south.	2,000	Early Lower Ordovician rocks (Beekmantown).	Swan Peak quartzite. Garden City limestone (Beekmantown).	Lower Ordovician.
Cambrian (?).	Bayhorse dolomite.	Generally massive thick-bedded dolomite, in part oolitic.	1,000+		St. Charles limestone.	Upper Cambrian.
	Garden Creek phyllite.	Intensely sheared and metamorphosed argillaceous rock.	Base not exposed. At least several hundred.		Nounan limestone, Bloomington formation, Blacksmith limestone, Ute limestone. Langston limestone.	Middle Cambrian.
					Brigham quartzite.	Lower Cambrian.
				East Fork and Hyndman formations (Algonkian?).		

[1] U. S. Geol. Survey Bull. 814, 1930. [2] U. S. Geol. Survey Prof. Paper 152, 1928. [3] This column relates to both the Wood River region and southeastern Idaho.

Figure 2.9: An initial correlation of the Ordovician and older units of the Bayhorse region to the stratigraphy of the Wood River region, central Idaho, and the stratigraphy of southeastern Idaho (Ross, 1937). Note the Ramshorn Slate age constraint has been since proved a mis-correlation (Hobbs et al., 1990), and the Kinnikinic Quartzite has been redefined (Hobbs et al., 1968).

The quartzites that crop out so prominently at the original type locality, in the lower reaches of Kinnikinic Creek, are now excluded from the Kinnikinic Quartzite as redefined. Hobbs et al. (1968) redefined the Kinnikinic Quartzite as the uppermost quartzite unit exposed in the Clayton quadrangle, lying in apparent conformity above at least 200 meters of massive and sandy "Ella" Dolomite in the anticlinal structure along the Salmon River canyon west of the town of Clayton. The type section of the Ella Dolomite (NE 1/4 SE 1/4 sec 23, T. 11 N. R. 17 E.) contains brachiopods and conodonts that clearly date to early Middle Ordovician time (Hobbs et al., 1968). Stratigraphically below the Middle Ordovician Kinnikinic Quartzite and Ella Dolomite (redefined by Hobbs et al., 1968) is a thick (>600 m) coarse- to medium-grained feldspathic quartzite, with thin conglomerate lenses and scattered pebbles within the upper two-thirds of the section, which has been redefined as the Clayton Mine Quartzite.

> "The fact that the formation [Clayton Mine Quartzite] lies with apparent conformity below the basal fossil-bearing zone of the Middle Ordovician Ella Dolomite suggests an Early Ordovician age for at least the upper part of the quartzite. However, the contact may be a disconformity representing a hiatus of indefinite duration, and all the quartzite may be older than Ordovician. (Hobbs et al., 1968)"

Hobbs and Hays (1990) demonstrated that the initial correlation of the Ramshorn Slate (Ross, 1937) to the Ordovician Kappa Phi Formation is incorrect. Thus, the only age constraint present in the stratigraphic section of Hobbs et al. (1968) is within the Middle Ordovician Ella Dolomite. The underlying Clayton Mine Quartzite, Ramshorn Slate, Bayhorse Dolomite, and Garden Creek Phyllite may be older than Early Ordovician beneath an unidentified unconformity.

Additionally, a ~650 m thick stratigraphic sequence on Squaw Creek in the Clayton quadrangle was also shown to be erroneously included in the original Kinnikinic Quartzite (Hobbs et al., 1968). This sequence was identified by Hobbs et al. (1968) to consist of a group of very distinctive strata (from bottom to top): (1) a massive, clean, sub-vitreous, unsorted quartzite (Quartzite of Boundary Creek), (2) impure dolomite, impure limestone, fissile siltstone, and flaggy siltstone (lower carbonate of Squaw Creek), (3) a pebbly, relatively pure quartzite (Cash Creek Quartzite), and (4) an overlying thin (<50 m), fossil-bearing shale. The upper shale contains trilobites of unequivocally Early and Middle Cambrian age, suggesting a possible correlation to the Wolsey Shale and Flathead Sandstone of southwestern Montana (Hobbs et al., 1968; Hobbs and Hays, 1990). The remaining stratigraphy lies in apparent conformity beneath the Cash Creek Quartzite, but no additional fossils were found.

The next significant work (Hobbs and Hays, 1990; Hobbs et al., 1991) identified a 215 m thick upper carbonate of Cash Creek in the Squaw Creek section that contains conodonts of Ordovician age, suggesting a possible correlation with the Ella Dolomite. Hobbs and Hays (1990) observed the basal contact of this unit to be a near-planar erosion surface that cuts down section to the south/southwest. West of Squaw Creek, the upper carbonate rests with apparent conformity on Cash Creek Quartzite of Middle or Early Cambrian age and within a thousand feet along strike, on the Middle Cambrian shale that stratigraphically overlies the Cash Creek Quartzite (Hobbs and Hays, 1990). Hobbs and Hays (1990) observed a possible pre-upper carbonate steeply dipping fault that separates the two localities.

> "The relations at both upper carbonate (of Cash Creek) outcrops indicate a situation where the upper carbonate was deposited upon an eroded surface cut across Middle Cambrian strata that had been uplifted, locally faulted, but not notably folded during Late Cambrian or possibly Early Ordovician time (Hobbs and Hays, 1990)".

The accompanying 1:62,500 scale mapping of Hobbs et al., (1991) and subsequent 1:24,000 scale mapping of the Clayton quadrangle by Krohe (2016) does not document this pre- "upper carbonate of Cash Creek" fault. However, Hobbs et al., (1991) and Krohe (2016) do map a clear erosional surface that cuts the Middle Cambrian shale and Cash Creek Quartzite and is overlain by the upper carbonate of Cash Creek. This requires exhumation of both the Middle Cambrian shale and Cash Creek Quartzite prior to upper carbonate of Cash Creek deposition; however, there is an inconsistency on whether this exhumation was fault-influenced or not.

Hobbs and Hays (1990) and the accompanying 1:62,500 scale mapping of Hobbs et al. (1991) split the Paleozoic and older stratigraphy of the Bayhorse region into six “terranes,” or essentially intact stratigraphic packages whose relationship to the other stratigraphic packages was not certain. The packages of interest to this study include: (A) Cambrian and Meso- to Neoproterozoic (?) sequence of quartzite and lesser amounts of siltstone and minor dolomite of the Leaton Gulch area, which crops out primarily in the Challis quadrangle to the north, (B) Middle to Lower Cambrian sequence of Squaw Creek, (C) The Bayhorse anticline, containing a folded sequence (of unknown age but tentatively assigned to Early Ordovician), consisting of the Ramshorn Slate, underlying Bayhorse Dolomite, Garden Creek Phyllite, and basal dolomite of Bayhorse Creek, and (D) A Middle Ordovician sequence (Kinnikinic Quartzite, Ella Dolomite, and Clayton Mine Quartzite). The Clayton Mine Quartzite of sequence (D) was thought to lie in thrust contact over the Ramshorn Slate and underlying units of sequence (C), although locally the contact was also mapped as conformable (Ross, 1937; Hobbs et al., 1968). A large “terrane-bounding” fault was also thought to separate the Middle Ordovician sequence (D) from the Cambrian sequence of Squaw Creek (B). How “terrane A” containing the Cambrian and Meso- to Neoproterozoic (?) sequence of Leaton Gulch fits in the larger stratigraphic framework of the Bayhorse area is not well understood. A simplified diagram of the various proposed stratigraphic arrangements of the Bayhorse region can be seen in figure 2.10.

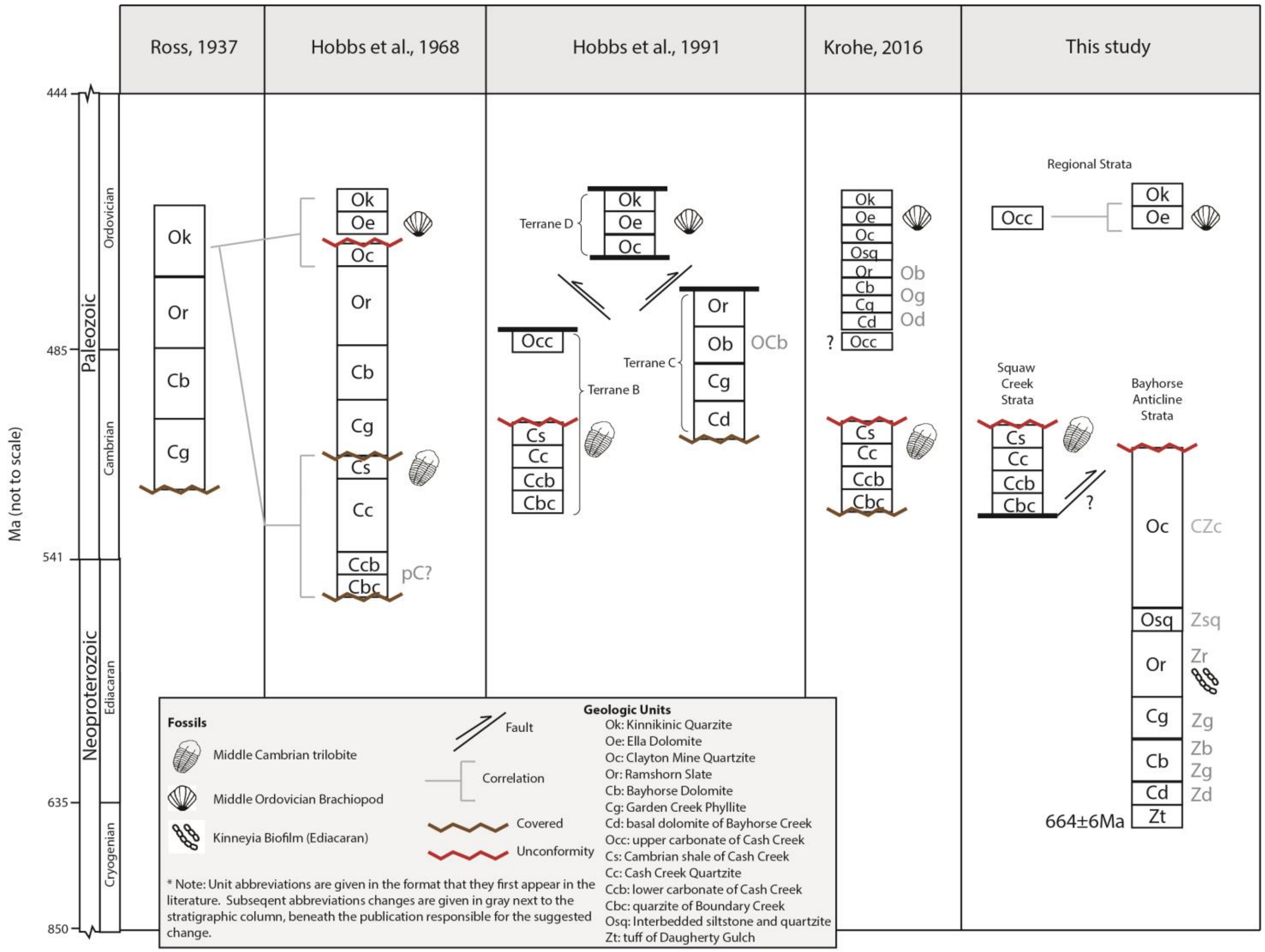

Figure 2.10- The proposed stratigraphic relations of the Ordovician and older stratigraphy of the Bayhorse area as discussed in the text above. For the sake of clarity, Hobbs et al. (1991) shows a simplified diagram omitting the stratigraphy of Leaton Gulch. Note that unit abbreviations are given in the same format as the unit abbreviation appears first in the literature. Subsequent abbreviation changes are given in gray next to the stratigraphic column, beneath the publication responsible for the suggested change. The proposed stratigraphy of this study will be covered at length in the Discussion.

The Lemhi Arch

Approximately 50 km northeast of Bayhorse, in the Lemhi and Beaverhead ranges, Middle Ordovician Kinnikinic Quartzite lies in angular unconformity above Mesoproterozoic Belt Supergroup rocks, forming the Lemhi arch (Scholten, 1957; Ruppel 1986; McCandless, 1982; Link et al., 2017b). The Lemhi arch is a northwest-trending landmass that influenced Neoproterozoic, early Paleozoic, and late Paleozoic to early Mesozoic marine sedimentary patterns across central Idaho and southwestern Montana (Ruppel, 1986; Bush et al., 2012). The Lemhi arch unconformity currently encompasses a poorly defined area approximately 250 km long and 100 km wide (Link et al., 2017b) where Neoproterozoic Windermere Supergroup (and correlative rocks) are missing. Belt Supergroup beneath the Lemhi arch may have experienced minor tilting during the enigmatic "East Kootenay orogeny" of British Columbia (1300-1350 Ma) or the younger "Goat River orogeny" (800-900 Ma) (McMechan and Price, 1982). Late Cambrian exhumation of the arch is better constrained (Link et al., 2017b). Recent mapping in central Idaho suggests that the Lemhi arch is at least partially a rotated fault block stranded within the miogeocline, which is interpreted to account for most of the Proterozoic tilting of Belt Supergroup within the Lemhi arch (Hansen, 2015; Pearson et al., 2016). This fundamental difference during rifting is interpreted to result from previous strengthening of the lower crust during ca. 1370 Ma mafic magmatism (Doughty and Chamberlain, 1996; Hansen, 2015; Pearson et al., 2016).

In some places across this feature, small isolated patches of post-Mesoproterozoic Belt Supergroup, pre-Middle Ordovician Kinnikinic Quartzite, strata are present. These thin isolated strata have been mapped as Lower Ordovician Summerhouse Formation (Ruppel, 1975; McCandless, 1982) as well as Neoproterozoic to Lower Cambrian sandstones of the Lower

Cambrian Tyler Peak Formation (McCandless 1982; Ruppel and Lopez, 1988) and the Lower Cambrian to Neoproterozoic Wilbert Formation (McCandless, 1982; Ruppel 1986, Ruppel and Lopez, 1988, Skipp and Link, 1992). The Summerhouse Formation is composed of pure quartzite, carbonate-cemented sandstone, and carbonate rocks (McCandless, 1982), and underlies the Kinnikinic conformably (McCandless, 1982) or in a slight angular unconformity (Ruppel, 1975). Due to its similar stratigraphic position beneath the Kinnikinic, the Summerhouse has been suggested to be an eastern equivalent of the Ella Dolomite (Hobbs and Hays, 1990; McCandless, 1982). The Lower Cambrian to Neoproterozoic sandstones of the Tyler Peak and Wilbert Formations, where present, unconformably overlie Mesoproterozoic strata and are unconformably overlain by Summerhouse or Kinnikinic (McCandless, 1982). It has been suggested that the Tyler Peak and Wilbert Formations are correlative to the quartzites of the Brigham Group (Skipp and Link, 1992).

Leaton Gulch

Approximately half way between Bayhorse and the Lemhi Range, at Leaton Gulch, isolated Neoproterozoic to Lower Ordovician strata are present (Carr and Link, 1999; Hargraves et al., 2007). At Leaton Gulch, Wilbert Formation overlies Belt Supergroup rocks in an apparent angular unconformity. The Wilbert Formation underlies Lower Ordovician, Summerhouse Formation and Middle Ordovician, Kinnikinic Quartzite in apparent slight angular unconformity (Hargraves et al., 2007).

Several Upper Cambrian feldspathic sandstones deposited across southeast Idaho Montana, and Wyoming contain distinctive 500-490 Ma detrital zircon grains, derived from the Late Cambrian Beaverhead plutons that intrude Belt Supergroup strata of the Lemhi arch. This indicates the Lemhi arch was undergoing active exhumation during Late Cambrian time (Link et al., 2017b). One detrital zircon sample (151PL02, Link et al., 2017b) at Leaton Gulch, from the upper "Wilbert" Formation, contains a large population of these Beaverhead grains. However, the Wilbert name has been used for several isolated beds of post-Belt, pre-Kinnikinic quartzite of likely different ages and correlations (McCandless, 1982; Skipp and Link, 1992).

The occurrence of Middle Ordovician to Neoproterozoic (?) units at Leaton Gulch begs a correlation to the Middle Ordovician and older units exposed ~20 km to the west in the Bayhorse region. Isolated outcrops, similar lithologies, varying age correlations and inconsistent use of formation nomenclature complicates our understanding of these thin, discontinuous Neoproterozoic to Lower Ordovician units. Significant discrepancies also exist between structural and stratigraphic interpretations of Leaton Gulch (Carr and Link, 1999; Hargraves et al., 2007) that require additional attention.

North-Central Idaho Windermere Supergroup

In west-central Idaho, rocks equivalent to the Windermere Supergroup are generally absent or unrecognized. However, metamorphosed Neoproterozoic and Cambrian strata have been found in roof pendants at Big Creek (Lund et al., 2003), in the Sawtooths (Ma et al., 2016), and at Stibnite (Stewart et al., 2017). Although metamorphism has complicated the stratigraphic relationships, the Big Creek and Stibnite composite sections contain two diamictites interlayered with mafic to felsic volcanic rocks, dated at 685 ± 7 Ma and 684 ± 4 Ma, which are overlain by a lower argillaceous/carbonate/dolomitic sequence which, in turn, is overlain by thick siliciclastic units. These have been correlated to the Windermere Supergroup (Lund et al., 2003; Isakson, 2017; Stewart et al., 2017). At Stibnite, only ~410 m of Upper Cambrian and Lower Ordovician strata were mapped (Stewart et al., 2017). Mapping at Edwardsburg did not find any strata above middle Brigham Group equivalents (Lund et al., 2003). Cretaceous-aged metamorphism may obscure the thicknesses at Stibnite and Edwardsburg.

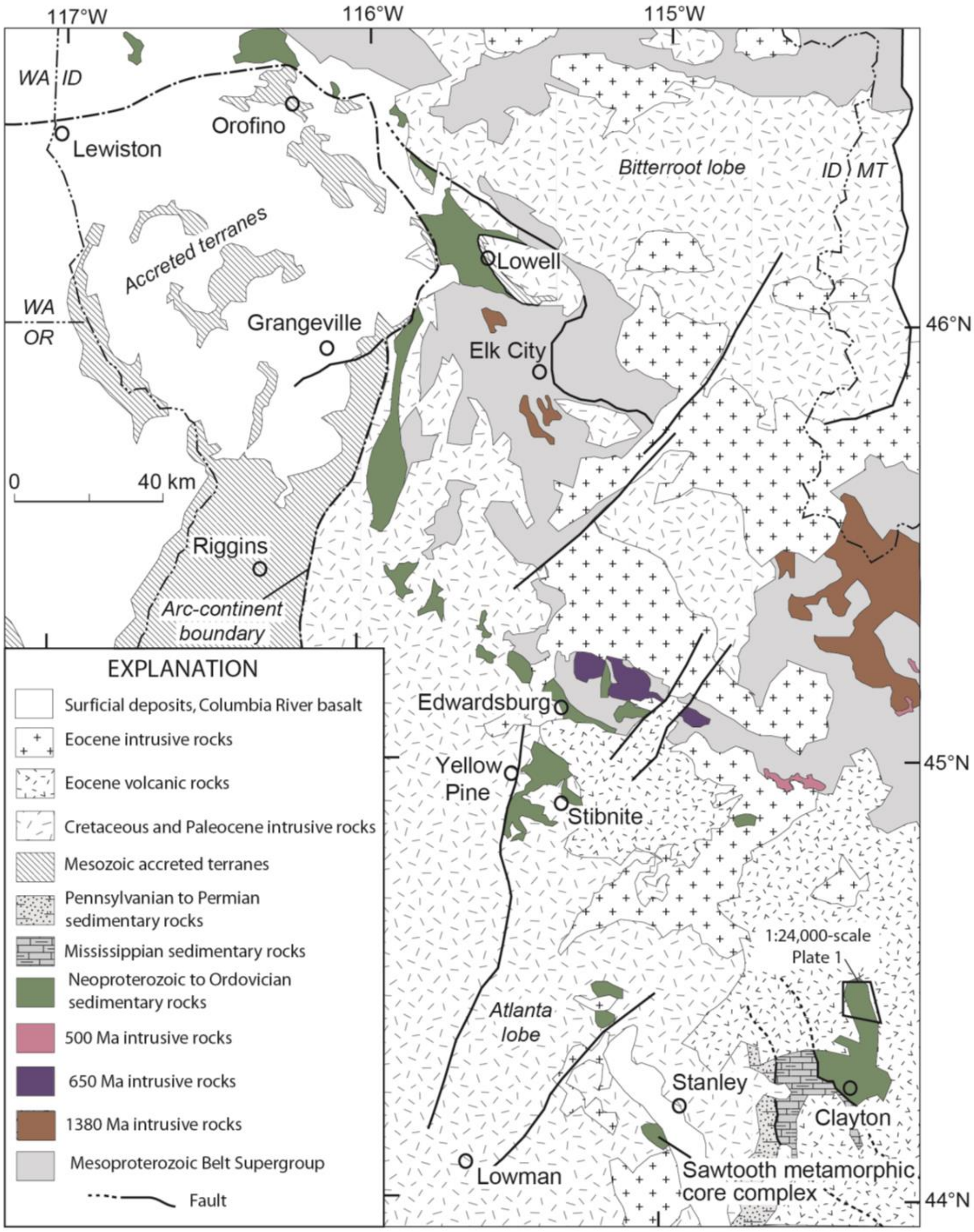

Figure 2.11- Simplified geologic map of central Idaho showing locations for roof pendants of Neoproterozoic to Ordovician sedimentary rocks, intrusive rocks of the ca. 500 Ma Beaverhead (pink), ca. 650 Ma Big Creek (purple), and ca. 1380 Ma Elk City Domain intrusive rocks. Adapted from Isakson, 2017.

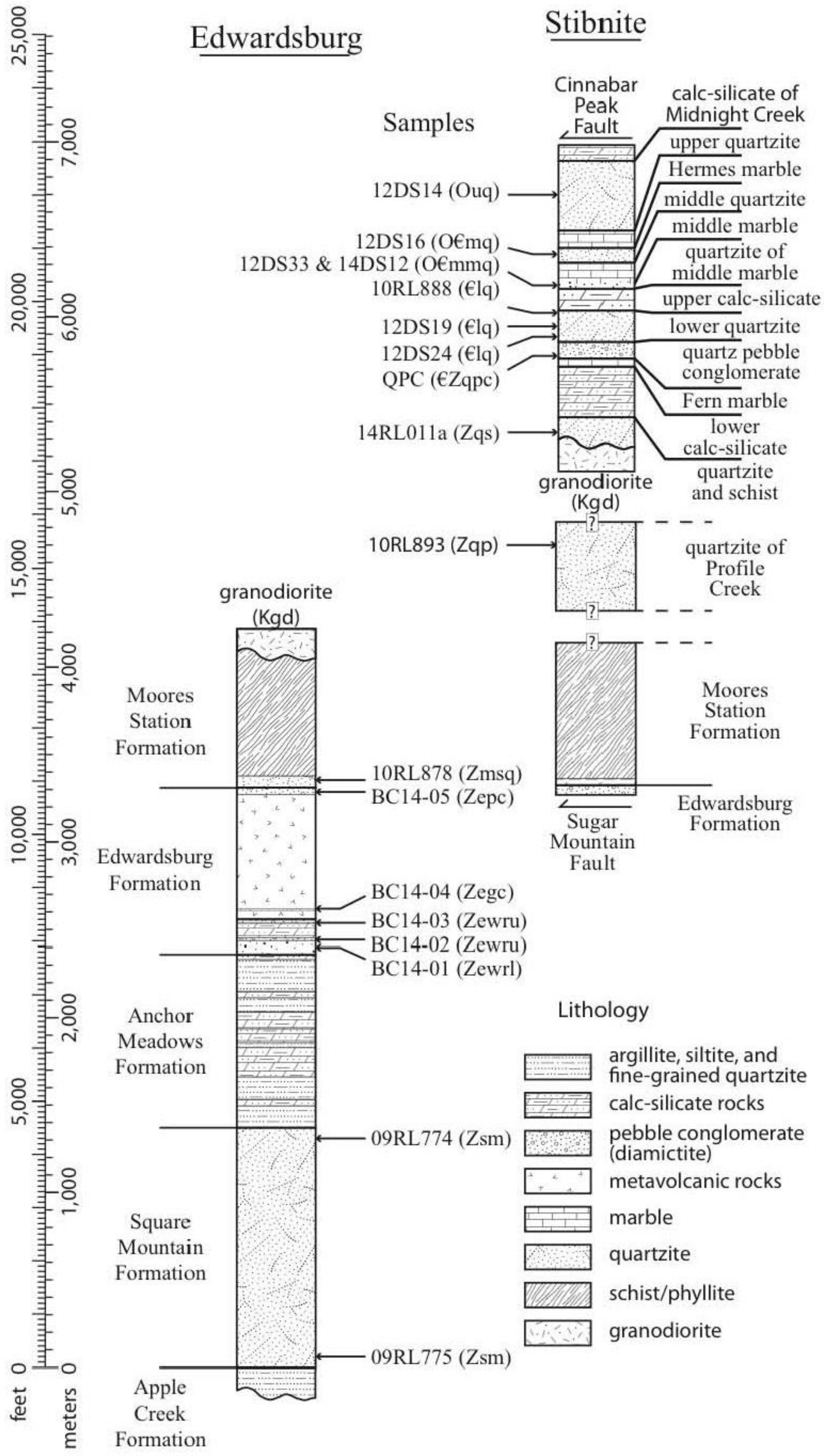

Figure 2.12- Composite stratigraphic sections for Neoproterozoic to Cambrian strata of the Edwardsburg and Stibnite areas (Isakson, 2017).

In central Idaho, three Cyrogenian plutons (Ramey Ridge, Acorn Butte, and Rush Creek Point) compose the Big Creek plutonic suite, and four Ordovician-Cambrian plutons (Yellowjacket, Deep Creek, Arnett Creek, and Beaverhead) compose the Beaverhead plutonic suite (Lund et al., 2010; Link et al., 2017b). The hypabyssal Beaverhead plutons (500-485 Ma) intrude Belt Supergroup and are unconformably overlain by Middle Ordovician Kinnikinic Quartzite; thus the Beaverhead plutons intruded the Lemhi arch (Fig. 2.2; Fig. 2.5; Lund et al., 2010; Link et al., 2017b). The Big Creek plutons (665-650 Ma) also intruded Belt Supergroup (Evans and Zartman, 1988; Lund et al., 2010; Lewis et al., 2012; Link et al., 2017b). However, recent mapping identified Neoproterozoic-Cambrian strata at Edwardsburg and Stibnite (Fig. 5.5; Lund et al., 2010; Stewart et al., 2013; Isakson, 2017; Stewart et al., 2017), indicating that the part of the strata missing across the Lemhi arch is present where the Big Creek plutons crop out, suggesting they did not intrude the Lemhi arch there(Fig. 2.2; Fig 2.5). The mildly bimodal, alkalic nature of the Big Creek and Beaverhead plutons suggests that they originated as lithospheric melts intruded during progressive lithospheric extension (Lund et al., 2010). The Big Creek and Beaverhead plutons are correlated with the initial and final stages of western Laurentian rifting (Yonkee et al., 2014) and have been interpreted to reflect recurrent extension along an inherited structural weakness (Lund et al., 2010).

Daugherty Gulch Borehole

A 3749-foot vertical exploration drill hole near the northeastern extent of the field area (Plate 1) intersected a volcanic unit, located at the bottom of the hole beneath the lower Bayhorse anticline sequence of Hobbs and Hays (1990) terrane C (Jacob, 1990). The hole, on the eastern limb of the Bayhorse anticline, intersected 11 ft of overburden, 488 feet of Bayhorse Dolomite, 2866 feet of Garden Creek Phyllite, 196 feet of Bayhorse Creek Dolomite, and 189 feet of silicic, lithic tuff, in which the hole was terminated. The top of the tuff was interpreted to have been weakly sorted by sedimentary processes and to rest conformably beneath the dolomite (Jacob, 1990).

After an unsuccessful TIMS (Thermal-Ionization Mass Spectrometry) dating attempt, zircons from the tuff of Daugherty Gulch were successfully U-Pb dated using a SHRIMP (Sensitive High-Resolution Ion MicroProbe Mass Spectrometry). Zircons from this tuff are euhedral and blocky. SHRIMP isotopic data from 15 of these zircon grains forms a coherent grouping with an age of 664 ± 6 Ma (Fig. 2.11), which is interpreted to approximate the extrusion date of the tuff (Lund et al., 2010).

Recent chemical abrasion thermal ionization mass spectrometry (CA-IDTIMS) dating of this same tuff yielded concordant a similar weighted mean date of 667.8 ± 0.22 Ma (Isakson, 2017).

Given the Neoproterozoic age, Lund et al. (2010) reinterpreted the rocks in the borehole to be part of a Neoproterozoic section not exposed at the surface in east-central Idaho, in part due to Late Cambrian to Early Ordovician age assignment and mapped structural complexity of the rocks exposed directly adjacent to the borehole in the Bayhorse anticline (Hobbs et al., 1991). Juxtaposition of the Cryogenian tuff (Lund et al., 2010) against significantly younger (allegedly) lower Paleozoic strata (Hobbs et al., 1991) would require major faulting between this drill hole and the adjacent outcrops (Lund et al., 2010). This relationship is testable by detailed field mapping.

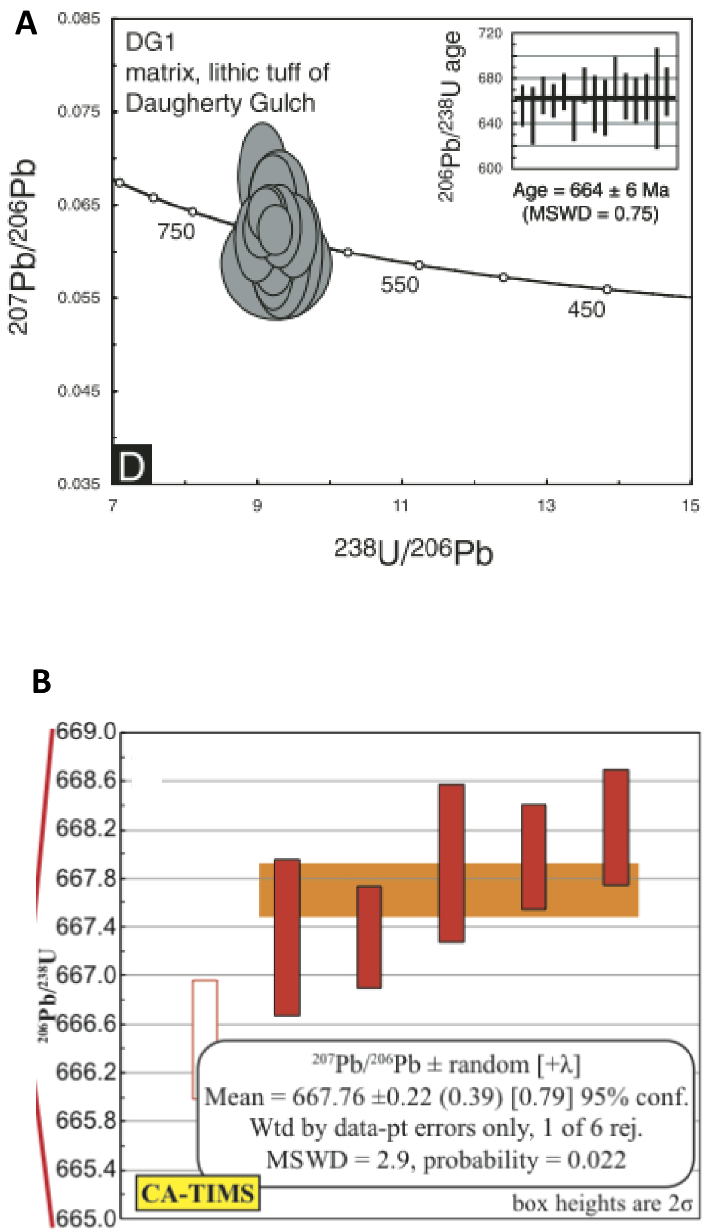

Figure 2.13- (A) Terra-Wasserburg plot of sensitive high-resolution ion microprobe (SHRIMP) U-Pb zircon dates from the tuff of Daugherty Gulch showing an age of 664 ± 6 Ma (Lund et al., 2010). MSWD: mean square of weighted deviates. (B) Ranked 206Pb/238U weighted mean plot for CA-IDTIMS analysis of single zircons from the tuff of Daugherty Gulch showing an age of 667.76 ± .79 Ma (Isakson, 2017).

Recent Mapping of the Clayton Quadrangle

Recent work has attempted to reconcile the issues remaining with the stratigraphy of the Bayhorse region. Mapping of the Clayton quadrangle (Krohe, 2016) suggested that Hobbs' "terrane C" (basal dolomite of Bayhorse Creek, Garden Creek Phyllite, Bayhorse Dolomite, Clayton Mine), is stratigraphically beneath the better dated Middle Ordovician "terrane D" and above Middle Cambrian "terrane B" (Fig. 2.10), making the stratigraphy of "terrane C" Early Ordovician in age. This inference was due in part to what appears to be stratigraphic continuity between the Clayton Mine Quartzite and the Ramshorn Slate, suggesting that Hobbs et al. (1991) were incorrect in their interpretation of a large terrane-bounding fault separating the Middle Ordovician section (of terrane D) and the section without fossil constraints (of terrane C). The result of this proposed stratigraphic correlation is an anonymously thick Lower Ordovician section at Bayhorse when compared to similar aged-strata in southeast Idaho (Fig. 2.12). Also, the dominantly clastic (conglomeratic at certain intervals) lithologies and detrital zircon populations (Krohe, 2016) within this anonymously thick section are not consistent with the carbonate-dominated lithologies of Lower Ordovician stratigraphy along the rest of the Laurentian margin (Yonkee et al., 2014).

Figure 2.14- Generalized map of Neoproterozoic to Early Cambrian strata (gray) along the North American Cordilleran margin. Also shown are the 87Sr/86Sr 0.706 line that approximates the western end of North American Precambrian crust and the eastern front of the Cordilleran thrust belt (adapted from Yonkee et al., 2014). Column of Ordovician stratigraphy in southeast Idaho adapted from the Preston 1:250,000 scale quad (Oriel and Platt, 1980). Column of Ordovician stratigraphy in the Bayhorse region, Idaho, adapted from 1:24,000 scale mapping of the Clayton Quadrangle (Krohe, 2016). Note the drastically greater thickness of the proposed Ordovician strata at Bayhorse as compared to the correlative section in southeast Idaho.

CHAPTER 3: METHODS

Fieldwork

Preliminary field evaluation during fall 2016 was followed by a major field season during the late spring and summer of 2017, with concluding field work during fall 2017. Mapping was conducted using standard geology field-mapping practices. Geologic units, attitudes, contacts, and structures were identified in the field and located on a USGS, 1:24,000-scale topographic map, accompanied with notes in a field notebook. Attitudes were measured using an azimuth Brunton transit compass, set to a 13° east magnetic declination for central Idaho. An Estwing rock hammer and Bausch & Lomb (10x) hand lens were used for field mineral identification. Pervasive pressure solution cleavage commonly obscured bedding in fine-grained units. However, under detailed analysis of fresh rock outcrops, measurable bedding laminations were often visible on two or more oblique faces; cleavage measurements were collected where bedding was not apparent. Emphasis was given to detailed mapping of the strata adjacent to the Daugherty Gulch Borehole, as well as the contact between the Ramshorn Slate and the overlying Clayton Mine Quartzite.

Sampling

Samples for detrital zircon analysis were collected from the Ramshorn Conglomerate, the siltite and quartzite unit that grades upwards into the Clayton Mine Quartzite, and throughout the Clayton Mine Quartzite at strategic stratigraphic intervals to constrain provenance changes within the Ramshorn Slate through Clayton Mine Quartzite (see Appendix A). These samples were collected to test the hypothesis that a significant portion of the Bayhorse section is Ediacaran and correlative to the upper Pocatello Formation and lower Brigham Group of southeastern Idaho instead of Ordovician as previously suggested (Krohe, 2016). Detrital zircon

U-Pb dating by Laser-Ablation Inductively-Coupled Plasma Mass-Spectrometry (LA-ICPMS) was utilized to constrain the provenances and maximum depositional ages of this stratigraphic section. Regionally consistent shifts in sediment transport systems and the resulting patterns in detrital zircon populations have been shown to be a powerful correlation tool along the Neoproterozoic to lower Paleozoic miogeocline of western Laurentia (e.g. Linde, 2014; Yonkee et al., 2014; Link et al., 2017b). Specific detrital zircon age-populations were targeted with Lu-Hf isotope geochemistry to further constrain provenance and magmatic evolution of key source rocks. Samples for analysis were collected in the field and secured in sample bags. Outcrop description, geographic location, lat/long, elevation, and estimated stratigraphic position were recorded.

Sample Preparation

Samples were separated for analysis at Idaho State University and mounted at the University of Arizona LaserChron facility. Individual samples were pulverized using a jaw crusher and disk mill. Zircon concentrate was obtained using standard separation techniques (Wilfley table, Frantz magnetic separator, and methylene iodide). Brennan was responsible for separation of samples DTB17-11 and DTB17-14, and undergraduate research assistant Braedon Warner separated samples DTB17-04, DTB17-05, DTB17-17, DTB17-18, and DTB17-19. Zircon separates were sent to the University of Arizona LaserChron Center, poured onto epoxy mounts to limit picking bias and mounted with U-Pb standards including Sri Lanka, FC-1 and R33 and additional standards Mud Tank, 91500, Temora, FC52, and Plesovice for Hafnium (Hf) analysis. Mounts were sanded to a depth of ~20 microns, polished, Back-scatter electron (BSE) imaged, and cleaned. Mounts that were set up for Hf analysis were also cathodoluminescence (CL) imaged. BSE imaging was used to confirm the minerals we analyzed were zircon and identify strongly zoned grains to exclude in analyses. CL imaging provided a higher level of detail for examination of changes in composition, growth, and mineral quality within individual zircon grains as required for more sensitive Hf analysis.

U-Th-Pb Geochronology

The U-Th-Pb (Uranium-Thorium-Lead) isotopic system (often referred to as the U-Pb system) has been widely applied in dating detrital zircon grains since the 1990s. The U-Pb system is a very powerful isotope system because there are three decay systems with very different half-lives (Fig. 3.1). Zircon is a useful geochronometer because it incorporates measurable levels of parent product during its crystallization and small levels of daughter isotopes, the latter of which can be accounted for in the common Pb correction. Zircon also retains daughter isotopes at high temperatures, essentially “starting the isotopic clock” at crystallization. Additionally, it is long-lived in the sedimentary system and ubiquitous in felsic rocks.

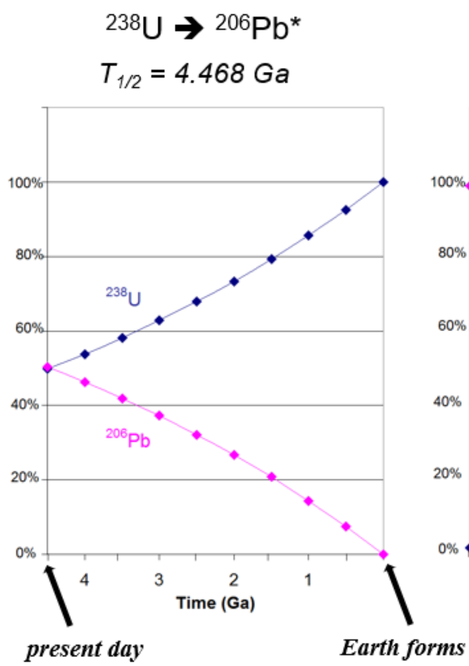

Figure 3.1- The three decay systems in the U-Th-Pb isotope system. The $^{232}Th/^{208}Pb$ system is usually not used for zircon (due to low Th). $^{206}Pb/^{238}U$ change is nearly linear due to the long half-life, making it well-suited to dating grains younger than 1000 Ma. $^{235}U/^{207}Pb$ changed rapidly during the Archean, due to lots of parent ^{235}U and a short half-life, making the 206/207 Pb system valuable for dating grains older than 1000 Ma. (from Gehrels et al., 2017)

The three decay-species allow autonomous confirmation of ages, as the isotope ratios will differ but should give the same calculated age. When interpreting U-Pb ages, it is important to consider that the different decay species have varying precision, depending on the age of the grain. $^{206}Pb/^{238}U$ is very precise for young analyses (< 1400 Ma) while $^{206}Pb/^{207}Pb$ is precise for ages >1400 Ma. However, the cutoff is usually applied at 1000 Ma due to the $^{206}Pb/^{207}Pb$ being more accurate for ages older than 1000 Ma, even though the $^{206}Pb/^{238}U$ age is more precise (Gehrels, 2012). The cutoff for the analyses displayed in this study was set at 900 Ma to avoid "splitting" the Grenville-aged (1.0-1.3 Ma) populations, an approach consistent with Gehrels et al., (2008) and Gehrels (2012). When using the U-Pb system, it is important to remember that ^{235}U is not measured, as very little ^{235}U is usually present, due to the short half-life. However, the ratio of $^{238}U/^{235}U$ is constant ($^{238}U/^{235}U$=137.82). This allows the $^{207}Pb/^{235}U$ ratio to be calculated from the $^{206}Pb/^{238}U$ measurement and the 137.82 ratio following the equation (Gehrels, 2012; Gehrels et al., 2017) (Fig. 3.2).

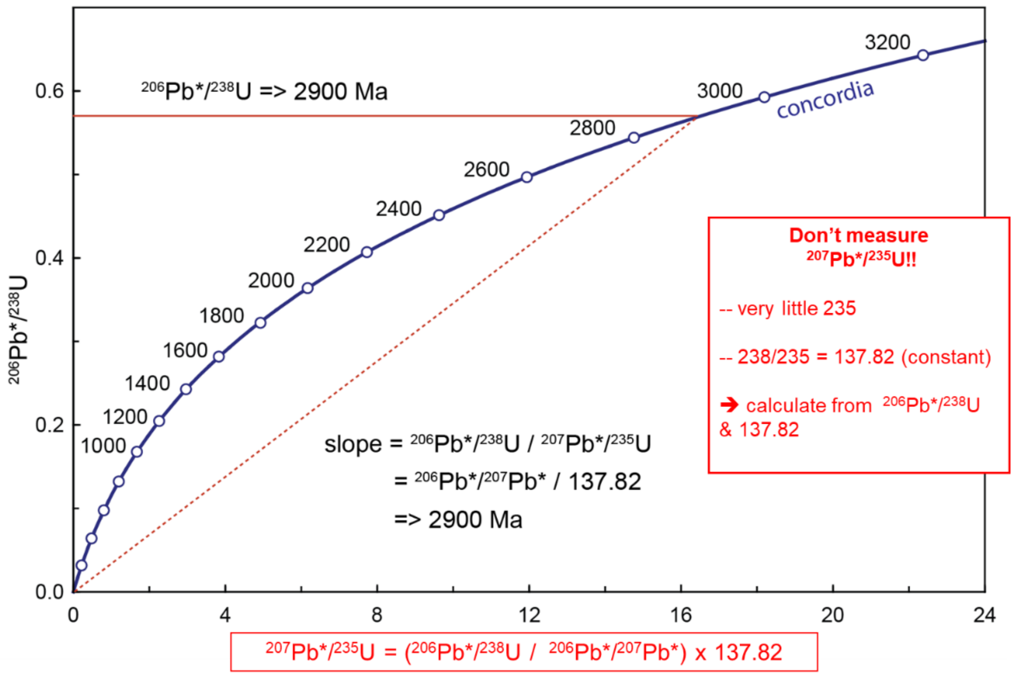

Figure 3.2- A U-Pb concordia diagram. Ages that fall along the blue line, have matching measured ages in both $^{206}Pb/^{238}U$ and $^{207}Pb/^{235}U$ systems. The red boxes outline how ^{235}Pb is calculated from measured $^{206}Pb/^{238}U$ and $^{206}Pb/^{207}Pb$ (from Gehrels et al., 2017).

When the different decay systems give the same age, the date is known as "concordant," and should plot along the concordia line. When the ages differ, these dates are known as "discordant," and the ages are often due to complexities in the U-Pb system, such as Pb loss. Inheritance of older grains, and overgrowths from younger crystallization events can also lead to misleading U-Pb ages.

LA-ICPMS analysis of the unknown zircons was conducted at the Arizona LaserChron Center. Brennan analyzed samples DTB17-04, DTB17-05, DTB17-11, and DTB17-14 in November of 2017, dating 315 unknown grains for each sample. Arizona Laserchron personnel analyzed samples DTB17-17, DTB17-18, and DTB17-19 in January of 2018, dating 110 unknown grains for each sample.

U-Pb isotope analysis involved ablation of zircon with a Photon Machines Analyte G2 excimer laser equipped with a HelEx ablation cell, using a spot diameter of 20 microns. For U-Pb dating, the grains were targeted as randomly as possible, with spots centered on the grain and guided by BSE images. The ablated material was carried via helium gas in to the plasma source of an Element 2 HR ICPMS. Grains were ablated for ~10 seconds, drilling down ~12 microns into the grain. Each analysis consisted of 5 seconds on peaks with the laser off (for backgrounds), 10 seconds with the laser firing, and a 20 second delay to purge the previous sample. Samples were analyzed using standard-sample bracketing procedure followed at 5:1, unknowns to standard ratio. Additional analytical details can be found in Gehrels et al. (2006).

Lu-Hf System

As discussed above, the U-Pb system is effective in determining a crystallization age for a zircon grain, but an additional isotope system holds valuable information about the evolution and history of a zircon grain. The Lu-Hf system relies on the decay of ^{176}Lu (Lutetium) to ^{176}Hf (Hafnium) with a half-life of ~35.7 Ga. All other Hf isotopes are stable. The ratio of interest in this system is ^{176}Hf/^{177}Hf. During mantle partial melting, silicate melts are enriched in Hf but depleted in Lu; zircon is very enriched in Hf. Thus, zircons yield a measurable ^{176}Hf/^{177}Hf ratio that has changed only slightly from the time that Hf was extracted from the mantle. Comparison of the evolution of ^{176}Hf/^{177}Hf in crustal rocks with the evolution of ^{176}Hf/^{177}Hf in the mantle can constrain the time when the crustal rock was extracted from the mantle (Fig. 3.3).

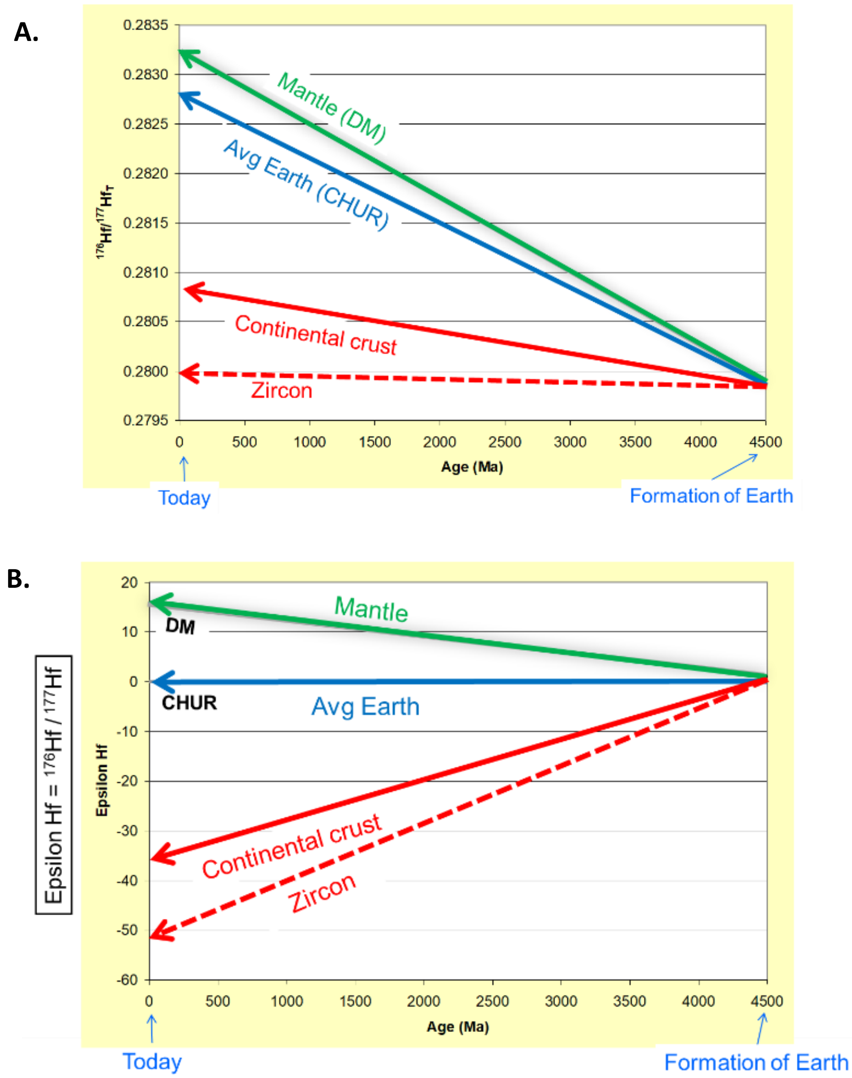

Figure 3.3- Graph A illustrates the $^{176}Hf/^{177}Hf$ evolution of the mantle, average Earth, continental crust, and zircon. Note the $^{176}Hf/^{177}Hf$ evolution in zircon occurs at a much lower rate than the mantle, due to the zircon being enriched in stable ^{177}Hf and having small amounts of parent ^{176}Lu. Graph B shows how this data is usually presented. Essentially the evolution rates are normalized vs. the Chondritic Uniform Reservoir (CHUR) or average Earth. Thus, negative epsilon Hf rocks are considered "evolved" and have older mantle extraction ages and positive epsilon Hf rocks are considered "primitive," with younger extraction ages (Gehrels et al., 2017).

LA-ICPMS Analysis

Hf isotope analyses were conducted with a Nu High-Resolution multi-collector Inductively Coupled Plasma Mass Spectrometer (HR ICPMS) connected to a Photon Machines Analyte G2 excimer laser. Instrument settings were established via calibration with a known solution, followed by analysis of seven different standards (Mud Tank, 91500, Temora, R33, FC52, Plesovice, and Sri Lanka). When the precision and accuracy were acceptable, unknowns were analyzed using the same parameters. Laser ablation analyses were conducted using a larger spot diameter of 40 microns, located on top of the U-Pb analysis pits. Grains with approximately 650 Ma and 1370 Ma U-Pb ages were targeted. Each analysis consisted of one 40-second background integration (no laser firing) followed by 60 one-second integrations with the laser firing. Each standard (all seven) was analyzed once for every 20 unknowns (Gehrels et al., 2006; 2008).

Data Analysis

Following analysis, data reduction was performed by lab personnel with an Arizona Laserchron python decoding routine and an Excel spreadsheet (E2agecalc). Isoplot, a Microsoft Excel "add-in" program was used for generating normalized probability density plots (Ludwig, 2008). These plots were produced by normalizing each curve by the number of constituent analyses so that they all contain the same area, allowing analyses of different number of grains to be visually compared. A maximum discordance filter of 20% for normal discordance and 5% for negative discordance was applied, as our study benefited more from identifying the presence and absence of broad age populations rather than narrowing in on precise ages within those peaks. The age picks of population peaks were evaluated using the Microsoft excel "add-in" Age Pick (available at https://sites.google.com/a/laserchron.org/laserchron/). Age Pick defines a peak as a maximum in age-probability that comprises age-probability contributions (at 2□) from 3 or more analyses. Maximum depositional ages (MDA) were calculated using the youngest cluster of (n≥2) of grain ages that overlap in age at 1□, which has been shown to be a reliable measure of the youngest age (Dickinson and Gehrels, 2009). However, in Neoproterozoic and lower Paleozoic Cordilleran rocks, detrital zircon MDA is often a poor constraint on true depositional age due to a relative lack of constant magmatic sources during this time interval (Yonkee et al., 2014, Link et al., 2017b).

Results of the detrital zircon U-Pb analyses are shown in Probablity Density Plots (PDPs). These plots have long been the most widespread method for visualizing detrital age distributions. PDPs are calculated by summing a number of Gaussian distributions whose means and standard deviations correspond to the individual ages and their respective analytical uncertanities (Ludwig, 2003). Issues have been raised with this method of visualizing detrital age distributions (Vermeesch, 2012). Specifically, the PDP is produced by stacking a normal distribution on top of each measurement whose bandwith is determined by the analytical precision, which can result in over-emphasizing precise measurements. The alternative visualization method proposed by Vermeesh (2012) is the Kernel Density Estimator (KDE). This method produces a similar looking result, and also relies on stacking normal distributions but rather than varying the width by analytical precision, the width is varied according to local density (Vermeesch, 2012). Where lots of data are available, a narrower bandwitch is used, allowing the KDE to provide a high resolution estimate in those parts of the distribution and smooth the plot in areas where data density is sparse. While this new method has been successfully applied, we chose to present our data as PDPs as it presents more consistent comparision to previously published datasets that rely primarily on PDPs. Corresponding KDE plots to the PDPs seen in this section can be found in Appendix D.

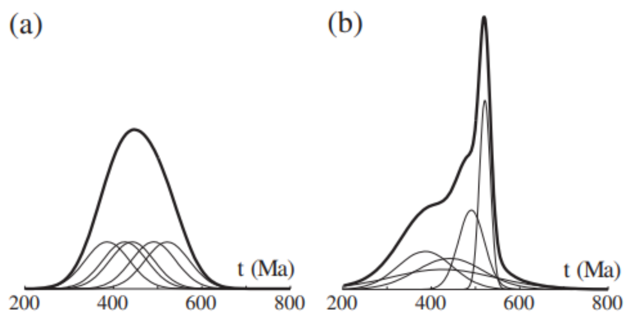

Figure 3.4- (a) The 'Kernel Density Estimator' showing stacked Gaussian curves on top of each measurement whose standard deviation determined by the local probability density. (b) The 'Probability Density Plot' also stacks a Gaussian curve on top of top of each measurement, but whose standard deviation is determined by the analytical precision (Vermeesch, 2012).

Multidimensional scaling (MDS) was used to aid in visualizing the statistical differences among the large number of samples included in this study. MDS also allowed for more objective grouping of similar detrital zircon populations than the standard method of visual comparison of PDP's. In this study (following the methodology of Matthews et al., 2018), the maximum difference between the cumulative probability density functions for each pair of samples—the D statistic of the Kolmogorov-Smirnov test—is used to quantify the dissimilarity of the samples. The D statistic is measured between each pair of samples to create a matrix of dissimilarity. The MDS approach then plots the samples on a Euclidean plane while attempting to honor the differences between samples in the dissimilarity matrix. As such, the distance between samples in the MDS plot is roughly equal to the dissimilarity between the samples based on the D statistic, and samples containing similar detrital zircon populations will plot in the same region. The addition of normally distributed unimodal synthetic populations has been shown to aid in visualizing the differences between samples on an MDS plot (Spencer and Kirkland, 2016). Synthetic populations were generated using Excel's (2016) NORMINV function, which generates a normally distributed dataset with a set standard deviation. Standard deviations were estimated from published data to create a representative synthetic population.

Free DZ Stats software (Saylor and Sundell, 2016), available at http://easd.geosc.uh.edu/saylor/dzstats.php, was utilized for this analysis. See Vermeesch (2013) and Saylor and Sundell (2016) for further discussion on comparing large detrital chronology datasets.

Subsidence Modeling

Generalized tectonic subsidence curves were generated for the Ordovician and older strata at Bayhorse, and the correlative section in the Bannock Range, southeast Idaho. Subsidence was calculated using BasinMod software developed by Platte River Associates, Inc. (www.platte.com/software/basinmod -2012.html). The software takes input for geologic age (top of the unit), thickness, lithology, and general depositional environment. This allows calculation of water depth and compaction. Compaction was calculated using the Statoil fluid flow porosity reduction method: $\Phi = \phi 0 \times \exp(-C \times Seff)$: ϕ = calculated porosity; $\Phi 0$ = initial porosity; C = Statoil compaction exponent; and Seff = effective stress.

Thin Sections

Thin section billets were sent to Wagner Petrographic for thin section preparation. Samples were cut to a standard 30-micron thickness and mounted on 24 by 46 mm slides. Carbonate slides were stained for calcite, and clastic slides were stained for potassium feldspar. Petrographic thin section analysis was conducted using a Nikon Optishot-Pol at Idaho State University's Microscope lab. A two-axis "stepping-stage" was used for (n=300) point counts of sandstones (see Appendix A). Polycrystalline quartz was counted as a lithic, thus compositions were plotted on the appropriate QmFLt diagram (monocrystalline Quartz, Feldspar, total Lithics; Dickinson et al., 1983). Thin section photomicrographs can be found in Appendix B.

Map Production

The 1:24,000 scale geologic map of the northern Bayhorse region (Plate 1) was digitized from georeferenced, scanned office maps using ArcMap 10.5 in Idaho State University's Digital Mapping Lab. Cross sections were digitized in Adobe Illustrator CS6 from 1:24,000 scale, hand-drawn and scanned illustrations. Structural analysis was conducted using Allmendinger's Stereonet 10 (http://www.geo.cornell.edu/geology/faculty/RWA/programs/stereonet.html). Isoplot 4.15 was utilized for geochronologic data presentation. Map elements were combined in Adobe Illustrator CS6 for final formatting.

CHAPTER 4: RESULTS

1:24,000-scale geologic mapping and structural analysis of a region within the Bayhorse and Bayhorse Lake 7.5-minute quadrangles southwest of Challis, central Idaho refined 1:62,500-scale geologic mapping from Hobbs et al., (1991), constrained the structural context of the Daugherty Gulch borehole, and evaluated the critical contact between the Clayton Mine Quartzite and Ramshorn Slate. Additionally, several detrital zircon samples were analyzed from key stratigraphic intervals and compared to previous detrital zircon results from southeast and central Idaho (Yonkee et al., 2014; Link et al., 2017b; and references therein). As discussed in the Geologic Background, previous mapping (Hobbs et al., 1991) designated the rocks as Late Cambrian to Middle Ordovician in age, due in part to a miscorrelation with outcrops of the Ordovician Phi Kappa Formation.

Geologic Units

Thin section point counts and photomicrographs can be found in Appendix B and C.

Neoproterozoic to Lower Paleozoic strata

Basal Dolomite of Bayhorse Creek (Neoproterozoic)- Light to medium gray, weathers grayish orange to brown, thin to medium tabular bedded, sandy dolomicritic mudstone. A maximum of the upper 20 m is exposed along Bayhorse Creek near center of the Bayhorse anticline. True interpreted thickness is approximately 50 m in the Daugherty Gulch drill hole. Lower contact is thought to be in apparent depositional conformity with the 667.76 ± 0.22 (Isakson, 2017) Ma tuff of Daugherty Gulch.

Garden Creek Phyllite (Neoproterozoic)- Dark gray to nearly black, slightly calcareous phyllite. Weathers to thin, smooth, flakes and chips, breaking often along irregular, wavy bedding planes. Otherwise, bedding is indistinct. Unit is poorly exposed except where deeply eroded by Garden and Bayhorse creeks. Exposures with southern aspect often do not sustain conifer growth. Overlies in apparent conformity the basal dolomite of Bayhorse Creek. Estimated thickness of approximately 500 meters.

Bayhorse Dolomite (Neoproterozoic)- Approximately 375 meter thick unit consisting of gray to tan/orange, primarily dolo-micritic mudstone (Fig. 4.1). Locally contains thin chert nodules, sometimes as localized (~3 cm) thick beds, dark gray silicified chert lithic (pisolite?) grainstone beds, and rare fine-grained sandy laminations that infrequently show cross-stratification. Stratigraphically lower portions show thin tabular bedding, stratigraphically higher levels show less defined bedding except for an interval of dark gray/brown laminated siltstone and argillite (~15 m) interval. Contains poorly defined stromatolitic bioherms, calcite veins (often as en echelon tension gashes), and localized cross laminations. Dolostone is heavily brecciated along faults and near the upper contact with Ramshorn Slate. Breccia ranges up to ~20 cm in diameter and is commonly supported in a dark red or gray siliceous matrix. Abundant fluorite mineralization is common where faulted and brecciated. Brecciated horizons are likely pipe breccias associated with Cenozoic volcanism or an irregular paleokarst surface. Overlies Garden Creek Phyllite in apparent ~10 m gradational contact.

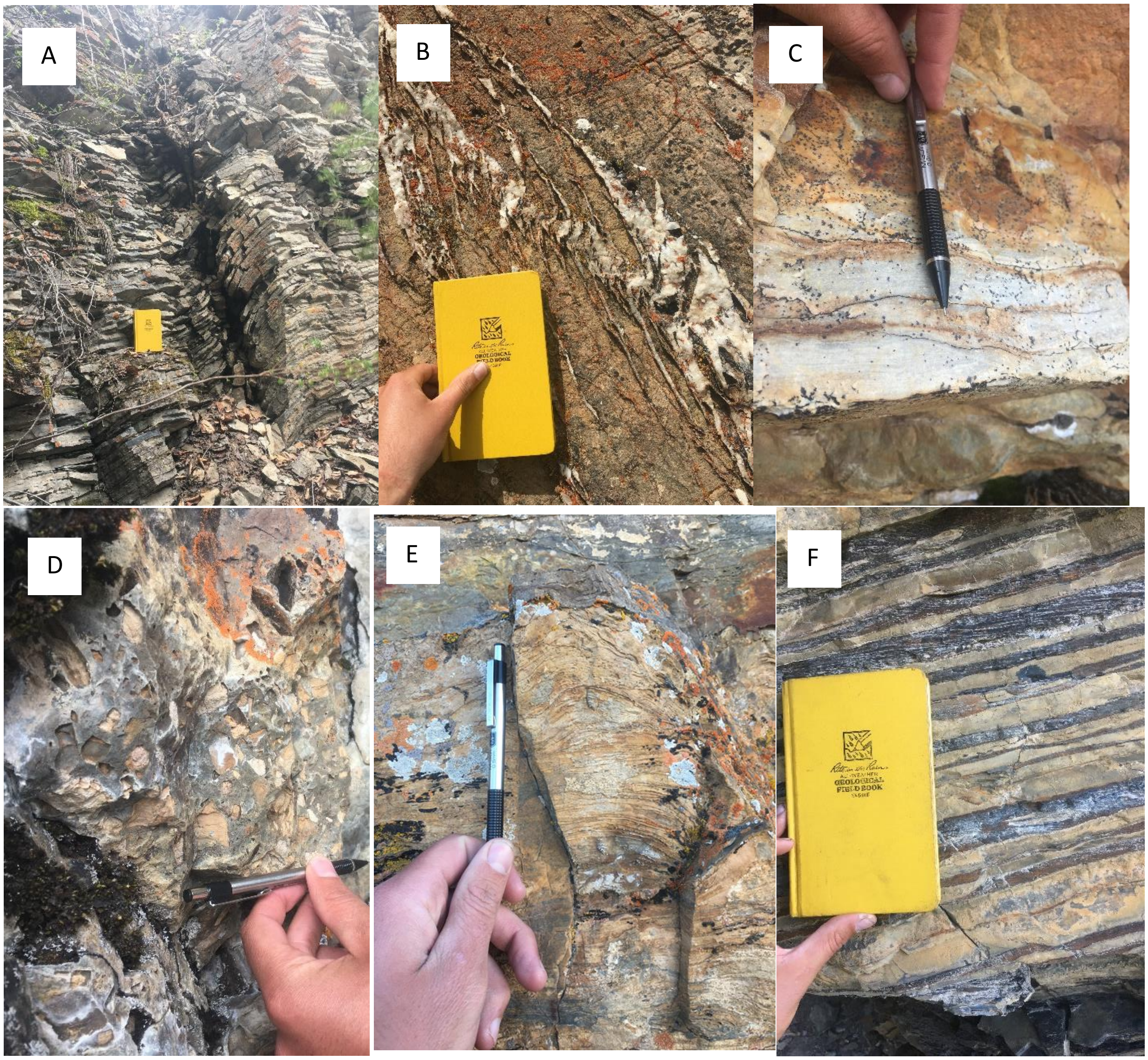

Figure 4.1- Bayhorse Dolomite outcrops showing (A) thin tabular bedding, (B) quartz-filled en echelon veins, (C) cross laminae, (D) breccia in siliceous matrix, (E) stromatolitic bioherms, and (F) banded calc-silicate hornfels where metamorphosed by Juliette stock. Field book is approximately 12 by 18.5 cm, pencil is approximately 14 cm.

Ramshorn Slate (Neoproterozoic)- Approximately 650 meter thick unit of medium gray to blueish gray to olive green to reddish brown, fine-grained, medium-laminated to fine bedded, slate with a subtle sheen, showing localized foliation and crenulation (Fig. 4.2). Often displays Leisegang banding. Where present, the Ramshorn Conglomerate may overlie the Bayhorse Dolomite in a slight erosional unconformity, which is suggested by thinned Bayhorse Dolomite.

Pervasively cleaved at high angles to bedding with lesser amounts of pencil cleavage. Breaks along cleavage except where slightly coarser grained to very fine sand. Often exhibits cyclic (~1 cm) thick, normally-graded laminations indicative of fine-grained turbidite deposition with a noticeable lack of bioturbation. Flute cast swarms are abundant near contact with incised Ramshorn Conglomerate. Locally contact-metamorphosed to hornfels near the Juliette stock, with muscovite and andalusite visible. Chiastolite/andalusite is often weathered out, leaving lath-like depressions. Appears to overlie Bayhorse Dolomite in apparent conformity.

Ramshorn Conglomerate (Neoproterozoic)- Reddish pink, well-rounded, poorly sorted, matrix-supported, coarse to medium pebbles in a fine sand matrix, vein quartz conglomerate (Fig. 4.2) with rare clasts of red jaspilite, and sandstone/siltstone pebbles (likely intrabasinal). Laterally interfingers with reddish brown, coarse-grained, well-rounded, moderately sorted, quartz arenite and medium grey, fine bedded, slate with abundant flute casts. Contains unusual, tight parallel wrinkle marks in mudstone facies interpreted as Kinneyia which may represent a microbial biofilm (see Hagadorn and Bottjer, 1997). Genesis and preservation of these structures will be covered in the Discussion. This unit is likely a submarine canyon deposit. Appears to interfinger with Ramshorn Slate, and potentially be deposited into a paleochannel cut into the Bayhorse Dolomite. Maximum thickness of approximately 200 meters.

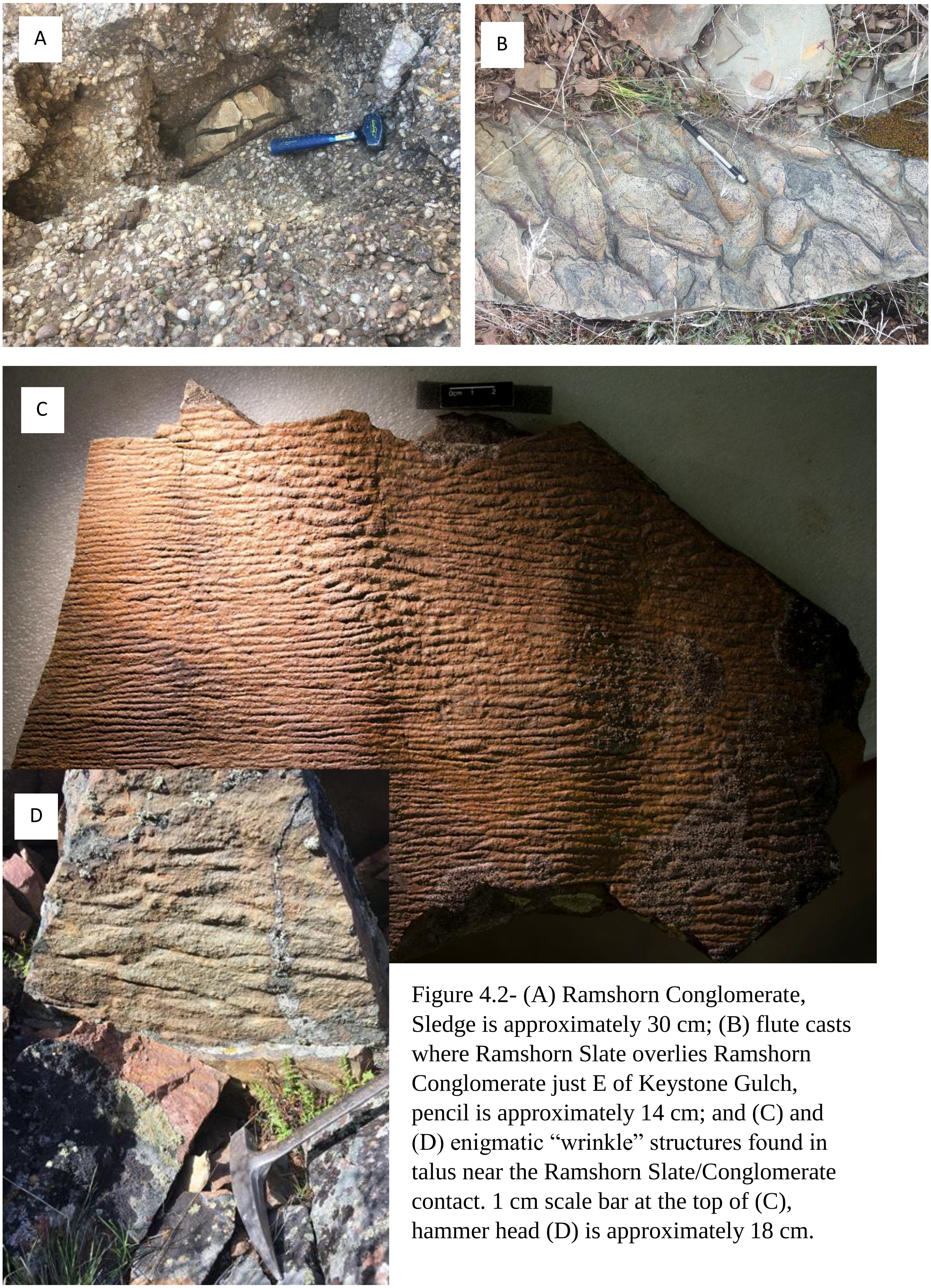

Figure 4.2- (A) Ramshorn Conglomerate, Sledge is approximately 30 cm; (B) flute casts where Ramshorn Slate overlies Ramshorn Conglomerate just E of Keystone Gulch, pencil is approximately 14 cm; and (C) and (D) enigmatic “wrinkle” structures found in talus near the Ramshorn Slate/Conglomerate contact. 1 cm scale bar at the top of (C), hammer head (D) is approximately 18 cm.

Interbedded Siltite and Quartzite (Neoproterozoic)- Approximately 250-meter thick unit showing cyclically interbedded mudstone and sandstone consistent with a gradational contact between Ramshorn Slate and Clayton Mine Quartzite. Primarily medium- to coarse-grained, subfeldspathic arenite with finer beds containing more detrital feldspar and muscovite. Quartzite is interbedded with meter-scale (3-4 m), thick laminated siltstone. One distinct bed of orange to fresh gray, locally oolitic, dolomite with laminations of distinct scattered subangular coarse quartz sand to fine pebbles is present.

Clayton Mine Quartzite (Neoproterozoic to Cambrian)- Over 800 m of dominantly quartzitic rocks that are heterogenous in color, degree of sorting, and bedding (Fig. 4.3). Formation ranges from orange, well-sorted, medium-grained quartz sandstone with variable feldspar content to reddish purple, matrix supported pebble conglomerate, to clean quartz arenite. The lower Clayton Mine unit is dominantly tightly quartz-cemented, medium to thick tabular cross stratified, feldspathic arenite with distinct thin, shiny green silt interlaminations on top of bedding planes. Locally small (<2 cm in diameter) reduction spots are abundant. The unit is interpreted to record variable fluvial and shallow marine deposition and likely contains one or more undocumented unconformities. Within this mapping area (Plate 1) the upper contact is covered by Tertiary volcanic rocks and/or faulted. To the south in Clayton Quadrangle, the Middle Ordovician Ella Dolomite overlies the Clayton Mine Quartzite. Recently this contact has been considered likely conformable (Krohe, 2016), however previous work acknowledges that this contact could be either a disconformity or low-angle unconformity (Hobbs et al., 1968; Hobbs and Hays, 1990).

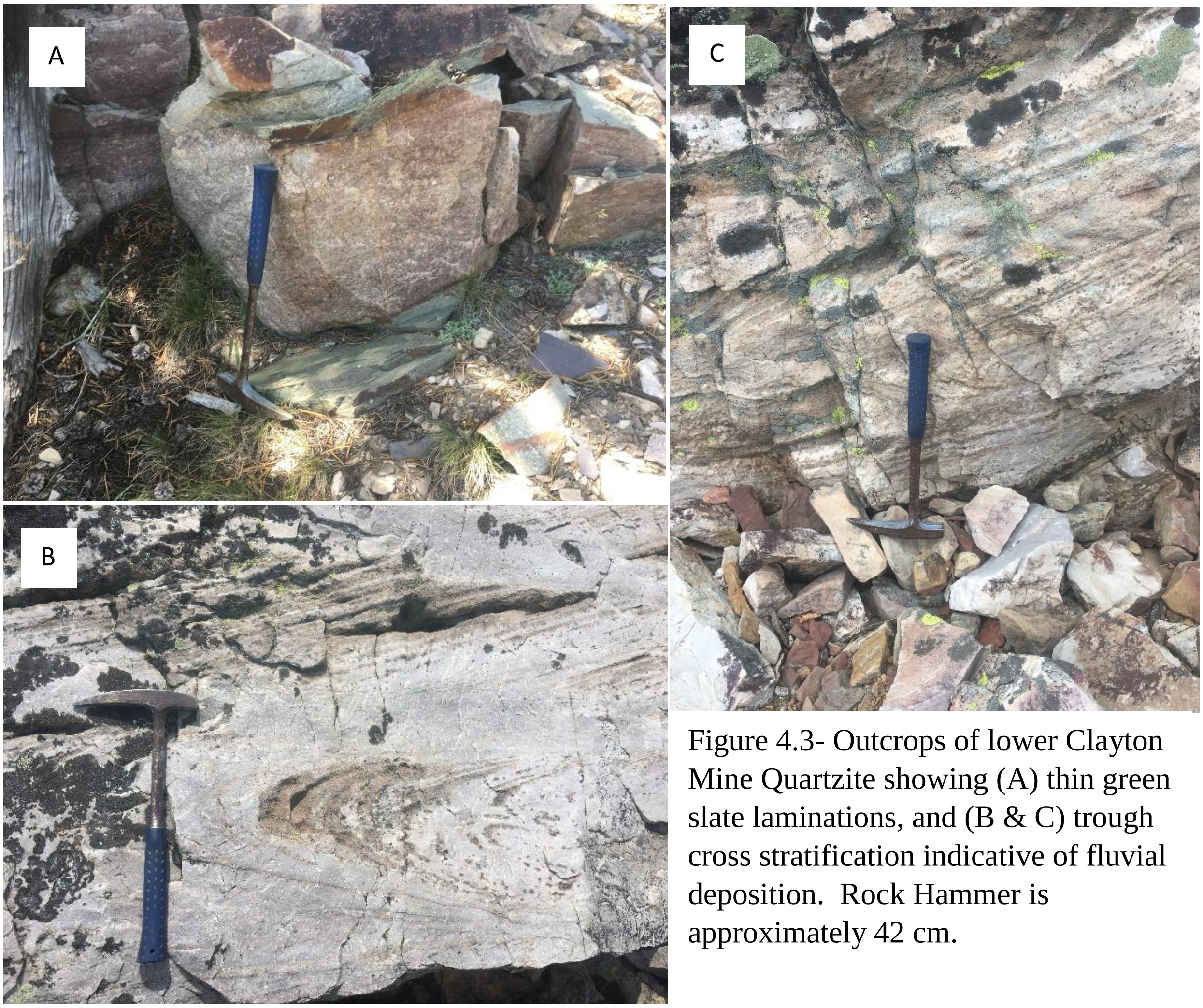

Figure 4.3- Outcrops of lower Clayton Mine Quartzite showing (A) thin green slate laminations, and (B & C) trough cross stratification indicative of fluvial deposition. Rock Hammer is approximately 42 cm.

Intrusive Rocks

Gabbro (Neoproterozoic?)- Grayish green, amphibole, clinopyroxene (augite?) gabbro found as 10 to 100-meter scale sill-like bodies near the stratigraphic contact between Ramshorn Slate and Interbedded siltite and quartzite. Contains phenocrysts of amphibole, plagioclase, and clinopyroxene and accessory pyrite generally < 2 mm in length in a fine-grained groundmass showing chlorite and epidote alteration. Locally shows an inflation/bedding shift above the gabbro interpreted to indicate laccolithic intrusion. Fission track date from an immediately adjacent quartzite revealed an annealing age of 140.1 ± 17.4 Ma (R.A. Zimmerman, written commun., 1983 in Hobbs et al., 1991). Our attempts to separate baddeleyite and zircon for U-Pb analysis were not successful. Mafic sills within a correlative stratigraphic interval in Utah are undated, but generally considered to record waning stages of Neoproterozoic rift-related igneous activity (Crittenden, 1988; Yonkee et al., 2014). Thus, I interpret that a Neoproterozoic age is more likely and the Jurassic fission track age likely records annealing due to burial. A relation to the 650-665 Ma plutonism ~100 km to the north at Big Creek is alluring but unproven.

Juliette Stock (Cretaceous)- Gray to pink, equigranular moderately coarse-grained, granite to quartz monzonite, with secondary muscovite. K-Ar age of biotite from main stock is 98.1 ± 3.3 Ma (McIntyre et al., 1976) and U-Pb age of zircon from main stock is dated 96.9 ± 0.9 Ma (Krohe, 2016), falling within the magmatic age range of the Atlanta lobe of the Idaho batholith (Gaschnig et al., 2010). Where in contact with the Ramshorn Slate, mica- and andalusite-rich contact aureoles are present. Zircons yielded εHf value of -5.7 to -13.9 (Krohe, 2016).

Challis Volcanic Group

Potassium-rich Basalt and Andesite (Eocene)- Orange to very dark-gray/black when fresh, basalt lava. ~3% (< 2mm) bottle-green olivine in a dark aphanitic groundmass. Occurs as a discrete local accumulation along the western margin of the mapping area. Likely less than 150 m thick. Potassium-argon age is 50.3 ± 1.5 Ma (Armstrong, 1975b).

Lithic Tuff (Eocene)- Light-orange to greenish-beige, un-welded, matrix-supported, volcanic lithic tuff. Contains angular volcanic clasts ranging in size from fine pebbles to small cobbles. Surrounded by an aphanitic (ashy?), matrix. Partially reworked by sedimentary processes.

Tertiary Dacite (Eocene)- Orange to light-gray sometimes altered to teal or bright-red, dacite lava. Contains variable phenocrysts assemblages but is primarily (< 20%) plagioclase (~5 mm) and (< 7%) hornblende (~2 mm) in an aphanitic groundmass. Full thickness is not exposed but estimated to be less than 600 m (Hobbs and Hays, 1991). Potassium-argon age is 49.3 ± 1.4 Ma (Armstrong, 1975b). Locally appears to overlie some thin flows of basalt.

Buster Lake Breccia (Eocene)- Reddish-orange, weathers to brown, well-cemented, pumaceous, breccia. Contains pumaceous lava fragments (<5 cm) as well as grayish-purple (mafic?) fragments.

Sedimentary Deposits

Glacial (Pleistocene)- Unsorted to poorly sorted cobbles, gravel, boulders in a clayey matrix, often poorly drained with thick soil accumulation. Located near and above Bayhorse and Little Bayhorse Lake.

Diamicton (Quaternary)- Unsorted terrigenous sediment, ranging in size from clay to boulders in an organic rich soil matrix. Often poorly drained. Possibly of periglacial origin but not conclusive.

Protalus Rampart (Quaternary)- Locally-derived, distinct ramparts of unsorted angular cobbles and boulders that accumulated at the toes of Clayton Mine Quartzite cliffs and talus fields. Likely of periglacial origin.

Lacustrine (Quaternary)- Very well-sorted, unlithified sediment, with thinly laminated beds of silt and clay. Located in seasonally inundated low-lying areas surrounding Bayhorse and Little Bayhorse Lake.

Talus (Quaternary)- Locally-derived loose masses of angular rock cobbles and boulders that mantle slopes of moderate angle. Primarily restricted to slopes below cliffs of Ramshorn Slate or Clayton Mine Quartzite.

Landslide (Quaternary)- Angular to subangular and poorly sorted, silt to boulder-sized debris. Formed by slope failure and characterized by a hummocky surface, with the main scarp commonly identifiable. Vegetated soil overburden is often present near the toe of the landslide. Common in heavily cleaved Ramshorn Slate.

Alluvium (Quaternary)- Silt, sand, pebbles, and cobbles associated with drainage systems of Daugherty Gulch, Garden Creek, and Bayhorse Creek (Fig. 4.4). May include terrace deposits along Garden Creek. Clasts are generally rounded and show crude stratification, sorting, and imbrication.

Figure 4.4- Alluvial deposit exposed on the north side of Bayhorse Creek along road approximately 1.5 km east of Bayhorse State Park entrance. Field book is approximately 12 by 18.5 cm

Structural Analysis

Overall, the map area (Plate 1) consists of a north to south-trending anticline of a slightly metamorphosed, yet intact, >2.5 km thick stratigraphic section consisting of a lower argillaceous and dolomitic sequence that is overlain by quartzite. Trending approximately perpendicular to the fold axis, three significant (E-W) drainages have incised into the section, exposing the stratigraphically lower units. Several north-trending, smaller amplitude folds were also recognized west of the main Bayhorse anticline. A series of N-S to SE-NW striking faults, with primarily normal offset, cross cut the older folds. Along these faults, syn-kinematic mineralization and a lack of noticeable offset on Quaternary features was observed.

The only significant thrust fault recognized by Hobbs et al., (1991) was reinterpreted as a gradational stratigraphic contact. Within the mapping area, along the eastern extent of Garden Creek, a shallowly east-dipping normal fault is interpreted to duplicate steeper dipping strata along the eastern limb of the Bayhorse anticline. Approximately 1 mile west, up Garden Creek, a west-dipping normal fault along the Ramshorn Slate/Bayhorse Dolomite contact resulted in the formation of a roll-over anticline within the Ramshorn Slate; this fault can be traced to the south in the Bayhorse Creek, a small roll-over anticline is also present. Another east-dipping fault runs approximately north-south through the ghost town of Bayhorse and exposes large Bayhorse Dolomite cliffs to the east that are also folded into a gentle anticline.

The older sedimentary sequence is covered to the east and west by extrusive, primarily dacitic to andesitic lava and tuffs. Previous interpretations (Hobbs and Hays, 1990) involved normal faults along the edges of the Bayhorse anticline to account for the relatively straight line contact between the Bayhorse anticline and these younger volcanic deposits. Potentially these volcanic rocks were deposited against a scarp of these inferred faults (Hobbs and Hays, 1990).

A granitic stock (U-Pb age 92.92±0.85 Ma) with a recognizable contact aureole intrudes the southern extent of the field area.

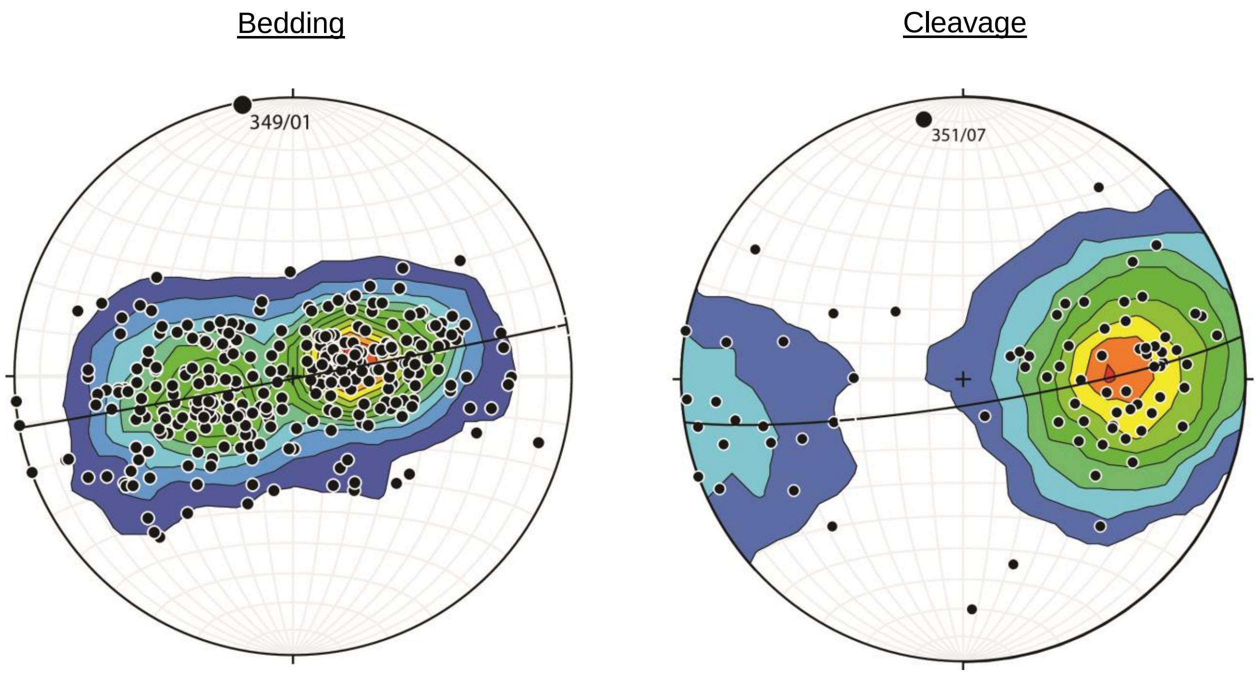

Figure 4.5- Stereonet diagrams (http://www.geo.cornell.edu/geology/faculty/RWA/programs/stereonet.html) of attitudes measured from the Bayhorse anticline. On the left are the bedding measurements, and on the right, are cleavage measurements. The poles to the planes were plotted and a cylindrical best fit was applied to the poles. The pole of this best fit great circle is the fold axis (labeled 3). For bedding, the fold axis was calculated to be 349/01 RHR, and for the cleavages, it was calculated to be 351/07 RHR. This is interpreted to suggest that the bedding and cleavages are folded around the same fold axis

Structural relations around large-scale folds constrain timing relations of internal strain relative to folding (Weil and Yonkee, 2012). One mechanism of internal strain accommodation is pressure solution cleavage, which accommodates shortening through the dissolution of grains at the grain to grain contact boundary and reprecipitation in the pressure shadow, this results in pervasive fabrics that form in planes perpendicular to □1. Often this cleavage fabric forms during folding, and the cleavage planes will parallel the axial plane of the fold (Van der Pluijm and Marshak, 2004).

In other instances, cleavage remains sub-perpendicular to bedding along fold limbs, indicating that cleavage formed early during layer parallel shortening and was subsequently tilted during large-scale folding and thrusting (Mitra and Yonkee, 1985). Stereonet analysis (Fig. 4.5) shows that the cleavages and the bedding in the Ramshorn Slate lie along a similar great circle.

Daugherty Gulch Borehole

My field mapping documented continuity in surface geology adjacent to and within strata where the Daugherty Gulch borehole containing the 667 Ma tuff (Isakson, 2017) was drilled. From the drill core a conformable contact was observed between the Cryogenian volcanic tuff and the overlying dolomite unit (Jacob, 1990; Lund et al., 2010). Gradational contacts were also observed from the dolomite and phyllite units overlying the ca. 667 Ma tuff in the Daugherty Gulch borehole (Jacob, 1990; Lund et al., 2010). In this study, gradational contacts were also observed between the basal dolomite of Bayhorse Creek, the overlying Garden Greek Phyllite, and the Bayhorse Dolomite where exposed along Bayhorse and Garden creeks.

Just west of Daugherty Spring, a small paired syncline/anticline fold exists on the eastern limb of the regional Bayhorse anticline. Approximately 500 m west of where the Daugherty borehole was drilled, a west-dipping normal fault juxtaposes the Ramshorn Slate against the stratigraphically higher Bayhorse Dolomite, suggesting at most ~200 meters of offset. West of this fault, the borehole was drilled into the east dipping limb of this small anticline (Plate 1).

Ramshorn Slate/Clayton Mine Quartzite Contact

Additionally, instead of previously-interpreted relations that involve a major thrust fault (Hobbs et al., 1991), our mapping documents that stratigraphically higher quartzites (Clayton Mine Quartzite) lie above shales (Ramshorn Slate) with an approximately 20 m gradational stratigraphic contact that consists of upward-coarsening shale and siltstone to interlayered quartzite, shaly quartzite, and finally predominantly quartzite. A distinct (1-7 m) interval of very fine to medium crystalline, partly oolitic, dolomite and similar beds of dolomitic sandstone occurs near the base of this unit. These observations are consistent with a gradational contact between the Ramshorn Slate and Clayton Mine Quartzite. These field observations suggest a relatively intact stratigraphic section exists westward from Daugherty Gulch. The section is composed of the Neoproterozoic Daugherty Gulch Tuff and overlying basal Bayhorse Dolomite, Garden Creek Phyllite, Bayhorse Dolomite, Ramshorn Slate, siltite and quartzite unit, and finally the Clayton Mine Quartzite.

Detrital Zircon U-Pb Geochronology

Basement rocks of the region comprise various blocks that influenced rift patterns and were sediment sources for younger strata. These blocks include the Archean Wyoming province, Neoarchean Grouse Creek block, evolved Paleoproterozoic Farmington zone and Mojave province, and juvenile Paleoproterozoic Yavapai and Mazatzal provinces (Fig. 4.6; Yonkee et al., 2014). This brief overview is given for preliminary context when analyzing the results presented below. Further dialogue on the changing provenance and detrital zircon ages seen throughout the Bayhorse section, and the geologic implications of these results will be presented at greater depth in the Discussion.

To provide stratigraphic context, the following results will be given alongside simplified stratigraphic sections, with the inferred stratigraphic position of the sample labeled. The first four samples (DTB17-04, DTB17-05, DTB17-11, and DTB17-14) were located within the mapping area, along Garden Creek, and collected in part to compare the Bayhorse strata with the Neoproterozoic to Ordovician stratigraphy of southeastern Idaho. South of the mapping area along the Salmon River and Highway 75, three additional samples were collected and analyzed (DTB17-17, DTB17-18, and DTB17-19) to constrain the relationship between the Ella Dolomite and thick underlying Clayton Mine Quartzite. The seven samples presented below augment the detrital zircon dataset from the Clayton region (Krohe, 2016; Link et al., 2017b). To maintain context with the Discussion, from here forward the age of the stratigraphic units (and abbreviations) are held consistent with the reinterpreted ages of this study.

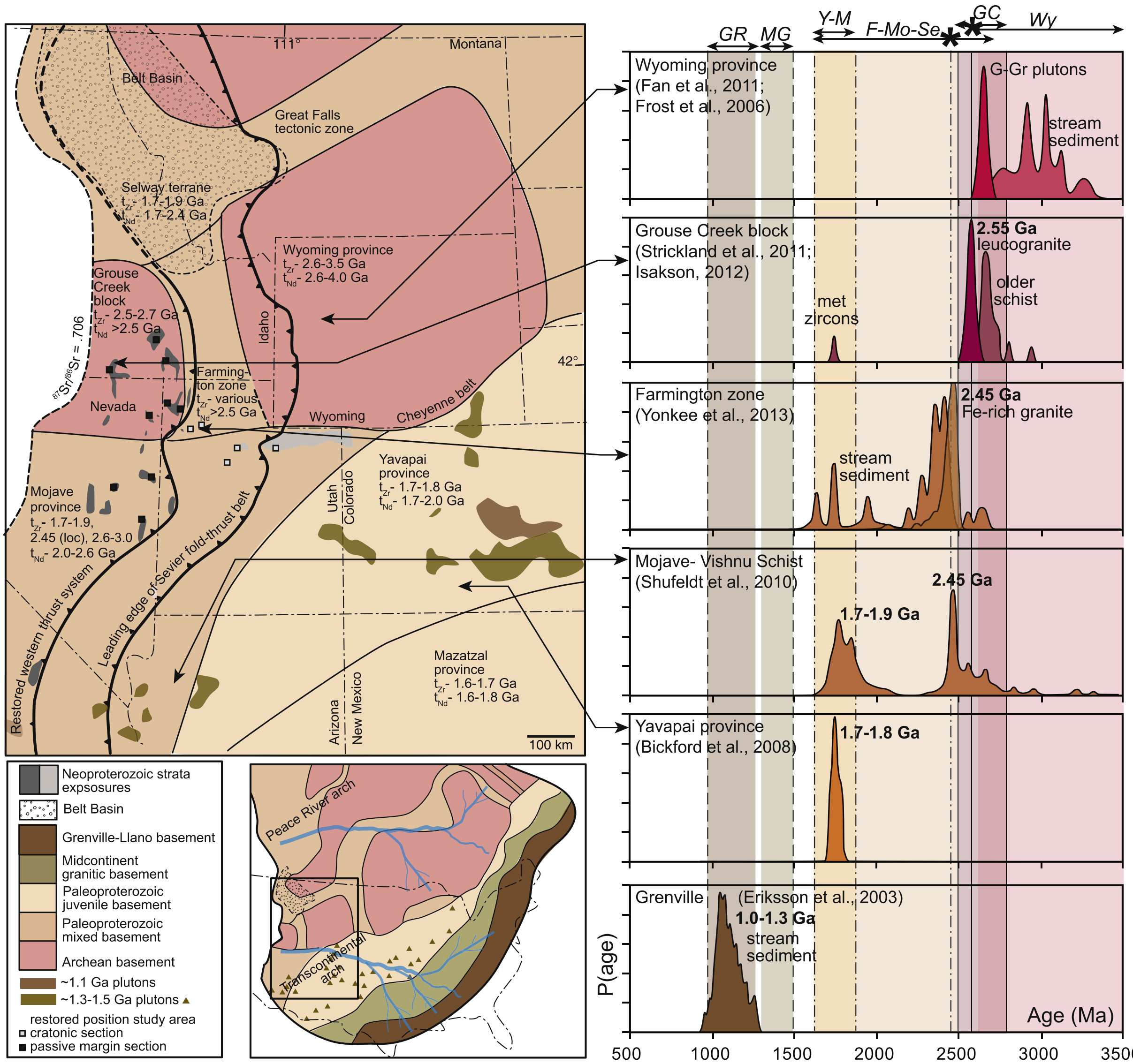

Figure 4.6- Generalized map of basement provinces shows local sediment sources for Neoproterozoic to Cambrian strata. Inset map of Laurentia shows locations of distal sediment sources. Zircon spectra from different basement sources have distinctive age patterns: Wyoming province (Wy) has a range of 2.6–3.0 Ga grains; Grouse Creek block (GC) has a prominent 2.55 Ga peak; Farmington zone, Mojave province, and Selway terrane (F-Mo-Se) have a mix of 1.7–1.9 Ga metamorphic grains, 2.45 Ga grains from local Fe-rich granitic plutons, and reworked Archean grains; Yavapai and Mazatzal provinces (Y-M) have a 1.7–1.8 Ga peak (Bickford et al., 2008); mid-continent granite (MG) and A-type granite intrusions in the SW U.S. have 1.3–1.5 Ga grains; and Grenville-Llano province (GR) has a range of 1.0–1.3 Ga grains with multiple subpeaks, along with ~1.1 Ga late granite intrusions in the SW U.S. (Yonkee et al., 2014 and references therein).

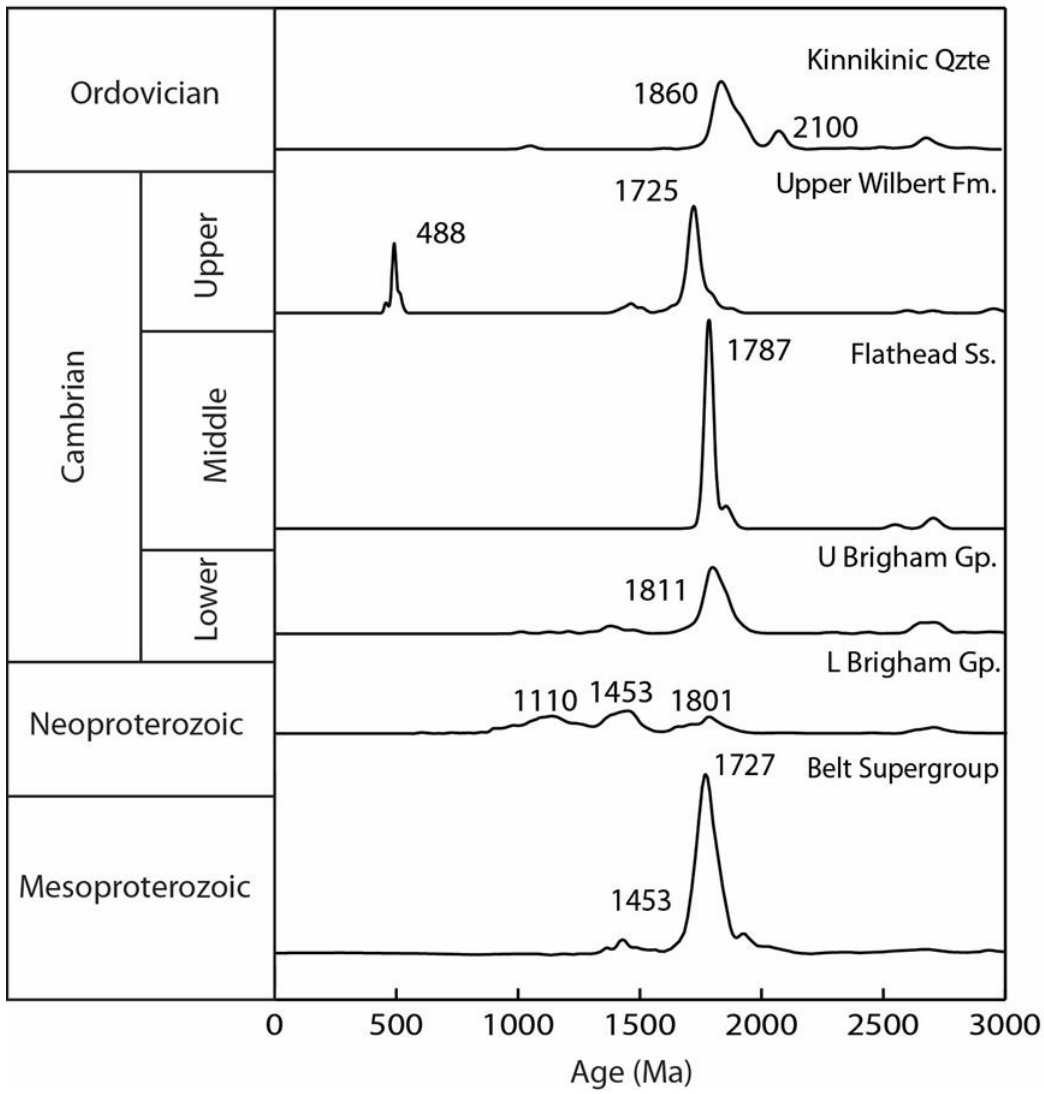

Figure 4.7- Comparative normalized U-Pb detrital zircon relative probability age plots from Mesoproterozoic to Ordovician sandstones of Idaho, Montana, and Wyoming. Ages (Ma) of prominent peaks are shown. Middle Ordovician Kinnikinic Quartzite, central Idaho (samples 5TA09, 9TD10, and 09LR01; from Beranek et al., 2016). Upper Cambrian Wilbert Formation (upper-most formation of Leaton Gulch), south of Challis, Idaho (Carr and Link, 1999; Hargraves et al., 2007; sample 151PL02). Middle Cambrian Flathead Sandstone, Teton Pass, Wyoming (1PL13) and Lower Cambrian upper Brigham Group, Gibson Jack Formation and Windy Pass Argillite (samples 9JK08, and 11JK08; from Yonkee et al., 2014). Neoproterozoic (Cryogenian) lower Brigham Group, Portneuf Range, Idaho and Utah; Caddy Canyon, Mutual, Browns Hole, and lower Camelback Mountain Formations (from Yonkee et al., 2014) (Z083, Z084, Z085 1JK08,). Mesoproterozoic Belt Supergroup from the Beaverhead and Lemhi Ranges (samples 2PL11, 6PL11, JS1103, 3TS09, 9TS09, 12RL214, 8PL12, 7PL12, 5PL10, 49ES08, 46ES08; from Link et al., 2016, Fig. 7 therein). These regionally consistent signatures are used in this study as a chronostratigraphic correlation tool. Interpretation of these regional trends will be covered in the Discussion.

Garden Creek Section

Four samples were collected and analyzed along the Garden Creek stratigraphic section (Plate 1; Fig. 4.8). The lack of coarse clastic lithologies in the lower portion of the section resulted in collection of the stratigraphically lowest sample (DTB17-04) from the coarse sandstone member of the lower Ramshorn conglomerate (Orc) that interfingers with the Ramshorn Slate. This sample yielded a dominant Grenville-aged population (~1.0-1.3 Ga) with lesser modes at ~1400 (Mid-continent granite), ~1760, and ~2700 Ma. The three grains younger than 975 Ma do not overlap in age and thus do not constitute a population from which to extract a robust MDA (Gehrels et al., 1995).

The next sample (DTB17-05) was collected from the first outcrop of quartzite above the Ramshorn Slate indicating a stratigraphic position near the lower contact of the siltite and quarztite (Osq of Hobbs et al., 1991). This fine-grained siltite and quartzite unit is in gradational contact with coarse sandstone of the Clayton Mine Quartzite. This sample contains a large age peak around 665-650 Ma. We further tested the provenance of this population using Hf isotope analysis discussed below. The remaining populations were similar in age to DTB17-04 with (1.0-1.3 Ga) Grenville, ~1.4 Ga (Mid-continent Granite), ~1760 and ~2700 Ma modes. However, the older populations are present in relatively greater amount than seen in DTB17-04.

The absence of significant fine-grained shale beds indicates proximity to the lower contact of the Clayton Mine Quartzite (Oc of Hobbs et al., 1991). DTB17-11 was collected in the Clayton Mine unit approximately 50 meters above its lower contact. This sample is dominated by the 665-650 Ma population, with an absence of any Grenville-aged grains, and lesser amounts of ~1450 (Mid-continent granite) and ~1700 Ma grains, with a small scattering of Archean dates.

The stratigraphically highest sample was collected on the top of the quartzite cliff near Buster Lake, approximately 600-700 meters above the lower contact of the Clayton Mine Quartzite. This sample (DTB17-14) shows a return of the Grenville grains, with a relatively larger population at ~1440 (Mid-continent Granite), but overall is dominated by a large Paleoproterozoic (~1760 Ma) population, and a large zircon population at ~2450 Ma.

Figure 4.8- The Garden Creek stratigraphy with detrital zircon probably plots and approximate stratigraphic position indicated. Note that abbreviations from Hobbs et al., 1991 are used. Tuff position was constrained by mapping in this study and dated by Lund et al., 2010. Tan represents primarily coarse clastic lithology; green, a shale or slate; and blue, a carbonate.

Figure 4.8

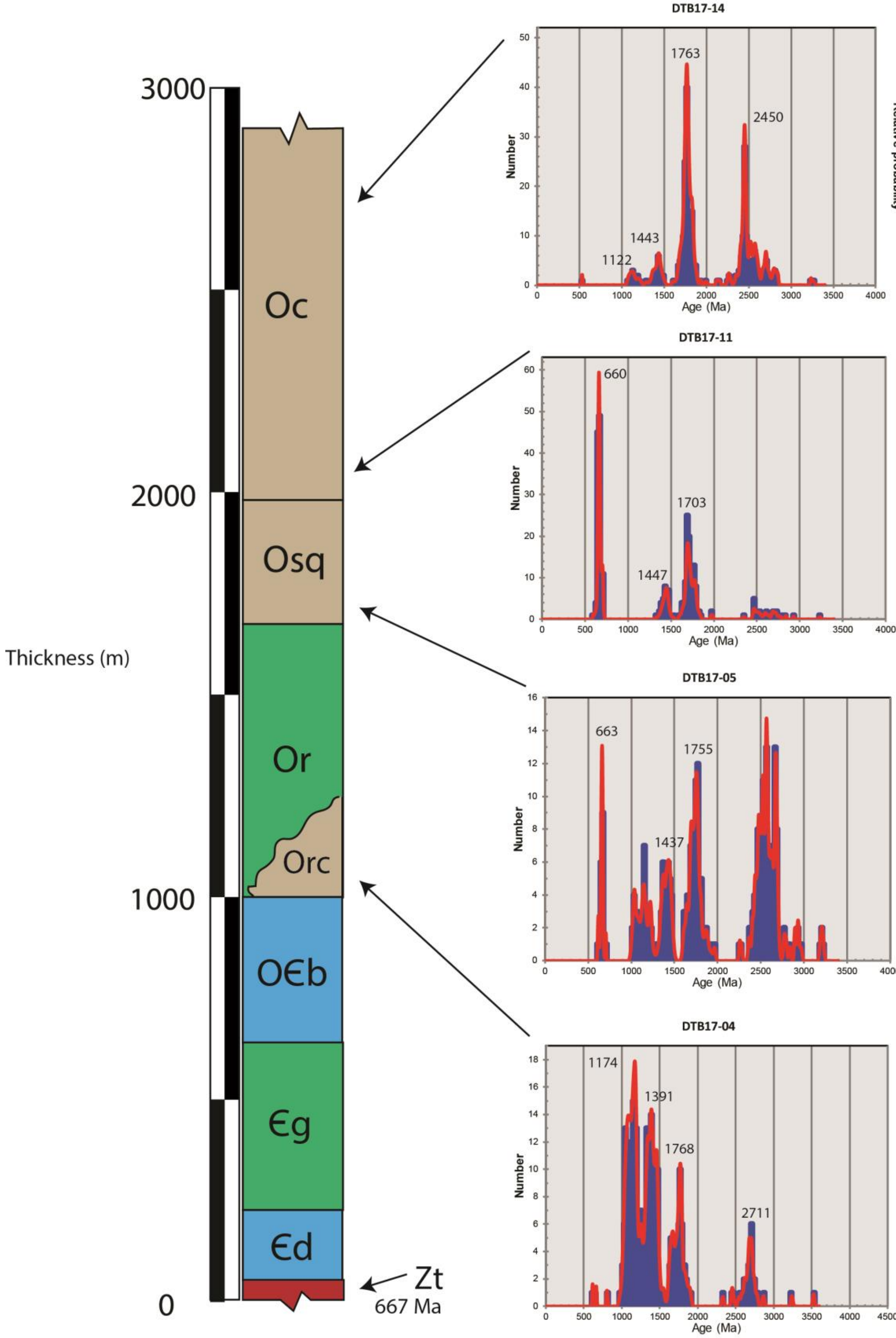

3000
2000
1000
0
Thickness (m)
Oc
Osq
Or
Orc
O€b
€g
€d
Zt
667 Ma
DTB17-14
1763
2450
1443
1122
Number
Relative probability
Age (Ma)
DTB17-11
660
1703
1447
DTB17-05
663
1755
1437
DTB17-04
1174
1391
1768
2711

Salmon River Section

Three samples were collected from a stratigraphic traverse along the Salmon River and Highway 75 (Fig. 4.9; Appendix C). These samples were collected to constrain the correlation of the quartzite that crops out prominently to the west of Clayton (mapped as Clayton Mine Quartzite by Hobbs et al., 1991). This sample traverse was analyzed to test the nature of the poorly exposed Clayton Mine Quartzite/Ella Dolomite contact as well as the possibility that the underlying quartzite is an Upper Cambrian unit of similar lithology. The nature of this contact is unclear; it has been variously mapped as conformable or as a low angle unconformity (Hobbs et al., 1968; Hobbs et al., 1991). The first sample, DTB17-16, was collected in the quartzite unit from less than 100 meters below the contact with the type section of the Middle Ordovician Ella Dolomite. This sample shows a scattering of Archean zircon grains but overall is dominated by a large Paleoproterozoic population with a normal distribution centered around ~1760 Ma.

The next sample, DTB17-18, was collected from the center of the anticline just west of Clayton, from the stratigraphically lowest exposure of the quartzite directly below the contact in question (~500 m below the Ella Dolomite contact). This sample contained a large population of Grenville-age grains with decreasing older zircon age peaks at ~1440, 1750, and 2650 Ma.

The final sample along this Highway 75 traverse, DTB17-19, was collected from the Clayton Mine Quartzite just east of the confluence of the East Fork and the main Salmon River. This final sample, DTB17-19, was collected approximately 10 m above the lower contact of the Clayton Quartzite with the siltite and quartzite gradational unit (Osq of Hobbs et al., 1991). This sample contained a large Grenville (1.0-1.3 Ga), ~1440, 1780, a >2500 Ma peaks. It also contained a small number (n=2 of 108) ca. 665-650 Ma grains that overlap in age.

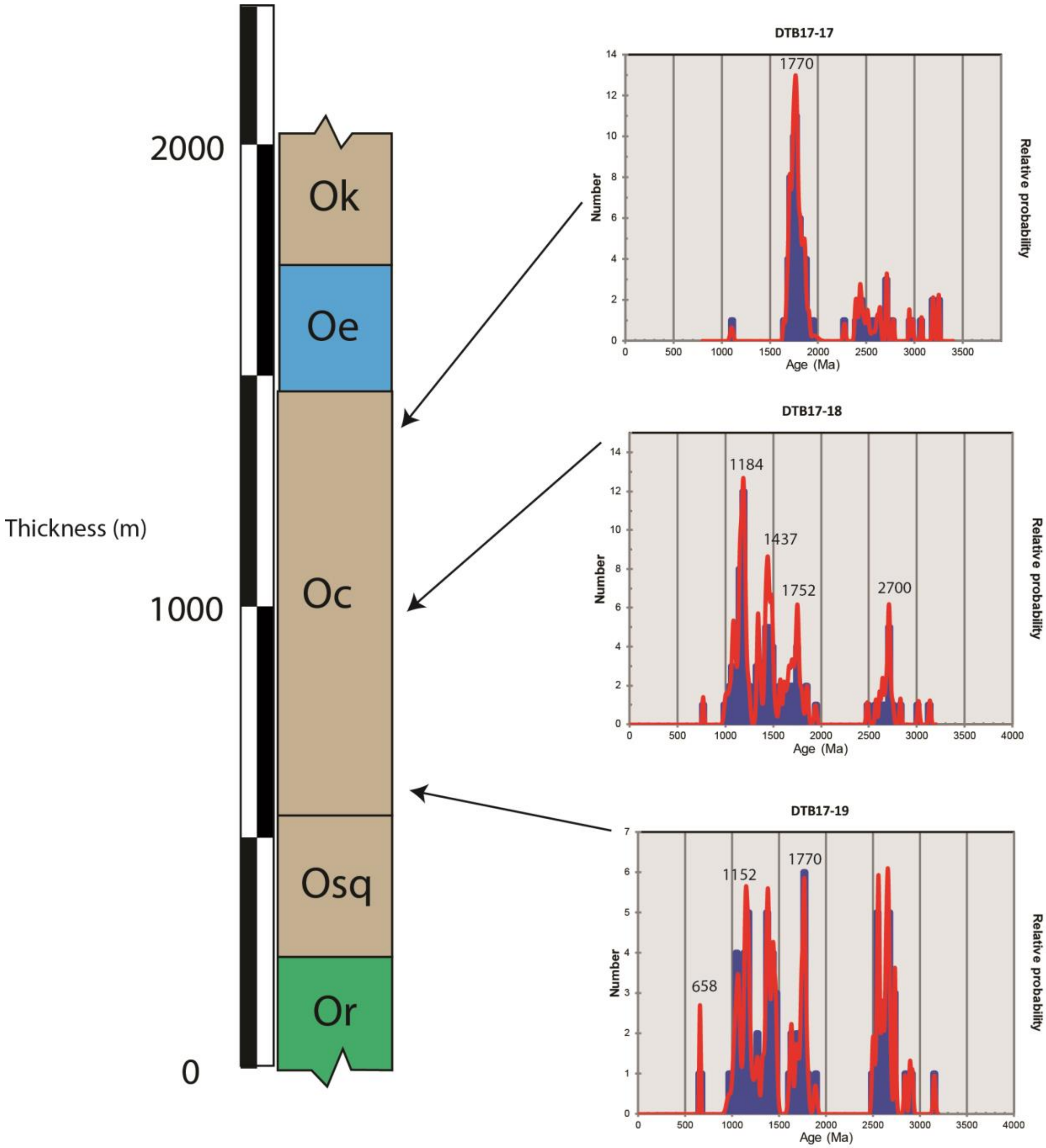

Figure 4.9- The samples collected along Highway 75 near Clayton. Detrital zircon probably plots and approximate stratigraphic position indicated. Note that abbreviations from Hobbs et al., (1991) are used. Tan represents primarily coarse clastic lithology; green, a shale or slate; and blue, a carbonate.

Detrital Zircon Lu-Hf

Lu-Hf geochronology was further applied to test the possibility that the 665-650 Ma grains originated from a point source and to evaluate the isotopic composition of the source rocks from which the zircons were derived. The ca. 665-650 Ma detrital zircons show initial εHf values ranging from 7.2 to 0.1, indicating an intermediate to moderately juvenile composition (Bahlburg et al., 2011).

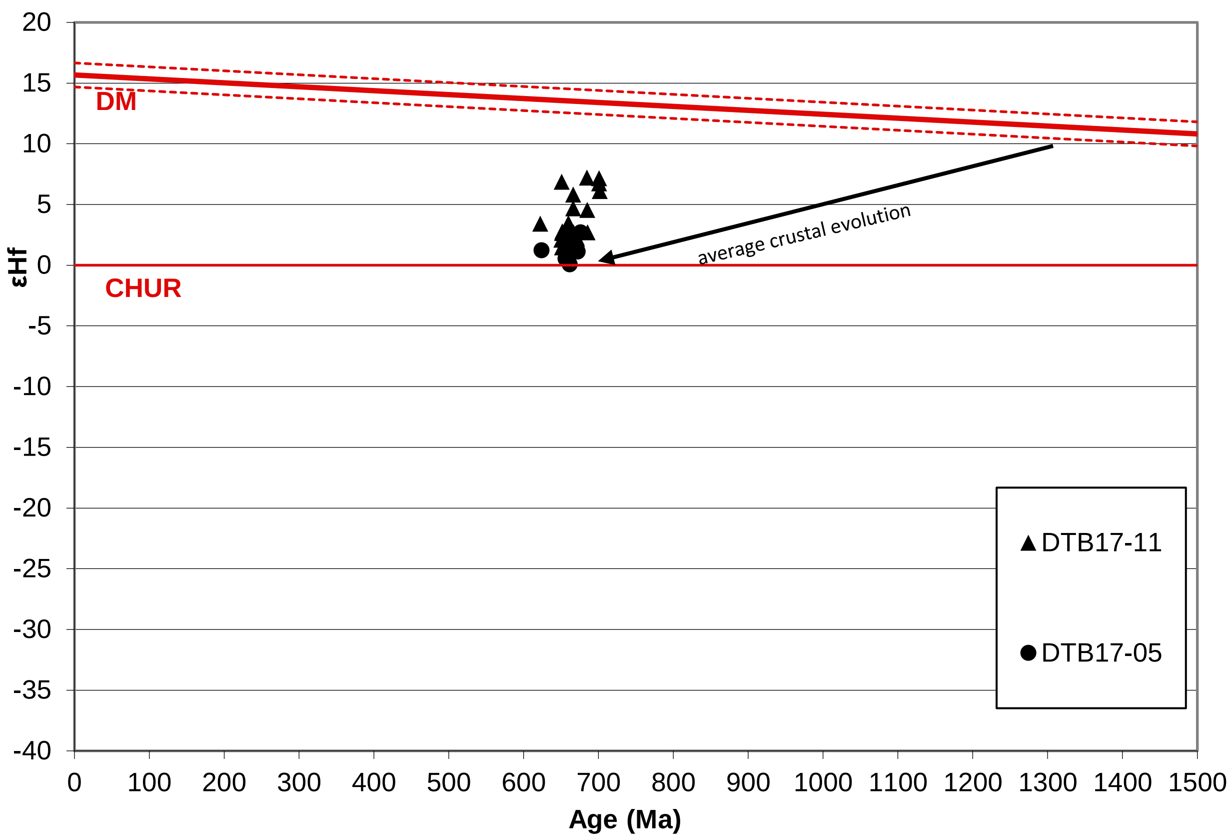

Figure 4.10- Detrital zircon (n=28) initial εHf values versus age (Ma) for the two samples (DTB17-11, and DTB17-05) that showed significant detrital age populations centered around ~665-650 Ma. The εHf is $^{176}Hf/^{177}Hf$. DM is depleted mantle; CHUR is chondritic uniform reservoir and represents the εHf of the average Earth. The average crustal evolution of $^{176}Hf/^{177}Hf$ is shown.

CHAPTER 5: DISCUSSION

Age Reassignment of the Bayhorse Stratigraphy

Lithologic characteristics of sedimentary rocks and detrital zircon patterns of Neoproterozoic to early Paleozoic strata along the North American Cordilleran margin follow a consistent stratigraphic framework (Yonkee et al., 2014). I argue that the stratigraphic relations seen in the field, detrital zircon patterns, regional correlation of lithologies, presence of Kinneyia biofilms, absence of any other fossils, and geochronologic constraints of the Bayhorse sequence (basal dolomite of Bayhorse Creek through the Clayton Mine Quartzite) confirm a Neoproterozoic to Early Cambrian, rather than Ordovician, age of deposition. This signifies a miscorrelation in previous studies (Ross, 1937; Hobbs et al., 1968; Hobbs et al., 1991 and Krohe, 2016).

Rise of Transcontinental Arch

Detrital zircon populations of Neoproterozoic North American Cordilleran units typically contain an abundance of Grenville-aged grains. The Grenville-aged grains are often associated with Paleoproterozoic and other Mesoproterozoic grain-age populations, suggesting a transcontinental river system tapping Grevillian sources with mixing of populations within the Grenville foreland and clastic wedge to the east (Link et al., 1993; Mueller et al., 2007; Dehler et al., 2010; Rainbird et al., 2012; Balgord et al., 2014; Linde et al., 2014; Yonkee et al., 2014, Matthews et al., 2018). Detrital zircon evidence from Neoproterozoic and Cambrian sandstones in Idaho as well as in the Roberts Mountains allochthon in central Nevada suggests that in Early Cambrian time, the Transcontinental Arch rose in the central United States, cutting off the supply of Grenville-aged zircons to the western continental margin (Amato and Mack, 2012; Linde et al., 2014; Yonkee et al., 2014; Link et al., 2017b; Matthews et al., 2018).

The Grenville aged grains in Neoproterozoic sandstones may also be recycled from Uinta Mountain Group (UMG) equivalents. The Uinta Mountain Group was deposited in an intracratonic basin from ca. 770-740 Ma and is dominated by detrital zircons from the Grenville orogeny. The UMG crops out in the east-west trending Uinta Mountains of Utah and shows thickening from ~4 km near Salt Lake City to over 7 km near the Utah/Colorado border. The Uinta Mountain Group is unconformably overlain by the Lower Cambrian Tintic Quartzite (Dehler et al., 2010; Yonkee et al., 2014). Burial of the Uinta Mountain is then generally coeval with the rise of the Transcontinental Arch. It is possible that the Uinta Mountain Group or an equivalent may have been contributing "recycled" Grenvillian zircons to the younger Neoproterozoic strata between ca. 740 and 540 Ma and that the disappearance of Grenville grains in the Early Cambrian may represent a cutting off from this source. It is unknown how much upper Uinta Mountain Group was eroded before its burial in the Early Cambrian.

Nevertheless, the supply of Grenville-age grains to western Laurentia was clearly cut off in the Early Cambrian. Thus, a significant concentration of detrital Grenville aged grains suggests a pre-Early Cambrian depositional age. In Idaho and Montana, the cut-off of Grenville-aged grains in the Early Cambrian is followed by appearance of a dominant 1780 Ma population in Middle Cambrian sandstones (Matthews et al., 2018). The provenance of these Paleoproterozoic grains is unclear. They were potentially sourced from the Yavapai province that was uplifted as part of the Transcontinental Arch (Malone et al., 2017), the Great Falls Tectonic Zone (Mueller et al., 2002), or the Swift Current anorogenic province (Collerson et al., 1988; Matthews et al., 2018).

Daugherty Gulch Borehole

My mapping near Daugherty Gulch Borehole did not identify any significant structures offsetting the borehole from the adjacent Bayhorse anticline. The observed structure, thicknesses, lithologies, and gradational nature of stratigraphic contacts described by the borehole log (Jacob, 1990) are all consistent with what is observed between correlative units when mapping. Minor discrepancies in thicknesses from the borehole units and the correlative units of the Bayhorse anticline are likely due to internal deformation.

Assuming an average 30° dip for all units within the borehole but the upper dolomite (where bedding dips near 15°, and steepens near 30 degrees at depth), true estimated thickness is 471 feet, 2482 feet, 170 feet, and 164 feet for the upper dolomite, phyllite, lower dolomite, and tuff of Daugherty Gulch respectively (Jacob, 1990). This suggests that the ridges adjacent to and above the borehole would fall within the 500 to 700-ft. stratigraphic interval of the Bayhorse dolomite. Hobbs and Hays (1990) noted a distinctly laminated argillite-siltstone interval and abundant pisolitic lithologies at the 500 to 700-foot stratigraphic height within the Bayhorse Dolomite. Field observations from the current study noted similar distinct lithologies on the dolostone ridges adjacent to the borehole. Irregular, sometimes concentric, silty laminations that vaguely resembled stromatolitic (?) bioherms were observed within the dolostone that crops out adjacent to the borehole as well as in the Bayhorse Dolomite in the main anticline to the west.

Lund et al. (2010) observed subtle lithologic differences from the Daugherty Gulch core to the rocks exposed nearby. The lower dolomite had been converted to marble and the carbonaceous phyllite from the core was “significantly less phyllitic and friable and contains more carbonate than the exposed Garden Creek Phyllite.” Previous studies (Grew, 1974 and references therein) have demonstrated that carbonaceous content of pelitic and calcareous rocks increases during low-grade burial metamorphism. This suggests that the observed lithologic differences may be a product of slight variation in metamorphic facies. These observations support my interpretation that the Basal Dolomite of Bayhorse Creek, Garden Creek Phyllite, Bayhorse Dolomite and the rest of the Bayhorse Section stratigraphically overlie the 667 Ma tuff.

The Ramshorn Slate overlies this lower dolomitic and phyllitic sequence (Basal Dolomite of Bayhorse Creek, Garden Creek Phyllite, Bayhorse Dolomite) here interpreted to be conformable with the 667 Ma Daugherty Gulch tuff. The two detrital zircon samples (10NK15: Krohe, 2016; DTB17-05: this study) analyzed from the Ramshorn Slate are dominated by Grenville-aged grains, consistent with an Ediacaran age.

Kinneyia

Additionally, wrinkle structures found in the lower Ramshorn Slate are interpreted to be Kinneyia biofilm. The genesis of these problematic sedimentary structures remains enigmatic; however, most authors interpret that the formation of these structures is related to an algal-mat microbial film (Hagadorn and Bottjer, 1997; Harazim et al., 2013; Kovalchuck, 2017). Similar wrinkle structures are found on bedding plane-exposures in the Mesoproterozoic upper Missoula Group and Spokane Formation (Montana) (Kovalchuk, 2017), the Neoproterozoic Wyman, Deep Springs, Johnnie, and Stirling Formations (Nevada and eastern California), and the Lower Cambrian Poleta and Harkless Formations (eastern California) (Hagadorn and Bottjer, 1997). While most modern siliciclastic microbial mats are limited to shallow-water environments such as tidal flats, lagoons, and sabkahs, many ancient biomats were well established in deep-water settings (Harazim et al., 2013) as may be the case for the Ramshorn Slate. The preservation of these structures suggests deposition before organisms developed that would have bioturbated the sediment, destroying the algal-mat (Hagadorn and Bottjer, 1997). The presence of these wrinkle structures in Late Cambrian and younger rocks is rare and often requires formation in areas of intermittent subaerial exposure and elevated salinities. These rare environments are needed to effectively suppress bioturbation and foster growth of patchy microbial communities (Hagadorn and Bottjer, 1997). Thus, I interpret the presence of Kinneyia biofilms, a complete lack of bioturbation in the Ramshorn slate, the failure of this study, and all previous studies (Ross, 1937; Patton, 1948; Hobbs, 1968, Hobbs et al., 1991; Krohe, 2016) to identify any fossils in the Garden Creek Phyllite, Ramshorn Slate, or interbedded siltite and quartzite, despite prevalent fine-grained lithologies with high fossil preservation potential, to be consistent with a pre-Middle Cambrian depositional age.

Ramshorn Slate/Clayton Mine Quartzite Contact

My recent mapping has reinterpreted the basal contact of the Clayton Mine Quartzite with the underlying Ramshorn slate to consist of a ~250 m coarsening upwards gradational contact, not a fault contact as mapped by Hobbs et al. (1991). Thus, this Cryogenian to Ediacaran, dolomitic, and argillaceous succession (Daugherty Gulch tuff, basal Dolomite of Bayhorse Creek, Garden Creek Phyllite, Bayhorse Dolomite, and Ramshorn Slate) is overlain in stratigraphic continuity by a thick, relatively coarse siliciclastic unit (the Clayton Mine Quartzite). The detrital zircon analyses from the lower portion of the Clayton Mine unit contain significant Grenville aged populations (DTB17-05, DTB17-18, DTB17-19, and 4PL14 from Krohe, 2016) consistent with a Neoproterozoic depositional age. Several samples also show a unique ~650-665 Ma population (DTB17-05 and DTB17-11, DTB17-19). The trough cross-bedded nature of this unit suggests fluvial to shallow marine deposition.

The depositional environment as well as the detrital zircon populations of this stratigraphic interval suggest a local, first order sedimentary system containing the 665-665 Ma grains that mixed with a continental, third order sedimentary system. (Ingersoll, 1990; Ingersoll et al., 1993; Link et al., 2005). I Interpret the ~665-650 grains to be sourced from the Cryogenian Big Creek plutons. I consider the lack of any Grenville-aged grains in DTB17-11, and a significant ~1450 and ~1700 aged population to record a first order system sourced from the Big Creek plutons and the surrounding Belt Supergroup (with similar ~1450 and 1700 age peaks).

The clustering of initial εHf values also suggests a point source for these ~665-650 Ma zircons. The intermediate to moderately juvenile values suggest that the melt likely involved limited reintegration of evolved Archean lithosphere and instead likely indicate a Mesoproterozoic lithospheric source with a small juvenile component. This interpretation is consistent with the Big Creek plutons resulting primarily from melting of the ca. 1370 Ma Elk City Domain (Dougherty and Chamberlain, 1996; Gaschnig et al., 2013; Link et al., 2017b). Hf analysis of Big Creek plutonic grains could help further constrain this provenance correlation.

The prevalence of the ~650-665 Ma grains in the lower Clayton Mine Quartzite appears to be a unique sedimentary signature that is not present in the correlative southeastern Idaho section. This suggests a drainage divide from southeast Idaho to central Idaho during Ediacaran time. However, both southeast and central Idaho appear to have received detritus from a third order, transcontinental river system that tapped Grevillian sources and resulted in a mixing of populations within the Grenville foreland and clastic wedge to the east

In the stratigraphically highest Clayton Mine sample, <100 m below the base of the Middle Ordovician Ella Dolomite, sample DTB17-17 contains no Grenville grains. Other stratigraphically higher Clayton Mine samples show a similar pattern (1TA09 from Krohe, 2016). The lack of Grenville-age grains is interpreted to signify deposition after the rise of Transcontinental Arch disrupted the continent-scale sediment transport system and presents an upper age constraint of Early to Middle Cambrian for the Clayton Mine Quartzite. However, significant unconformities or hiatuses likely exist within the Clayton Mine Quartzite as correlative strata in southeastern Idaho are approximately 3 times thicker. It also suggests that near Clayton, a period of erosion or non-depositional separates the Lower Cambrian, upper Clayton Mine Quartzite from the overlying Middle Ordovician Ella Dolomite.

The Middle Cambrian and older Squaw Creek section shows the same provenance change interpreted to represent the rise of the Transcontinental Arch. This suggests the Squaw Creek section overlaps in age with the Clayton Mine Quartzite.

Regional Correlation

It is important to note that these proposed correlations and subsequent tectonic models assume that the rocks of the Bayhorse region are not an “allochthonous” slice of Cordilleran margin translated by Mesozoic dextral strike-slip faults or part of an accreted ribbon continent. The Bayhorse strata shows a Laurentian provenance and are located approximately 150 km inboard from the nearest documented strike/slip faulting in the western Idaho shear zone (Schmidt et al., 2017). In addition, the identification of Neoproterozoic and lower Paleozoic strata ~100 km to the north at Stibnite and Big Creek (Lund et al., 2010; Stewart et al., 2017) and ~60 km to the southwest within the Sawtooth Metamorphic Core Complex (Ma et al., 2016), validate that the Bayhorse strata is native to central Idaho.

Bayhorse Section

Litho- and chronostratigraphic patterns in northeastern Washington and southeastern Idaho exhibit similarities to the newly reassigned Neoproterozoic to Cambrian stratigraphy of the Bayhorse section. In southeastern Idaho, the upper Scout Mountain Member of the Pocatello Formation contains a reworked fallout tuff bed, U-Pb SHRIMP dated to 667 ± 5 Ma (Fanning and Link, 2004). This Cryogenian tuff is overlain by limestone and argillite of the upper member of the Pocatello Formation (Link 1987; Fanning and Link, 2004), which in turn is overlain by the micritic, oolitic, sandy carbonate of the Blackrock Canyon Limestone which contains poorly defined stromatolites (Corsetti et al., 2007). Based on matching volcanic tuff ages and lithological similarity, I correlate the upper Scout Mountain Member to the ca. 667 Ma tuff of Daugherty Gulch (Lund et al., 2010; Isakson, 2017) and the overlying basal dolomite of Bayhorse Creek. The Garden Creek Phyllite overlies the basal dolomite of Bayhorse Creek in central Idaho, and in southeastern Idaho the upper member of the Pocatello Formation overlies the Scout Mountain Member. Both the Garden Creek Phyllite and the upper member of the Pocatello Formation are fine-grained argillaceous lithologies and are overlain by the Bayhorse Dolomite and Blackrock Canyon Limestone, respectively.

The Bayhorse Dolomite and Blackrock Canyon Limestone share similar lithologies with diagnostic oolitic and stromatolitic intervals. This Blackrock Canyon Limestone has been suggested to correlate to the Noonday Dolomite of Death Valley, which contains a karsted upper surface (Summa, 1993) and may represent sea-level drawdown during Marinoan glaciation (Corsetti et al., 2007; Mahon et al., 2014). The upper contact of the Bayhorse Dolomite has also been proposed to be a karst surface (Hobbs and Hays, 1990), and could chronostratigraphically correlate. However, the Marinoan glaciation interval has also been proposed to exist at the base of the Inkom Formation (Link et al., 1987) and within the Scout Mountain member of the Pocatello Formation (Isakson, 2017). An integrated chemostratigraphic study of the Bayhorse stratigraphy may help refine these correlations.

The Blackrock Canyon Limestone and the Bayhorse Dolomite are both overlain by fine grained units of the Papoose Creek Formation and Ramshorn Slate respectively. In northern Utah, within a similar (albeit slightly older) stratigraphic interval, the Kelley Canyon Formation contains graded, fine-grained beds, deposited from suspension and as distal turbidites; increasing quartzite content and mafic igneous sills are also noted in the upper Kelley Canyon Formation (Crittenden, 1988; Yonkee et al., 2014). I observed similar lithologies in the Ramshorn Slate/siltite and quartzite of the Bayhorse section. The mafic sills within the Kelley Canyon Formation are undated but hypothesized to record waning stages of Neoproterozoic rift related igneous activity (Crittenden, 1988; Yonkee et al., 2014). I suggest that the Kelly Canyon Formation and these sills may correlate with the similar stratigraphic interval at Bayhorse containing the gabbroic sills within the Ramshorn Slate/siltite and quartzite.

Detrital zircon samples from this stratigraphic interval at Bayhorse also exhibit abundant 1.0-1.3 Ga and 1.3-1.5 Ga detrital grains originating from distal Laurentian sources as seen in southeast Idaho and Utah (Yonkee et al., 2014). Considering these lithologic, stratigraphic, provenance and chronologic similarities, I interpret the Bayhorse stratigraphic section from the Daugherty Gulch tuff upwards through the lower Clayton Mine Quartzite to be chrono- and litho-stratigraphically correlative to the Scout Mountain Member of the Pocatello Formation through the Papoose Creek Formation of southeast Idaho.

Figure 5.1- Simplified Neoproterozoic to Ordovician stratigraphy of Bayhorse and southeastern Idaho. Southeastern Idaho stratigraphic column after Link and Phoenix (1996).

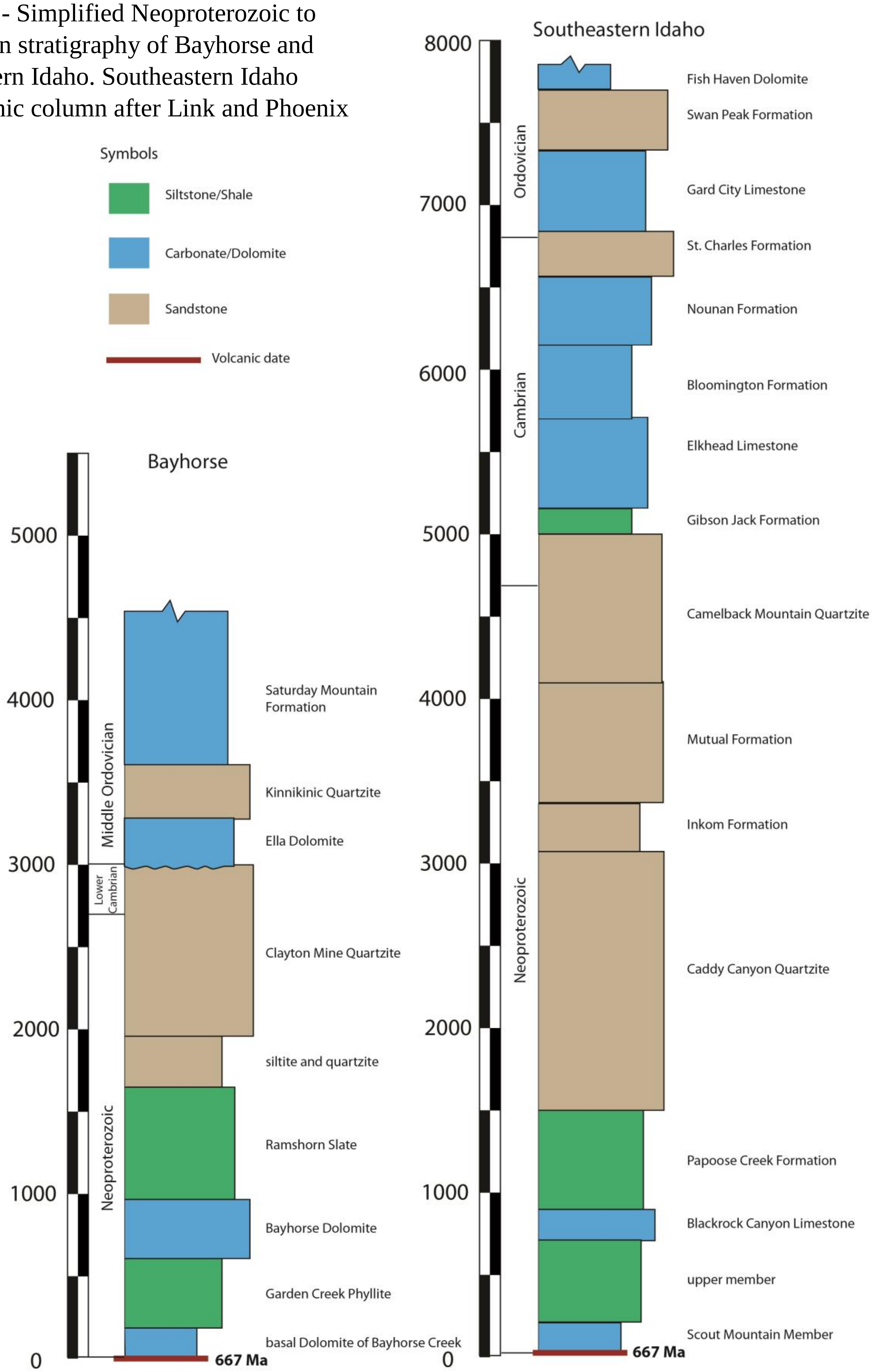

Above this stratigraphic interval, the correlation from Bayhorse to the rest of the miogeocline increases in complexity. In southeastern Idaho, ~3.5 km of the Caddy Canyon Quartzite, Inkom Formation, Mutual Formation, and Camelback Mountain Quartzites of the Brigham Group overlie the Papoose Creek/Kelly Canyon Formation. At Bayhorse, the ~1 km thick Clayton Mine Quartzite overlies the Ramshorn Slate. Additionally, Neoproterozoic (665-650 Ma) and Late Cambrian-Early Ordovician (500-485 Ma) alkalic igneous rocks of the Big Creek-Beaverhead belt are found in central Idaho but generally absent south of the Snake River Plain (Lund et al., 2010; Link et al., 2017b). The stratigraphic position of the Clayton Mine Quartzite, lying conformably above the Ramshorn Slate (a correlative to the Papoose Creek), suggests correlation to the Caddy Canyon Quartzite. Stratigraphically higher within the Clayton Mine Quartzite, a shift is evident in the detrital zircon populations with the absence of Grenville grains and the transition to a significant ca. 1780 Ma peak. This same provenance shift is recognized within several other basal Cambrian sandstones, including the Camelback Mountain Quartzite of the Brigham Group in southeast Idaho, Cash Creek Quartzite in central Idaho, and the Flathead Sandstone in southwest Montana (Matthews et al., 2018); this suggests that the Clayton Mine Quartzite is correlative to the Caddy Canyon, Inkom, Mutual, and Camelback Mountain formations of southeast Idaho. However, it is likely that several unrecognized unconformities exist within the Clayton Mine Quartzite. The 665-650 Ma population of detrital grains in the Clayton Mine Quartzite are also found in a similarly correlated quartzite ~80 km to the northwest at Stibnite (Fig. 5.2; Stewart et al., 2016; Isakson, 2017). Zircon grains of this age have not been found in units outside of central Idaho.

Based on lithology, the Clayton Mine Quartzite could reasonably be correlative to the Caddy Canyon, Mutual, and Camelback Mountain quartzites as they all consist of variably sorted and sized, quartzose to subfeldspathic arenites with subordinate argillite, indicative of deposition in a fluvial to shallow marine environment (Link et al., 1987). However, in central Idaho, discrete lithostratigraphic intervals within the Clayton Mine Quartzite intervals must be missing. In central Idaho, the 100-200 m thick distinctive argillite regional marker of the Inkom is not present. If this chrono-stratigraphic correlation holds true, the Clayton Mine Quartzite is also approximately 1/3 the thickness of the chronostratigraphic correlative units in southeast Idaho.

This stratigraphic difference is likely due to decreased accommodation space within the developing margin of central Idaho, potentially due to a lower crustal strengthening along the margin of the Mesoproterozoic Belt/Purcell basin. Intermittent fluvial and shallow marine clastic deposition of the Clayton Mine Quartzite was likely interrupted by hiatuses and periods of erosion while central Idaho struggled to subside at rate that could accommodate the influx of sediment. These periods of erosion/non-deposition in the Clayton Mine could coincide with the several regional unconformities in the correlative upper Brigham Group of southeast Idaho section, however this is quite speculative. Unconformities in the southeast Idaho section occur above and below the Inkom Formation as well as within the Camelback Mountain Quartzite (Christie-Blick et al., 1988).

In southeast Idaho, the Camelback Mountain Quartzite is interpreted to span the Neoproterozoic to Early Cambrian boundary and records the end of rifting, and transition to thermal subsidence of the now passive margin (Yonkee et al., 2014). In southeastern Idaho, thick carbonate units overlie the Camelback Mountain Quartzite. These carbonate units include (moving up section) the Cambrian Gibson Jack Formation, Elkhead Limestone, Bloomington Formation, Nounan Dolomite, and St. Charles Formation (Fig. 5.1; Link et al., 2017b). The Upper Cambrian St. Charles Formation includes the feldspathic Worm Creek Member that records Late Cambrian tectonism and exhumation of the Lemhi arch in central Idaho (Link et al., 2017b).

However, in central Idaho, the Middle Ordovician Ella Dolomite and Kinnikinic Quartzite (correlatives to the Garden City Limestone and Swan Peak Quartzite of southeastern Idaho) lie directly above the Lower (to Middle?) Cambrian Clayton Mine Quartzite at several localities. This suggests that correlatives to the Gibson Jack Formation, Elkhead Limestone, Bloomington Formation, Nounan Dolomite and St. Charles Formation of southeastern Idaho are missing at Bayhorse, representing approximately 40 million years of missing strata.

Squaw Creek Section

In contrast to the partially eroded stratigraphic section near Bayhorse, less than 10 km to the northwest, a >650 m Cambrian section is preserved in the Squaw Creek section. The Middle Cambrian quartzite (Cash Creek Quartzite) and shale interval of Squaw Creek has drawn comparisons to the Middle Cambrian Flathead and Wosley Shale of southwestern Montana and northwestern Wyoming (Hobbs and Hays, 1990; Krohe, 2016).

The same stratigraphic provenance trend seen in the upper Clayton Mine is present in the Squaw Creek Section (Fig. 5.2 and 5.3). The two samples of the stratigraphically lowest unit in the Squaw Creek section (lower Quartzite of Boundary Creek samples 3TA09 and 15NK15; Krohe, 2016) contain significant Grenville aged grains. Up-section, recent detrital zircon analysis 4TA09 and 5NK15 (Krohe, 2016) shows a large ca. 1780 Ma population in the Cash Creek Quartzite and the absence of Grenville (1.0-1.3 Ga) grains. The shale overlying the Cash Creek Quartzite contains trilobites of early Middle Cambrian age (Hobbs and Hays, 1990). This is consistent with our interpretation that the presence and subsequent absence of Grenville-aged detritus as an Early Cambrian chronostratigraphic indicator. This also suggests that the Squaw Creek section is a chronostratigraphic (albeit slightly more complete) correlative to the upper Clayton Mine Quartzite.

This Middle Cambrian shale is variably preserved beneath a dolostone of generalized Ordovician age (Hobbs and Hays, 1990). This Ordovician dolostone (carbonate of Cash Creek) may tentatively be correlated to the Middle Ordovician Ella Dolomite; Eocene volcanic rocks cover the top contact of this unit. This suggests the Squaw Creek section also experienced Late Cambrian erosion that may have been coeval with the erosional surface between the Clayton Mine Quartzite and Ella Dolomite.

Additionally, this also suggests that the upper Clayton Mine Quartzite is correlative to the Squaw Creek section below the Middle Cambrian Shale. However, a ~175 m thick carbonaceous siltite interval present in the Squaw Creek section (lower carbonate of Squaw Creek) is not recognized within the Clayton Mine Quartzite. It is possible this interval could have been eroded within the Clayton Mine Quartzite. If this is true, the juxtaposition of two lithologically similar quartzite units (Cash Creek and lower quartzite of Boundary Creek) in the upper Clayton Mine Quartzite could have gone unrecognized by Hobbs et al., (1991) and Krohe (2016). It is also possible that the lower carbonate of Squaw Creek is a distal facies of the Clayton Mine Quartzite, and it was only deposited deeper on the continental shelf, or possibly during a time of minor regression and hiatus in the fluvial/nearshore Clayton Mine Quartzite.

Following the interpretation of Hobbs and Hays (1990), I suggest that the Middle Cambrian and older strata of the Squaw Creek section were transported from the west on a thrust fault. Instead of a terrane-bounding fault (Hobbs et al., 1991), I suggest that the Squaw Creek section was transported on the hanging-wall of a relatively bedding-parallel thrust fault. This fault juxtaposed the similar-aged, albeit slightly more complete and potentially more offshore (western) facies of the basal quartzite of Boundary Creek, lower carbonate of Squaw Creek, and Cash Creek Quartzite against the Clayton Mine Quartzite. It is probable this thrust strikes north to south along the east side of Squaw Creek, where Tertiary volcanic rocks and younger Quaternary deposits obscure recognition of the fault. It is also likely that this thrust is cut by younger normal faults, adding further complication to its identification.

Stereonet analysis (Fig. 4.1) shows that the cleavages and the bedding in the Ramshorn Slate lie along a similar great circle. This is interpreted to suggest that the cleavage formed prior to significant folding. The formation of cleavage early in the deformational history of an area may be aided by elevated temperatures and pressures caused by increased overburden due to emplacement of earlier overriding thrust sheets (Mitra et al., 1984), potentially suggesting that the rocks of the Bayhorse anticline were previously buried beneath the Copper Basin or inferred Squaw Creek Thrust plate.

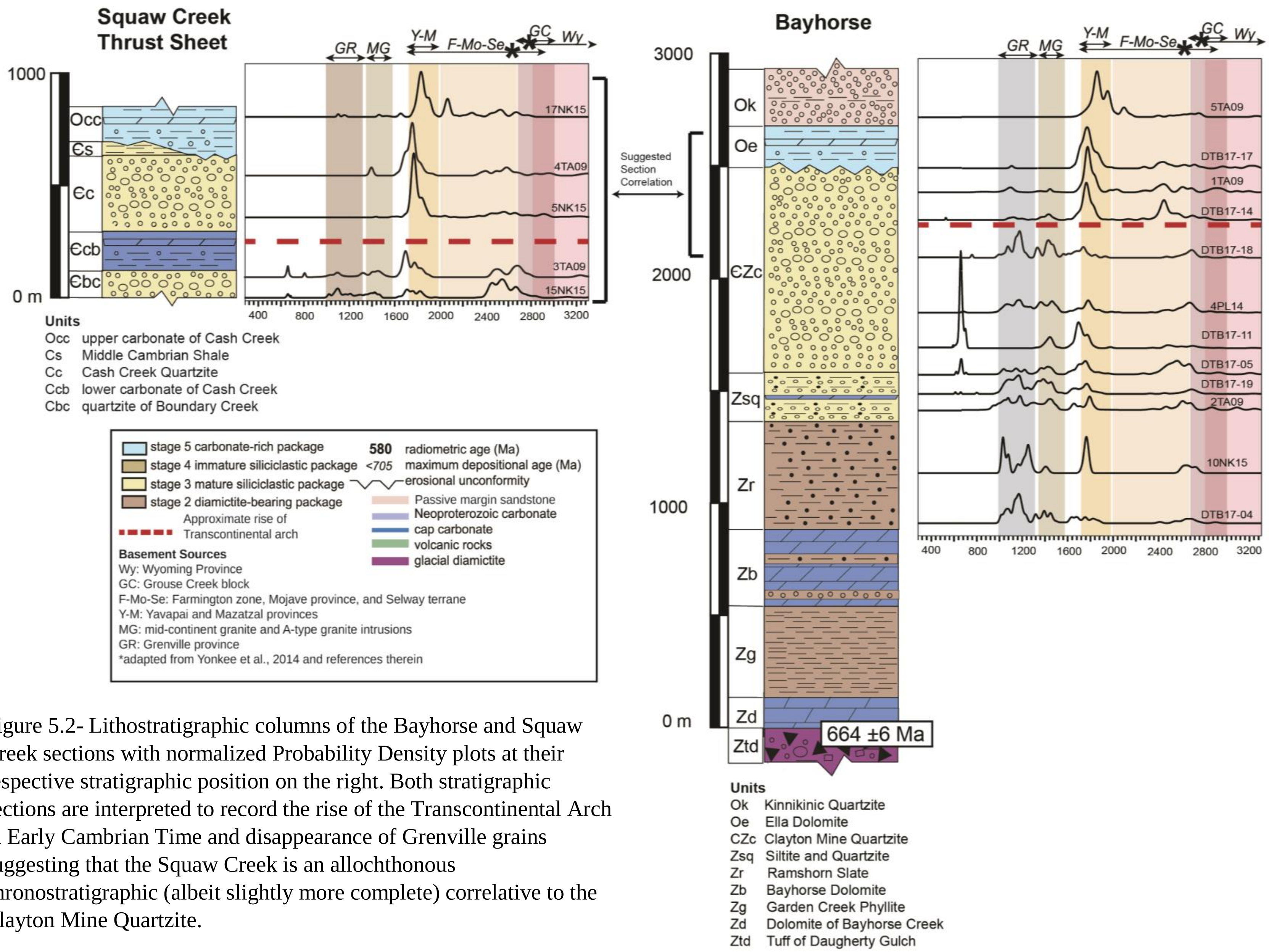

Figure 5.2- Lithostratigraphic columns of the Bayhorse and Squaw Creek sections with normalized Probability Density plots at their respective stratigraphic position on the right. Both stratigraphic sections are interpreted to record the rise of the Transcontinental Arch in Early Cambrian Time and disappearance of Grenville grains suggesting that the Squaw Creek is an allochthonous chronostratigraphic (albeit slightly more complete) correlative to the Clayton Mine Quartzite.

Figure 5.3

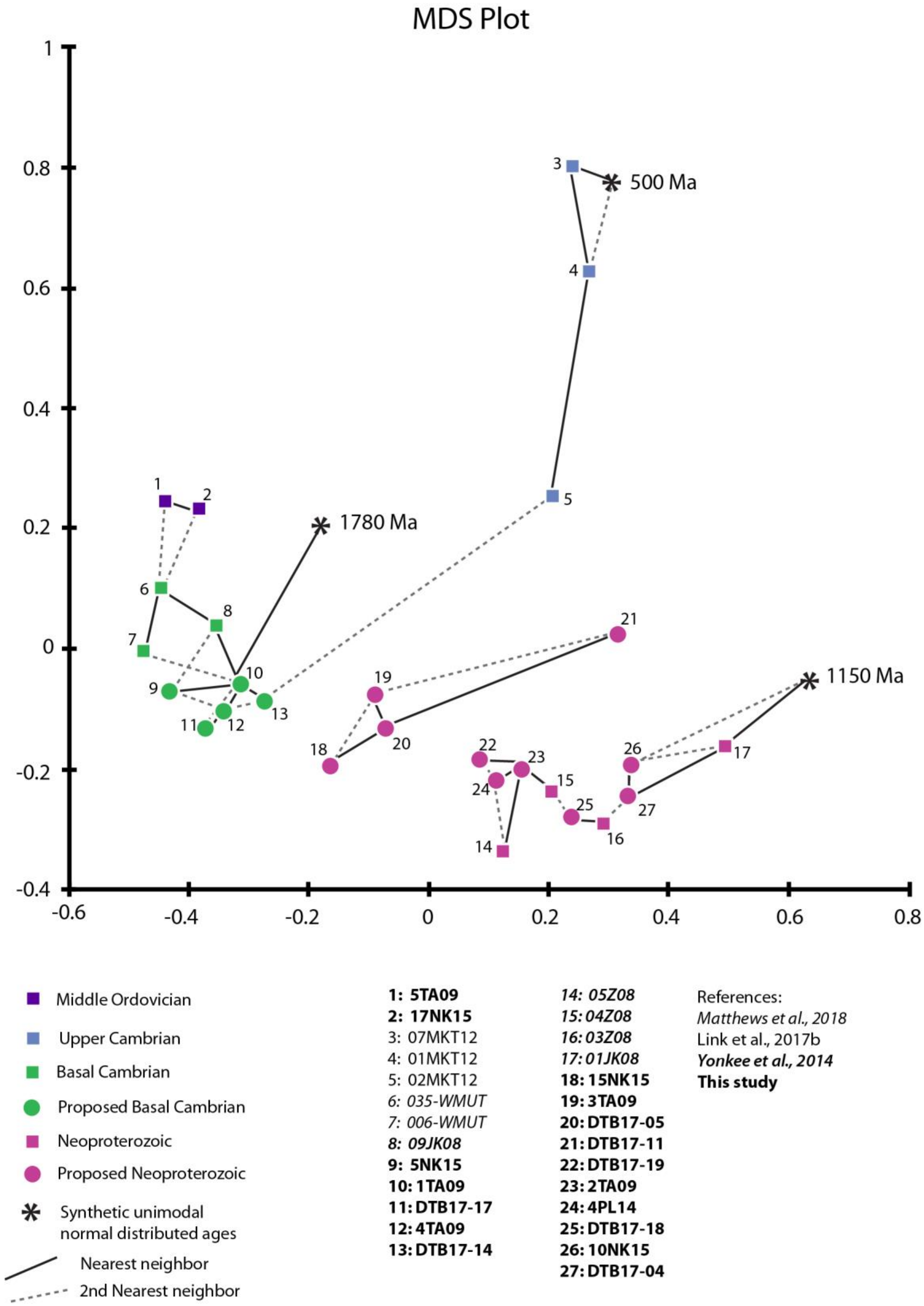

MDS Plot
1
0.8
0.6
0.4
0.2
0
-0.2
-0.4
-0.6
-0.4
-0.2
0
0.2
0.4
0.6
0.8
500 Ma
1780 Ma
1150 Ma
Middle Ordovician
Upper Cambrian
Basal Cambrian
Proposed Basal Cambrian
Neoproterozoic
Proposed Neoproterozoic
Synthetic unimodal normal distributed ages
Nearest neighbor
2nd Nearest neighbor
1: 5TA09
2: 17NK15
3: 07MKT12
4: 01MKT12
5: 02MKT12
6: 035-WMUT
7: 006-WMUT
8: 09JK08
9: 5NK15
10: 1TA09
11: DTB17-17
12: 4TA09
13: DTB17-14
14: 05Z08
15: 04Z08
16: 03Z08
17: 01JK08
18: 15NK15
19: 3TA09
20: DTB17-05
21: DTB17-11
22: DTB17-19
23: 2TA09
24: 4PL14
25: DTB17-18
26: 10NK15
27: DTB17-04
References:
Matthews et al., 2018
Link et al., 2017b
Yonkee et al., 2014
This study

Figure 5.3- Two-dimensional scaling plot of KS test dissimilarity values. The axes are arbitrarily calculated values to illustrate similarity of each dataset in 2D space. Each point represents one entire detrital zircon sample, the squares represent published samples of a known age-correlation, and circles are samples of this study. The points that plot closer together are statistically more similar with solid lines indicating the nearest neighbor, and dashed lines indicating the second nearest neighbor. The results show 5 distinct groupings. The Middle Ordovician and Upper Cambrian samples plot in separate distinct groupings. Note none of the Bayhorse samples plot within these groupings. The Basal Cambrian samples also plot together and are defined by their general lack of Grenville grains. The Neoproterozoic samples also generally plot together, defined by their prevalence of Grenville grains. However, several samples from Bayhorse plot slightly apart from the other known Neoproterozoic samples due to presence of the unique 665-650 Ma grains.

North-Central Idaho Correlations

The developing consensus (Lund et al., 2003; Ma et al., 2016; Isakson, 2017, Stewart et al., 2017; this study) is that Neoproterozoic and Lower Cambrian rocks exists west of the Lemhi arch in central Idaho. At Stibnite, >600 m of fine-grained carbonaceous quartzite, marble, and phyllite of the Moores Station Formation likely correlates to the basal Dolomite of Bayhorse Creek, Garden Creek Phyllite, Bayhorse Dolomite, and Ramshorn Slate. The Moores Station Formation is overlain by a <1000 m (?) dominantly quartzite with a lesser calc-silicate interval (quartzite of Profile Creek, lower calc-silicate, Fern marble, quartz pebble conglomerate, lower quartzite). Detrital zircon samples from the quartzite of Profile Creek (10RL893), quartzite and schist (14RL011a), and quartz pebble conglomerate (QPC) show significant Grenville-aged detritus along with a small population of ca. 660 Ma grains. These ca. 660 Ma grains have also been interpreted to be sourced from the Big Creek plutons. In the stratigraphically higher samples within the lower quartzite (12DS24, 12DS19, 10RL888), the ca. 660 Ma and Grenville-aged grains disappear, and a ca. 1780 peak is dominating (Isakson, 2017). This interval is interpreted to span the Cambrian/Neoproterozoic boundary and likely correlates to the Clayton Mine Quartzite and interbedded siltite and quartzite at Bayhorse and the Middle Cambrian and older section at Squaw Creek (Fig. 5.4). This suggests that the Neoproterozoic to middle Cambrian section at Stibnite and Bayhorse show similar thicknesses and lithologies. Stibnite does appear to have approximately 450 m (?) of strata within the upper Cambrian to lower Ordovician interval that is missing at Bayhorse including several detrital zircon samples with an abundance of Beaverhead ca. 500 Ma grains (14DS12, 12DS33).

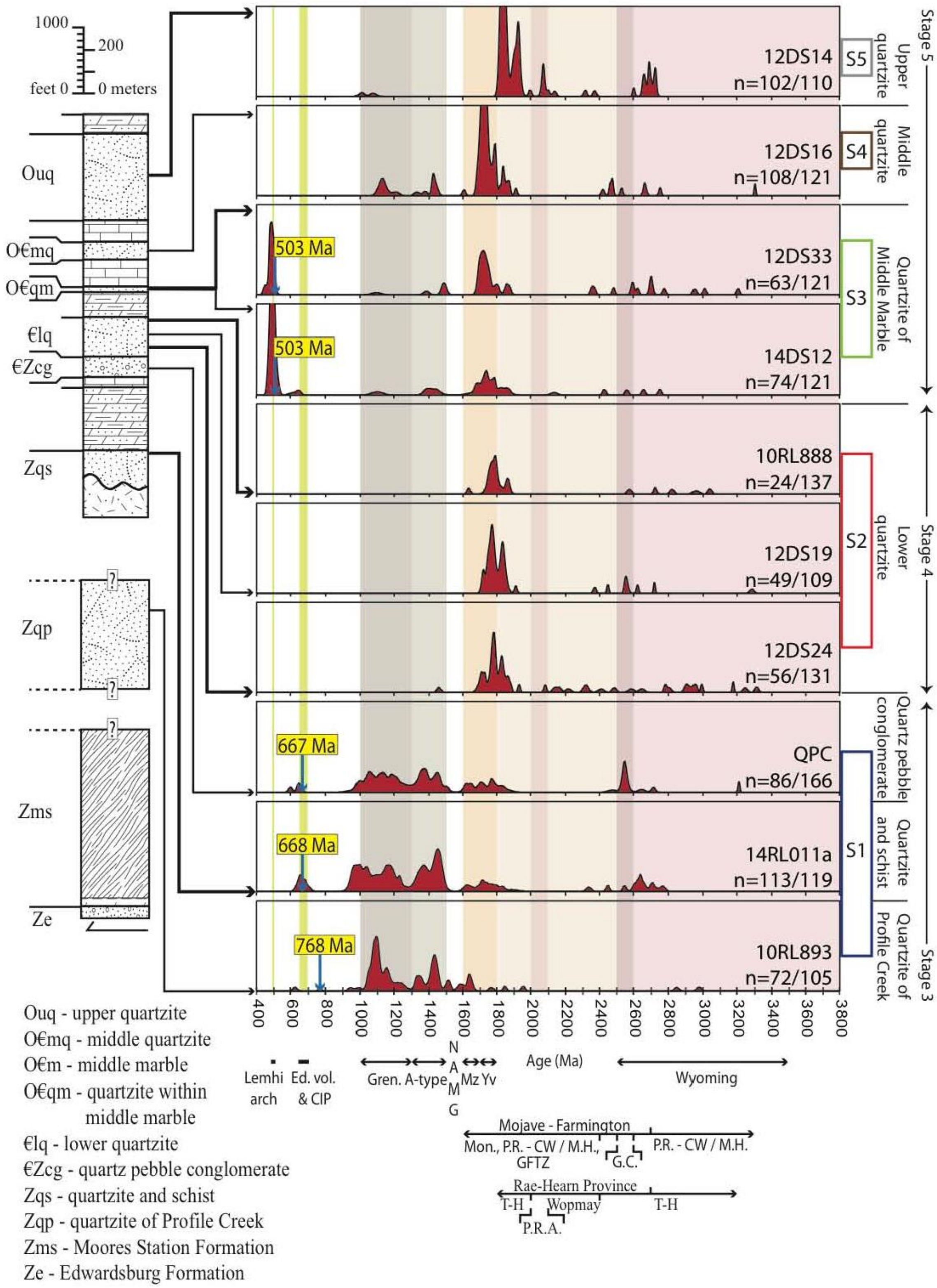

Figure 5.4- Generalized stratigraphy of the Stibnite area alongside stacked relative probability plots (from Isakson, 2017). This section at Stibnite spans a similar time interval as the strata at Bayhorse.

Implications for Rodinian Rifting

Tectonostratigraphic Differences from Bayhorse to Southeast Idaho

The reassignment of the Bayhorse section from Ordovician to Cryogenian, Ediacaran, and Lower Cambrian requires recharacterization of the stratigraphic architecture, sediment thickness, facies distribution, and subsidence patterns through central Idaho during the Neoproterozoic and early Paleozoic. I interpret these similarities between the newly identified Cryogenian to Ediacaran Bayhorse section (basal Dolomite of Bayhorse Creek, Garden Creek Phyllite, Bayhorse Dolomite, and Ramshorn Slate), and the chronostratigraphically correlative section in southeastern Idaho (upper member of Pocatello Formation, Blackrock Canyon Limestone, and Papoose Creek Formtion), to record a period of Neoproterozoic extension and contemporaneous basin subsidence in both central and southeastern Idaho. Along most of the developing Cordilleran margin, a similar litho- and chronologic interval is recognized. This interval is interpreted to coincide with initial extension and the onset the regional subsidence (Yonkee et al., 2014).

This interval of initial extension is usually followed by an interval of final rifting, and transition to drift around the Neoproterozoic/Cambrian boundary marked by the deposition of thick Ediacaran shallow marine and fluvial siliciclastic strata overlain by Cambrian basal sandstones and overlying thick Cambrian carbonates (Yonkee et al., 2014). I interpret the notable absence of Upper Cambrian and Lower Orodovician strata at Bayhorse, and thinning of the Clayton Mine Quartzite compared to correlative Ediacaran Quartzites of the Brigham Group to suggest that this interval of final rifting in central Idaho was likely prolonged (by approximately 50 myr) compared to southeast Idaho, with significantly less subsidence and enigmatic periods of exhumation. The presence of a local (650-665 Ma) detrital zircon population in the Clayton Mine Quartzite is interpreted to record intermittent local basins of the Ediacaran central Idaho marginal basin.

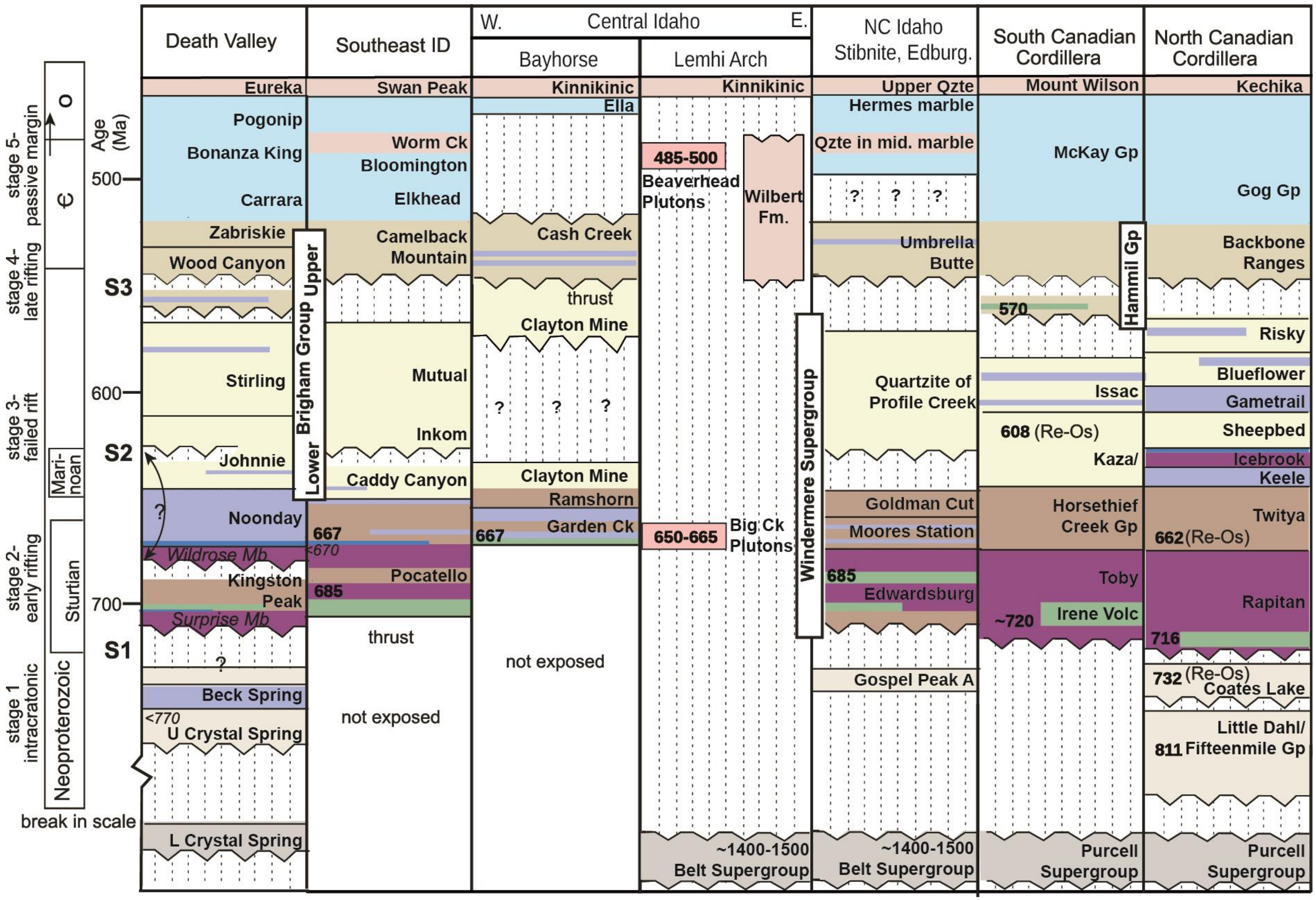

Figure 5.5- Chronostratigraphic correlation of Neoproterozoic to Ordovician stratigraphy along the Cordillera margin. Southeast Idaho stratigraphy adapted from Link et al. (1987), Oriel and Platt (1980), and Yonkee et al. (2014). Lemhi arch stratigraphy adapted from McCandless (1982), Lund et al. (2010), and Link et al. (2017b). North-central Idaho stratigraphy compiled from Stibnite (Stewart et al., 2017) and Edwardsburg (Lund et al., 2010) and Isakson (2017). Bayhorse stratigraphy from this study. Rift stages (stage 1 - stage 5) from Yonkee et al. (2014). Major sequence boundaries (S1 – S3) from Link et al. (1987).

Punctuated Subsidence in the Bayhorse Region

To visualize the variations in subsidence from southeast Idaho to Bayhorse, tectonic subsidence curves were generated (Fig. 5.6). Thickness and depositional environment on this model started at the tuff of Daugherty Gulch and the correlative Scout Mtn. member of the Pocatello Formation. The model ends in the Middle Ordovician at the top contact of the Kinnikinic Quartzite and Swan Peak Formation in central and southeast Idaho respectively. Bannock Range stratigraphy is from Oriel and Platt (1980), Link et al. (1987), and Fanning and Link (2004). Neoproterozoic eustatic changes have large uncertainties (Yonkee et al., 2014) and thus for simplification sea level was held constant in this model.

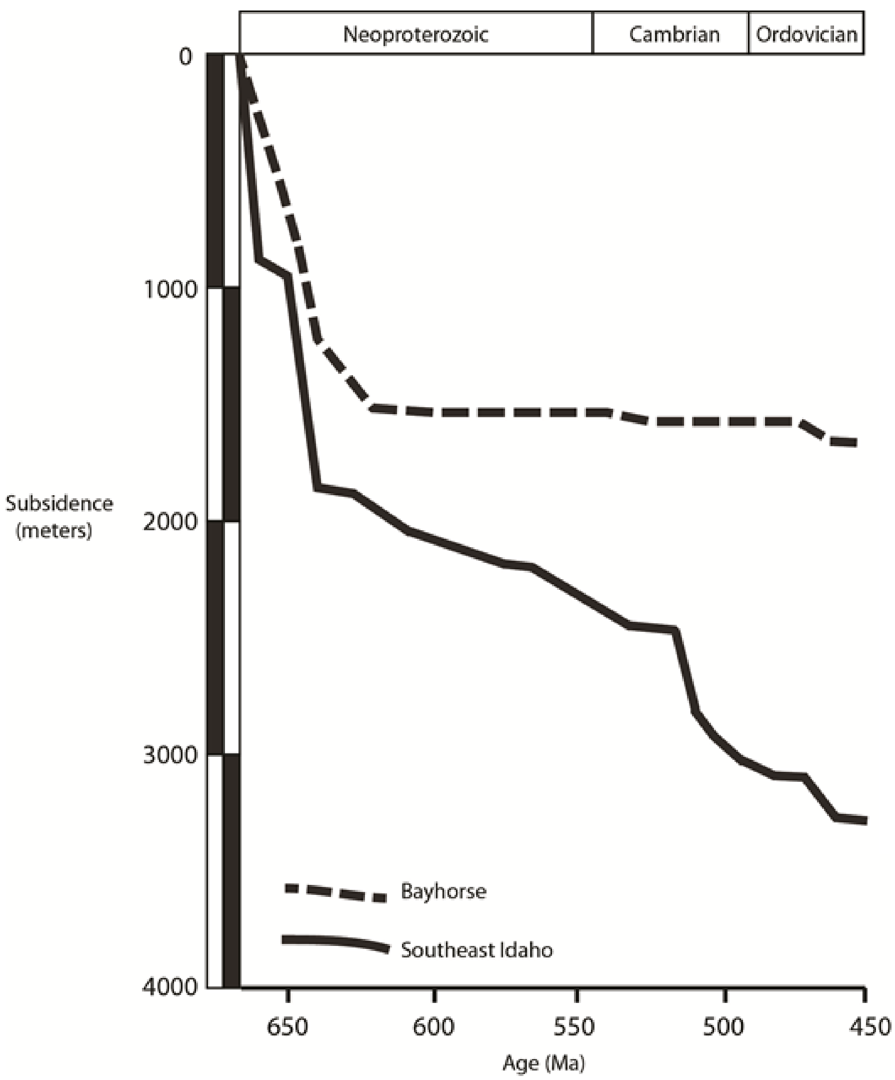

Figure 5.6- Cryogenian to Middle Ordovician generalized tectonic subsidence curves for the Bayhorse region (dashed line) and southeast Idaho (solid line). Note how southeast Idaho shows two distinct concave up intervals at approximately 650 and 520 Ma, interpreted here to represent two distinct rifting intervals. The initial concave up shape at Bayhorse is like southeast Idaho until about 600 Ma, after which Bayhorse experiences minimal subsidence.

Proposed Depth-Dependent Extension Model

Lund (2008) applied the detachment model (Lister, 1986) to the Cordilleran margin and proposed an “upper-plate” domain for central Idaho. Observations of: (1) relatively thin miogeoclinal strata, and relatively narrow continental shelf facies belt (Sloss, 1950; Scholten 1957; Armstrong, 1975a), (2) the Cryogenian and Late Cambrian-Early Ordovician Big Creek-Beaverhead belt (Lund et al., 2010), (3) the Lemhi arch (Sloss, 1954; Scholten 1957; Ruppel 1986), (5) the Late Cambrian Worm Creek basin along an oblique Snake River transfer fault (Link et al., 2017b) and (6) aeromagnetic and isotopic data indicating that North American basement is present and extended but not offset across central Idaho beneath the miogeocline (Armstrong et al., 1977; Sims et al., 2005) have been cited as evidence to support an “upper-plate” domain. This model has been applied to other “ancient” rifted margins (Karner and Driscoll, 1999; Thomas, 2011).

However, studies of modern rifted margins display a first-order structural similarity consisting of a seaward arrangement of distinct domains (Peron-Pinvidic et al., 2013; Cadenas et al., 2018) that are not easily explained by the detachment model. I argue that current models as applied to ancient rifted margins fail to explain these features observed in modern margins. This failure, in addition to the newly recognized presence of regionally correlative stratigraphy at Bayhorse, requires re-evaluation of central Idaho as an “upper-plate” domain.

Finite-element thermomechanical numerical modeling has suggested that the two end members of magma-poor margins can be explained by depth-dependent extension resulting from lower crustal rheological differences (Huismans and Beaumont, 2011). In this depth-dependent extensional modeling, strengthened lower lithosphere prevents decoupling between the lower and upper lithosphere. In these regions, the lower lithosphere necks viscously while the upper lithosphere fails by faulting. This results in a narrow region across which the crust thins abruptly and resulting sedimentation is minimal; the adjacent rift flank experiences uplift and exhumation, and the transition to a true passive margin with establishment of a spreading center is delayed (Huismans and Beaumont, 2011). This is consistent with our observations in central Idaho during the deposition of thinned and missing Upper Ediacaran to Lower Ordovician strata.

Regions of extension within a weak lower-crustal domain result in the upper lithosphere decoupling from the lower lithosphere over a wide region; this results in distributed extension across a wide region and shallow water conditions in wide spread 'sag basins' (Huismans and Beaumont, 2011). This appears to be consistent with relations in southeast Idaho, during the deposition of thick upper Cambrian and Lower Ordovician carbonate rocks. The marine platform lithologies of these rocks require long-lived relatively shallow depositional conditions, consistent with this model.   However, in the depth-dependent model, the proposed Snake River Transfer fault (Lund, 2008; Link et al., 2017b) likely separated a region of strengthened crust to the north from one of weaker crust to the south, as opposed to an "upper-plate" domain to the north from a "lower-plate" domain to the south as previously suggested (Lund, 2008).

Applying this numerically-derived depth-dependent model to "real-world" observations in the analogous magma-poor modern Iberia-Newfoundland system (Peron-Pinvidic et al., 2013; Beranek et al., 2017), it appears that during the first phase of Laurentian rifting from ca. 720 to 660 and early regional, broad subsidence from ca. 660 to 580 Ma (Yonkee et al., 2014), the necking domain (where extension is localized) was outboard (oceanward) of the Mesoproterozoic-strengthened lower crust in central Idaho. Thus, the focused extension and crustal thinning of the "necking domain" was taking place in relatively homogenous lithosphere throughout central and southeast Idaho. This resulted in similar subsidence rates and associated correlative sedimentation during the initial phase of rifting recognized west of the Lemhi arch.

During the final phase of rifting, volcanism, and transition to drift from ~570 to 530 Ma (Yonkee et al., 2014), the original necking domain was unsuccessful and abandoned, resulting in a new domain of focused extension forming inboard (towards the continent). In southeast Idaho, the lack of a strengthened lower crust allowed decoupling and quick oceanward migration of the necking domain, resulting in the transition to a passive margin by the Early Cambrian. In central Idaho, the new necking domain encountered strengthened lower crust that resisted decoupling (Fig. 5.8). This resulted in the upper crust failing by faulting at the inboard "proximal domain," forming the rotated fault block of the Lemhi arch (Hansen, 2015; Pearson et al., 2016) with associated rift flank uplift and exhumation occurring simultaneously. These processes could account for the exhumation of the Lemhi arch, the regionally extensive Late Cambrian unconformity west of the Lemhi arch, and a later transition to a passive margin observed in central Idaho.

It is also possible that this stranded fault block of the Lemhi arch and its resistance to extension resulted in localized loading, flexural subsidence, and minor magnitudes of extension that were accommodated east of the arch in southwestern Montana (Fig. 5.7). Potentially this is observed in the Neoproterozoic (and Cambrian?) reactivation of Mesoproterozoic extensional features in the Central Montana trough (Sloss, 1950; Price and Sears, 2000; Sears, 2007) as well as resulted in the ~600 m of Middle and Upper Cambrian strata deposited in southwest Montana during Lemhi arch exhumation (Link et al., 2017b).

Hypothetically, if these minor rates of extension east of the Lemhi arch were to have continued, I suggest that this ancient structure would be analogous to the modern Le Danois

High, found just north of the Iberian Peninsula (Cadenas et al., 2018). The Le Danois High is considered a rift-related stranded continental block and separates two distinctive extensional domains (Cadenas et al., 2018). Sedimentary cover is observed to thin toward the Le Danois High. Additionally, seismic data suggests an exhumation and/or erosional surface of tilted basement underlies this thin sedimentary cover on the Le Danois High (Cadenas et al., 2018).

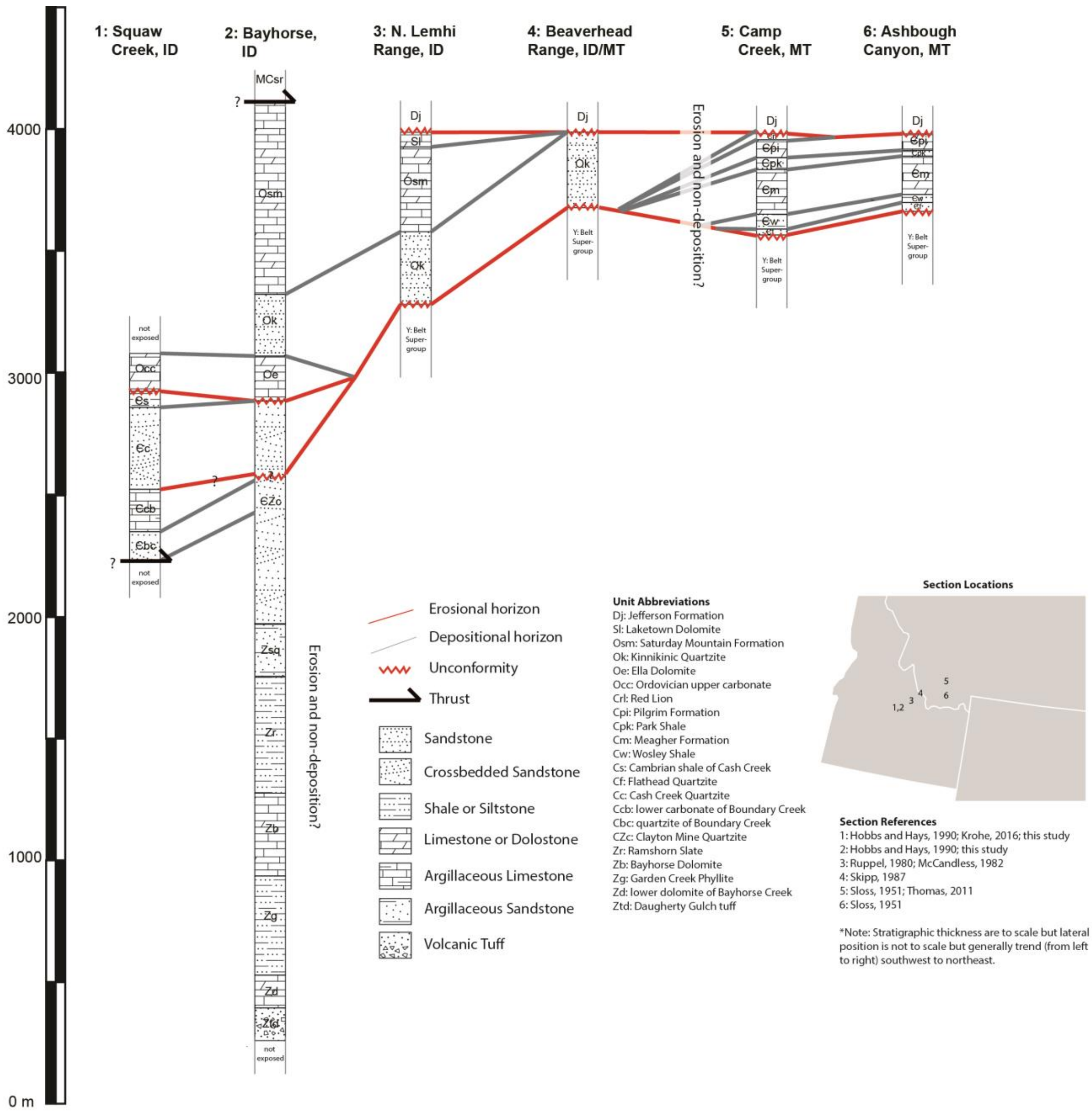

Figure 5.7- Lithostratigraphic columns from a southwest to northeast traverse across the Lemhi Arch. Stratigraphic section locations and references are listed above. The comparison of these lithologies and thickness emphasizes the differences present in tectonostratigraphic architecture, west of the Lemhi arch (sections 1 and 2), the Lemhi Arch (3 and 4) and east of the Lemhi Arch in the Montana Trough (4 and 5). This traverse is generally perpendicular to the trend of the Lemhi Arch and the inferred Neoproterozoic and Cambrian rifted margin of Laurentia through central Idaho.

When compared to other magma-poor rifted margins, the breakup and rift evolution of the Cordilleran margin is more prolonged (Beranek, 2017). I also speculate that this may be due to a long period of tectonic quiescence prior to rifting in the Cordilleran margin. The most recent orogenic event affecting the Cordillera margin of Laurentia dates roughly a billion years prior to rifting (recorded as metamorphism within the Farmington zone; Mueller et al., 2011). In contrast, modern analogous margins (such as the Iberian-Newfoundland system), prior crustal thickening predates the opening of the Atlantic by < 150 million years (Silurian, Acadian orogenesis; Dunning et al., 1990; followed by the onset of rifting in Permian time; Peron-Pinvidic et al., 2013). It has long been proposed (Holmes, 1926) that previously thickened crust is predisposed to gravitational collapse and related extension (Spencer and Kirkland, 2016).

Figure 5.8- Paleogeographic maps showing interpreted sediment sources, depositional environments, and schematic fault geometry (SRTF- Inferred Snake River transfer fault, LA-Lemhi arch). Basement rocks are labeled (adapted from Balgord et al., 2013; Yonkee et al., 2014). Note the location of Bayhorse is approximate, as Sevier shortening magnitudes in central Idaho are not well constrained. Phase A – Deposition of UMG in intracratonic basin. Phase B – Initial rifting resulted in relatively uniform subsidence and sedimentation across central and southeast Idaho. Phase C – Depth-dependent extension. North of the SRTF, central Idaho resisted extension due to the rift encountering strengthened crust. This resulted in minimal sedimentation, initial Lemhi arch (Salmon River arch?) exhumation (contributing detritus off the Big Creek plutons), and a curved margin separated by a dextral fault. Potentially the margin was intermittently isolated north of the hypothesized SRTF. South of the SRTF, the margin experienced a wide region of thinning and subsidence. Schematic cross sections adapted from Huismans and Beaumont (2011). Note how the central Idaho continental and mantle lithosphere were coupled due to strengthening by the Elk City Domain. Phase D – The margin south of the SRTF is passive by this time. North of the SRTF, central Idaho experienced final rifting while actively being exhumed and shedding detritus off the Beaverhead plutons.

Figure 5.8

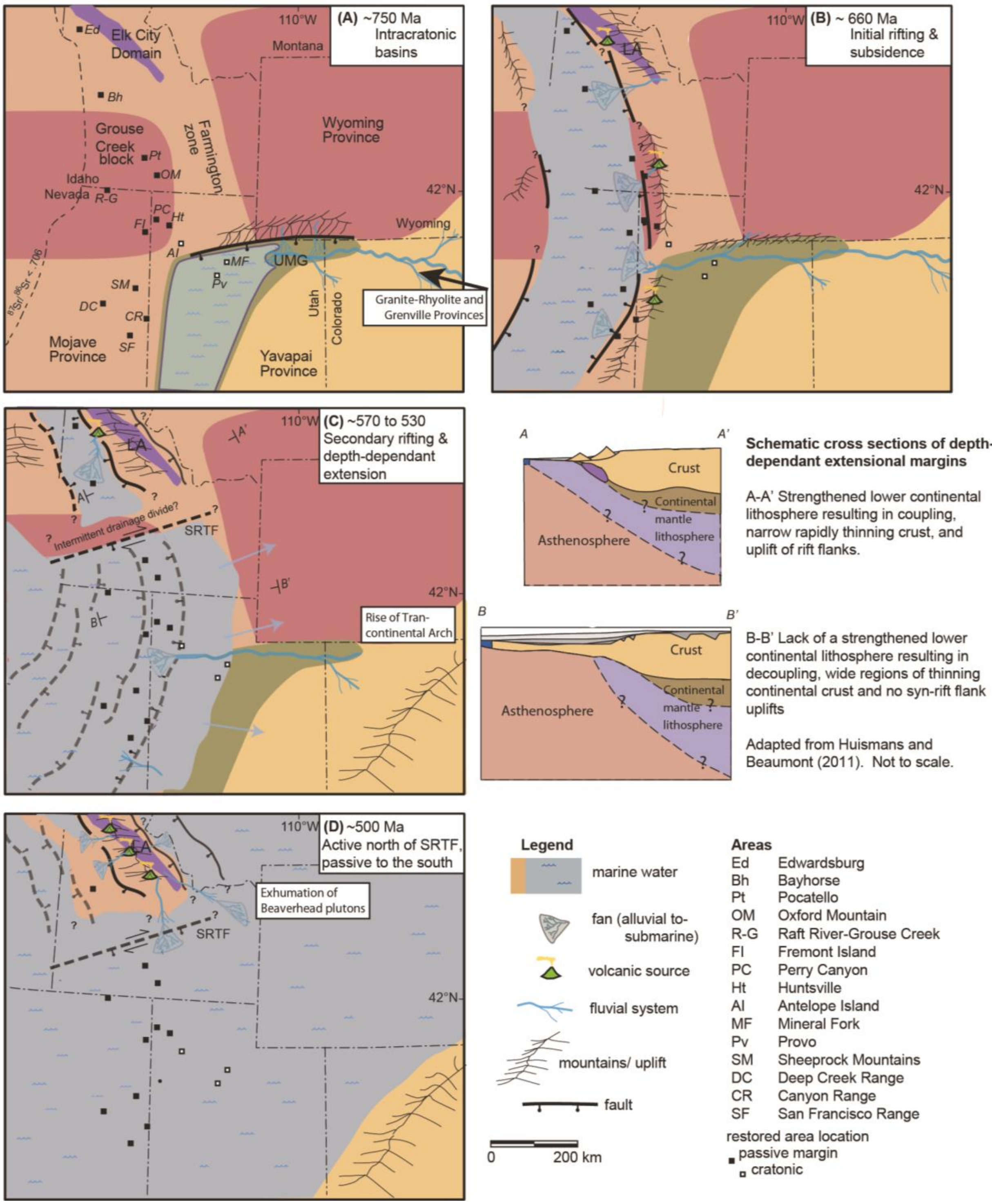
(A) ~750 Ma Intracratonic basins
Elk City Domain
Grouse Creek block
Farmington zone
Wyoming Province
Montana
Idaho
Nevada
Wyoming
Utah
Colorado
Mojave Province
Yavapai Province
UMG
Granite-Rhyolite and Grenville Provinces
(B) ~ 660 Ma Initial rifting & subsidence
LA
(C) ~570 to 530 Secondary rifting & depth-dependant extension
Intermittent drainage divide?
SRTF
Rise of Tran-continental Arch
(D) ~500 Ma Active north of SRTF, passive to the south
Exhumation of Beaverhead plutons
110°W
42°N
Schematic cross sections of depth-dependant extensional margins
Crust
Continental mantle lithosphere
Asthenosphere
A-A' Strengthened lower continental lithosphere resulting in coupling, narrow rapidly thinning crust, and uplift of rift flanks.
B-B' Lack of a strengthened lower continental lithosphere resulting in decoupling, wide regions of thinning continental crust and no syn-rift flank uplifts
Adapted from Huismans and Beaumont (2011). Not to scale.
Legend
marine water
fan (alluvial to-submarine)
volcanic source
fluvial system
mountains/ uplift
fault
0 200 km
Areas
Ed Edwardsburg
Bh Bayhorse
Pt Pocatello
OM Oxford Mountain
R-G Raft River-Grouse Creek
FI Fremont Island
PC Perry Canyon
Ht Huntsville
AI Antelope Island
MF Mineral Fork
Pv Provo
SM Sheeprock Mountains
DC Deep Creek Range
CR Canyon Range
SF San Francisco Range
restored area location
passive margin
cratonic

CHAPTER 6: CONCLUSIONS

Cryogenian to Cambrian sedimentary units have long been known to be absent in east-central Idaho across the Lemhi arch and were generally thought to also be absent west of this feature in central Idaho. However, the results of this study establish the presence of a relatively intact and unmetamorphosed section of Cryogenian to Lower Cambrian sedimentary units, west of the Lemhi arch in central Idaho, that were formerly thought to be Ordovician (Hobbs et al., 1991; Krohe, 2016). Furthermore, the newly identified section demonstrates a strong correlation to the similar-age sections in southeast Idaho. This suggests that Neoproterozoic stratigraphy was once continuous from southeast Idaho through central Idaho. The primary conclusions from this study include:

1: The stratigraphy of the Bayhorse anticline lies in stratigraphic continuum above the 667 Ma tuff of the Daugherty Gulch borehole.

2: Instead of previously interpreted relations that involve major thrust faults, our mapping documents that stratigraphically higher quartzites (Clayton Mine Quartzite) lie above shales (Ramshorn Slate) with an approximately 200-meter gradational stratigraphic contact that consists of upwards-coarsening shale and siltstone to interlayered quartzite, shaly quartzite, and finally predominantly quartzite.

3: The lithologies, detrital zircon populations, and volcanic ages found in the Bayhorse section (tuff of Daugherty Gulch through the Ramshorn Slate) and in the lower Clayton Mine Quartzite show strong similarities to the Pocatello Formation and lower Brigham Group of southeast Idaho.

4: Approximately 2.5 km of Upper Cambrian and Lower Ordovician carbonates present in the correlative southeast Idaho section are missing at Bayhorse, as Middle Ordovician Ella Dolomite unconformably overlies the Lower Cambrian Clayton Mine Quartzite.

5. A slightly more complete Cambrian section is present at Squaw Creek. Following the interpretation of Hobbs et al. (1991), I interpret this section to lie on the hanging wall of a thrust. This section likely partially correlates with the upper Clayton Mine Quartzite.

6: The Clayton Mine Quartzite, Cash Creek Quartzite, and Camelback Mountain Formation record the uplift of the Transcontinental Arch and the resulting disruption of a sediment transport network sourcing a distal provenance (Grenville) and subsequent sourcing to a more proximal provenance (Yavapai-Mazatzal, GFTZ, and/or Swift Anorogenic Province) at approximately 540 Ma.

7. The widespread absence of Upper Cambrian and Lower Ordovician strata in central Idaho supports previous evidence that central Idaho was tectonically active until the Early Ordovician, while southeast Idaho transitioned to a passively subsiding margin by the Early Cambrian.

Considering these new observations, I suggest that the initial Neoproterozoic rifting (~720 to 660 Ma) was relatively uniform in timing and structure from southeast Idaho through central Idaho west of the Lemhi arch. However, during the next stage (~660 to 580 Ma) of broad subsidence with deposition of mature siliciclastic strata of the lower Brigham Group and its correlatives, central Idaho began to deviate in its evolution from the rest of Cordilleran margin. During this time, sedimentation in central Idaho may have occurred in isolated basins. While the rest of the margin was experiencing final rifting, volcanism, and transition to drift from ~570 to

520 Ma, central Idaho experienced minimal subsidence. After this period of final rifting, most of the margin transitioned to regional subsidence along a now passive margin, marked by the deposition of Middle Cambrian and Ordovician carbonate-rich strata. However, while the rest of the margin had transitioned to passive subsidence, central Idaho experienced volcanism, exhumation, and final rifting. This is indicated by the absence of thick carbonate platform strata west of the Lemhi arch, and active exhumation of the Beaverhead plutons.

I further suggest that these variations in the tectonostratigraphic architecture of the Laurentian margin advocate for a style of rifting that can allow two different proposed structural domains to experience similar initial rifting processes, followed by significant deviation between these domains during the final rifting process. I propose that a magma-poor, depth-dependent rifting model, controlled principally by the rheology of the pre-rifted lithosphere, can explain these tectonostratigraphic differences observed in the Neoproterozoic to lower Paleozoic strata of Idaho and southwestern Montana.

References

Amato, J.M., and Mack, G.H., 2012, Detrital zircon geochronometry from the Cambrian–Ordovician Bliss Sandstone, New Mexico: Evidence for contrasting Grenville-age and Cambrian sources on opposite sides of the transcontinental Arch: Geological Society of America Bulletin, v. 124, p. 1826–1840, doi: 10 .1130 /B30657 .1.

Anderson, H.E., and Davis, D.W. 1995. U–Pb geochronology of the Moyie Sills, Purcell Supergroup, southeastern British Columbia: Implications for the Mesoproterozoic geological history of the Purcell (Belt) Basin: Canadian Journal of Earth Sciences, v. 32, no. 8, p. 1180–1193, doi:10.1139/e95-097.

Armstrong, F.C., and Oriel, S.S., 1982, Tectonic development of the Idaho-Wyoming thrust Belt: in Peterson, J. A., ed., Paleotectonics and Sedimentation, American Association of Petroleum Geologists Memoir 41, p. 243-279.

Armstrong, R.L., 1975a, Precambrian (1500 m.y. old) rocks of central Idaho - The salmon river arch and its role in cordilleran sedimentation and tectonics: American Journal of Science, v. 275, p. 437–467.

Armstrong, R.L., 1975b, The geochronometry of Idaho: Isochron/West, no. 14, p. 1-50.

Armstrong, R.L., Taubeneck, W.H., and Hales, P.O., 1977, Rb-Sr and K-Ar geochronometry of Mesozoic granitic rocks and their Sr isotopic composition, Oregon, Washington, and Idaho: Geological Society of America Bulletin, v. 88, p. 397–411.

Armstrong, R.L., and Ward, Peter, 1991, Evolving geographic patterns of Cenozoic magmatism in the North American Cordillera—The temporal and spatial association of magmatism and metamorphic core complexes: Journal of Geophysical Research, v. 96, no. B8, p. 13201–13224.

Bahlburg, H., Vervoort, J.D., Andrew DuFrane, S., Carlotto, V., Reimann, C., and Cárdenas, J., 2011, The U-Pb and Hf isotope evidence of detrital zircons of the Ordovician Ollantaytambo Formation, southern Peru, and the Ordovician provenance and paleogeography of southern Peru and northern Bolivia: Journal of South American Earth Sciences, v. 32, p. 196–209, doi: 10.1016/j.jsames.2011.07.002.

Balgord, E.A., Yonkee, W.A., Link, P.K., and Fanning, C.M., 2013, Stratigraphic, geochronologic, and geochemical record of the Cryogenian Perry Canyon Formation, Northern Utah: Implications for Rodinia rifting and snowball earth glaciation: Bulletin of the Geological Society of America, v. 125, p. 1442–1467, doi: 10.1130/B30860.1.

Bennett, E.H., 1986, Relationship of the trans-Challis fault system in central Idaho to Eocene and Basin and Range extensions: Geology, v. 14, no. 6, p. 481-484, doi: 10.1130/0091-7613(1986)14<481:ROTTFS>2.0.CO;2.

Beranek, L.P., 2017, A magma-poor rift model for the Cordilleran margin of western North America: Geology, v. 45, p. 1115–1118, doi: 10.1130/G39265.1.

Beranek, L.P., Link, P.K., and Fanning, C.M., 2016, Detrital zircon record of mid-Paleozoic convergent margin activity in the northern U.S. Rocky Mountains: Implications for the Antler orogeny and early evolution of the North American Cordillera: Lithosphere, v. 8, p. 533–550, doi: 10 .1130 /L557 .1

Berry, R.F., Holm, O.H., Steele, D.A., 2005. Chemical U–Th–Pb monazite dating and the Proterozoic history of King Island, southeast Australia: Australian Journal of Earth Science, v. 52, p. 461–471.

Borg, S.G., and DePaolo, D.J., 1994. Laurentia, Australia, and Antarctica as a Late Proterozoic supercontinent: constraints from isotopic mapping: Geology, v. 22, p. 307–310.

Bickford, M.E., Mueller, P.A., Kamenov, G.D., Hill, B.M., 2008. Crustal evolution of southern Laurentia during the Paleoproterozoic: insights from zircon Hf isotopic studies of ca. 1.75 Ga rocks in central Colorado: Geology, v. 36, p. 555–558.

Brennan, D., Pearson, D.M., and Link, P.K., 2017, Rodinia, Rifting, and the Ramshorn Slate: Geologic mapping of the Bayhose area, central Idaho reassigns the age of poorly understood stratigraphy from Ordovician to Neoproterozoic, GSA Abstracts with Programs.

Burchfiel, B.C., and Royden, L.H., 1991, Antler orogeny: a Mediterranean-type orogeny: Geology, v. 19, p. 66–69, doi: 10.1130/0091-7613(1991)019<0066:AOAMTO>2.3.CO;2.

Burmester, R.F., Lonn, J.D., Lewis, R.S., and Mcfaddan, M.D., 2016, Stratigraphy of the Lemhi subbasin of the Belt Supergroup: GSA Special Paper, v. 522, p. 1–17, doi: 10.1130/2016.2522(05).

Bush, J., Thomas, R.C., and Pope, M.C., 2012, Sauk megasequence deposition in northeastern Washington, northern Idaho, and western Montana, in Derby, J.R., Fritz, R.D., Longacre, S.A., Morgan, W.A., and Stomach, C.A., eds., The great American carbonate bank: The geology and economic resources of the Cambrian-Ordovician megasequence of Laurentia: American Association of Petroleum Geologists Memoir 98, p. 751-768.

Cadenas, P.,G. Fernández-Viejo, J. A. Pulgar, J. Tugend, G. Manatschal, and T. Minshulll, 2018, Constraints imposed by rift inheritance on the compressional reactivation of a hyperextended margin: Mapping rift domains in the North Iberian margin and in the Cantabrian Mountains: Tectonics, 28 p., doi: 10.1002/2016TC004454.

Carr, J., and Link, P.K., 1999, Neoproterozoic conglomerate and breccia in the formation of Leaton Gulch, Grouse Peak, northern Lost River Range, Idaho: Relation to Beaverhead impact structure, in Hughes, S.S., and Thackray, G.D., eds., Guidebook to the geology of eastern Idaho: Pocatello, Idaho Museum of Natural History, p. 21–29.

Camp, V.E., Pierce, K.L., Morgan, L.A., Survey, U.S.G., Rocky, N., and Science, M., 2015, Yellowstone plume trigger for Basin and Range extension, and coeval emplacement of the Nevada – Columbia Basin magmatic belt: Geosphere, v. 11, p. 203–225, doi: 10.1130/GES01051.1.

Cheney, E.S., and Doughty, P.T., 2017, Overview of Laurentian Rocks in the Pacific Northwest, in Cheney, E.S., ed., The Geology of Washington and Beyond: Washington Division of Geology and Earth Resources, p. 23-27.

Crittenden, M.D., Jr., 1988, Bedrock Geologic Map of the Promontory Mountains, Box Elder County, Utah: U.S. Geological Survey Open-File Report 88–646, scale 1:100,000.

Christiansen, R.L., Foulger, G.R., Evans, J.R., 2002. Upper mantle origin of the Yellowstone hotspot. Geological Society of America Bulletin 114, 1245–1256.

Christie-Blick, N., Grotzinger, J.P., and van der Borch, C.C., 1988, Sequence stratigraphy in Proterozoic successions: Geology, v. 16, p. 100–104.

Collerson, K.D., Van Schmus, R.W., Lewry, J.F., and Bickford, M.E., 1988, Buried Precambrian basement in south-central Saskatchewan: Provisional results from Sm-Nd model ages and U-Pb zircon geochronology, in Macdonald, R., ed., Summary of Investigations 1988, Saskatchewan Geological Survey: Saskatchewan Department of Energy and Mines Miscellaneous Report 88-4, p. 142–150.

Colpron, M., Logan, J. M., and Mortensen, J. K., 2002, U-Pb zircon age constraint for late Neoproterozoic rifting and initiation of the lower Paleozoic passive margin of western Laurentia: Canadian Journal of Earth Sciences, v. 39, p. 133–143, doi: 10.1139/e01-069.

Coney, P.J., and Harms, T.A., 1984, Cordilleran metamorphic core complexes: Cenozoic extensional relics of Mesozoic compression: Geology, v. 12, p. 550–554.

Corsetti, F.A., Link, P.K., and Lorentz, N.J., 2007, δ13 chemo stratigraphy of the Neoproterozoic succession near Pocatello, Idaho: Implications for glacial chronology and regional correlations, in Link, P.K., and Lewis, R.S., eds., Proterozoic Geology of Western North America and Siberia: SEPM (Society for Sedimentary Geology) Special Publication 86, p. 193–208.

Dalziel, I.W.D., 1991, Pacific margins of Laurentia and East Antarctica- Australia as a conjugate rift pair: Evidence and implications for an Eocambrian supercontinent: Geology, v. 19, p. 598-601.

DeCelles, P.G., 2004, Late Jurassic to Eocene evolution of the Cordilleran thrust belt and foreland basin system, western USA: American Journal of Science, v. 304, p. 105–168, doi: 10.2475/ajs.304.2.105.

Dehler, C.M., Prave, A.R., Crossey, L.J., Karlstrom, K.E., Atudorei, V., and Porter, S.M., 2001, Linking mid-Neoproterozoic successions in the western U.S.: The Chuar Group–Uinta Mountain Group–Pahrump Group connection (CHUMP): Geological Society of America Abstracts with Programs, v. 33, no. 5, p. 20–21.

Dehler, C.M., Fanning, C.M., Link, P.K., Esther, M., Kings-bury, E.M., and Rybczynski, D., 2010, Incipient Rodinia breakup, marine transgression, and peri-Gondwanan sediment source in western Laurentia at <766 to 742 Ma: New SHRIMP data from the Uinta

Mountain Group and Big Cottonwood Formation, northern Utah: Geological Society of America Bulletin, v. 122, p. 1686–1699, doi: 10.1130 /B30094.1.

Dickinson, W.R., 2004, Evolution of the North American Cordillera: Annual Review of Earth and Planetary Sciences, v. 32, p. 13-45.

Dickinson, W. R., and Snyder, W. S., 1978, Plate tectonics of the Laramide orogeny, in Matthews, V., Ill, ed., Laramide folding associated with basement block faulting in the western United States: Geological Society of America Memoir 151, p. 355-366.

Dickinson, W.R., and Gehrels, G.E., 2009, Use of U-Pb ages of detrital zircons to infer maximum depositional ages of strata: A test against a Colorado Plateau Mesozoic database: Earth and Planetary Science Letters, v. 288, p. 115–125, doi:10.1016/j.epsl.2009.09.013.

Dostal, J., Breitsprecher, K., Church, B.N., Thorkelson, D., and Hamilton, T.S., 2003, Eocene melting of Precambrian lithospheric mantle: Analcime-bearing volcanic rocks from the Challis-Kamloops belt of south central British Columbia: Journal of Volcanology and Geothermal Research, v. 126, p. 303-326.

Doughty, P.T., and Chamberlain, K.R., 1996, Salmon River Arch revisited: new evidence for 1370 Ma rifting near the end of deposition in the Middle Proterozoic Belt basin: Canadian Journal of Earth Sciences, v. 33, p. 1037–1052, doi: 10.1139/e96-079.

Doughty, P.T., and Chamberlain, K.R. 2008. Protolith age and timing of Precambrian magmatic and metamorphic events in the Priest River complex, northern Rockies. Canadian Journal of Earth Sciences, v. 45, no. 1, p. 99–116, doi:10.1139/E07-067.

Evans, K.V., and Zartman, R.E., 1988, Early Paleozoic alkalic plutonism in east-central Idaho: Geological Society of America Bulletin, v. 100, p. 1981–1987, doi: 10 .1130 /0016 -7606 (1988) 100 <1981: EPAPIE>2 .3 .CO;2.

Faccenna, C., Becker, T.W., Lallemand, S., Lagabrielle, Y., Funiciello, F., and Piromallo, C., 2010, Subduction-triggered magmatic pulses: A new class of plumes?: Earth and Planetary Science Letters, v. 299, p. 54–68, doi:10.1016 /j.epsl.2010.08.012

Fanning, C.M., and Link, P.K., 2004, U-Pb SHRIMP ages of Neoproterozoic (Sturtian) glaciogenic Pocatello Formation, southeastern Idaho: Geology, v. 32, p. 881– 884, doi: 10.1130 /G20609.1.

Fioretti, A.M., Black, L.P., Foden, J., Visona, D., 2005. Grenville-age magmatism at the South Tasman Rise (Australia): a new piercing point for the reconstruction of Rodinia: Geology, v. 33, p. 769–772.

Fisher, F.S., McIntyre, D.H., and Johnson, K.M., 1992, Geologic Map of the Challis 1°x2° Quadrangle, Idaho: U.S. Geological Survey Miscellaneous Investigations Series Map, v. I-1819, scale 1:250,000.

Foster, D.A., Mueller, P.A., Mogk, D.W., Wooden, J.L., Vogl, J.J., 2006. Proterozoic evolution of the western margin of the Wyoming craton: implications for the tectonic and magmatic evolution of the northern Rocky Mountains: Canadian Journal of Earth Sciences, v. 43, p. 1601–1619.

Gaschnig, R.M., Vervoort, J.D., Lewis, R.S., and McClelland, W.C., 2010, Migrating magmatism in the northern US Cordillera: In situ U-Pb geochronology of the Idaho batholith: Contributions to Mineralogy and Petrology, v. 159, p. 863–883, doi: 10.1007/s00410-009-0459-5.

Gaschnig, R.M., Vervoort, J.D., Lewis, R.S., and Tikoff, B., 2013, Probing for Proterozoic and Archean crust in the northern U.S. Cordillera with inherited zircon from the Idaho batholith: Bulletin of the Geological Society of America, v. 125, p. 73–88, doi: 10.1130/B30583.1.

Gehrels, G., 2012, Detrital Zircon U-Pb Geochronology: Current Methods and New Opportunities: Tectonics of Sedimentary Basins, p. 45–62, doi: 10.1002/9781444347166.ch2.

Gehrels, G. E., and Pecha, M., 2014, Detrital zircon U-Pb geochronology and Hf isotope geochemistry of Paleozoic and Triassic passive margin strata of western North America: Geosphere, v. 10, p. 49–65, doi:10.1130/GES00889.1.

Gehrels, G.E., Dickinson, W.R., Ross, G.M., Stewart, J.H., and Howell, D.G., 1995, Detrital zircon reference for Cambrian to Triassic miogeoclinal strata of western North America: Geology, v. 23, p. 831–834, doi: 10.1130/0091-7613(1995)023<0831:DZRFCT>2.3.CO;2.

Gehrels, G.E., Valencia, V., Pullen, A., 2006, Detrital zircon geochronology by Laser-Ablation Multicollector ICPMS at the Arizona LaserChron Center, in Loszewski, T., and Huff, W., eds., Geochronology: Emerging Opportunities, Paleontology Society Short Course: Paleontology Society Papers, v. 11, 10 p.

Gehrels, G.E., Valencia, V., Ruiz, J., 2008, Enhanced precision, accuracy, efficiency, and spatial resolution of U-Pb ages by laser ablation–multicollector–inductively coupled plasma–mass spectrometry: Geochemistry, Geophysics, Geosystems, v. 9, Q03017, doi:10.1029/2007GC001805.

Gehrels, G., Chapman, J., Valley. J., 2017, U-TH-Pb Geochronology, O and Hf Isotopes, and Trace Element Geochemistry Applied to Detrital Minerals: Seattle WA, GSA Short Course.

Grew, E.S., 1974, Carbonaceous Material in some Metamorphic Rocks of New England and other areas: The Journal of Geology, v. 82, p. 50–73.

Hagadorn, J.W. and Bottjer, D.J., 1997, Wrinkle structures: Microbially mediated sedimentary structures common in subtidal siliciclastic settings at the Proterozoic-Phanerozoic transition: Geology, v. 25, p. 1047–1050.

Hansen, C.M., 2015, An investigation into the Poison Creek thrust: A Sevier thrust with Proterozoic Implications. [M.S. thesis]: Pocatello, Idaho State University, 79 p.

Harazim, D., Callow, R.T., McIlroy, D., 2013. Microbial mats implicated in the generation of intrastratal shrinkage ('synaeresis') cracks: Sedimentology 60, 1621–1638.

Hargraves, R.B., Ruppel, E.T., and Gephart, J.W., 2007, The Leaton Gulch breccia in east-central Idaho, U.S.A., and its relation to the Beaverhead meteorite impact, in Link, P.K., and Lewis, R.S., eds., Proterozoic geology of western North America and Siberia: SEPM (Society for Sedimentary Geology) Special Publication 86, p. 167–174, doi: 10 .2110 /pec .07 .86 .0167.

Harlan, S.S., Heaman, L., LeCheminant, A.N., Premo, W.R., 2003, Gunbarrel mafic magmatic event: a key 780 Ma time marker for Rodinia plate reconstructions: Geology, v. 31, p. 1053–1056.

Hayward, N., 2015, Geophysical investigation and reconstruction of lithospheric structure and its control on geology, structure, and mineralization in the Cordillera of northern Canada and eastern Alaska: Tectonics, v. 34, p. 2165–2189, doi: 10.1002/2015TC003871.

Hildebrand, R.S., 2009, Did westward subduction cause Cretaceous-Tertiary orogeny in the North American Cordillera: Geological Society of America Special Paper 457, 71 p.

Hobbs, S.W., 1985. Precambrian and Paleozoic sedimentary terranes in the Bayhorse area of the Challis quadrangle, in McIntyre, D. H., eds., Symposium on the geology and mineral deposits of the Challis 1 degree x 2 degree quadrangle, Idaho: U.S. Geological Survey Bulletin, v. 1658, p. 59–68.

Hobbs, S.W. and Hays, W.H., 1990, Ordovician and Older Rocks of the Bayhorse area, Custer County, Idaho: U.S. Geological Survey Bulletin, v., 1891, 40 p.

Hobbs, S. W., W. H. Hays, and R.J. Ross, Jr., 1968, The Kinnikinic Quartzite of central Idaho - redefinition and subdivision: U.S. Geological Survey Bulletin 1254-J, 22 p.

Hobbs, S.W., Hays, W.H., and Mclntyre, D.H., 1975, Geologic map of the Clayton quadrangle, Custer County, Idaho—Description of map units: U.S. Geological Survey Open-File Report 7:5-76, scale 1:62,500.

Hobbs, S.W., Hays, W.H., and McIntyre, D.H., 1991, Geologic map of the Bayhorse area, central Custer county, Idaho: U.S. Geological Survey Miscellaneous Investigations Series Map I-1882, scale 1:62,500.

Hoffman, P.F., 1991, Did the breakout of Laurentia turn Gondwanaland inside-out?: Science, v. 252, p. 1409-1412.

Holmes, A., 1926, Contributions to the theory of magmatic cycles: Geological Magazine, v. 63, p. 306, doi:10.1017/S001675680008448X.

Huismans, R., and Beaumont, C., 2011, Depth-dependent extension, two-stage breakup and cratonic underplating at rifted margins: Nature, v. 473, p. 74–78, doi: 10.1038/nature09988.

Humphreys, E.D., Dueker, K.G., Schutt, D.L., Smith, R.B., 2000, Beneath Yellowstone: evaluating plume and nonplume models using teleseismic images of the upper mantle: GSA Today, v. 10, p. 1–6.

Ingersoll, R.V., 1990, Actualistic sandstone petrofacies: Discriminating modern and ancient source rocks: Geology, v. 18, p. 733–736, doi: 10 .1130 /0091 -7613 (1990) 018 <0733: ASPDMA >2 .3 .CO;2.

Ingersoll, R.V., Kretchmer, A.G., and Valles, P.K., 1993, The effect of sampling scale on actualistic sandstone petrofacies: Sedimentology, v. 40, p. 937–953, doi: 10 .1111 /j .1365 -3091.1993 .tb01370.x.

Isakson, V. H., 2017, Geochronology of the tectonic, stratigraphic, and magmatic evolution of Neoproterozoic to early Paleozoic, North American Cordillera and Cryogenian glaciation [Ph.D. thesis]: Boise State University, 477 p.

Jacob, T., 1990, Late Proterozoic(?) tuff near Challis, Idaho, in Moye, F.J., eds., Geology and Ore Deposits of the Trans-Challis Fault System/Great Falls Tectonic Zone: Guidebook of the Fifteenth Annual Tobacco Root Geological Society Field Conference, Northwest Geology, v. 19, p. 97–106.

Janecke, S.U., Hammond, B.F., Snee, L.W., and Geissman, J.W., 1997, Rapid extension in an Eocene volcanic arc: Structure and paleogeography of an intra-arc half graben in central Idaho: Geological Society of America Bulletin, v. 109, p. 253–267, doi: 10.1130/0016-7606(1997)109<0253: REIAEV>2.3.CO;2.

Johnston, S.T., 2008, The Cordilleran Ribbon Continent of North America: Annual Review of Earth and Planetary Sciences, v. 36, p. 495-530, doi: 10.1146/annurev.earth.36.031207.124331.

Jones, C.H., Sonder, L.J., Unruh, J.R., 1998. Lithospheric gravitational potential energy and past orogenesis: implications for conditions of initial Basin and Range and Laramide deformation: Geology, v. 26, p. 639–642.

Karlstrom, K.E., Williams, M.L., McLelland, J., Geissman, J.W., Ahall, K.I., 1999, Refining Rodinia: geological evidence for the Australia–western U.S. connection in the Proterozoic: GSA Today, v. 9, p. 1–7.

Karner, G.D., and Driscoll, N.W., 1999, Tectonic and stratigraphic development of the West African and eastern Brazilian Margins: insights from quantitative basin modelling: Geological Society, London, Special Publications, v. 153, p. 11–40, doi: 10.1144/GSL.SP.1999.153.01.02.

King, S.D., 2007, Hotspots and edge-driven convection: Geology, v. 35, p. 223–226, doi:10.1130/G23291A.1.

Kovalchuk, O., 2017, Microbial Mat-Related Structures: Laboratory Experiments and Observations from the Mesoproterozoic Belt Supergroup, Southwestern Montana [M.S. Thesis]: University of Alberta 105 p.

Krohe, Nicholas, 2016, Structural Framework and Detrital Zircon Provenance of the Southern Portion of the Clayton Quadrangle Custer County, Idaho. [M.S. Thesis] Pocatello, Idaho State University, 206 p, 1 plate.

Lewis, R.S., Vervoort, J.D., Burmester, R.F., and Oswald, P.J., 2010, Detrital zircon analysis of Mesoproterozoic and Neoproterozoic metasedimentary rocks of north-central Idaho: Implications for development of the Belt-Purcell basin: Canadian Journal of Earth Sciences, v. 47, no. 11, p. 1383–1404.

Lewis, R.S., Link, P.K., Stanford, L.R., and Long, S.P., 2012, Geologic map of Idaho: Idaho Geological Survey Map M-9, scale 1:750,000.

Li, Z.X., Zhang, L., Powell, C.M., 1995. South China in Rodinia: part of the missing link between Australia–East Antarctica and Laurentia?: Geology, v. 23, p. 407–410.

Li, Z.X., Bogdanova, S.V., Collins, A.S., Davidson, A., De Waele, B., Ernst, R.E., Fitzsimons, I.C.W., Fuck, R.A., Gladkochub, D.P., Jacobs, J., Karlstrom, K.E., Lu, S., Natapov, L.M., Pease, V., Pisarevsky, S.A., Thrane, K., and Vernikovsky, V., 2008, Assembly, configuration, and break-up history of Rodinia: A synthesis: Precambrian Research, v. 160, no. 1–2, p. 179–210, doi:10.1016/j.precamres.2007.04.021.

Linde, G.M., Cashman, P.H., Trexler, J.H., and Dickinson, W.R., 2014, Stratigraphic trends in detrital zircon geochronology of upper Neoproterozoic and Cambrian strata, Osgood Mountains, Nevada, and elsewhere in the Cordilleran miogeocline: Evidence for early Cambrian uplift of the Transcontinental Arch: Geosphere, v. 10, p. 1402–1410, doi: 10.1130 /GES01048.1.

Link, P.K., and Janecke, S.U., 1999, Geologic Roadlogs for the Big and Little Lost River, Lemhi, and Salmon River Valleys, in Hughes, S.S., and Thackray, G.D., eds. Guidebook to the Geology of Eastern Idaho: Idaho Museum of Natural History, v. 1, p. 295-334.

Link, P. K., and Phoenix, E. C., 1996, Rocks, Rails, and Trails: Idaho Museum of Natural History, Pocatello, 194 p.

Link, P.K., Jansen, S.T., Halimdihardja, P., Lande, A., Zahn, P., 1987, Stratigraphy of the Brigham Group (Late Proterozoic–Cambrian), Bannock, Portneuf, and Bear River Ranges, southeastern Idaho: Thirty-eighth Field Conference, Wyoming Geological Association Guidebook, pp. 133–148.

Link, P.K., and Janecke, S.U., 1999, Geology of east-central Idaho: Geologic roadlogs for the Big and Little Lost River, Lemhi, and Salmon River valleys, in Hughes, S.S., and Thackray, G.D., eds., Guidebook to the geology of eastern Idaho: Pocatello, Idaho Museum of Natural History, p. 295–334.

Link, P.K., et al., 1993, Middle and Late Proterozoic stratified rocks of the western U.S. Cordillera, Colorado Plateau, and Basin and Range Province, in Reed, J.C., et al., eds., Precambrian: Conterminous U.S.: Boulder, Colorado, Geological Society of America, Geology of North America, v. C-2, p. 463–595, doi: 10 .1130 /DNAG -GNA -C2 .463.

Link, P.K., Fanning, C.M., Beranek, L.P., 2005. Reliability and longitudinal change of detrital-zircon age spectra in the Snake River system, Idaho and Wyoming: an example of reproducing the bumpy barcode. Sedimentary Geology 182, 101–142.

Link, P.K., Fanning, C.M., Lund, K.I., and Aleinikoff, J.N., 2007, Detrital-zircon populations and provenance of Mesoproterozoic strata of east-central Idaho, U.S.A.: Correlation with Belt Supergroup of southwest Montana, in Link, P.K., and Lewis, R.S., eds., Proterozoic geology of western North America and Siberia: Society of Economic Paleontologists and Mineralogists Special Publication 86, p. 101–128, doi: 10.2110 /pec .07 .86. 0101.

Link, P.K., Mahon, R.C., Beranek, L.C., Campbell-Stone, E.A., and Lynds, R., 2014, Detrital Zircon Provenance of Pennsylvanian to Permian Sandstones from the Wyoming Craton and Wood River Basin, Idaho, U.S.A.: Rocky Mountain Geology, v. 49, p. 115–136, doi: 10.2113/gsrocky.49.2.115.

Link, P.K., Stewart, E.D., Steel, T., Sherwin, J.-A., Hess, L.T., and McDonald, C., 2016, Detrital zircons in the Mesoproterozoic upper Belt Supergroup in the Pioneer, Beaverhead and Lemhi Ranges, Montana and Idaho: The Big White arc, in Maclean J.S, and Sears, J.W. eds., Belt Basin: Window to the Mesoproterozoic Earth: Geological Society of America Special Paper 522, doi: 10 .1130 /2016 .2522 (07).

Link, P.K., Autenrieth-Durk, K.M., Cameron, A., Fanning, C.M., Vogl, J.J., and Foster, D.A., 2017a, U-Pb zircon ages of the Wildhorse gneiss, Pioneer Mountains, south-central idaho, and tectonic implications: Geosphere, v. 13, p. 681–698, doi: 10.1130/GES01418.1.

Link, P.K., Todt, M.K., Pearson, D.M., and Thomas, R.C., 2017b, 500–490 Ma detrital zircons in Upper Cambrian Worm Creek and correlative sandstones, Idaho, Montana, and Wyoming: Magmatism and tectonism within the passive margin: Lithosphere, v. 9, p. 1–17, doi: 10.1130/L671.1.

Lister, G.S., Etheridge, M.A., and Symonds, P.A., 1986, Detachment faulting and the evolution of passive continental margins: Geology, v. 14, p. 246–250, doi: 10 .1130 /0091 -7613 (1986) 14 <246: DFATEO>2 .0 .CO;2.

Livaccari, R.F., Burke, K., and Sengor, A.M.C., 1981, Was the Laramide orogeny related to the subduction of an Oceanic plateau? Nature, v. 289, p. 276-278.

Ludwig, K.R., 2008, User’s manual for Isoplot 3.70: a geochronological toolkit for Microsoft Excel: Berkeley Geochronology Center Special Publication no. 4, p. 1-76.

Lund, K., 2008, Geometry of the Neoproterozoic and Paleozoic rift margin of western Laurentia: Implications for mineral deposit settings: Geosphere, v. 4, p. 429–444, doi: 10.1130/GES00121.1.

Lund, K., Aleinikoff, J.N., Evans, K.V., Fanning, C.M., 2003, SHRIMP U–Pb geochronology of Neoproterozoic Windermere Supergroup, central Idaho; implications for rifting of western Laurentia and synchroneity of Sturtian glacial deposits: Geological Society of America Bulletin, v. 15, p. 349–372.

Lund, K., Aleinikoff, J.N., Evans, K.V., duBray, E.A., Dewitt, E.H., and Unruh, D.M., 2010, SHRIMP U-Pb dating of recurrent Cryogenian and Late Cambrian–Early Ordovician alkalic mag- matism in central Idaho: Implications for Rodinian rift tectonics: Geological Society of America Bulletin, v. 122, p. 430–453, doi: 10 .1130 /B26565 .1.

Ma, Chong, Bergeron, P., Foster, D.A., Dutrow, B.L., Mueller, P.A., and Allen, C., 2016, Detrital zircon geochronology of the Sawtooth metamorphic complex, Idaho: Evidence for metamorphosed lower Paleozoic shelf strata within the Idaho batholith: Geosphere, v. 12, p. 1136–1153, doi: 10 .1130 /GES01201 .1.

Mahon, R.C., Dehler, C.M., Link, P.K., Karlstrom, K.E., and Gehrels, G.E., 2014, Geochronologic and stratigraphic constraints on the Mesoproterozoic and Neoproterozoic Pahrump Group, Death Valley, California: A record of the assembly, stability, and breakup of Rodinia: Bulletin of the Geological Society of America, v. 126, p. 652–664, doi: 10.1130/B30956.1.

Malone, D.H., Craddock, J.P., and Kenderes, S., 2017, Detrital zircon geochronology and prov- enance of the Middle Cambrian Flathead Sandstone, Park County, Wyoming: The Mountain Geologist, v. 54, p. 86–103.

Matthews, W., Guest, B., and Madronich, L., 2018, Latest Neoproterozoic to Cambrian detrital zircon facies of western Laurentia: Geosphere, v. 14, p. 243–264, doi: 10.1130/GES01544.1.

McCandless, D.O., 1982, A reevaluation of Cambrian through Middle Ordovician stratigraphic of the southern Lemhi Range [M.S. Thesis]: University Park, The Pennsylvanian State University, 235 p.

McInyre, D.H., and Hobbs, S.W., 1987. Geologic map of the Challis Quadrangle, Custer and Lemhi Counties, Idaho: U.S. Geological Survey Geologic Quadrangle Map GQ-1599, scale 1:62,500.

McIntyre, D. H., Hobbs, S. W., Marvin, R.F., and Mehnert, H. H., 1976, Late Cretaceous and Eocene ages for hydrothermal alteration and mineralization, Bayhorse district and vicinity, Custer County, Idaho: Isohron/West, no. 16, p. 11-12.

McIntyre, D.H., Ekren, E.D. and Hardyman, R.F., 1982, Stratigraphic and structural framework of the Challis volcanics in the eastern half of the Challis 1 x 2 quadrangle, Idaho: Bulletin of Idaho Bureau of Mines and Geology, v. 26, p. 155-177.

McMechan M. E. and Price R. A., 1982, Superimposed low-grade metamorphism in the Mount Fisher area, southeastern British Columbia- implications for the East Kootenay orogeny: Canadian Journal of Earth Sciences, v. 19, p. 476-489.

McQuarrie, N., and Rodgers, D.W., 1998, Subsidence of a volcanic basin by flexure and lower crustal flow: The eastern Snake River Plain, Idaho: Tectonics, v. 17, p. 203–220, doi: 10.1029/97TC03762.

Medig, K.P.R., 2016, Sedimentology, Geochemistry, and Geochronology of unit PR1 of the lower Fifteenmile group and the Pinguicula Group, Wernecke and Ogilvie Mountains, Yukon, Canada: Mesoproterozoic environments and paleocontinental reconstructions. [Phd Thesis]: Simon Fraser University, 263 p.

Meyers, J., 2014, Eocene magmatic evolution and synchronous to subsequent extensional faulting, Little Wood River Reservoir Quadrangle, Blaine County Idaho, [M.S. Thesis]: Pocatello, Idaho State University, 64 p.

Mitra, G., Yonkee, W.A., Gentry, D., 1984, Solution cleavage and its relationship to major structures in the Idaho-Utah-Wyoming thrust belt: Geology, no. 12, p. 354–358.

Mitra, G., Yonkee, W.A., 1985, Spaced cleavage and its relationship to folds and thrusts in the Idaho-Utah-Wyoming thrust belt of the Rocky Mountain Cordilleras: Journal of Structural Geology, no. 7, p. 361–373.

Moores, E.M., 1991, Southwest U.S.-East Antarctic (SWEAT) connection: A hypothesis: Geology, v. 19, p. 425-428.

Moye, F.J., Hackett, W.R., Blakley, J.D., and Snider, L.G., 1988, Regional Geologic Setting and Volcanic Stratigraphy of the Challis Volcanic Field, Central Idaho: Guidebook to the geology of central and Southern Idaho: Idaho Geological Survey Bulletin, v. 27, p. 87–98.

Mueller, P.A., Heatherington, A.L., Kelly, D.M., Wooden, J.L., and Mogk, D.W., 2002, Paleoproterozoic crust within the Great Falls tectonic zone: Implications for the assembly of southern Laurentia: Geology, v. 30, p. 127–130.

Mueller, P.A., Foster, D.A., Mogk, D.W., Wooden, J.L., Kamenov, G.D., and Vogl, J.J., 2007, Detrital mineral chronology of the Uinta Mountain Group: Implications for the Grenville flood in southwestern Laurentia: Geology, v. 35, no. 5, p. 431–434, doi:10.1130/G23148A.1.

Mueller, P.A., Wooden, J.L., Mogk, D.W., and Foster, D.A., 2011, Paleoproterozoic evolution of the Farmington zone: Implications for terrane accretion in southwestern Laurentia: Lithosphere, v. 3, p. 401–408, doi: 10.1130/L161.1.

Nelson, W. H., and C. P. Ross, 1968, Geology of part of the Alder Creek mining district, Custer County, Idaho: U. S. Geol. Survey Bull. V. 1252A, p. A1-A30.

Nordsvan, A.R., Collins, W.J., Li, Z., Spencer, C.J., Pourteau, A., Withnall, I.W., Betts, P.G., and Volante, S., 2018, Laurentian crust in northeast Australia : Implications for the assembly of the supercontinent Nuna: Geology, p. 1-4.

Oriel, S.S., and Platt, L.B., 1980, Geologic Map of the Preston 1°x2° Quadrangle, southeastern Idaho and western Wyoming, U.S. Geological Survey Miscellaneous Investigations Series Map I-1127, scale 1:250,000.

Parsons, T., Thompson, G.A., and Smith, R.P., 1998, More than one way to stretch: A tectonic model for extension along the plume track of the Yellowstone hotspot and adjacent Basin and Range Province: Tectonics, v. 17, p. 221–234, doi: 10.1029/98TC00463.

Patton, W.W., 1948, Geology of the Clayton area, Custer County, Idaho: [M.S. thesis] Cornell University, 43 p.

Payne, S.J., McCaffrey, R., and King, R.W., 2008, Strain rates and contemporary deformation in the Snake River Plain and surrounding Basin and Range from GPS and seismicity: Geology, v. 36, p. 647–650, doi: 10.1130/G25039A.1.

Payne, S.J., McCaffrey, R., King, R.W., Kattenhorn, S.A., 2012, A new interpretation of deformation rates in the Snake River Plain and adjacent basin and range regions based on GPS measurements: Geophysical Journal International, v. 189, no. 1, p. 101-122

Pearson, D.M., Link, P.K., Todt, M.K., Hansen, C.M., Krohe, N.J., and Mahoney, J.B., 2016, The Lemhi arch of east-central Idaho: A stranded fault block within the western Laurentian rift margin: Geological Society of America Abstracts with Programs, v. 48, no. 6, doi: 10.1130 /abs /2016RM -276022.

Peron-Pinvidic, G., Manatschal, G., and Osmundsen, P.T., 2013, Structural comparison of archetypal Atlantic rifted margins: A review of observations and concepts: Marine and Petroleum Geology, v. 43, p. 21–47, doi: 10.1016/j.marpetgeo.2013.02.002.

Pierce, K.L., Morgan, L.A., 1992. The track of the Yellowstone hot spot: volcanism, faulting, and uplift. In: Link, P.K., Kuntz, M.A., Platt, L.B. (Eds.), Regional Geology of Eastern Idaho and Western Wyoming: Geological Society of America Memoir, vol. 179, p. 1–53.

Pierce, K.L., and Morgan, L.A., 2009, Is the track of the Yellowstone hotspot driven by a deep mantle plume? - Review of volcanism, faulting, and uplift in light of new data: Journal of Volcanology and Geothermal Research, v. 188, p. 1–25, doi: 10.1016/j.jvolgeores.2009.07.009.

Pierce, K.L., Morgan, L.A., Saltus, R.W., 2002. Yellowstone plume head: postulated tectonic relations to the Vancouver slab, continental boundaries, and climate, *in* Bonnichsen, Bill, White, C.M., McCurry, Micheal (Eds.), Tectonic and Magmatic Evolution of the Snake River Plain Volcanic Province: Idaho Geological Survey Bulletin, v. 30, p. 5–33.

Pisarevsky, S.A., Natapov, L.M., Donskaya, T.V., Gladkochub, D.P., Vernikovsky, V.A., 2008, Proterozoic Siberia: a promontory of Rodinia: Precambrian Research, v. 160, p. 66–76.

Pisarevsky, S.A., Elming, S.Å., Pesonen, L.J., and Li, Z.X., 2014, Mesoproterozoic paleogeography: Supercontinent and beyond: Precambrian Research, v. 244, p. 207–225, doi: 10.1016/j.precamres.2013.05.014.

Price, R.A., 1964, The Precambrian Purcell system in the Rocky Mountains of southern Alberta and British Columbia: Bulletin of Canadian Petroleum Geology, v. 12, Special Issue, p. 399–426.

Price, R.A., and Sears, J.W., 2000, A preliminary palinspastic map of the Mesoproterozoic Belt Purcell Super-group, Canada and USA: Implications for the tectonic setting and structural evolution of the Purcell anticlinorium and the Sullivan deposit, in Lydon, J.W., Höy, T., Slack, J.F., and Knapp, M.E., eds., The Geological Environment of the Sullivan Deposit, British Columbia: Geological Association of Canada, Mineral Deposits Division, Special Publication 1, p. 61–81.

Rainbird, R., Cawood, P., and Gehrels, G.E., 2012, The Great Grenvillian sedimentation episode: Record of supercontinent Rodinia's assembly, in Busby, C., and Antonio, A., eds., Tectonics of Sedimentary Basins: Recent Advances, Chichester, UK, John Wiley & Sons, Ltd., p. 583–601, doi: 10.1002/9781444347166.ch29.

Rodgers, D.W., and Janecke, S., 1992, Tertiary Paleogeologic maps of the western Idaho-Wyoming-Montana Thrust Belt, *in* Link, P.K., Kuntz, M.A., and Platt, L.B., eds., Regional Geology of Eastern Idaho and Western Wyoming: Geological Society of America Memoir 179, 312 p.

Ross, C. P., 1937, Geology and ore deposits of the Bayhorse region, Idaho: U.S. Geological Survey Bulletin 877, 161 p.

Ross, G.M., Parrish, R.R., and Winston, D., 1992, Provenance and U-Pb geochronology of the Mesoproterozoic Belt Supergroup (northwestern United States): Implications for age of deposition and pre-Panthalassa plate reconstructions: Earth and Planetary Science Letters, v. 113, p. 57-76.

Rogers, J.J.W., and Santosh, M., 2002, Configuration of Columbia, a Mesoproterozoic Supercontinent: Gondwana Research, v. 5, p. 5–22, doi: 10.1016/S1342-937X(05)70883-2.

Ruppel, R.T., 1975, Precambrian Y sedimentary rocks in east-central Idaho: U.S. Geological Survey Professional Paper 889-A, 23 p.

Ruppel, E.T., 1986, The Lemhi Arch: A Late Proterozoic and early Paleozoic landmass in central Idaho, in Peterson, J.A., ed., Paleotectonics and sedimentation in the Rocky Mountain region, United States: American Association of Petroleum Geologists Memoir 41, p. 119–130, doi: 10 .1306 /M41456C6.

Ruppel, E. T., and Lopez, D. A., 1988, Regional geology and mineral deposits in and near the central part of the Lemhi Range, Lemhi County, Idaho: U.S. Geological Survey Professional Paper 1480, 122 p.

Sanford, R.F., 2005, Geology and stratigraphy of the Challis Volcanic Group and related rocks, Little Wood River area, south-central Idaho, with a section on Geochronology by Lawrence W. Snee: U.S. Geological Survey Bulletin 2064-II, 22 p.

Saylor, J.E., and Sundell, K.E., 2016, Quantifying comparison of large detrital geochronology data sets [Geosphere, 12, (203-220)] doi:10.1130/GES01237.1: Geosphere, v. 12, p. 1881–1881, doi: 10.1130/GES01237.1.

Saylor, J.E., Jordan, J.C., Sundell, K.E., Wang, X., Wang, S. and Deng, T., 2017, Topographic growth of the Jishi Shan and its impact on basin and hydrology evolution, NE Tibetan Plateau: Basin Research

Schmidt, K.L., Lewis, R.S., Vervoort, J.D., Stetson-Lee, T.A., Michels, Z.D., and Tikoff, B., 2017, Tectonic evolution of the Syringa embayment in the central North American Cordilleran accretionary boundary: Lithosphere, v. 9, p. 184–204, doi: 10.1130/L545.1.

Scholten, R., 1957, Paleozoic evolution of the Geosynclinal margin north of the Snake River Plain, Idaho-Montana: Bulletin of the Geological Society of America, v. 68, p. 151-170.

Schusler, K.L., Pearson, D.M., McCurry, M., 2017, Whose fault is it? A kinematic analysis of high angle faults adjacent to the eastern Snake River plain near Arco, ID: GSA Abstracts with Programs, v. 49, no. 6.

Sears, J.W., 2007, Belt-Purcell Basin: Keystone of the Rocky Mountain fold-and-thrust belt, United States and Canada, in Sears, J.W., Harms, T.A., and Evenchick, C.A., eds., Whence the Mountains? Inquiries into the Evolution of Orogenic Systems: A Volume in Honor of Raymond A. Price: Geological Society of America Special Paper 433, p. 147–166, doi:10.1130/2007.2433(07).

Sears, J.W., and Price, R.A., 2000, New look at the Siberian connection: no SWEAT; Geology v. 28, p. 423–426.

Shields, A., 2017, Characterizing Basin and Range Fault Activity near Challis, Idaho, using Novel Remote Sensing Techniques [M.S. Thesis]: Idaho State University, 118 p.

Sims, P.K., Lund, K., and Anderson, E., 2005, Precambrian crystalline basement map of Idaho—An interpretation of aeromagnetic anomalies: U.S. Geological Survey Scientific Investigations Map 2884.

Skipp, B., 1987, Basement thrust sheets in the Clearwater orogenic zone, central Idaho and western Montana: Geology, v. 115, p. 220-224.

Skipp, B., and Link, P.K., 1992, Middle and late Proterozoic rocks and late Proterozoic tectonics in the southern Beaverhead Mountains, Idaho and Montana: A preliminary report, in Link, P.K., et al., eds., Regional geology of eastern Idaho and western Wyoming: Geological Society of America Memoir 179, p. 141–154, doi: 10 .1130 /MEM179 -p141.

Sloss, L.L., 1950, Paleozoic sedimentation in Montana area: American Association of Petroleum Geologists Bulletin, v. 34, p. 423–451.

Sloss, L.L., 1954, Lemhi Arch, a mid-Paleozoic positive element in south-central Idaho: Geological Society of America Bulletin, v. 65, p. 365–368, doi: 10 .1130 /0016 -7606 (1954)65 [365: LAAMPE]2 .0 .CO;2.

Sloss, L.L., 1963, Sequences in the cratonic interior of North America: Geological Society of America Bulletin, v. 74, p. 93–114, doi: 10 .1130 /0016 -7606 (1963)74 [93: SITCIO]2 .0 .CO;2.

Speed, R.C., and Sleep, N.H., 1982, Antler orogeny and foreland basin: A model: Discussion and reply: Geological Society of America Bulletin, v. 93, p. 81.

Spencer, C.J., and Kirkland, C.L., 2016, Visualizing the sedimentary response through the orogenic cycle: A multidimensional scaling approach: Lithosphere, v. 8, p. 29–37, doi: 10.1130/L479.1.

Stewart, D.E., Lewis, R.S., Stewart, E.D., and Link, P.K., 2013, Geologic Map of the Central and Lower Big Creek Drainage, Central Idaho: Idaho Geological Survey, scale 1:75,000.

Stewart, D. E., Stewart, E. D., Lewis, R. S., Weppner, K. N., Isakson, V. H., and Freed, J. S., 2017, Geologic Map of the Stibnite Quadrangle, Valley County, Idaho: Idaho Geological Survey, scale 1:24,000.

Stewart, E.D., Link, P.K., Fanning, C.M., Frost, C.D., and McCurry, M., 2010, Paleogeographic implications of non-North American sediment in the Mesoproterozoic upper Belt Supergroup and Lemhi Group, Idaho and Montana, USA: Geology, v. 38, no. 10, p. 927–930, doi: 10 .1130/G31194 .1 .

Stewart, J.H., 1972, Initial deposits in the Cordilleran geo- syncline: Evidence of a late Precambrian (<850 m.y.) continental separation: Geological Society of America Bulletin, v. 83, p. 1345–1360, doi: 10 .1130 /0016 -7606 (1972)83 [1345: IDITCG]2 .0 .CO;2 .5-828.

Strickland, A., Miller, E.L., Wooden, J.L., 2011, The timing of Tertiary metamorphism and deformation in the Albion–Raft River–Grouse Creek metamorphic core complex, Utah and Idaho: The Journal of Geology, v. 119, p. 185–206.

Summa, C.L., 1993, Sedimentologic, Stratigraphic, and Tectonic Controls of a Mixed Carbonate-Siliciclastic Succession: Neoproterozoic Johnnie Formation, Southern California [Ph.D. Dissertation], Cambridge, Massachusetts, Massachusetts Institute of Technology, 616 p.

Tackley, P.J., Stevenson, D.J., Glatzmaier, G.A., and Schubert, G., 1993, Effects of an endothermic phase transition at 670 km depth in a spherical model of convection in the Earth’s mantle: Nature, v. 361, p. 699–704, doi: 10.1038/361699a0.

Thomas, W.A., 1993, Low-angle detachment geometry of the late Precambrian-Cambrian Appalachian-Ouachita rifted margin of southeastern North America: Geology, v. 21, p. 921–924, doi: 0.1130/0091-7613(1993)021<0921:LADGOT>2.3.CO;2.

Thomas, W.A., 2011, The Iapetan rifted margin of southern Laurentia: Geosphere, v. 7, p. 97–120, doi: 10.1130/GES00574.1.d

Tikoff, B., Benford, B., and Giorgis, S., 2008, Lithospheric control on the initiation of the Yellowstone hotspot: Chronic reactivation of lithospheric scars: International Geology Review, v. 50, p. 305–324, doi:10.2747/0020 -6814.50.3.305.

Van der Pluijm BA, Marshak S., 2004, Earth structure: New York, W.W. Norton and Company, 656 p.

Vermeesch, P., 2012, On the visualisation of detrital age distributions: Chemical Geology, v. 312–313, p. 190–194, doi: 10.1016/j.chemgeo.2012.04.021.

Vermeesch, P., 2013, Multi-sample comparison of detrital age distributions: Chemical Geology, v. 341, p. 140–146, doi: 10.1016/j.chemgeo.2013.01.010.

Vervoort, J.D., Lewis, R.S., Fisher, C., Gaschnig, R.M., Jansen, A.C., and Brewer, R., 2016, Neoarchean and Paleoproterozoic crystalline basement rocks of north-central Idaho: Constraints on the formation of western Laurentia: Bulletin of the Geological Society of America, v. 128, p. 94–109, doi: 10.1130/B31150.1.

Walker, J.D., Geissman, J.W., Bowring, S.A., and Babcock, L.E., 2013, The Geological Society of America Geologic Time Scale: Geological Society of America Bulletin, v. 125, p. 259–272, doi: 10.1130/B30712.1.

Weil, A.B., and Yonkee, W.A., 2012, Layer-parallel shortening across the Sevier fold-thrust belt and Laramide foreland of Wyoming: Spatial and temporal evolution of a complex geodynamic system: Earth and Planetary Science Letters, v. 357–358, p. 405–420, doi: 10.1016/j.epsl.2012.09.021.

Wilson, E., Preacher, J.M., and Link, P.K., 1994, New constraints on the nature of the Early Mississippian sedimentary basin in Idaho, in Embry, A.F., et al., eds., Pangaea: Global environments and resources: Canadian Society of Petroleum Geologists Memoir 17, p. 155–174.

Wingate, M.T.D., Pisarevsky, S.A., Evans, D.A.D., 2002, Rodinia connections between Australia and Laurentia: no SWEAT, no AUSWUS?: Terra Nova, v. 14, p. 121–128.

Winston, D., 1986a, Sedimentation and tectonics of the Middle Proterozoic Belt Basin and their influence on Phanerozoic compression and extension in western Montana and northern Idaho, in Peterson, J.A., ed., Sedimentation and Tectonics: American Association of Petroleum Geologists Memoir 41, p. 87–118.

Winston, D., Link, P.K., 1993. Middle Proterozoic rocks of Montana, Idaho and eastern Washington: the Belt Supergroup, *in* Reed, J.C., Jr., et al., eds., Precambrian: Conterminous U.S.: Boulder, Colorado, Geological Society of America, Geology of North America, v. C-2, p. 487-517.

Yonkee, W.A., and Weil, A.B., 2015, Tectonic evolution of the Sevier and Laramide belts within the North American Cordillera orogenic system: Earth-Science Reviews, v. 150, p. 531–593, doi: 10.1016/j.earscirev.2015.08.001.

Yonkee, W.A., Dehler, C.D., Link, P.K., Balgord, E.A., Keeley, J.A., Hayes, D.S., Wells, M.L., Fanning, C.M., and Johnston, S.M., 2014, Tectono-stratigraphic framework of Neoproterozoic to Cambrian strata, west-central U.S.: Protracted rifting, glaciation, and evolution of the North American Cordilleran margin: Earth-Science Reviews, v. 136, p. 59–95, doi: 10 .1016 /j .earscirev .2014 .05 .004.

Zhao, M.F., Yan, D.P., Kennedy, A.K., Li, Y.Q., Ding, J., 2002, SHRIMP U–Pb zircon geochronological and geochemical evidence for Neoproterozoic arc- magmatism along the western margin of the Yangtze Block South China. Earth Planet. Sci. Lett. 196, 51–67.

Zirakparvar, N.A., Vervoort, J.D., McClelland, W., and Lewis, R.S., 2010, Insights into the metamorphic evolution of the Belt–Purcell basin; evidence from Lu–Hf garnet geochronology: Canadian Journal of Earth Sciences, v. 47, p. 161–179, doi: 10.1139/E10-001.

APPENDICES

Appendix A: Point Count Data

Figure A.1

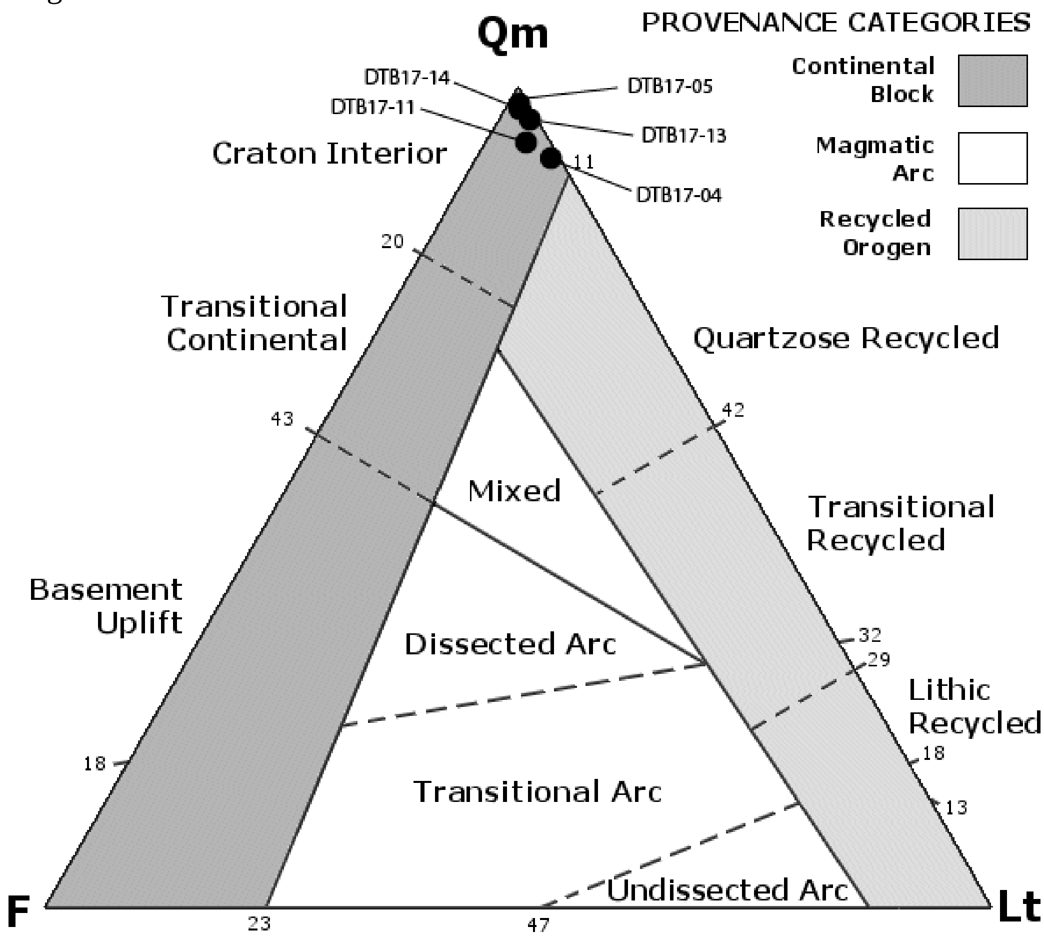

Qm: Monocrystalline Quartz, F: Feldspar, Lt: Total Lithics

Table A.1

Sample	Unit	Grain Counts					
		Qm		F		Lt	
		#	%	#	%	#	%
DTB17-04	Zr	274	91.3	0	0	26	8.6
DTB17-05	Zsq	294	98	0	0	6	2
DTB17-11	CZc	278	95	7	2.3	15	5
DTB17-13	CZc	292	97.3	0	0	8	2.7
DTB17-14	CZc	293	97.7	5	1.7	2	0.7

Figure A.1 and Table A.1- The point counts of the lower Ramshorn Slate (Zr) shows ~9% lithics, mostly polycrystalline quartz, consist with the abundance of vein quartz clasts in the Ramshorn Conglomerate. The Clayton Mine Quartzite (CZc) is dominantly a quartz arenite. The Clayton Mine and Ramshorn Slate samples plot within the cratonic interior as is expected for rifting and passive margin sandstones. Polycrystalline quartz was counted as a lithic indicated by the QmFLt diagram. Ternary diagram after Dickinson et al., 1983. Please note that these point counts are representative of the hand samples from which the detrital zircons were separated and do not reflect the full heterogeneity of some units.

Appendix B: Thin Section Photomicrographs

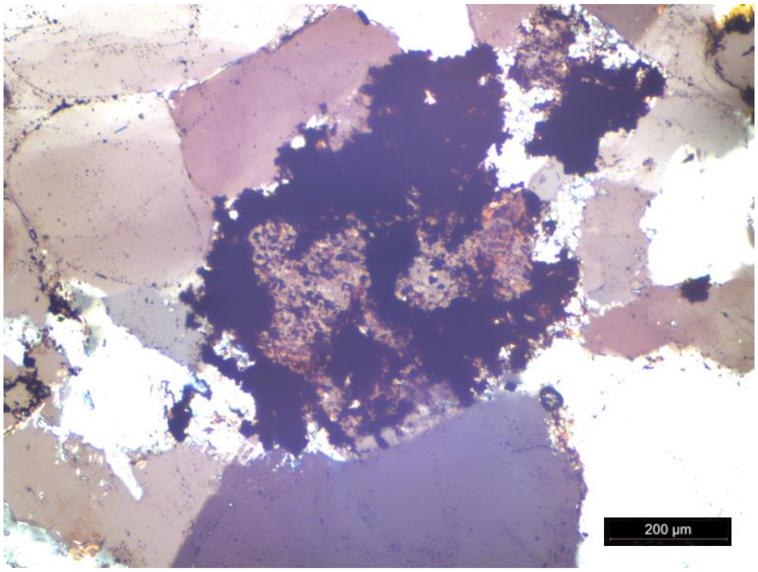

Figure B.1- Ramshorn Slate: Polycrystalline quartz lithic surrounded by monocrystalline quartz in cross polarized light.

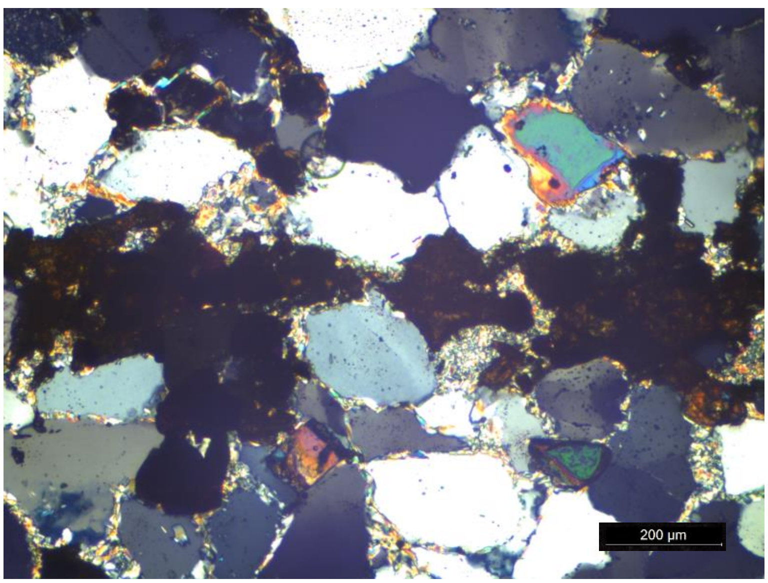

Figure B.2- Siltite and Quartzite: Heavy mineral (zircon) concentrated along a lamination with interstitial hematite in cross polarized light.

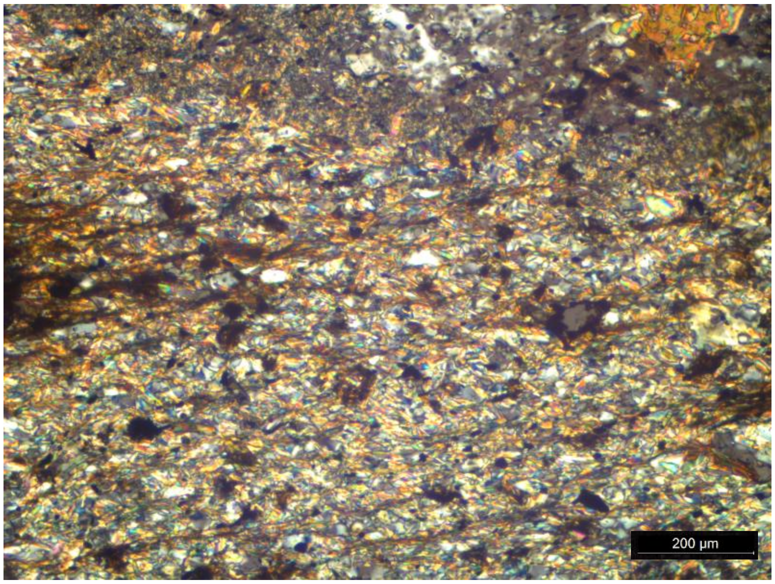

Figure B.3 - Contact Metamorphosed Aureole within Ramshorn Slate showing finer grain size and distinct foliation under cross polarized light.

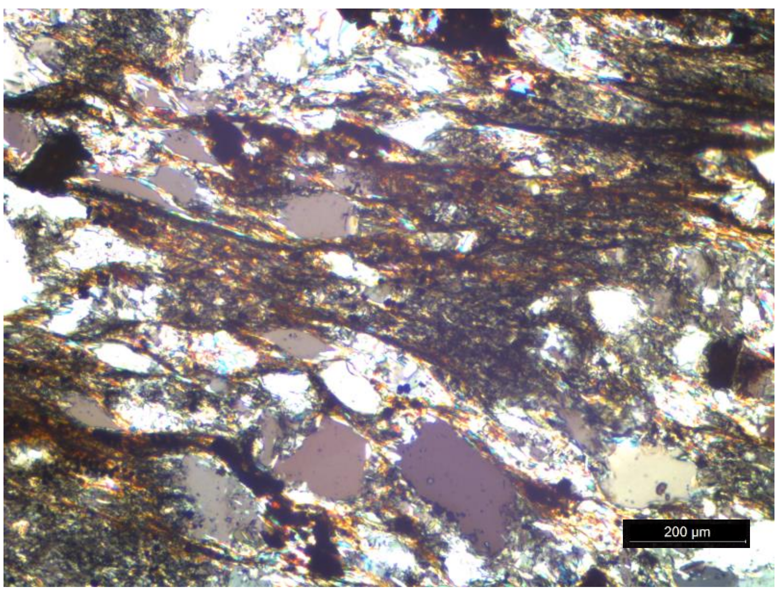

Figure B.4 - Ramshorn Slate: Showing quartz grains surrounded by fine-grained foliated (micaeous) matrix in cross polarized light.

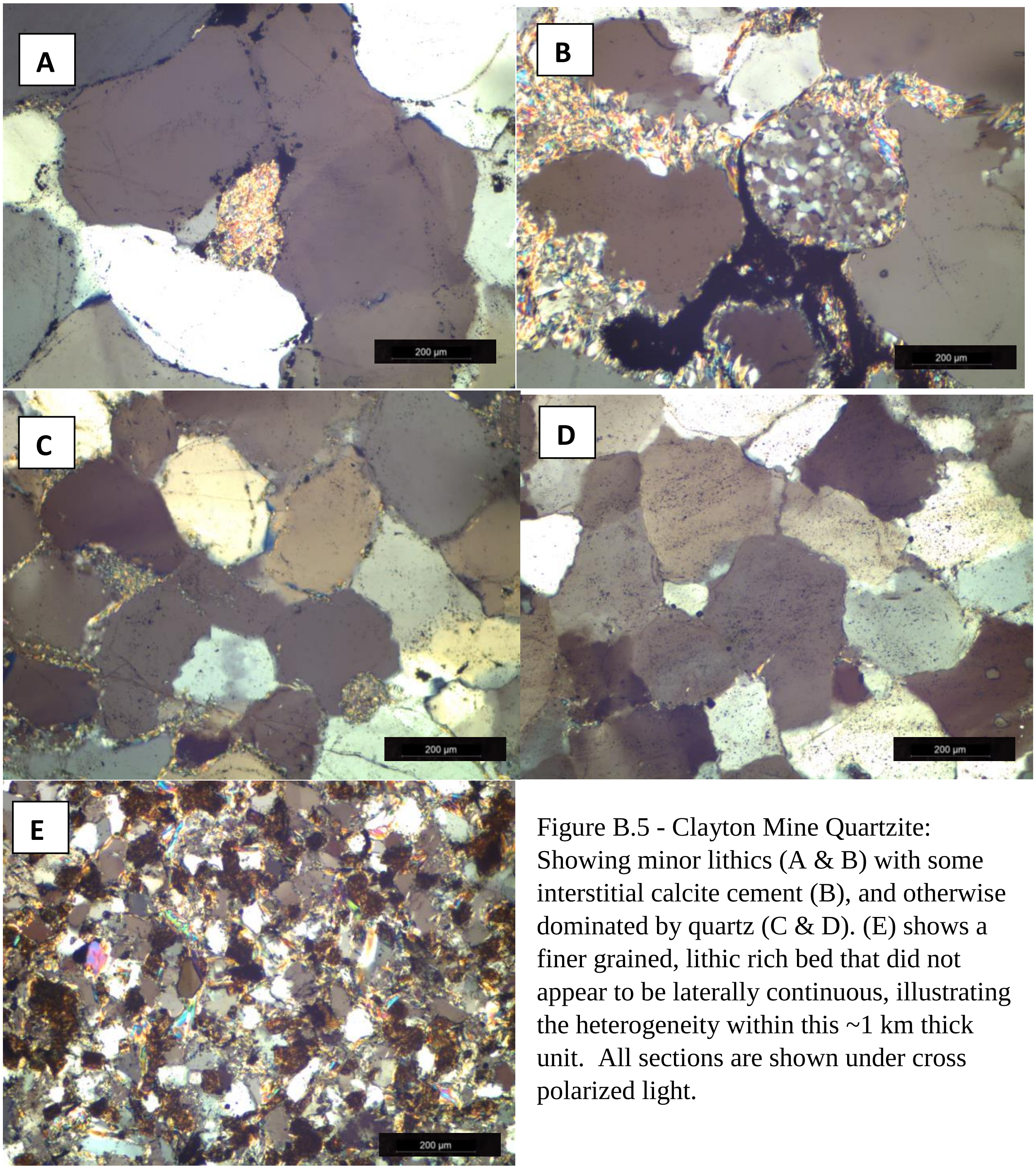

Figure B.5 - Clayton Mine Quartzite: Showing minor lithics (A & B) with some interstitial calcite cement (B), and otherwise dominated by quartz (C & D). (E) shows a finer grained, lithic rich bed that did not appear to be laterally continuous, illustrating the heterogeneity within this ~1 km thick unit. All sections are shown under cross polarized light.

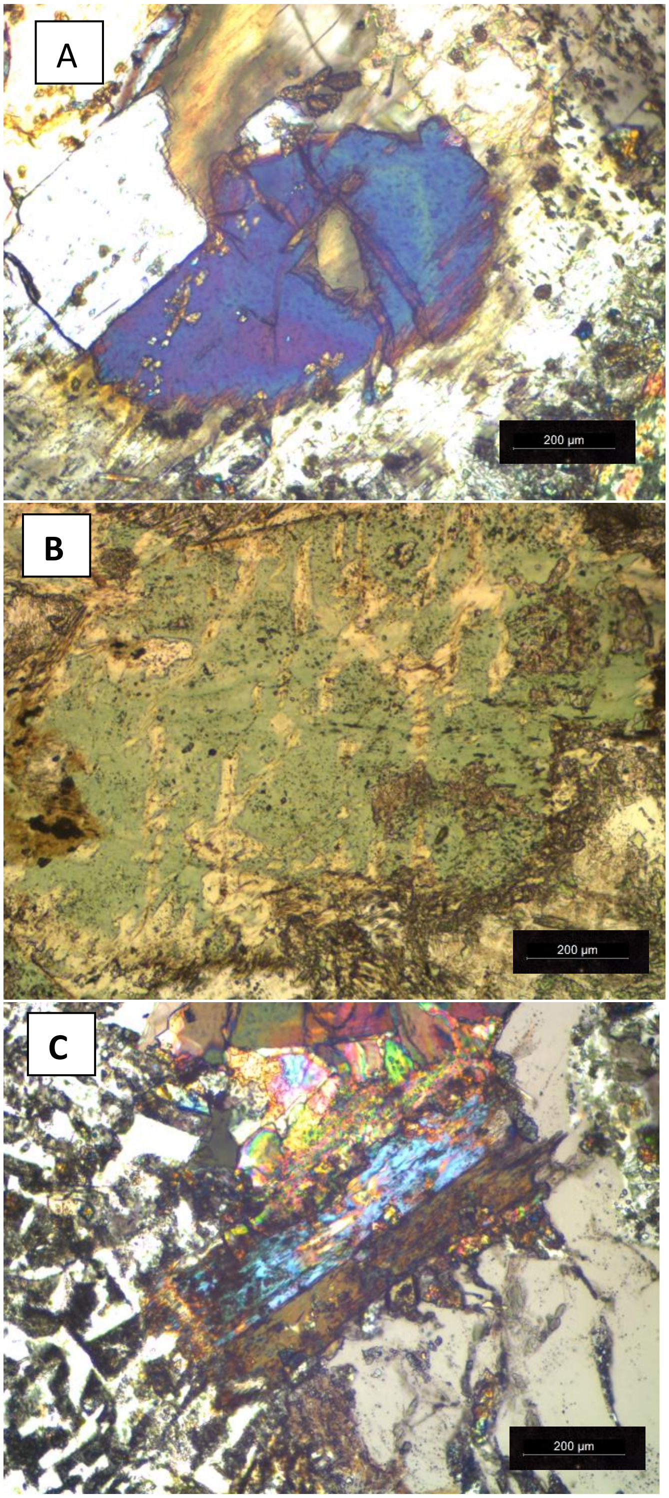

Figure B. 6 - Gabbro: Showing (A) Ca-Pyroxene (Augite?) in cross polarized light; (B) Authigenic chlorite in plane polarized light; (C) Simple twinned hornblende in cross polarized light.

All images were taken under 100x magnification.

Appendix C: Detrital Zircon sample locations and descriptions

Table C.1

Sample number	Sampler	Latitude	Longitude	Elevation (ft. asl)	Location	Unit	Unit name	Description	Analyst	Analyses conducted	Concordant analyses	Results
DTB17-04	Daniel Brennan	44.48422	114.34827	7969	Ridge N. of Daugherty Gulch, S. of Ski Lift	Zrc	Ramshorn Conglomerate	Well sorted, coarse grained Qtz arenite. Basal conglomerate member of Ramshorn Slate	Daniel Brennan	315	297	Numerous grains at ca. 1000-1300 Ma. Decreasing modes at ca. 1400, 1780 and 2700 Ma.
DTB17-05	Daniel Brennan	44.45187	114.39072	8500	Up North Gulch on E. facing slope	Zsq	Interbedded Siltite and Quartzite	Medium-grained Qtz Arenite interbedded with 10 m thick shale.	Daniel Brennan	315	275	Significant ca. 650 Ma population with following modes at ca. 1000-1300, 1400, 1780, and 2700 Ma.
DTB17-11	Daniel Brennan	44.44048	114.40026	7997	Up Garden Crk, W. of switch backs, near cattle guard	CZc	Clayton Mine Quartzite	Coarse-grained, poorly sored, Qtz. Arenite. Stratigraphically lowest, Clayton Mine Qzte.	Daniel Brennan	315	296	Dominated by a ca. 650 Ma population, with lesser modes at ca. 1450, 1700, and <2500 Ma.
DTB17-14	Daniel Brennan	44.43656	114.40365	9294	Top of Quartzite cliff, above Garden Crk.	CZc	Clayton Mine Quartzite	Medium-grained Qtz arenite. Stratigraphically highest Clayton Mine Qzte up Garden Creek.	Daniel Brennan	315	298	Principal modes at ca. 1760 and 2450 Ma. With lesser from 1000-1300 and ca. 1440 Ma.
DTB17-17	Daniel Brennan	44.25961	114.40344	5584	Just N. of Clayton Fire station, W. of Kinniknic Crk.	CZc	Clayton Mine Quartzite	Medium-grained, Qtz Arenite, < 100m below Ella contact	Univ. AZ Laserchron	110	93	Principal mode at ca. 1780 Ma. Lesser mode at ca. 2500 Ma.
DTB17-18	Daniel Brennan	44.26327	114.41557	5712	~1.2 km W. of Clayton, N. of HWY 75, up talus slope	CZc	Clayton Mine Quartzite	Micaceous fine grained Qtz arenite. Near center of Anticline, low in Clayton Mine Qtz section in Clayton quad.	Univ. AZ Laserchron	110	99	Principal mode at ca. 1000-1300 Ma. Decreasing modes at ca. 1440, 1780 and 2700 Ma.
DTB17-19	Daniel Brennan	44.27372	114.32705	5527	N of Salmon River, ~500m NE of Confluence w/ E. Fork of Salmon	CZc	Clayton Mine Quartzite	Coarse to medium Qtz arenite, Near Gabbro and mapped Osq. Lower Clayton Mine.	Univ. AZ Laserchron	110	103	Modes at ca. 100-1300, 1440, 1780 and 2700 Ma. A few grains at ca. 650 Ma.

Appendix D: KDE Plots

Figure D.1 - Garden Creek traverse KDE plots

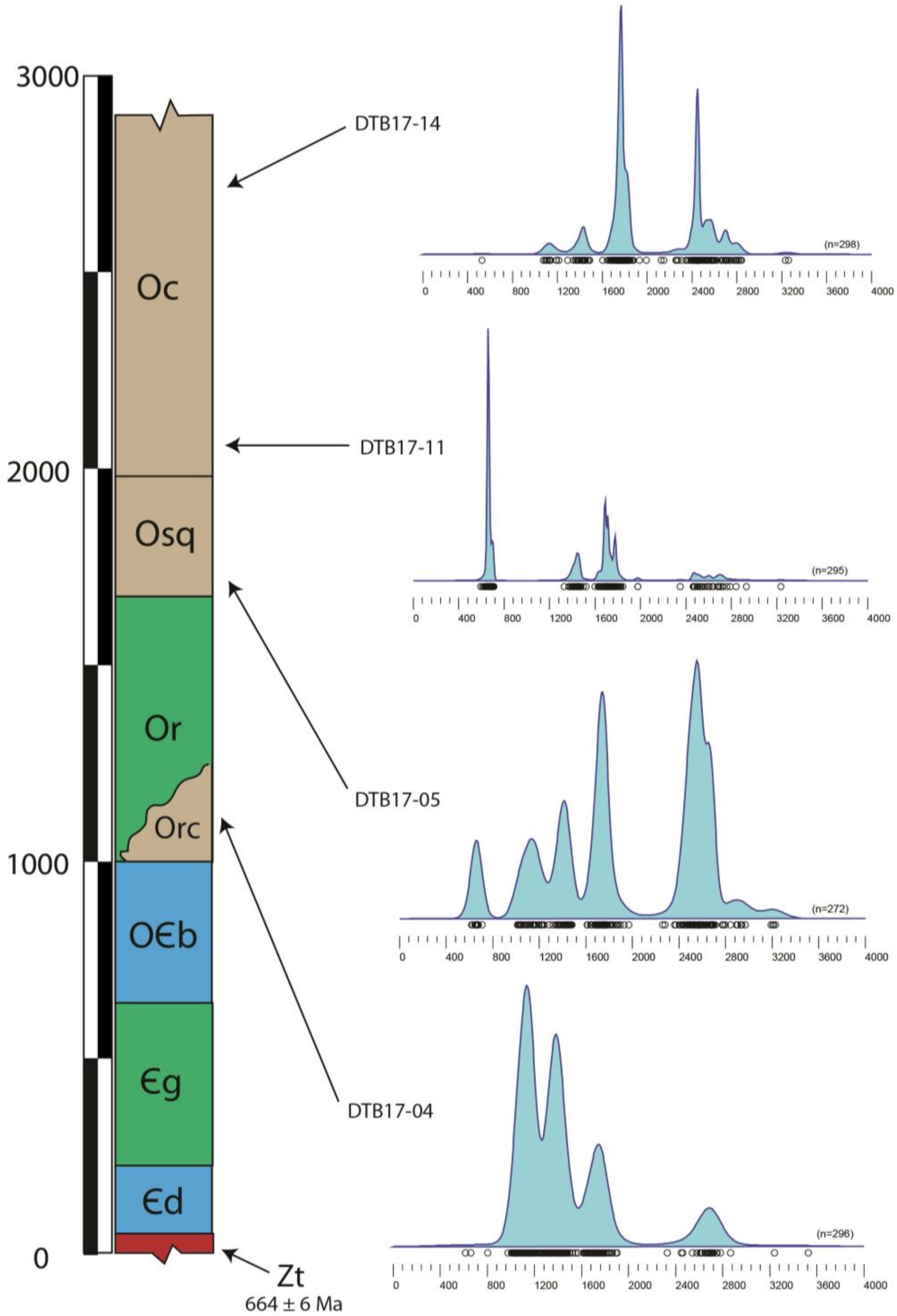

Figure D. 2 - Salmon River Traverse KDE Plots

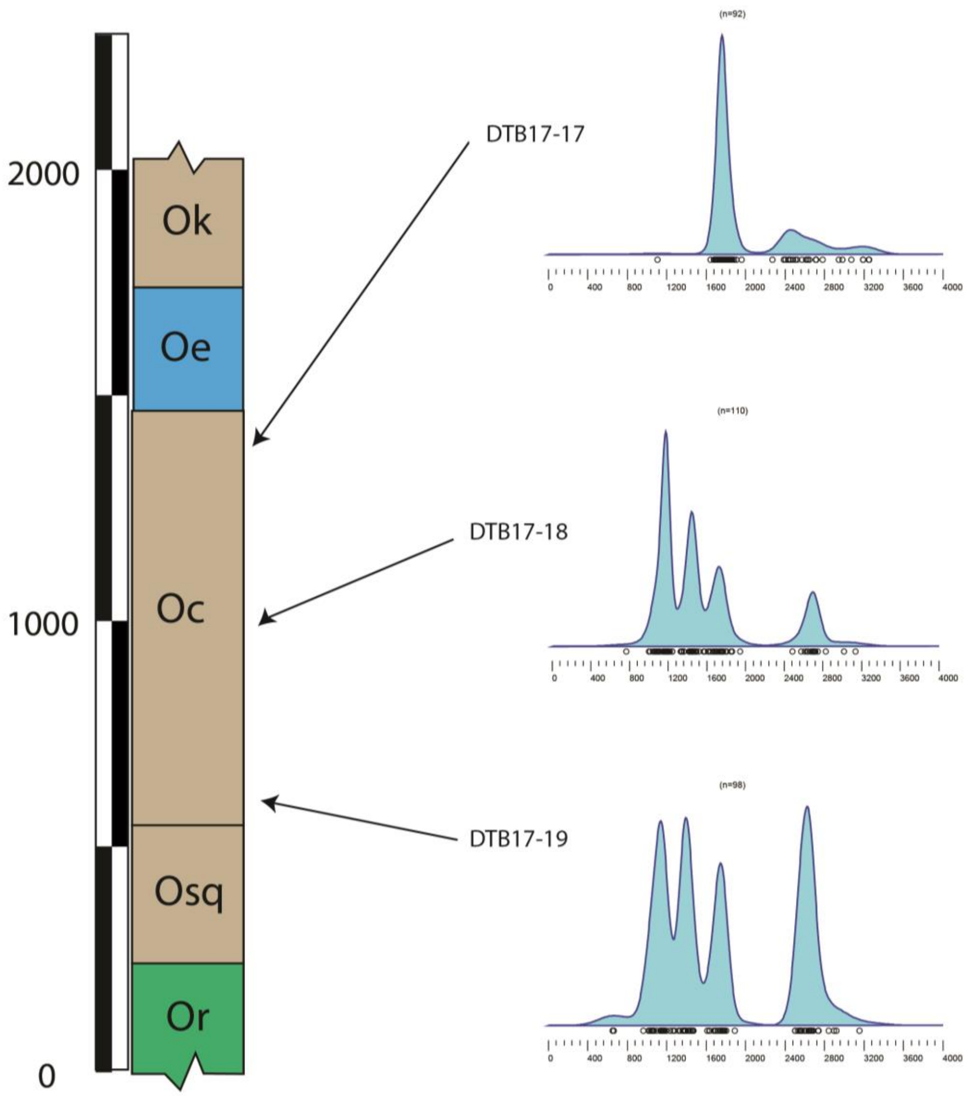

Appendix E: LA-ICPMS data tables

Table DTB17-04 . U-Pb geochronologic analyses.																			
						Isotope ratios						Apparent ages (Ma)							
Analysis	U (ppm)	206Pb 204Pb	U/Th	206Pb* 207Pb*	± (%)	207Pb* 235U*	± (%)	206Pb* 238U	± (%)	error corr.	206Pb* 238U*	± (Ma)	207Pb* 235U	± (Ma)	206Pb* 207Pb*	± (Ma)	Best age (Ma)	± (Ma)	Conc (%)
-04-Spot 4	977	74384	0.8	16.7451	0.6	0.8202	1.2	0.0997	1.1	0.87	612.4	6.3	608.1	5.7	592.5	13.4	612.4	6.3	103.4
4-Spot 101	69	44686	1.5	15.7174	1.1	0.9446	1.6	0.1077	1.1	0.71	659.5	7.0	675.3	7.7	728.2	23.3	659.5	7.0	90.6
4-Spot 226	1385	56313	13.4	14.0357	0.8	1.3001	1.4	0.1324	1.2	0.82	801.6	8.9	845.8	8.3	963.6	16.9	801.6	8.9	83.2
4-Spot 202	541	300119	3.1	13.9501	0.8	1.6525	1.6	0.1673	1.4	0.88	997.0	13.1	990.5	10.2	976.1	15.5	976.1	15.5	102.1
04-Spot 11	139	1714098	1.2	13.7556	0.7	1.7355	1.3	0.1732	1.2	0.87	1029.8	11.1	1021.8	8.7	1004.6	13.7	1004.6	13.7	102.5
4-Spot 174	604	729653	15.3	13.7013	0.9	1.6098	1.9	0.1600	1.7	0.89	957.0	15.4	974.0	12.2	1012.7	17.7	1012.7	17.7	94.5
04-Spot 51	460	65820	1.6	13.6658	0.6	1.7492	1.3	0.1734	1.2	0.88	1031.1	11.1	1026.9	8.6	1017.9	12.8	1017.9	12.8	101.3
4-Spot 223	45	8230	0.8	13.6366	1.7	1.7771	2.4	0.1758	1.6	0.70	1044.2	15.8	1037.1	15.3	1022.2	34.2	1022.2	34.2	102.1
04-Spot 70	877	174247	22.0	13.5956	0.9	1.5935	1.7	0.1572	1.5	0.86	941.2	13.0	967.7	10.8	1028.3	17.9	1028.3	17.9	91.5
04-Spot 40	123	15380	1.1	13.5658	1.1	1.7760	1.7	0.1748	1.3	0.76	1038.6	12.8	1036.7	11.3	1032.8	22.8	1032.8	22.8	100.6
-04-Spot 1	314	132735	3.1	13.5523	0.6	1.8576	1.3	0.1827	1.1	0.88	1081.5	11.1	1066.1	8.4	1034.8	12.3	1034.8	12.3	104.5
04-Spot 75	80	11584	2.6	13.5444	0.7	1.7633	1.5	0.1733	1.3	0.89	1030.2	12.8	1032.1	9.8	1036.0	14.0	1036.0	14.0	99.4
4-Spot 105	232	33056	0.9	13.5223	0.9	1.7118	1.5	0.1680	1.2	0.79	1000.8	11.4	1013.0	9.9	1039.3	19.1	1039.3	19.1	96.3
4-Spot 167	97	23445	1.3	13.5130	1.3	1.8208	1.8	0.1785	1.2	0.69	1058.9	12.1	1053.0	11.8	1040.7	26.2	1040.7	26.2	101.8
4-Spot 160	30	9608	1.5	13.4842	1.4	1.7944	2.3	0.1756	1.9	0.79	1042.7	17.8	1043.4	15.3	1045.0	28.9	1045.0	28.9	99.8
4-Spot 274	36	14147	1.5	13.4679	1.5	1.8449	2.0	0.1803	1.3	0.66	1068.5	13.1	1061.6	13.2	1047.4	30.3	1047.4	30.3	102.0
04-Spot 61	169	463426	3.2	13.4616	0.8	1.7825	1.5	0.1741	1.3	0.85	1034.7	12.2	1039.1	9.8	1048.4	16.2	1048.4	16.2	98.7
4-Spot 140	66	36273	1.0	13.4549	1.0	1.8055	1.6	0.1763	1.2	0.77	1046.5	11.8	1047.4	10.3	1049.4	20.3	1049.4	20.3	99.7
4-Spot 108	259	130429	2.6	13.4538	0.9	1.8299	1.7	0.1786	1.4	0.83	1059.5	13.5	1056.2	10.9	1049.5	18.6	1049.5	18.6	100.9
4-Spot 246	82	163992	3.3	13.4534	0.9	1.7862	1.7	0.1744	1.4	0.84	1036.1	13.4	1040.4	11.0	1049.6	18.7	1049.6	18.7	98.7
04-Spot 73	118	100636	1.2	13.4518	0.9	1.7752	1.4	0.1733	1.1	0.79	1030.1	10.8	1036.4	9.4	1049.8	18.0	1049.8	18.0	98.1
4-Spot 109	747	1909876	13.9	13.4367	0.8	1.7081	1.5	0.1665	1.2	0.83	993.0	11.4	1011.6	9.5	1052.1	16.5	1052.1	16.5	94.4
04-Spot 62	46	12436	1.7	13.4291	1.0	1.8737	1.9	0.1826	1.6	0.83	1081.0	15.5	1071.9	12.3	1053.2	20.8	1053.2	20.8	102.6
04-Spot 47	208	34832	1.3	13.4250	0.9	1.5279	2.3	0.1488	2.2	0.93	894.4	18.1	941.7	14.3	1053.9	17.3	1053.9	17.3	84.9
4-Spot 255	68	13973	3.0	13.4023	1.0	1.7366	1.6	0.1689	1.2	0.76	1005.9	11.1	1022.2	10.2	1057.3	20.8	1057.3	20.8	95.1
4-Spot 218	123	53801	3.8	13.3911	0.8	1.8689	1.4	0.1816	1.2	0.85	1075.7	12.2	1070.1	9.6	1058.9	15.4	1058.9	15.4	101.6
-04-Spot 7	292	93960	4.0	13.3276	0.7	1.8586	1.2	0.1797	0.9	0.80	1065.5	9.2	1066.5	7.7	1068.5	13.9	1068.5	13.9	99.7
4-Spot 148	820	252229	5.9	13.3229	0.8	1.7810	1.5	0.1722	1.2	0.83	1024.0	11.7	1038.5	9.6	1069.2	16.4	1069.2	16.4	95.8
4-Spot 299	403	37953	2.2	13.3137	0.8	1.8732	1.4	0.1810	1.1	0.78	1072.2	10.5	1071.7	9.0	1070.6	17.0	1070.6	17.0	100.1
4-Spot 236	225	182340	2.4	13.2977	1.1	1.8907	1.6	0.1824	1.1	0.73	1080.2	11.3	1077.8	10.4	1073.0	21.6	1073.0	21.6	100.7
04-Spot 27	322	141879	3.2	13.2944	0.9	1.9156	1.5	0.1848	1.2	0.81	1093.1	12.2	1086.5	10.0	1073.5	17.6	1073.5	17.6	101.8
4-Spot 125	104	139868	1.9	13.2731	0.9	1.9292	1.6	0.1858	1.3	0.81	1098.5	12.7	1091.2	10.4	1076.7	18.4	1076.7	18.4	102.0
4-Spot 259	174	81675	2.5	13.2573	0.9	1.9012	1.6	0.1829	1.4	0.85	1082.7	13.7	1081.5	10.8	1079.1	17.3	1079.1	17.3	100.3
4-Spot 275	156	44090	1.2	13.2536	1.0	1.8737	1.8	0.1802	1.5	0.83	1068.0	14.7	1071.8	11.8	1079.7	19.8	1079.7	19.8	98.9
04-Spot 74	52	14239	2.3	13.2503	1.0	1.8849	1.5	0.1812	1.1	0.71	1073.6	10.5	1075.8	9.9	1080.2	21.0	1080.2	21.0	99.4
4-Spot 117	319	72593	3.6	13.2470	0.8	1.9226	1.5	0.1848	1.3	0.86	1093.1	13.2	1089.0	10.2	1080.6	15.4	1080.6	15.4	101.2
4-Spot 187	118	125852	2.9	13.2362	0.9	1.8900	1.4	0.1815	1.1	0.76	1075.3	10.6	1077.6	9.3	1082.3	18.3	1082.3	18.3	99.3
4-Spot 294	180	1854760	1.6	13.2236	0.8	1.9295	1.3	0.1851	1.0	0.76	1094.9	9.6	1091.4	8.4	1084.2	16.4	1084.2	16.4	101.0
04-Spot 49	51	33103	1.7	13.2114	0.9	1.9501	1.9	0.1869	1.7	0.89	1104.8	17.6	1098.5	13.1	1086.1	17.7	1086.1	17.7	101.7
4-Spot 238	175	59897	1.4	13.2030	0.9	1.7985	1.5	0.1723	1.3	0.81	1024.8	11.8	1044.9	10.0	1087.3	17.9	1087.3	17.9	94.2
4-Spot 180	507	158989	2.6	13.1804	0.8	1.6868	1.5	0.1613	1.3	0.84	964.1	11.6	1003.6	9.7	1090.8	16.3	1090.8	16.3	88.4
4-Spot 256	204	78005	0.6	13.1574	0.8	1.9101	1.4	0.1824	1.1	0.80	1079.8	10.8	1084.6	9.1	1094.3	16.5	1094.3	16.5	98.7
-04-Spot 9	78	49229	1.7	13.1454	1.0	1.9201	1.7	0.1831	1.3	0.78	1084.1	13.0	1088.1	11.2	1096.1	20.9	1096.1	20.9	98.9
04-Spot 55	115	27908	1.4	13.1224	1.0	1.9641	1.5	0.1870	1.2	0.75	1105.1	11.8	1103.3	10.3	1099.6	20.1	1099.6	20.1	100.5
4-Spot 311	228	79258	3.7	13.1193	0.8	1.8715	1.3	0.1781	1.0	0.76	1056.8	9.5	1071.0	8.5	1100.1	16.7	1100.1	16.7	96.1
4-Spot 307	87	35373	1.1	13.1109	0.8	1.9032	1.5	0.1810	1.2	0.82	1072.7	11.9	1082.2	9.8	1101.3	16.9	1101.3	16.9	97.4
4-Spot 200	81	48949	2.0	13.0883	1.0	1.8813	1.7	0.1787	1.4	0.80	1059.6	13.3	1074.5	11.2	1104.8	20.2	1104.8	20.2	95.9
4-Spot 290	88	202516	1.6	13.0839	1.0	2.0084	1.5	0.1907	1.2	0.76	1125.0	11.9	1118.3	10.2	1105.5	19.4	1105.5	19.4	101.8
4-Spot 211	753	327987	2.5	13.0715	0.7	1.9811	1.6	0.1879	1.4	0.89	1109.9	14.5	1109.1	10.8	1107.4	14.5	1107.4	14.5	100.2
04-Spot 45	125	109375	1.5	13.0628	1.0	1.8782	1.7	0.1780	1.4	0.83	1056.2	14.0	1073.4	11.5	1108.7	19.3	1108.7	19.3	95.3
4-Spot 149	224	89800	1.5	13.0602	0.9	1.9391	1.6	0.1837	1.3	0.84	1087.4	13.1	1094.7	10.5	1109.1	17.1	1109.1	17.1	98.0
4-Spot 308	118	27152	2.4	13.0380	0.9	1.8765	1.6	0.1775	1.3	0.80	1053.4	12.2	1072.8	10.4	1112.5	18.5	1112.5	18.5	94.7
4-Spot 228	132	134505	1.6	13.0304	1.3	1.9687	1.9	0.1861	1.4	0.74	1100.4	14.0	1104.9	12.6	1113.7	25.0	1113.7	25.0	98.8
4-Spot 267	669	4711634	2.1	13.0216	0.7	1.9207	1.2	0.1815	1.0	0.81	1075.0	9.9	1088.3	8.2	1115.0	14.2	1115.0	14.2	96.4
04-Spot 15	71	44224	2.1	13.0181	1.1	2.0796	1.5	0.1964	1.1	0.72	1156.1	11.5	1142.1	10.4	1115.6	21.2	1115.6	21.2	103.6
04-Spot 72	100	9737	1.4	13.0125	1.1	2.0233	1.5	0.1910	1.1	0.73	1127.0	11.6	1123.4	10.4	1116.4	21.0	1116.4	21.0	100.9
4-Spot 122	146	51519	3.0	12.9632	0.8	1.9426	1.4	0.1827	1.1	0.80	1081.8	10.7	1095.9	9.1	1124.0	16.3	1124.0	16.3	96.2
04-Spot 41	416	72854	3.2	12.9525	0.8	1.9936	1.5	0.1874	1.2	0.85	1107.1	12.7	1113.3	10.0	1125.6	15.6	1125.6	15.6	98.3
4-Spot 288	101	32418	2.0	12.9245	0.8	2.1329	1.9	0.2000	1.7	0.91	1175.4	18.4	1159.5	13.1	1129.9	15.9	1129.9	15.9	104.0
04-Spot 50	94	48551	2.2	12.9081	1.0	1.9803	1.8	0.1855	1.5	0.82	1096.8	14.7	1108.8	12.0	1132.5	20.4	1132.5	20.4	96.9
04-Spot 82	224	219065	2.7	12.8975	0.7	2.0102	1.3	0.1881	1.1	0.85	1111.2	11.1	1119.0	8.7	1134.1	13.4	1134.1	13.4	98.0
4-Spot 251	41	12842	2.6	12.8902	1.3	2.1310	1.9	0.1993	1.3	0.70	1171.6	14.0	1158.9	12.9	1135.2	26.5	1135.2	26.5	103.2
4-Spot 131	17	16508	0.6	12.8773	1.4	2.0140	1.9	0.1882	1.3	0.67	1111.5	12.9	1120.2	12.7	1137.2	27.5	1137.2	27.5	97.7
4-Spot 145	544	367629	17.2	12.8732	1.0	2.0783	1.4	0.1941	1.0	0.72	1143.7	10.3	1141.7	9.4	1137.9	19.0	1137.9	19.0	100.5
04-Spot 46	31	11528	4.3	12.8631	1.3	2.1339	1.8	0.1992	1.2	0.68	1170.8	13.2	1159.8	12.5	1139.4	26.3	1139.4	26.3	102.8
4-Spot 119	198	66373	2.9	12.8564	0.9	2.1300	1.5	0.1987	1.1	0.77	1168.3	12.0	1158.6	10.1	1140.5	18.4	1140.5	18.4	102.4
04-Spot 10	32	9300	0.5	12.8519	1.4	2.1362	1.9	0.1992	1.3	0.69	1171.1	14.3	1160.6	13.4	1141.1	27.8	1141.1	27.8	102.6
04-Spot 25	115	101836	2.2	12.8457	0.9	2.1108	1.6	0.1967	1.3	0.83	1157.8	13.9	1152.3	10.9	1142.1	17.5	1142.1	17.5	101.4
04-Spot 14	919	644197	2.0	12.8374	0.7	2.1052	1.5	0.1961	1.3	0.88	1154.3	14.0	1150.5	10.3	1143.4	13.9	1143.4	13.9	101.0
4-Spot 127	180	40878	3.0	12.8370	0.8	2.1071	1.5	0.1963	1.2	0.83	1155.2	13.0	1151.1	10.2	1143.5	16.4	1143.5	16.4	101.0
4-Spot 205	59	12638	1.9	12.8338	1.2	2.0733	1.8	0.1931	1.3	0.72	1138.0	13.3	1140.0	12.2	1143.9	24.6	1143.9	24.6	99.5
4-Spot 121	63	22781	3.6	12.8186	0.9	2.1863	1.6	0.2033	1.3	0.83	1193.3	14.4	1176.7	11.1	1146.3	17.8	1146.3	17.8	104.1
4-Spot 293	106	23551	2.0	12.8156	1.0	2.1955	1.4	0.2042	1.0	0.70	1197.6	10.8	1179.6	9.8	1146.8	19.8	1146.8	19.8	104.4
04-Spot 95	443	288163	5.8	12.7800	0.6	2.1260	1.1	0.1971	0.9	0.82	1160.0	9.8	1157.3	7.8	1152.3	12.7	1152.3	12.7	100.7
4-Spot 100	149	214122	3.4	12.7689	0.8	2.1598	1.4	0.2001	1.2	0.84	1175.9	12.8	1168.2	9.9	1154.0	15.4	1154.0	15.4	101.9
04-Spot 23	119	70831	2.7	12.7614	1.0	2.1798	1.5	0.2018	1.2	0.75	1185.2	12.5	1174.6	10.7	1155.2	20.2	1155.2	20.2	102.6
04-Spot 89	68	11395	0.8	12.7571	0.9	2.1274	1.4	0.1969	1.1	0.78	1158.7	11.6	1157.7	9.7	1155.8	17.3	1155.8	17.3	100.3
-04-Spot 2	128	30032	2.4	12.7459	0.8	2.1424	1.4	0.1981	1.1	0.80	1165.3	11.7	1162.6	9.6	1157.6	16.5	1157.6	16.5	100.7
4-Spot 279	90	19544	2.5	12.7432	1.1	2.1864	1.6	0.2022	1.2	0.76	1186.9	13.6	1176.7	11.5	1158.0	21.2	1158.0	21.2	102.5
4-Spot 233	33	7337	3.0	12.7400	1.1	2.1645	1.7	0.2001	1.3	0.77	1175.8	13.9	1169.7	11.7	1158.5	21.4	1158.5	21.4	101.5
4-Spot 310	82	70471	2.4	12.7293	0.9	2.2234	1.6	0.2054	1.3	0.82	1204.0	14.2	1188.4	11.1	1160.2	18.1	1160.2	18.1	103.8
04-Spot 24	34	23649	3.2	12.7255	1.3	2.1276	2.0	0.1964	1.5	0.75	1156.2	15.8	1157.8	13.9	1160.8	26.5	1160.8	26.5	99.6
4-Spot 184	431	48022	4.0	12.6966	0.8	1.8852	1.6	0.1737	1.4	0.87	1032.3	13.5	1075.9	10.8	1165.3	16.2	1165.3	16.2	88.6
4-Spot 152	28	11251	1.8	12.6954	1.6	2.1446	2.1	0.1976	1.4	0.67	1162.2	14.9	1163.3	14.5	1165.4	31.0	1165.4	31.0	99.7
4-Spot 215	129	809812	2.7	12.6915	1.0	2.2102	1.6	0.2035	1.2	0.75	1194.3	13.0	1184.3	11.1	1166.1	20.6	1166.1	20.6	102.4
04-Spot 84	243	52724	2.7	12.6837	0.7	2.1000	1.2	0.1933	0.9	0.79	1139.0	9.8	1148.8	8.1	1167.3	14.4	1167.3	14.4	97.6
04-Spot 81	246	51587	2.0	12.6745	0.7	2.1499	1.3	0.1977	1.1	0.84	1163.0	11.6	1165.0	9.0	1168.8	14.1	1168.8	14.1	99.5
4-Spot 194	639	557050	2.7	12.6639	1.0	2.0717	1.7	0.1904	1.4	0.82	1123.4	13.9	1139.5	11.3	1170.4	18.9	1170.4	18.9	96.0
04-Spot 34	82	24577	2.5	12.6626	0.9	2.1597	1.7	0.1984	1.5	0.87	1166.9	15.9	1168.2	11.9	1170.6	16.9	1170.6	16.9	99.7
4-Spot 298	564	189559	3.4	12.6510	0.6	2.1608	1.2	0.1983	1.0	0.87	1166.4	10.9	1168.5	8.1	1172.4	11.3	1172.4	11.3	99.5

4-Spot 158	183	147909	2.7	12.6449	0.9	2.1965	1.4	0.2015	1.1	0.79	1183.5	12.0	1179.9	9.8	1173.4	17.3	1173.4	17.3	100.9
4-Spot 166	200	296260	2.5	12.6347	0.9	2.1962	1.4	0.2013	1.1	0.77	1182.5	11.7	1179.8	9.8	1175.0	17.5	1175.0	17.5	100.6
4-Spot 276	301	111513	5.8	12.6320	0.9	2.1821	1.5	0.2000	1.2	0.80	1175.4	13.2	1175.4	10.7	1175.4	18.0	1175.4	18.0	100.0
4-Spot 312	261	169663	3.6	12.6082	0.7	2.1562	1.2	0.1973	1.0	0.84	1160.6	10.9	1167.0	8.5	1179.1	13.3	1179.1	13.3	98.4
04-Spot 99	169	38343	3.2	12.6023	0.8	2.1145	1.8	0.1934	1.6	0.89	1139.5	17.2	1153.6	12.7	1180.1	16.7	1180.1	16.7	96.6
04-Spot 71	273	1550330	2.5	12.5965	0.7	2.0383	1.4	0.1863	1.2	0.85	1101.3	11.7	1128.4	9.2	1181.0	13.9	1181.0	13.9	93.3
04-Spot 32	91	20130	1.9	12.5902	1.0	2.2263	1.5	0.2034	1.1	0.74	1193.4	11.9	1189.3	10.4	1181.9	19.8	1181.9	19.8	101.0
4-Spot 123	547	62483	2.0	12.5814	0.6	1.9064	1.1	0.1740	0.9	0.84	1034.3	8.9	1083.3	7.4	1183.3	11.8	1183.3	11.8	87.4
4-Spot 271	40	76179	0.8	12.5802	1.5	1.9545	2.0	0.1784	1.3	0.65	1058.3	12.8	1100.0	13.6	1183.5	30.5	1183.5	30.5	89.4
04-Spot 53	196	64730	3.0	12.5593	0.9	2.2009	1.4	0.2006	1.0	0.72	1178.4	10.5	1181.3	9.5	1186.8	18.5	1186.8	18.5	99.3
4-Spot 199	116	22923	3.0	12.5438	1.1	2.3092	1.4	0.2102	0.9	0.64	1229.7	10.0	1215.1	9.9	1189.2	21.3	1189.2	21.3	103.4
4-Spot 116	106	91274	2.1	12.5331	0.9	2.2850	1.5	0.2078	1.2	0.79	1217.0	12.9	1207.6	10.4	1190.9	17.6	1190.9	17.6	102.2
4-Spot 161	124	70131	2.9	12.5292	1.1	2.2427	1.5	0.2039	1.1	0.69	1196.1	11.6	1194.5	10.8	1191.5	21.9	1191.5	21.9	100.4
4-Spot 234	155	65388	1.7	12.5204	0.8	2.2214	1.6	0.2018	1.4	0.87	1185.0	15.2	1187.8	11.4	1192.9	16.0	1192.9	16.0	99.3
4-Spot 257	226	101336	1.5	12.5203	0.8	2.1260	1.5	0.1931	1.3	0.87	1138.4	13.8	1157.3	10.6	1192.9	15.1	1192.9	15.1	95.4
04-Spot 93	43	19733	1.9	12.5056	0.9	2.2191	1.4	0.2014	1.0	0.74	1182.6	11.0	1187.1	9.6	1195.3	18.3	1195.3	18.3	98.9
4-Spot 172	203	73133	2.5	12.4957	0.8	2.2558	1.3	0.2045	1.0	0.78	1199.6	11.5	1198.6	9.5	1196.8	16.7	1196.8	16.7	100.2
4-Spot 237	151	44005	1.5	12.4199	1.0	2.2171	1.5	0.1998	1.2	0.78	1174.2	13.0	1186.4	10.8	1208.8	18.9	1208.8	18.9	97.1
4-Spot 230	94	14355	2.4	12.4005	1.0	2.2797	1.7	0.2051	1.4	0.81	1202.8	15.0	1206.0	11.9	1211.9	19.5	1211.9	19.5	99.2
4-Spot 235	60	48786	1.8	12.3662	1.3	2.2169	1.9	0.1989	1.3	0.71	1169.5	14.1	1186.4	13.0	1217.3	25.7	1217.3	25.7	96.1
4-Spot 164	214	54936	1.8	12.2699	0.9	2.3679	1.7	0.2108	1.5	0.86	1233.2	16.4	1233.0	12.1	1232.7	16.8	1232.7	16.8	100.0
4-Spot 212	227	54979	2.0	12.2164	1.3	2.2691	2.2	0.2011	1.7	0.80	1181.4	18.8	1202.7	15.3	1241.3	25.3	1241.3	25.3	95.2
4-Spot 224	94	32023	2.0	12.2154	0.9	2.4389	1.6	0.2162	1.4	0.85	1261.6	15.7	1254.1	11.7	1241.4	17.0	1241.4	17.0	101.6
4-Spot 132	199	85277	2.6	12.2116	0.7	2.3550	1.3	0.2087	1.1	0.85	1221.7	12.5	1229.1	9.5	1242.0	13.9	1242.0	13.9	98.4
4-Spot 139	234	113415	1.8	12.1983	0.8	2.2541	1.5	0.1995	1.3	0.85	1172.7	14.1	1198.1	10.8	1244.1	15.8	1244.1	15.8	94.3
04-Spot 30	167	55332	2.3	12.1578	0.8	2.3784	1.3	0.2098	1.0	0.80	1227.8	11.7	1236.1	9.4	1250.6	15.4	1250.6	15.4	98.2
4-Spot 196	115	47479	2.0	12.1568	1.1	2.3865	1.7	0.2105	1.3	0.77	1231.5	14.6	1238.6	12.1	1250.8	21.3	1250.8	21.3	98.5
4-Spot 162	256	75983	1.6	12.1143	0.8	2.4603	1.6	0.2163	1.3	0.86	1262.1	15.5	1260.5	11.4	1257.7	16.0	1257.7	16.0	100.4
04-Spot 86	29	11417	1.1	12.0989	2.2	2.0720	2.6	0.1819	1.3	0.50	1077.3	12.6	1139.6	17.5	1260.1	43.3	1260.1	43.3	85.5
4-Spot 282	90	90005	1.6	12.0824	1.0	2.3661	1.6	0.2074	1.3	0.78	1215.1	14.1	1232.4	11.7	1262.8	20.2	1262.8	20.2	96.2
04-Spot 60	231	212034	1.9	12.0399	0.8	2.4213	1.5	0.2115	1.2	0.83	1236.9	13.8	1248.9	10.6	1269.7	15.9	1269.7	15.9	97.4
4-Spot 273	197	34029	3.6	11.9978	0.9	2.3373	1.5	0.2035	1.2	0.81	1193.9	13.2	1223.7	10.7	1276.5	17.4	1276.5	17.4	93.5
4-Spot 181	141	23405	2.1	11.9789	1.1	2.4716	1.8	0.2148	1.5	0.79	1254.5	16.7	1263.8	13.3	1279.6	21.9	1279.6	21.9	98.0
04-Spot 90	170	61349	4.7	11.8986	0.9	2.4548	1.6	0.2119	1.3	0.80	1239.1	14.1	1258.8	11.3	1292.7	18.4	1292.7	18.4	95.9
04-Spot 85	67	34982	2.9	11.8959	0.9	2.4702	1.5	0.2132	1.3	0.83	1245.9	14.5	1263.4	11.2	1293.1	16.9	1293.1	16.9	96.3
4-Spot 272	266	112165	3.3	11.8154	0.8	2.6503	1.2	0.2272	1.0	0.79	1319.9	11.8	1314.7	9.2	1306.3	14.9	1306.3	14.9	101.0
04-Spot 35	234	147141	2.3	11.8143	0.7	2.6116	1.6	0.2239	1.4	0.90	1302.3	16.6	1303.9	11.5	1306.5	13.6	1306.5	13.6	99.7
4-Spot 134	144	60473	2.5	11.8140	0.8	2.6670	1.4	0.2286	1.1	0.80	1327.3	13.1	1319.4	10.2	1306.6	16.2	1306.6	16.2	101.6
4-Spot 305	264	66652	1.8	11.7626	1.0	2.4579	1.6	0.2098	1.3	0.79	1227.6	14.4	1259.7	11.7	1315.0	19.2	1315.0	19.2	93.4
04-Spot 29	115	91321	2.9	11.7327	1.1	2.6348	1.8	0.2243	1.4	0.77	1304.6	16.0	1310.4	12.9	1320.0	21.8	1320.0	21.8	98.8
04-Spot 18	183	40890	2.4	11.7314	0.9	2.7899	1.5	0.2375	1.2	0.82	1373.6	15.3	1352.8	11.3	1320.2	16.9	1320.2	16.9	104.0
04-Spot 39	210	235850	2.9	11.7261	0.7	2.4819	1.4	0.2112	1.2	0.84	1235.0	13.0	1266.8	9.9	1321.1	14.2	1321.1	14.2	93.5
4-Spot 278	211	71661	1.2	11.7195	0.8	2.5760	1.5	0.2190	1.2	0.82	1276.8	14.0	1293.8	10.8	1322.1	16.4	1322.1	16.4	96.6
4-Spot 179	72	65111	1.3	11.6998	1.0	2.7120	1.7	0.2302	1.4	0.81	1335.7	16.4	1331.8	12.5	1325.4	19.4	1325.4	19.4	100.8
4-Spot 296	48	15350	2.0	11.6916	1.1	2.6611	1.7	0.2257	1.4	0.79	1312.2	16.0	1317.7	12.7	1326.8	20.5	1326.8	20.5	98.9
04-Spot 44	458	94885	2.6	11.6598	0.9	2.4670	1.5	0.2087	1.2	0.82	1221.9	13.6	1262.4	10.8	1332.0	16.8	1332.0	16.8	91.7
04-Spot 79	275	79116	3.4	11.6510	0.6	2.7741	1.2	0.2345	1.0	0.86	1358.1	12.6	1348.6	9.0	1333.5	12.0	1333.5	12.0	101.8
4-Spot 182	299	135387	2.3	11.6486	1.2	2.4339	1.6	0.2057	1.1	0.68	1206.0	12.1	1252.7	11.7	1333.9	23.1	1333.9	23.1	90.4
4-Spot 253	70	26590	3.1	11.6324	1.0	2.7961	1.5	0.2360	1.1	0.76	1365.9	14.1	1354.5	11.3	1336.6	19.1	1336.6	19.1	102.2
4-Spot 247	218	350849	1.9	11.6202	1.0	2.7000	1.5	0.2276	1.1	0.76	1322.2	13.3	1328.5	10.9	1338.6	18.6	1338.6	18.6	98.8
4-Spot 242	52	29112	1.6	11.6175	0.9	2.7398	1.6	0.2309	1.3	0.81	1339.5	15.6	1339.3	11.8	1339.1	17.8	1339.1	17.8	100.0
4-Spot 309	64	11989	1.9	11.6173	0.9	2.6504	1.6	0.2234	1.2	0.80	1299.9	14.7	1314.8	11.5	1339.1	18.0	1339.1	18.0	97.1
04-Spot 88	303	160334	3.6	11.6138	0.8	2.7496	1.4	0.2317	1.1	0.82	1343.4	13.9	1342.0	10.5	1339.7	15.6	1339.7	15.6	100.3
4-Spot 315	164	105842	2.7	11.6103	0.7	2.6745	1.6	0.2253	1.4	0.89	1309.8	17.1	1321.4	12.0	1340.3	14.1	1340.3	14.1	97.7
4-Spot 241	277	70229	1.9	11.5920	0.7	2.4151	1.6	0.2031	1.4	0.88	1192.1	15.1	1247.1	11.2	1343.3	14.1	1343.3	14.1	88.7
4-Spot 188	197	66407	2.2	11.5802	0.9	2.7027	1.7	0.2271	1.5	0.84	1319.2	17.4	1329.2	12.8	1345.3	18.0	1345.3	18.0	98.1
04-Spot 12	137	41157	2.4	11.5722	0.8	2.7582	1.4	0.2316	1.1	0.81	1342.9	13.9	1344.3	10.6	1346.6	16.1	1346.6	16.1	99.7
04-Spot 17	63	46225	2.5	11.5412	1.0	2.9157	1.7	0.2442	1.4	0.80	1408.3	17.2	1386.0	12.8	1351.8	19.6	1351.8	19.6	104.2
4-Spot 150	106	85164	3.6	11.5319	0.8	2.8183	1.5	0.2358	1.2	0.81	1364.9	14.5	1360.4	10.9	1353.3	16.3	1353.3	16.3	100.9
4-Spot 254	165	62004	3.5	11.5287	0.9	2.7444	1.4	0.2296	1.1	0.76	1332.2	12.8	1340.6	10.5	1353.9	17.7	1353.9	17.7	98.4
4-Spot 155	132	54501	0.5	11.4960	0.8	2.7783	1.6	0.2317	1.4	0.86	1343.7	16.5	1349.7	11.8	1359.3	15.8	1359.3	15.8	98.8
4-Spot 306	243	168266	3.6	11.4808	0.7	2.7011	1.4	0.2250	1.2	0.85	1308.3	13.9	1328.8	10.2	1361.9	13.8	1361.9	13.8	96.1
04-Spot 94	270	78954	1.9	11.4691	0.8	2.8665	1.4	0.2385	1.1	0.81	1379.1	14.2	1373.2	10.7	1363.9	16.2	1363.9	16.2	101.1
4-Spot 143	350	114541	1.3	11.4261	0.8	2.8803	1.4	0.2388	1.2	0.82	1380.4	14.7	1376.8	10.9	1371.1	15.8	1371.1	15.8	100.7
4-Spot 114	92	26065	2.2	11.4184	0.7	2.9383	1.2	0.2434	1.0	0.82	1404.5	12.9	1391.8	9.4	1372.4	13.8	1372.4	13.8	102.3
4-Spot 291	175	59920	1.3	11.4108	0.8	2.8607	1.5	0.2368	1.2	0.81	1370.3	14.6	1371.6	10.9	1373.7	16.3	1373.7	16.3	99.8
04-Spot 48	64	486095	1.6	11.4096	1.1	2.9166	1.4	0.2415	0.9	0.65	1394.3	11.7	1386.2	10.9	1373.9	21.0	1373.9	21.0	101.5
4-Spot 206	201	66815	3.2	11.4054	0.7	2.9062	1.5	0.2405	1.3	0.88	1389.3	16.6	1383.5	11.5	1374.6	14.1	1374.6	14.1	101.1
4-Spot 260	212	275843	2.0	11.3846	1.0	2.8474	1.6	0.2352	1.2	0.78	1361.7	15.2	1368.1	11.9	1378.1	18.9	1378.1	18.9	98.8
4-Spot 163	58	48105	1.6	11.3685	1.0	2.8993	1.8	0.2392	1.5	0.82	1382.3	18.5	1381.7	13.7	1380.8	20.0	1380.8	20.0	100.1
4-Spot 129	118	31773	1.4	11.3586	0.8	2.8966	1.2	0.2387	0.9	0.73	1380.1	11.1	1381.0	9.3	1382.5	16.3	1382.5	16.3	99.8
4-Spot 204	165	70154	2.9	11.3549	0.9	2.8712	1.5	0.2366	1.2	0.81	1368.7	15.0	1374.4	11.3	1383.1	16.7	1383.1	16.7	99.0
4-Spot 217	103	106542	2.9	11.3527	1.0	3.0095	1.6	0.2479	1.2	0.76	1427.7	15.5	1410.0	12.2	1383.5	20.1	1383.5	20.1	103.2
04-Spot 43	395	125090	5.8	11.3496	0.7	2.9198	1.1	0.2405	0.8	0.75	1389.0	10.1	1387.1	8.1	1384.0	13.6	1384.0	13.6	100.4
04-Spot 36	55	29340	1.5	11.3439	0.9	2.8484	1.8	0.2345	1.6	0.87	1357.8	19.0	1368.4	13.3	1385.0	16.6	1385.0	16.6	98.0
4-Spot 159	81	23347	3.7	11.3381	0.7	2.9492	1.5	0.2426	1.4	0.89	1400.3	17.3	1394.6	11.7	1386.0	13.4	1386.0	13.4	101.0
4-Spot 157	344	119655	2.8	11.3265	0.8	2.8307	1.3	0.2326	1.0	0.80	1348.3	12.3	1363.7	9.5	1387.9	14.7	1387.9	14.7	97.1
4-Spot 232	135	269137	2.8	11.3027	1.0	2.9907	1.5	0.2453	1.2	0.77	1414.0	14.9	1405.3	11.6	1391.9	18.4	1391.9	18.4	101.6
4-Spot 262	380	151717	3.0	11.2901	1.0	2.8884	1.4	0.2366	1.0	0.72	1369.1	12.3	1378.9	10.4	1394.1	18.3	1394.1	18.3	98.2
4-Spot 292	133	94236	1.5	11.2841	0.9	2.8992	1.4	0.2374	1.0	0.74	1373.0	12.7	1381.7	10.5	1395.1	18.0	1395.1	18.0	98.4
4-Spot 136	195	3050114	1.8	11.2783	0.6	2.9361	1.2	0.2403	1.1	0.87	1388.1	13.6	1391.3	9.4	1396.1	11.6	1396.1	11.6	99.4
4-Spot 263	55	35335	0.8	11.2754	0.9	2.8818	1.5	0.2358	1.2	0.81	1364.6	14.6	1377.2	11.1	1396.6	16.6	1396.6	16.6	97.7
04-Spot 76	160	73473	2.7	11.2646	0.9	2.7205	1.5	0.2224	1.2	0.81	1294.3	14.1	1334.1	11.0	1398.4	16.7	1398.4	16.7	92.6
4-Spot 185	69	63334	2.6	11.2544	1.2	2.8990	1.8	0.2367	1.3	0.74	1369.7	16.6	1381.7	13.7	1400.2	23.3	1400.2	23.3	97.8
04-Spot 21	259	103310	2.1	11.2312	0.9	2.9104	1.6	0.2372	1.3	0.81	1372.0	16.5	1384.6	12.4	1404.1	18.2	1404.1	18.2	97.7
4-Spot 289	294	529136	3.8	11.2185	0.9	2.7992	1.6	0.2279	1.3	0.82	1323.2	15.7	1355.3	12.0	1406.3	17.5	1406.3	17.5	94.1
4-Spot 243	93	1182818	1.5	11.2146	0.8	3.0074	1.3	0.2447	1.0	0.80	1411.2	13.0	1409.5	9.7	1407.0	14.6	1407.0	14.6	100.3
4-Spot 133	135	210479	0.8	11.2069	0.8	2.9572	1.5	0.2405	1.2	0.83	1389.1	15.4	1396.7	11.3	1408.3	16.0	1408.3	16.0	98.6
4-Spot 280	54	66069	2.1	11.2024	0.9	2.9765	1.7	0.2419	1.4	0.84	1396.8	17.6	1401.6	12.7	1409.0	17.5	1409.0	17.5	99.1
04-Spot 77	321	425047	1.1	11.1671	0.8	3.0876	1.5	0.2502	1.2	0.82	1439.4	15.7	1429.6	11.3	1415.1	16.0	1415.1	16.0	101.7
4-Spot 213	281	91020	1.4	11.1532	0.9	2.9132	1.6	0.2358	1.4	0.85	1364.6	17.1	1385.3	12.4	1417.4	16.5	1417.4	16.5	96.3
4-Spot 239	145	204104	1.2	11.1311	0.8	2.9480	1.6	0.2381	1.3	0.84	1376.8	16.1	1394.3	11.8	1421.2	16.2	1421.2	16.2	96.9
04-Spot 65	20	68624	0.8	11.1072	1.3	2.9744	1.8	0.2397	1.2	0.70	1385.2	15.2	1401.1	13.3	1425.3	24.0	1425.3	24.0	97.2
04-Spot 20	224	159386	2.1	11.1062	1.0	2.4996	2.1	0.2014	1.9	0.88	1183.0	20.1	1271.9	15.3	1425.5	19.3	1425.5	19.3	83.0
4-Spot 169	92	22311	1.9	11.0957	0.9	3.0980	1.5	0.2494	1.2	0.80	1435.5	15.2	1432.2	11.3	1427.3	16.8	1427.3	16.8	100.6
4-Spot 153	358	62062	2.3	11.0869	0.9	2.9152	1.4	0.2345	1.1	0.80	1358.1	14.1	1385.9	10.9	1428.9	16.5	1428.9	16.5	95.0

4-Spot 112	330	63916	2.7	11.0747	0.8	2.9246	1.4	0.2350	1.1	0.80	1360.7	13.5	1388.3	10.5	1430.9	15.9	1430.9	15.9	95.1
4-Spot 258	81	337595	1.0	11.0578	1.1	2.9478	2.5	0.2365	2.3	0.90	1368.5	28.2	1394.3	19.3	1433.9	21.4	1433.9	21.4	95.4
4-Spot 124	278	1067132	1.9	11.0542	0.9	2.9754	1.4	0.2386	1.0	0.77	1379.7	13.0	1401.4	10.3	1434.5	16.4	1434.5	16.4	96.2
4-Spot 266	253	160452	3.0	11.0146	0.9	3.0978	1.6	0.2476	1.3	0.82	1426.0	17.1	1432.2	12.6	1441.3	17.9	1441.3	17.9	98.9
4-Spot 118	104	60076	1.5	11.0096	1.1	3.1886	2.0	0.2547	1.7	0.83	1462.7	21.8	1454.4	15.4	1442.2	21.1	1442.2	21.1	101.4
04-Spot 98	127	418360	2.2	10.9750	0.9	3.1429	1.4	0.2503	1.1	0.77	1439.9	13.9	1443.2	10.8	1448.2	17.1	1448.2	17.1	99.4
4-Spot 195	146	123566	2.4	10.9710	1.0	3.1286	1.6	0.2490	1.3	0.79	1433.6	16.8	1439.7	12.6	1448.9	19.0	1448.9	19.0	98.9
4-Spot 156	263	64692	2.1	10.9687	0.8	3.0955	1.6	0.2464	1.4	0.87	1419.7	17.5	1431.6	12.1	1449.3	14.9	1449.3	14.9	98.0
4-Spot 135	85	43110	1.4	10.9617	0.9	3.2509	1.5	0.2586	1.2	0.82	1482.5	16.3	1469.4	11.7	1450.5	16.5	1450.5	16.5	102.2
4-Spot 250	130	4206700	2.5	10.9430	0.8	3.1704	1.4	0.2517	1.2	0.84	1447.4	15.5	1450.0	11.0	1453.7	14.8	1453.7	14.8	99.6
4-Spot 183	200	163811	1.3	10.9414	0.7	3.3194	1.5	0.2635	1.3	0.87	1507.8	17.2	1485.6	11.5	1454.0	13.7	1454.0	13.7	103.7
4-Spot 176	219	161918	1.8	10.9334	0.8	3.1279	1.8	0.2481	1.6	0.90	1428.9	20.5	1439.6	13.7	1455.4	15.0	1455.4	15.0	98.2
4-Spot 126	154	37771	1.3	10.9062	0.8	3.2414	1.2	0.2565	0.9	0.77	1471.9	12.0	1467.1	9.2	1460.2	14.4	1460.2	14.4	100.8
4-Spot 302	81	749531	2.6	10.8992	1.0	3.2953	1.5	0.2606	1.1	0.76	1492.9	15.0	1479.9	11.5	1461.4	18.2	1461.4	18.2	102.2
4-Spot 270	618	4207214	2.7	10.8962	0.7	3.2027	1.4	0.2532	1.2	0.87	1455.0	16.1	1457.8	11.0	1461.9	13.0	1461.9	13.0	99.5
4-Spot 231	341	2087683	1.0	10.8901	0.8	3.1928	1.5	0.2523	1.3	0.84	1450.3	16.7	1455.4	11.8	1463.0	15.8	1463.0	15.8	99.1
4-Spot 144	141	45466	2.1	10.8598	0.8	3.1964	1.6	0.2519	1.3	0.84	1448.1	16.9	1456.3	12.0	1468.2	16.1	1468.2	16.1	98.6
04-Spot 19	75	51972	3.0	10.8524	0.8	3.2189	1.6	0.2535	1.4	0.87	1456.3	18.6	1461.7	12.6	1469.5	15.0	1469.5	15.0	99.1
4-Spot 283	60	36794	1.4	10.8357	0.9	3.2504	1.4	0.2556	1.1	0.78	1467.1	14.7	1469.3	11.1	1472.5	16.9	1472.5	16.9	99.6
4-Spot 285	449	479331	5.9	10.8258	0.8	3.2819	1.6	0.2578	1.4	0.88	1478.6	18.6	1476.8	12.5	1474.2	14.4	1474.2	14.4	100.3
4-Spot 106	159	50503	2.2	10.8060	0.7	3.3127	1.2	0.2597	0.9	0.79	1488.5	12.3	1484.1	9.1	1477.7	13.4	1477.7	13.4	100.7
04-Spot 57	167	80316	2.2	10.7983	1.0	3.2657	1.8	0.2559	1.5	0.82	1468.7	19.2	1472.9	13.9	1479.0	19.4	1479.0	19.4	99.3
4-Spot 264	226	285708	1.8	10.7168	0.7	3.2955	1.4	0.2563	1.2	0.86	1470.7	15.7	1480.0	10.8	1493.4	13.4	1493.4	13.4	98.5
4-Spot 281	157	788035	1.8	10.6786	0.9	3.3399	1.7	0.2588	1.4	0.85	1483.6	19.1	1490.4	13.2	1500.1	16.6	1500.1	16.6	98.9
4-Spot 286	138	74165	1.7	10.5329	0.9	3.1431	1.5	0.2402	1.2	0.82	1387.8	15.5	1443.3	11.7	1526.1	16.4	1526.1	16.4	90.9
4-Spot 314	200	67273	3.9	10.4130	0.7	3.6132	1.1	0.2730	0.9	0.78	1556.0	12.1	1552.4	8.9	1547.6	13.2	1547.6	13.2	100.5
4-Spot 209	128	5307	6.3	10.2940	1.8	3.3416	3.4	0.2496	2.9	0.84	1436.3	37.3	1490.8	26.9	1569.2	34.5	1569.2	34.5	91.5
4-Spot 313	526	42773	1.2	10.0499	0.7	3.1240	1.7	0.2278	1.6	0.92	1323.0	19.1	1438.6	13.4	1614.0	12.6	1614.0	12.6	82.0
04-Spot 42	189	37431	3.1	10.0060	0.8	4.0761	1.3	0.2959	1.1	0.82	1671.1	16.2	1649.5	10.9	1622.1	14.1	1622.1	14.1	103.0
4-Spot 248	357	299364	1.6	9.9657	0.9	3.8700	1.4	0.2798	1.1	0.78	1590.5	15.0	1607.4	11.0	1629.6	16.0	1629.6	16.0	97.6
4-Spot 287	166	176222	1.2	9.9225	0.9	3.8738	1.6	0.2789	1.3	0.81	1585.8	18.2	1608.2	12.9	1637.7	17.5	1637.7	17.5	96.8
04-Spot 52	373	327584	1.6	9.8822	0.9	4.0201	1.3	0.2883	1.0	0.74	1632.8	14.3	1638.3	11.0	1645.3	16.9	1645.3	16.9	99.2
4-Spot 295	321	115045	2.2	9.8808	0.8	3.6939	1.4	0.2648	1.2	0.82	1514.5	15.9	1570.0	11.4	1645.5	15.0	1645.5	15.0	92.0
4-Spot 170	151	56425	1.1	9.8757	0.9	4.0153	1.9	0.2877	1.6	0.87	1630.1	23.4	1637.3	15.3	1646.5	17.4	1646.5	17.4	99.0
4-Spot 171	160	135814	0.9	9.8649	1.0	3.4471	1.4	0.2467	1.0	0.70	1421.6	12.8	1515.2	11.3	1648.5	19.2	1648.5	19.2	86.2
-04-Spot 6	93	75360	1.0	9.8294	1.0	4.1205	1.4	0.2939	1.1	0.74	1660.9	15.7	1658.4	11.8	1655.2	17.8	1655.2	17.8	100.3
04-Spot 56	181	42229	2.6	9.7782	0.8	4.1424	1.2	0.2939	0.9	0.76	1661.0	12.9	1662.7	9.6	1664.9	14.1	1664.9	14.1	99.8
4-Spot 240	141	40335	1.3	9.7445	0.8	4.0775	1.6	0.2883	1.3	0.86	1633.0	19.2	1649.8	12.6	1671.2	14.8	1671.2	14.8	97.7
4-Spot 301	279	1085412	1.5	9.7130	0.8	4.1972	1.6	0.2958	1.4	0.86	1670.5	20.7	1673.5	13.4	1677.2	15.4	1677.2	15.4	99.6
4-Spot 197	51	64511	5.0	9.7054	1.0	3.9803	1.8	0.2803	1.5	0.83	1592.8	21.4	1630.2	14.9	1678.7	19.1	1678.7	19.1	94.9
-04-Spot 3	204	1177604	1.2	9.7051	0.7	4.2004	1.3	0.2958	1.1	0.83	1670.4	16.5	1674.1	11.1	1678.8	13.8	1678.8	13.8	99.5
4-Spot 300	81	208471	2.1	9.6797	0.9	4.3055	1.6	0.3024	1.4	0.84	1703.2	20.4	1694.4	13.4	1683.6	16.4	1683.6	16.4	101.2
4-Spot 210	88	185812	1.2	9.6436	1.1	4.2585	1.9	0.2980	1.6	0.82	1681.3	23.0	1685.4	15.7	1690.5	20.3	1690.5	20.3	99.5
4-Spot 107	271	127041	2.1	9.5523	0.9	4.2894	1.5	0.2973	1.2	0.79	1677.9	17.1	1691.3	12.0	1708.0	16.4	1708.0	16.4	98.2
4-Spot 220	276	70624	5.3	9.5422	0.7	4.3315	1.6	0.2999	1.4	0.88	1690.8	20.7	1699.4	13.0	1709.9	13.7	1709.9	13.7	98.9
4-Spot 304	51	49222	2.6	9.5280	0.9	4.4445	1.7	0.3073	1.5	0.84	1727.2	22.1	1720.7	14.4	1712.7	17.2	1712.7	17.2	100.8
4-Spot 225	482	76628	4.1	9.5186	0.7	3.6646	1.6	0.2531	1.4	0.90	1454.4	18.6	1563.7	12.7	1714.5	13.0	1714.5	13.0	84.8
4-Spot 190	32	9429	1.7	9.5057	1.9	3.6391	2.7	0.2510	2.0	0.71	1443.6	25.3	1558.1	21.8	1717.0	35.3	1717.0	35.3	84.1
4-Spot 284	112	24950	3.3	9.4865	0.9	4.3488	1.5	0.2993	1.2	0.82	1688.0	18.4	1702.7	12.5	1720.7	16.0	1720.7	16.0	98.1
4-Spot 151	595	247042	6.7	9.4548	0.8	4.0243	2.0	0.2761	1.9	0.93	1571.6	26.0	1639.1	16.3	1726.9	13.8	1726.9	13.8	91.0
4-Spot 244	170	1365935	2.6	9.4041	0.6	4.5190	1.4	0.3084	1.3	0.91	1732.6	20.1	1734.5	12.0	1736.7	10.8	1736.7	10.8	99.8
4-Spot 221	189	118209	3.7	9.3751	0.7	4.0762	1.8	0.2773	1.7	0.93	1577.6	23.6	1649.6	14.7	1742.4	12.1	1742.4	12.1	90.5
4-Spot 268	221	74033	1.8	9.3634	0.7	4.5002	1.4	0.3057	1.3	0.88	1719.7	19.0	1731.0	11.9	1744.7	12.3	1744.7	12.3	98.6
4-Spot 269	575	46270	2.3	9.3575	0.8	3.6960	1.3	0.2509	1.1	0.81	1443.3	13.6	1570.5	10.4	1745.8	14.1	1745.8	14.1	82.7
4-Spot 192	240	179086	2.5	9.3354	0.9	4.2374	1.5	0.2870	1.2	0.80	1626.6	16.8	1681.3	12.0	1750.2	16.0	1750.2	16.0	92.9
4-Spot 110	62	32443	4.3	9.3239	0.9	4.7211	1.4	0.3194	1.1	0.79	1786.8	17.7	1771.0	12.0	1752.4	16.2	1752.4	16.2	102.0
-04-Spot 5	541	203967	1.7	9.2864	0.6	4.6238	1.1	0.3116	1.0	0.84	1748.4	14.7	1753.6	9.5	1759.8	11.3	1759.8	11.3	99.4
4-Spot 222	116	83728	1.0	9.2817	0.8	4.8213	1.4	0.3247	1.2	0.82	1812.6	18.3	1788.6	11.9	1760.7	14.8	1760.7	14.8	102.9
04-Spot 97	347	136889	1.2	9.2755	0.6	4.7375	1.2	0.3188	1.0	0.85	1784.0	15.9	1773.9	10.1	1761.9	11.4	1761.9	11.4	101.3
04-Spot 83	303	182560	2.8	9.2658	0.7	4.6716	1.4	0.3141	1.1	0.85	1760.7	17.7	1762.2	11.3	1763.8	13.0	1763.8	13.0	99.8
4-Spot 138	283	150034	4.6	9.2522	0.7	4.8478	1.2	0.3254	0.9	0.79	1816.2	14.9	1793.2	10.0	1766.5	13.3	1766.5	13.3	102.8
04-Spot 13	259	149261	2.1	9.2355	0.8	4.5280	1.2	0.3034	0.9	0.78	1708.3	14.1	1736.1	10.0	1769.8	13.9	1769.8	13.9	96.5
4-Spot 277	304	71135	1.4	9.2322	0.8	4.6863	1.5	0.3139	1.2	0.84	1760.0	18.8	1764.8	12.2	1770.5	14.6	1770.5	14.6	99.4
4-Spot 198	74	38932	2.2	9.2309	1.0	4.7905	1.6	0.3209	1.2	0.77	1793.9	18.8	1783.2	13.1	1770.7	18.1	1770.7	18.1	101.3
04-Spot 80	352	76759	8.3	9.2189	0.7	4.6937	1.2	0.3140	1.0	0.81	1760.2	15.5	1766.1	10.4	1773.1	13.2	1773.1	13.2	99.3
4-Spot 214	567	64622	2.9	9.2139	0.9	4.2043	1.9	0.2811	1.7	0.88	1596.8	23.9	1674.9	15.8	1774.1	17.0	1774.1	17.0	90.0
4-Spot 173	237	108223	2.6	9.2000	0.6	4.7916	1.3	0.3199	1.1	0.87	1789.0	17.4	1783.4	10.7	1776.9	11.2	1776.9	11.2	100.7
04-Spot 96	195	65263	1.6	9.1586	0.7	4.7965	1.1	0.3187	0.9	0.79	1783.6	13.3	1784.3	9.0	1785.1	12.0	1785.1	12.0	99.9
4-Spot 115	102	114115	3.0	9.1556	1.0	4.8605	1.7	0.3229	1.4	0.81	1803.8	21.9	1795.4	14.4	1785.7	18.2	1785.7	18.2	101.0
4-Spot 103	234	291355	1.9	9.1553	0.8	4.7626	1.5	0.3164	1.3	0.86	1772.0	19.9	1778.3	12.5	1785.7	13.9	1785.7	13.9	99.2
4-Spot 229	112	1218834	1.0	9.1352	0.6	4.7850	1.6	0.3172	1.5	0.92	1775.9	23.0	1782.3	13.5	1789.7	11.5	1789.7	11.5	99.2
4-Spot 252	138	173183	4.6	9.1341	0.7	4.9281	1.4	0.3266	1.2	0.87	1821.9	18.8	1807.1	11.5	1790.0	12.3	1790.0	12.3	101.8
4-Spot 113	121	65154	3.2	9.1290	1.0	4.1329	1.5	0.2738	1.2	0.79	1559.8	16.9	1660.8	12.7	1791.0	17.4	1791.0	17.4	87.1
4-Spot 249	234	654706	3.9	9.0384	0.8	4.9865	1.2	0.3270	0.9	0.77	1823.9	14.5	1817.0	10.1	1809.1	13.9	1809.1	13.9	100.8
04-Spot 54	478	93435	2.1	8.9576	0.7	4.5047	1.3	0.2928	1.1	0.84	1655.4	15.5	1731.8	10.6	1825.4	12.6	1825.4	12.6	90.7
04-Spot 37	370	644867	1.8	8.9387	0.9	4.3995	1.7	0.2853	1.5	0.85	1618.2	20.8	1712.2	14.1	1829.3	16.1	1829.3	16.1	88.5
04-Spot 66	79	17981	9.9	8.8884	0.9	5.1956	1.6	0.3351	1.4	0.85	1863.0	22.0	1851.9	13.7	1839.5	15.5	1839.5	15.5	101.3
4-Spot 120	193	79933	3.8	8.8008	1.0	5.0331	1.4	0.3214	1.0	0.74	1796.6	16.4	1824.9	12.0	1857.4	17.3	1857.4	17.3	96.7
4-Spot 189	74	65253	11.8	8.7882	0.9	5.2882	1.6	0.3372	1.3	0.81	1873.2	21.0	1867.0	13.6	1860.0	16.9	1860.0	16.9	100.7
4-Spot 130	94	184792	0.5	8.6477	0.9	5.4491	1.4	0.3419	1.1	0.77	1895.9	17.4	1892.6	11.8	1889.0	15.9	1889.0	15.9	100.4
4-Spot 175	295	734232	1.7	8.5930	0.9	5.3345	1.5	0.3326	1.3	0.82	1851.0	20.5	1874.4	13.2	1900.5	15.7	1900.5	15.7	97.4
04-Spot 78	486	67651	3.0	6.7321	0.9	6.8609	1.5	0.3351	1.2	0.82	1863.2	19.5	2093.6	13.1	2328.4	14.7	2328.4	14.7	80.0
4-Spot 265	329	679689	1.7	6.2723	0.7	10.3046	1.3	0.4690	1.1	0.83	2479.0	23.1	2462.5	12.5	2448.9	12.6	2448.9	12.6	101.2
04-Spot 22	68	71810	1.6	6.2310	0.9	8.9437	1.6	0.4044	1.3	0.81	2189.0	24.3	2332.3	14.7	2460.1	15.9	2460.1	15.9	89.0
4-Spot 303	48	58592	1.6	5.9385	0.9	11.4037	1.4	0.4914	1.1	0.79	2576.6	24.3	2556.7	13.5	2541.0	14.9	2541.0	14.9	101.4
4-Spot 193	408	74320	0.6	5.8076	0.7	10.1422	1.1	0.4274	0.9	0.78	2293.9	17.1	2447.8	10.5	2578.3	11.9	2578.3	11.9	89.0
04-Spot 91	82	79713	1.3	5.7020	0.8	11.7163	1.6	0.4847	1.4	0.85	2547.8	28.7	2582.0	15.0	2608.9	13.9	2608.9	13.9	97.7
4-Spot 111	253	62766	1.4	5.6733	0.9	9.4886	1.4	0.3906	1.1	0.79	2125.6	19.9	2386.4	12.8	2617.3	14.3	2617.3	14.3	81.2
04-Spot 16	179	59312	1.4	5.6502	0.9	9.4441	1.8	0.3872	1.6	0.88	2109.7	29.1	2382.1	16.8	2624.1	14.3	2624.1	14.3	80.4
4-Spot 208	292	134635	2.1	5.5715	0.7	10.6316	1.4	0.4298	1.2	0.86	2304.8	24.1	2491.5	13.4	2647.4	12.2	2647.4	12.2	87.1
04-Spot 59	186	111719	2.8	5.5487	0.8	12.2271	1.3	0.4923	1.0	0.78	2580.5	21.8	2622.0	12.4	2654.2	13.8	2654.2	13.8	97.2
4-Spot 165	60	66525	1.2	5.4900	0.9	13.3892	1.6	0.5333	1.3	0.82	2755.5	29.5	2707.5	15.2	2671.8	15.2	2671.8	15.2	103.1
4-Spot 154	418	597294	2.9	5.4867	0.8	13.1334	1.5	0.5228	1.3	0.86	2711.2	29.0	2689.3	14.4	2672.8	13.1	2672.8	13.1	101.4
4-Spot 102	106	142959	1.3	5.4825	0.7	13.2054	1.2	0.5253	1.0	0.83	2721.7	21.1	2694.4	10.9	2674.1	10.8	2674.1	10.8	101.8
04-Spot 67	108	948959	1.0	5.4603	0.9	13.2302	1.6	0.5242	1.4	0.85	2716.8	30.8	2696.2	15.4	2680.8	14.2	2680.8	14.2	101.3
-04-Spot 8	121	176823	1.0	5.4571	0.7	13.2207	1.4	0.5235	1.2	0.87	2713.9	27.6	2695.5	13.5	2681.7	11.7	2681.7	11.7	101.2

4-Spot 147	13	1017	28.7	5.4325	2.4	11.1089	4.3	0.4379	3.6	0.83	2341.1	70.2	2532.3	40.0	2689.2	39.4	2689.2	39.4	87.1
4-Spot 128	180	1368202	1.0	5.4278	0.7	13.1565	1.6	0.5181	1.4	0.89	2691.3	30.9	2690.9	14.9	2690.6	12.0	2690.6	12.0	100.0
04-Spot 58	67	71083	1.0	5.3857	0.6	13.5756	1.3	0.5305	1.2	0.89	2743.6	26.7	2720.6	12.7	2703.5	10.3	2703.5	10.3	101.5
4-Spot 191	86	67546	2.4	5.3785	0.9	11.7776	1.4	0.4596	1.1	0.77	2437.9	22.3	2586.9	13.4	2705.7	15.1	2705.7	15.1	90.1
04-Spot 38	36	37957	6.4	5.3717	0.8	13.9268	1.4	0.5428	1.1	0.83	2795.2	25.8	2744.7	13.0	2707.8	12.7	2707.8	12.7	103.2
4-Spot 203	98	79119	1.1	5.3409	0.8	13.7907	1.8	0.5344	1.6	0.89	2760.1	35.5	2735.4	16.9	2717.3	13.5	2717.3	13.5	101.6
4-Spot 297	91	114020	1.4	5.3405	0.8	13.7472	1.4	0.5327	1.1	0.81	2752.8	24.8	2732.4	12.9	2717.4	13.1	2717.4	13.1	101.3
04-Spot 28	192	70380	2.0	5.3381	1.0	13.2736	1.6	0.5141	1.2	0.78	2674.2	27.1	2699.3	15.0	2718.2	16.3	2718.2	16.3	98.4
04-Spot 26	557	332773	2.4	5.2486	0.7	12.9695	1.3	0.4939	1.1	0.85	2587.6	24.3	2677.4	12.7	2746.0	11.8	2746.0	11.8	94.2
04-Spot 31	57	66505	3.0	5.2395	0.8	13.7471	1.5	0.5226	1.3	0.84	2710.3	28.8	2732.4	14.7	2748.8	13.8	2748.8	13.8	98.6
04-Spot 87	126	119180	3.3	5.1383	0.8	14.5436	1.8	0.5422	1.6	0.90	2792.8	36.1	2785.9	16.8	2780.9	12.5	2780.9	12.5	100.4
4-Spot 177	71	70609	1.0	4.8818	0.8	16.0139	1.5	0.5672	1.2	0.83	2896.5	28.9	2877.6	14.2	2864.4	13.4	2864.4	13.4	101.1
4-Spot 201	21	28844	1.7	3.8662	0.8	24.7141	1.4	0.6933	1.1	0.78	3395.2	28.2	3297.0	13.3	3237.8	13.4	3237.8	13.4	104.9
4-Spot 168	274	116369	0.8	3.2168	0.7	31.6016	1.4	0.7376	1.2	0.85	3561.7	33.0	3538.0	14.0	3524.6	11.5	3524.6	11.5	101.1

Table DTB17-05. U-Pb geochronologic analyses.																			
						Isotope ratios						Apparent ages (Ma)							
Analysis	U	206Pb	U/Th	206Pb*	±	207Pb*	±	206Pb*	±	error	206Pb*	±	207Pb*	±	206Pb*	±	Best age	±	Conc
	(ppm)	204Pb		207Pb*	(%)	235U*	(%)	238U	(%)	corr.	238U*	(Ma)	235U	(Ma)	207Pb*	(Ma)	(Ma)	(Ma)	(%)
5-Spot 289	397	54171	3.3	16.2881	0.8	0.8489	1.2	0.1003	1.0	0.78	616.3	5.6	624.1	5.7	652.1	16.1	616.3	5.6	94.5
5-Spot 294	2024	114308	2.5	16.4346	0.7	0.8521	1.1	0.1016	0.9	0.78	623.9	5.2	625.8	5.2	632.9	15.3	623.9	5.2	98.6
5-Spot 189	334	734285	1.3	16.1130	0.8	0.9012	1.5	0.1054	1.2	0.85	645.8	7.6	652.4	7.0	675.3	16.3	645.8	7.6	95.6
5-Spot 173	1161	95628	3.6	16.1601	0.7	0.8990	1.2	0.1054	0.9	0.80	646.0	5.7	651.2	5.5	669.1	14.9	646.0	5.7	96.6
5-Spot 244	416	362883	7.5	16.3832	0.7	0.9008	1.2	0.1071	0.9	0.81	655.8	5.9	652.2	5.6	639.7	14.5	655.8	5.9	102.5
5-Spot 238	256	120676	1.6	16.1399	0.8	0.9149	1.3	0.1071	1.1	0.81	656.1	6.7	659.6	6.4	671.8	16.4	656.1	6.7	97.7
05-Spot 39	635	267199	0.5	16.1960	0.7	0.9118	1.2	0.1071	0.9	0.79	656.2	5.7	658.0	5.6	664.3	15.1	656.2	5.7	98.8
5-Spot 141	428	37418	2.7	16.2960	0.9	0.9115	1.4	0.1078	1.0	0.76	659.8	6.5	657.8	6.7	651.1	19.4	659.8	6.5	101.3
5-Spot 237	414	693480	2.4	15.9776	0.7	0.9301	1.2	0.1078	1.0	0.82	660.1	6.3	667.7	6.0	693.3	14.9	660.1	6.3	95.2
5-Spot 120	252	454226	1.8	16.2380	0.7	0.9175	1.1	0.1081	0.8	0.76	661.7	5.2	661.0	5.3	658.8	15.0	661.7	5.2	100.4
05-Spot 70	158	758657	2.6	16.1020	0.8	0.9273	1.4	0.1083	1.1	0.78	663.1	6.6	666.2	6.6	676.8	18.1	663.1	6.6	98.0
5-Spot 144	208	62601	1.9	15.9732	1.0	0.9404	1.4	0.1090	1.0	0.70	666.9	6.2	673.1	7.0	693.9	21.6	666.9	6.2	96.1
5-Spot 212	355	199796	2.3	16.1022	0.7	0.9337	1.2	0.1091	1.0	0.85	667.5	6.6	669.6	6.0	676.7	13.9	667.5	6.6	98.6
5-Spot 191	220	98410	2.0	16.0299	0.6	0.9402	1.1	0.1094	0.9	0.80	669.0	5.4	673.0	5.3	686.4	13.8	669.0	5.4	97.5
5-Spot 283	294	70332	1.7	16.1712	1.0	0.9343	1.3	0.1096	0.9	0.69	670.6	5.9	669.9	6.6	667.6	20.6	670.6	5.9	100.4
5-Spot 138	254	33876	7.2	15.9084	0.7	0.9521	1.3	0.1099	1.1	0.83	672.2	7.0	679.2	6.5	702.6	15.4	672.2	7.0	95.7
5-Spot 239	375	511568	2.1	16.1871	0.8	0.9416	1.4	0.1106	1.1	0.80	676.2	7.1	673.7	6.8	665.5	17.7	676.2	7.1	101.6
5-Spot 269	676	410606	2.0	15.9956	0.6	0.9980	1.0	0.1158	0.8	0.79	706.5	5.5	702.8	5.3	690.9	13.6	706.5	5.5	102.3
5-Spot 107	352	182677	4.2	13.7097	0.7	1.7069	1.2	0.1698	1.0	0.80	1011.0	9.2	1011.1	7.9	1011.4	14.9	1011.4	14.9	100.0
5-Spot 305	330	268675	3.0	13.6680	0.9	1.7780	1.2	0.1763	0.9	0.70	1046.9	8.3	1037.4	8.0	1017.6	17.9	1017.6	17.9	102.9
5-Spot 168	236	103696	2.7	13.5882	0.7	1.6840	1.2	0.1660	0.9	0.79	990.2	8.7	1002.5	7.7	1029.4	15.0	1029.4	15.0	96.2
5-Spot 181	89	68609	1.9	13.5584	0.8	1.6369	1.4	0.1610	1.1	0.79	962.5	9.6	984.5	8.6	1033.9	17.1	1033.9	17.1	93.1
5-Spot 155	274	52222	4.5	13.5529	0.7	1.7550	1.2	0.1726	1.1	0.85	1026.3	10.0	1029.0	8.0	1034.7	13.3	1034.7	13.3	99.2
05-Spot 74	204	109210	3.2	13.5303	0.8	1.7484	1.2	0.1716	0.9	0.72	1021.2	8.2	1026.6	7.8	1038.1	16.9	1038.1	16.9	98.4
5-Spot 210	359	109330	4.0	13.5160	0.5	1.8492	1.4	0.1814	1.3	0.92	1074.3	12.5	1063.1	9.1	1040.2	11.1	1040.2	11.1	103.3
05-Spot 36	253	49183	2.8	13.4563	0.7	1.7780	1.2	0.1736	1.0	0.80	1031.9	9.2	1037.5	7.8	1049.2	14.5	1049.2	14.5	98.4
-05-Spot 2	415	287922	1.6	13.3813	0.7	1.7179	1.2	0.1668	1.0	0.80	994.4	9.1	1015.2	7.9	1060.4	14.7	1060.4	14.7	93.8
5-Spot 112	141	94815	2.2	13.2618	0.7	1.8490	1.1	0.1779	0.8	0.76	1055.6	7.8	1063.1	7.0	1078.4	13.9	1078.4	13.9	97.9
5-Spot 232	119	43548	3.1	13.2587	1.0	1.7843	1.5	0.1717	1.1	0.76	1021.2	10.8	1039.8	9.7	1078.9	19.3	1078.9	19.3	94.7
05-Spot 10	114	113388	0.9	13.2205	0.9	1.8151	1.4	0.1741	1.0	0.73	1034.7	9.7	1050.9	9.1	1084.7	18.9	1084.7	18.9	95.4
5-Spot 114	47	6364	1.4	13.1874	1.1	1.9096	1.7	0.1827	1.3	0.75	1081.8	12.8	1084.4	11.4	1089.7	22.8	1089.7	22.8	99.3
05-Spot 66	53	25546	4.0	13.0481	1.1	2.0374	1.6	0.1929	1.1	0.72	1137.0	11.7	1128.1	10.7	1110.9	21.9	1110.9	21.9	102.3
05-Spot 23	158	52420	4.0	13.0244	0.8	1.9768	1.3	0.1868	1.0	0.77	1104.1	10.3	1107.6	8.9	1114.6	16.8	1114.6	16.8	99.1
5-Spot 295	70	21389	1.1	12.9674	0.8	1.9624	1.3	0.1846	1.0	0.77	1092.3	10.1	1102.7	8.8	1123.3	16.8	1123.3	16.8	97.2
5-Spot 274	401	1019951	3.5	12.8518	0.7	2.1416	1.2	0.1997	1.0	0.84	1173.7	10.6	1162.3	8.2	1141.2	13.0	1141.2	13.0	102.9
5-Spot 176	328	92851	1.9	12.8295	0.9	2.0591	1.4	0.1917	1.1	0.76	1130.5	11.1	1135.3	9.6	1144.6	18.2	1144.6	18.2	98.8
5-Spot 275	365	354690	1.3	12.8259	0.8	2.0652	1.4	0.1922	1.1	0.81	1133.3	11.4	1137.3	9.3	1145.2	15.8	1145.2	15.8	99.0
5-Spot 174	108	67557	2.7	12.8034	1.0	2.0053	1.4	0.1863	1.0	0.70	1101.3	10.1	1117.3	9.8	1148.7	20.6	1148.7	20.6	95.9
5-Spot 132	65	15556	1.6	12.7901	1.1	2.1080	1.5	0.1956	1.0	0.69	1151.8	10.8	1151.4	10.3	1150.7	21.5	1150.7	21.5	100.1
5-Spot 207	52	39346	2.2	12.7891	1.5	1.9964	2.0	0.1853	1.3	0.67	1095.6	13.4	1114.3	13.4	1150.9	29.2	1150.9	29.2	95.2
5-Spot 214	188	102712	1.9	12.7841	0.8	2.1469	1.1	0.1991	0.8	0.72	1170.7	8.5	1164.1	7.6	1151.6	15.1	1151.6	15.1	101.7
5-Spot 131	222	129881	3.0	12.7291	0.9	2.1080	1.5	0.1947	1.1	0.76	1146.8	11.7	1151.4	10.0	1160.2	18.8	1160.2	18.8	98.8
05-Spot 99	165	111453	3.2	12.6631	0.8	2.1490	1.3	0.1975	1.0	0.79	1161.6	10.8	1164.7	9.0	1170.5	15.8	1170.5	15.8	99.2
05-Spot 13	35	331414	1.0	12.5318	1.2	2.0193	1.6	0.1836	1.0	0.62	1086.7	9.6	1122.0	10.5	1191.1	24.0	1191.1	24.0	91.2
5-Spot 126	65	218598	1.3	12.5095	0.9	2.1233	1.3	0.1927	0.9	0.71	1136.1	9.7	1156.4	9.1	1194.6	18.5	1194.6	18.5	95.1
5-Spot 103	156	99334	3.7	12.3810	1.0	2.3344	1.5	0.2097	1.1	0.74	1227.3	12.0	1222.8	10.3	1215.0	19.2	1215.0	19.2	101.0
05-Spot 69	168	86746	3.2	12.3595	0.7	2.2947	1.2	0.2058	1.0	0.83	1206.3	11.2	1210.7	8.7	1218.4	13.6	1218.4	13.6	99.0
05-Spot 60	423	4078110	1.5	12.3493	1.0	2.3283	1.4	0.2086	1.0	0.68	1221.5	10.7	1221.0	10.1	1220.0	20.4	1220.0	20.4	100.1
5-Spot 302	151	52052	2.0	12.3374	0.7	2.2544	1.2	0.2018	0.9	0.77	1185.0	9.8	1198.2	8.3	1221.9	14.7	1221.9	14.7	97.0
05-Spot 63	297	77878	2.8	12.3057	0.7	2.2551	1.1	0.2014	0.9	0.82	1182.6	10.1	1198.4	8.0	1227.0	12.9	1227.0	12.9	96.4
05-Spot 93	175	218707	1.1	12.2121	0.9	2.3321	1.5	0.2066	1.2	0.79	1210.9	12.8	1222.1	10.4	1241.9	17.6	1241.9	17.6	97.5
5-Spot 213	37	19285	2.0	11.9733	1.7	2.3375	2.0	0.2031	1.1	0.56	1191.8	12.2	1223.8	14.3	1280.5	32.4	1280.5	32.4	93.1
5-Spot 178	156	317958	2.2	11.7519	0.7	2.5896	1.2	0.2208	0.9	0.81	1286.2	10.9	1297.7	8.5	1316.8	13.2	1316.8	13.2	97.7
5-Spot 291	140	51053	1.2	11.6236	0.5	2.5261	1.0	0.2130	0.9	0.88	1245.0	10.4	1279.6	7.6	1338.0	9.6	1338.0	9.6	93.0
5-Spot 313	346	267723	2.0	11.5498	0.7	2.7455	1.0	0.2301	0.7	0.73	1334.9	8.6	1340.9	7.2	1350.3	12.8	1350.3	12.8	98.9
5-Spot 307	74	21564	2.4	11.5423	0.9	2.6580	1.4	0.2226	1.0	0.73	1295.6	11.7	1316.9	10.0	1351.6	17.7	1351.6	17.7	95.9
05-Spot 96	269	146808	1.3	11.5345	0.7	2.8979	1.3	0.2425	1.1	0.84	1399.8	14.1	1381.4	10.0	1352.9	13.8	1352.9	13.8	103.5
05-Spot 17	555	2679365	6.6	11.4791	0.7	2.4983	1.0	0.2081	0.8	0.77	1218.6	8.9	1271.5	7.5	1362.2	12.7	1362.2	12.7	89.5
05-Spot 16	158	337274	2.0	11.4498	0.7	2.7274	1.1	0.2266	0.8	0.78	1316.6	9.9	1335.9	7.9	1367.1	12.6	1367.1	12.6	96.3
05-Spot 49	37	49451	2.7	11.4290	1.0	2.7555	1.5	0.2285	1.1	0.74	1326.7	13.3	1343.6	11.1	1370.6	19.2	1370.6	19.2	96.8
5-Spot 250	226	191712	2.2	11.4093	0.6	2.8775	1.1	0.2382	0.9	0.85	1377.4	11.6	1376.0	8.3	1373.9	11.0	1373.9	11.0	100.3
5-Spot 265	103	485872	1.9	11.3848	0.8	2.7861	1.2	0.2302	0.9	0.75	1335.3	11.2	1351.8	9.2	1378.1	15.7	1378.1	15.7	96.9
5-Spot 226	551	241210	2.4	11.3826	0.5	2.5907	1.1	0.2140	0.9	0.87	1249.9	10.8	1298.0	8.0	1378.4	10.4	1378.4	10.4	90.7
5-Spot 235	253	113107	1.9	11.3567	0.8	2.8522	1.5	0.2350	1.2	0.82	1360.8	14.9	1369.4	11.1	1382.8	16.0	1382.8	16.0	98.4
5-Spot 281	238	98410	4.9	11.2584	0.7	3.0589	1.3	0.2499	1.1	0.85	1437.8	14.7	1422.5	10.3	1399.5	13.4	1399.5	13.4	102.7
05-Spot 26	120	50349	1.4	11.2540	0.7	2.8865	1.2	0.2357	1.0	0.83	1364.3	12.8	1378.4	9.4	1400.2	13.2	1400.2	13.2	97.4
05-Spot 75	354	528497	1.1	11.2473	0.6	2.3312	1.6	0.1902	1.5	0.94	1122.7	15.6	1221.8	11.5	1401.4	10.9	1401.4	10.9	80.1
5-Spot 276	441	333424	3.5	11.1959	0.7	3.0543	1.3	0.2481	1.0	0.82	1428.8	13.1	1421.3	9.6	1410.1	13.9	1410.1	13.9	101.3
05-Spot 98	177	462469	2.8	11.1655	0.7	3.0864	1.4	0.2500	1.1	0.83	1438.7	14.5	1429.3	10.4	1415.3	14.3	1415.3	14.3	101.7
5-Spot 288	150	117899	1.9	11.1533	0.7	3.0705	1.1	0.2485	0.9	0.77	1430.7	11.2	1425.4	8.7	1417.4	14.0	1417.4	14.0	100.9
05-Spot 90	152	92565	1.4	11.1371	0.6	2.9920	1.2	0.2418	1.0	0.84	1396.0	12.3	1405.6	8.9	1420.2	12.1	1420.2	12.1	98.3
5-Spot 222	112	69430	3.1	11.1165	0.8	3.1159	1.3	0.2513	1.0	0.80	1445.3	13.6	1436.6	10.0	1423.7	14.9	1423.7	14.9	101.5
5-Spot 186	294	173824	2.1	11.0877	0.8	3.0861	1.4	0.2483	1.1	0.79	1429.6	13.8	1429.2	10.5	1428.7	16.1	1428.7	16.1	100.1
05-Spot 37	403	268156	2.1	11.0542	0.6	2.9902	1.1	0.2398	1.0	0.86	1385.8	12.3	1405.1	8.7	1434.5	11.2	1434.5	11.2	96.6

5-Spot 190	175	829347	1.3	11.0451	0.7	3.1518	1.2	0.2526	1.0	0.84	1451.8	12.9	1445.4	9.2	1436.1	12.4	1436.1	12.4	101.1
5-Spot 134	140	102592	1.7	11.0295	0.9	3.0529	1.4	0.2443	1.1	0.78	1409.1	13.5	1421.0	10.5	1438.8	16.6	1438.8	16.6	97.9
5-Spot 296	124	99213	2.7	11.0143	0.7	3.1131	1.1	0.2488	0.9	0.79	1432.2	11.4	1435.9	8.7	1441.4	13.4	1441.4	13.4	99.4
5-Spot 193	641	41347	1.8	10.9559	1.0	3.0118	1.3	0.2394	0.9	0.69	1383.7	11.5	1410.6	10.3	1451.5	18.6	1451.5	18.6	95.3
5-Spot 180	160	196555	2.9	10.9518	0.6	3.1449	1.0	0.2499	0.8	0.80	1438.0	9.9	1443.8	7.4	1452.2	11.0	1452.2	11.0	99.0
5-Spot 143	215	241227	1.2	10.9101	0.8	3.1428	1.7	0.2488	1.5	0.89	1432.2	19.2	1443.2	13.0	1459.5	14.9	1459.5	14.9	98.1
5-Spot 216	185	109693	4.1	10.9081	0.7	3.2522	1.3	0.2574	1.1	0.85	1476.5	14.6	1469.7	10.1	1459.8	13.2	1459.8	13.2	101.1
05-Spot 55	103	28823	1.3	10.8855	0.9	3.1321	1.5	0.2474	1.2	0.79	1425.0	15.0	1440.6	11.5	1463.8	17.5	1463.8	17.5	97.3
05-Spot 86	127	33399	3.8	10.8537	1.5	3.1527	1.8	0.2483	1.0	0.54	1429.6	12.4	1445.7	14.0	1469.3	29.0	1469.3	29.0	97.3
5-Spot 156	109	202729	1.4	10.8111	0.8	3.1747	1.4	0.2490	1.2	0.83	1433.5	15.1	1451.0	10.9	1476.8	14.9	1476.8	14.9	97.1
05-Spot 29	84	57406	1.3	10.8047	1.0	3.1737	1.4	0.2488	1.1	0.75	1432.3	13.8	1450.8	11.1	1477.9	18.1	1477.9	18.1	96.9
5-Spot 130	184	149169	1.5	10.0719	0.7	3.8750	1.1	0.2832	0.9	0.78	1607.4	12.5	1608.5	9.2	1609.9	13.3	1609.9	13.3	99.8
05-Spot 32	131	144356	0.7	10.0585	0.9	3.6763	1.3	0.2683	1.0	0.75	1532.2	13.5	1566.2	10.5	1612.4	16.0	1612.4	16.0	95.0
-05-Spot 1	279	119354	1.7	10.0483	0.9	3.6223	1.6	0.2641	1.3	0.81	1510.8	17.7	1554.4	12.9	1614.3	17.6	1614.3	17.6	93.6
5-Spot 278	226	134956	1.9	9.9208	0.8	3.3812	1.4	0.2434	1.2	0.84	1404.3	14.7	1500.1	10.9	1638.0	14.1	1638.0	14.1	85.7
5-Spot 312	260	410087	2.1	9.8717	0.6	3.7790	1.1	0.2707	0.9	0.83	1544.3	12.9	1588.3	9.0	1647.2	11.6	1647.2	11.6	93.7
05-Spot 92	289	272149	1.4	9.8578	0.7	4.0340	1.0	0.2885	0.8	0.76	1634.2	11.1	1641.1	8.3	1649.9	12.3	1649.9	12.3	99.1
5-Spot 240	252	336239	2.0	9.8574	0.9	3.9448	1.5	0.2821	1.2	0.80	1602.2	17.3	1622.9	12.4	1649.9	17.1	1649.9	17.1	97.1
5-Spot 279	97	292863	0.8	9.8535	0.8	3.9381	1.5	0.2816	1.2	0.83	1599.2	17.3	1621.6	12.0	1650.7	15.5	1650.7	15.5	96.9
5-Spot 308	159	123314	2.0	9.7266	0.5	4.2793	0.9	0.3020	0.8	0.83	1701.3	11.7	1689.4	7.8	1674.6	9.9	1674.6	9.9	101.6
5-Spot 290	115	110892	2.3	9.7006	0.7	4.1476	1.1	0.2919	0.8	0.77	1651.2	12.3	1663.7	9.0	1679.6	12.9	1679.6	12.9	98.3
5-Spot 154	332	380249	4.7	9.6744	0.7	4.2444	1.2	0.2979	1.0	0.81	1681.1	14.8	1682.7	10.2	1684.6	13.4	1684.6	13.4	99.8
5-Spot 163	150	101599	3.0	9.6666	0.6	4.2981	1.0	0.3015	0.8	0.79	1698.6	12.3	1693.0	8.6	1686.1	11.7	1686.1	11.7	100.7
5-Spot 298	252	462401	2.4	9.6632	0.6	4.2743	1.2	0.2997	1.0	0.85	1689.8	15.0	1688.4	9.8	1686.7	11.6	1686.7	11.6	100.2
5-Spot 177	157	167600	3.5	9.6615	0.6	4.1747	1.1	0.2927	0.9	0.82	1654.8	12.7	1669.1	8.7	1687.1	11.3	1687.1	11.3	98.1
5-Spot 270	321	36755	2.0	9.6422	0.7	3.6023	1.2	0.2520	1.0	0.84	1448.9	12.8	1550.0	9.4	1690.7	12.0	1690.7	12.0	85.7
05-Spot 91	425	691862	6.1	9.6173	0.6	4.4896	1.1	0.3133	0.8	0.79	1756.9	12.9	1729.0	8.8	1695.5	11.8	1695.5	11.8	103.6
5-Spot 211	193	166559	1.4	9.6022	0.4	4.2907	1.0	0.2989	0.9	0.90	1686.1	13.4	1691.6	8.3	1698.4	8.2	1698.4	8.2	99.3
5-Spot 161	156	8930865	2.9	9.5914	0.6	3.9303	1.3	0.2735	1.1	0.86	1558.7	14.9	1619.9	10.1	1700.5	11.7	1700.5	11.7	91.7
05-Spot 79	306	141140	2.3	9.5771	0.8	4.4302	1.4	0.3079	1.1	0.82	1730.1	17.0	1718.0	11.2	1703.2	14.1	1703.2	14.1	101.6
5-Spot 217	127	84455	2.2	9.5538	0.8	4.3095	1.4	0.2987	1.1	0.81	1685.0	16.6	1695.2	11.4	1707.7	15.1	1707.7	15.1	98.7
05-Spot 28	49	3306950	2.3	9.5426	0.8	4.3194	1.4	0.2991	1.1	0.80	1686.7	16.5	1697.1	11.5	1709.9	15.4	1709.9	15.4	98.6
05-Spot 47	100	49711	3.7	9.5235	0.8	4.3998	1.2	0.3040	0.9	0.72	1711.3	13.1	1712.3	10.0	1713.5	15.5	1713.5	15.5	99.9
05-Spot 35	538	384323	3.8	9.5171	0.6	4.2812	1.3	0.2956	1.1	0.88	1669.6	16.3	1689.7	10.3	1714.8	11.0	1714.8	11.0	97.4
5-Spot 260	158	93524	2.4	9.5136	0.6	4.3452	1.2	0.2999	1.0	0.86	1691.0	14.9	1702.0	9.6	1715.5	11.0	1715.5	11.0	98.6
05-Spot 87	288	1608177	2.4	9.5064	0.6	4.3715	1.2	0.3015	1.0	0.85	1698.9	15.4	1707.0	10.0	1716.9	11.7	1716.9	11.7	99.0
05-Spot 97	160	292021	2.1	9.4735	0.6	4.3684	1.2	0.3003	1.0	0.84	1692.7	14.7	1706.4	9.7	1723.2	11.9	1723.2	11.9	98.2
5-Spot 247	399	582523	1.8	9.4708	0.6	4.4861	1.7	0.3083	1.6	0.93	1732.2	24.1	1728.4	14.2	1723.8	11.6	1723.8	11.6	100.5
5-Spot 147	125	860313	7.1	9.4462	0.6	4.3902	1.0	0.3009	0.8	0.79	1695.8	12.0	1710.5	8.4	1728.5	11.4	1728.5	11.4	98.1
05-Spot 18	86	91483	4.9	9.4143	0.6	4.4978	1.2	0.3072	1.0	0.86	1727.1	15.3	1730.6	9.7	1734.7	10.8	1734.7	10.8	99.6
5-Spot 230	169	197629	2.2	9.3871	0.6	4.5785	1.1	0.3118	0.9	0.83	1749.8	14.1	1745.4	9.3	1740.0	11.4	1740.0	11.4	100.6
05-Spot 33	426	114906	4.8	9.3778	0.6	4.5831	1.2	0.3119	1.0	0.87	1749.8	15.7	1746.2	9.8	1741.9	10.8	1741.9	10.8	100.5
5-Spot 192	192	103806	1.0	9.3762	0.6	4.6087	0.9	0.3135	0.7	0.79	1758.1	11.0	1750.9	7.6	1742.2	10.2	1742.2	10.2	100.9
5-Spot 258	70	168989	1.4	9.3666	0.8	4.5940	1.2	0.3122	0.9	0.77	1751.6	14.5	1748.2	10.3	1744.0	14.5	1744.0	14.5	100.4
5-Spot 297	213	36727	2.0	9.3645	0.8	4.2614	1.5	0.2896	1.3	0.84	1639.3	18.2	1685.9	12.3	1744.5	15.0	1744.5	15.0	94.0
05-Spot 43	142	91861	2.7	9.3533	1.0	4.2970	1.6	0.2916	1.2	0.79	1649.6	18.0	1692.8	12.9	1746.7	17.7	1746.7	17.7	94.4
5-Spot 284	268	127652	0.9	9.3468	0.6	4.6072	1.2	0.3125	1.1	0.87	1752.8	16.7	1750.6	10.4	1747.9	11.1	1747.9	11.1	100.3
5-Spot 203	193	1569138	3.0	9.3335	0.6	4.6855	1.1	0.3173	0.9	0.81	1776.6	13.7	1764.7	9.1	1750.5	11.5	1750.5	11.5	101.5
5-Spot 259	445	253510	2.9	9.3155	0.6	4.6013	1.1	0.3110	0.9	0.85	1745.7	14.1	1749.5	9.1	1754.1	10.4	1754.1	10.4	99.5
5-Spot 101	156	90881	1.7	9.2940	0.7	4.7287	1.3	0.3189	1.1	0.84	1784.3	17.4	1772.3	11.2	1758.3	13.4	1758.3	13.4	101.5
05-Spot 59	80	43781	3.0	9.2917	0.7	4.5782	1.2	0.3087	1.0	0.79	1734.1	14.5	1745.3	10.1	1758.7	13.7	1758.7	13.7	98.6
05-Spot 12	249	139354	2.2	9.2819	0.7	4.6115	1.1	0.3106	0.9	0.78	1743.5	13.4	1751.4	9.4	1760.7	12.9	1760.7	12.9	99.0
5-Spot 123	150	49473	2.1	9.2771	0.8	4.7034	1.0	0.3166	0.7	0.67	1773.1	10.7	1767.8	8.7	1761.6	14.0	1761.6	14.0	100.7
05-Spot 76	129	167493	3.5	9.2723	0.7	4.7697	1.2	0.3209	1.0	0.83	1794.1	15.6	1779.6	10.1	1762.6	12.3	1762.6	12.3	101.8
5-Spot 253	80	184447	1.8	9.2666	0.7	4.7539	1.1	0.3196	0.9	0.79	1788.0	13.9	1776.8	9.5	1763.7	12.6	1763.7	12.6	101.4
5-Spot 129	95	126203	2.1	9.2578	0.7	4.7862	1.4	0.3215	1.2	0.87	1797.1	19.2	1782.5	11.8	1765.4	12.4	1765.4	12.4	101.8
5-Spot 292	240	357720	4.8	9.2527	0.8	4.8364	1.3	0.3247	1.1	0.81	1812.6	17.2	1791.2	11.3	1766.4	14.3	1766.4	14.3	102.6
5-Spot 140	95	57000	1.8	9.2327	0.8	4.8151	1.1	0.3226	0.8	0.69	1802.3	12.2	1787.5	9.4	1770.4	14.7	1770.4	14.7	101.8
5-Spot 282	231	912804	4.4	9.2116	0.7	4.7262	1.3	0.3159	1.1	0.85	1769.6	16.8	1771.9	10.8	1774.6	12.5	1774.6	12.5	99.7
05-Spot 53	175	149688	1.2	9.2075	0.9	4.3954	1.4	0.2937	1.2	0.81	1659.7	17.0	1711.5	11.9	1775.4	15.6	1775.4	15.6	93.5
5-Spot 234	173	131159	2.5	9.2025	0.8	4.6468	1.4	0.3103	1.2	0.83	1742.1	17.7	1757.7	11.7	1776.4	14.4	1776.4	14.4	98.1
05-Spot 57	139	173506	4.0	9.1984	0.7	4.7960	1.3	0.3201	1.1	0.83	1790.2	17.3	1784.2	11.2	1777.2	13.4	1777.2	13.4	100.7
5-Spot 287	120	43865	3.5	9.1907	0.7	4.6074	1.1	0.3073	0.9	0.81	1727.2	13.8	1750.6	9.4	1778.7	12.0	1778.7	12.0	97.1
5-Spot 194	283	162659	2.5	9.1558	0.6	4.7967	1.2	0.3187	1.1	0.86	1783.2	16.6	1784.3	10.4	1785.6	11.4	1785.6	11.4	99.9
5-Spot 273	81	72404	3.0	9.0677	0.8	4.7402	1.2	0.3119	1.0	0.78	1749.9	14.6	1774.4	10.2	1803.2	13.8	1803.2	13.8	97.0
5-Spot 221	113	98742	1.8	9.0649	0.8	5.0232	1.3	0.3304	1.1	0.82	1840.3	17.5	1823.2	11.3	1803.8	13.8	1803.8	13.8	102.0
05-Spot 54	264	939578	3.6	9.0517	0.6	4.9729	1.2	0.3266	1.0	0.87	1821.9	15.9	1814.7	9.8	1806.5	10.3	1806.5	10.3	100.9
05-Spot 82	117	135093	3.1	9.0360	0.7	4.7952	1.3	0.3144	1.1	0.84	1762.3	16.3	1784.1	10.6	1809.6	12.4	1809.6	12.4	97.4
05-Spot 64	282	83163	2.3	8.9963	0.8	5.1272	1.2	0.3347	0.8	0.68	1861.0	12.8	1840.6	9.9	1817.6	15.4	1817.6	15.4	102.4
5-Spot 157	166	129371	2.0	8.9004	0.8	5.0311	1.3	0.3249	1.1	0.81	1813.6	17.2	1824.6	11.3	1837.1	14.0	1837.1	14.0	98.7
5-Spot 100	83	144319	2.4	8.8083	0.8	5.2645	1.5	0.3365	1.2	0.83	1869.6	19.8	1863.1	12.6	1855.8	15.0	1855.8	15.0	100.7
05-Spot 15	181	179065	2.2	8.7602	0.7	5.0957	1.2	0.3239	1.0	0.80	1808.7	15.2	1835.4	10.2	1865.7	12.9	1865.7	12.9	96.9
5-Spot 162	260	55997	1.2	8.7047	0.8	4.5617	1.4	0.2881	1.1	0.83	1632.1	16.3	1742.3	11.4	1877.2	13.7	1877.2	13.7	86.9
-05-Spot 9	136	77437	2.2	8.6285	0.7	5.2029	1.3	0.3257	1.0	0.82	1817.7	16.2	1853.1	10.7	1893.0	13.0	1893.0	13.0	96.0
5-Spot 255	720	10020	1.8	8.4729	1.0	4.5410	1.5	0.2792	1.1	0.75	1587.2	15.3	1738.5	12.1	1925.7	17.4	1925.7	17.4	82.4
5-Spot 206	480	147788	5.0	8.2808	0.7	5.9267	1.3	0.3561	1.0	0.84	1963.7	17.7	1965.2	10.9	1966.7	12.2	1966.7	12.2	99.8
05-Spot 38	167	111263	3.1	7.0174	0.5	7.7579	0.9	0.3950	0.8	0.86	2146.0	14.7	2203.3	8.4	2257.1	8.2	2257.1	8.2	95.1
5-Spot 311	199	214916	1.9	6.9349	0.5	8.6924	1.1	0.4374	0.9	0.86	2338.9	17.7	2306.3	9.6	2277.5	9.3	2277.5	9.3	102.7
5-Spot 271	197	187180	2.2	6.6066	0.6	9.2053	1.2	0.4413	1.0	0.84	2356.3	19.6	2358.6	10.8	2360.6	10.8	2360.6	10.8	99.8
5-Spot 242	171	92659	2.7	6.5539	0.6	9.3234	1.2	0.4434	1.0	0.85	2365.7	19.4	2370.3	10.6	2374.3	10.5	2374.3	10.5	99.6
5-Spot 148	413	58238	2.3	6.4422	0.7	7.6492	1.4	0.3575	1.3	0.89	1970.5	21.6	2190.7	12.8	2403.6	11.1	2403.6	11.1	82.0
5-Spot 252	215	264190	2.9	6.4380	0.5	9.4330	0.9	0.4406	0.8	0.86	2353.5	15.8	2381.0	8.6	2404.7	8.2	2404.7	8.2	97.9
5-Spot 184	291	99886	2.8	6.3944	0.7	9.0787	1.4	0.4212	1.2	0.88	2266.0	23.6	2346.0	12.8	2416.2	11.1	2416.2	11.1	93.8
5-Spot 256	412	6356786	3.0	6.3423	0.5	10.4457	1.0	0.4807	0.9	0.85	2530.3	18.4	2475.1	9.6	2430.1	9.1	2430.1	9.1	104.1
5-Spot 264	206	99154	2.6	6.3277	0.6	9.7662	1.3	0.4484	1.1	0.88	2388.1	21.9	2413.0	11.6	2434.0	10.3	2434.0	10.3	98.1
5-Spot 128	151	150249	3.3	6.3247	0.6	9.8493	1.2	0.4520	1.1	0.86	2404.1	21.6	2420.8	11.5	2434.8	10.7	2434.8	10.7	98.7
5-Spot 220	143	194250	2.8	6.3213	0.7	9.8611	1.3	0.4523	1.1	0.85	2405.4	22.6	2421.9	12.1	2435.7	11.7	2435.7	11.7	98.8
05-Spot 27	178	92114	3.2	6.2970	0.7	10.3406	1.4	0.4725	1.1	0.84	2494.3	23.5	2465.7	12.6	2442.2	12.6	2442.2	12.6	102.1
05-Spot 11	163	1062885	1.8	6.2879	0.8	9.9395	1.2	0.4535	0.9	0.77	2410.7	18.3	2429.2	10.9	2444.7	12.7	2444.7	12.7	98.6
5-Spot 215	227	130877	2.4	6.2529	0.4	10.0551	1.0	0.4562	0.9	0.89	2422.8	17.2	2439.9	8.9	2454.1	7.6	2454.1	7.6	98.7
5-Spot 202	224	109882	1.1	6.2490	0.7	8.7597	1.3	0.3972	1.1	0.85	2156.0	19.5	2313.3	11.5	2455.2	11.3	2455.2	11.3	87.8
05-Spot 46	137	167913	3.1	6.2264	0.8	10.0330	1.2	0.4533	0.9	0.77	2409.8	18.6	2437.8	11.2	2461.3	13.1	2461.3	13.1	97.9
5-Spot 219	353	241349	2.3	6.1914	0.6	10.7178	1.1	0.4815	0.9	0.81	2533.7	18.3	2499.0	10.0	2470.8	10.6	2470.8	10.6	102.5
-05-Spot 4	511	616127	3.0	6.1884	0.5	10.7792	1.1	0.4840	1.0	0.89	2544.7	21.3	2504.3	10.5	2471.7	8.7	2471.7	8.7	103.0
5-Spot 113	197	224411	2.5	6.1883	0.6	10.4397	1.1	0.4688	1.0	0.86	2478.1	20.1	2474.6	10.6	2471.7	10.0	2471.7	10.0	100.3
5-Spot 171	724	398694	1.3	6.1788	0.6	10.5610	1.1	0.4735	0.9	0.81	2498.8	18.0	2485.3	9.9	2474.3	10.5	2474.3	10.5	101.0

5-Spot 198	203	158307	1.4	6.1766	0.6	10.7676	1.0	0.4826	0.8	0.81	2538.4	17.2	2503.3	9.3	2474.9	9.8	2474.9	9.8	102.6
5-Spot 146	310	699628	1.0	6.1736	0.5	9.4097	1.1	0.4215	1.0	0.89	2267.3	18.9	2378.8	10.2	2475.7	8.5	2475.7	8.5	91.6
5-Spot 135	1114	113828	5.4	6.1614	0.6	8.8743	1.2	0.3967	1.1	0.88	2154.0	19.6	2325.2	11.0	2479.0	9.5	2479.0	9.5	86.9
5-Spot 125	478	376881	0.8	6.1271	0.6	11.1095	1.1	0.4939	0.9	0.82	2587.5	18.7	2532.4	10.0	2488.4	10.3	2488.4	10.3	104.0
5-Spot 150	354	1185448	1.8	6.1216	0.6	10.2522	1.1	0.4554	0.9	0.84	2419.1	18.6	2457.8	10.1	2489.9	9.8	2489.9	9.8	97.2
5-Spot 204	359	3525998	1.1	6.1167	0.5	10.9850	1.3	0.4875	1.1	0.90	2560.0	24.0	2521.9	11.7	2491.3	9.2	2491.3	9.2	102.8
5-Spot 267	275	604400	2.9	6.1142	0.7	10.7121	1.3	0.4752	1.1	0.86	2506.4	22.7	2498.5	11.9	2492.0	11.1	2492.0	11.1	100.6
05-Spot 51	199	220099	1.6	6.0985	0.7	10.6052	1.3	0.4693	1.1	0.85	2480.4	22.4	2489.2	11.9	2496.3	11.4	2496.3	11.4	99.4
5-Spot 293	521	105952	2.1	6.0949	0.7	8.4799	2.2	0.3750	2.1	0.95	2052.9	37.7	2283.8	20.4	2497.3	11.3	2497.3	11.3	82.2
05-Spot 83	412	231246	1.3	6.0802	0.6	10.7245	1.1	0.4731	1.0	0.85	2497.3	19.7	2499.5	10.5	2501.4	10.1	2501.4	10.1	99.8
5-Spot 124	535	782120	0.6	6.0788	0.5	10.2430	1.4	0.4518	1.3	0.92	2403.2	26.1	2457.0	13.0	2501.8	9.2	2501.8	9.2	96.1
5-Spot 286	26	12129	1.8	6.0435	0.8	10.6948	1.3	0.4690	1.0	0.76	2479.1	20.6	2497.0	12.2	2511.6	14.3	2511.6	14.3	98.7
05-Spot 41	191	103343	1.0	6.0375	0.7	10.8664	1.4	0.4760	1.2	0.87	2509.9	25.6	2511.8	13.2	2513.2	11.8	2513.2	11.8	99.9
5-Spot 153	196	402189	0.9	6.0293	0.5	10.9518	1.1	0.4791	0.9	0.88	2523.4	19.8	2519.0	10.0	2515.5	8.6	2515.5	8.6	100.3
05-Spot 72	212	107019	2.0	6.0289	0.7	10.8936	1.3	0.4765	1.1	0.82	2512.2	22.1	2514.1	12.0	2515.6	12.3	2515.6	12.3	99.9
5-Spot 165	176	116843	1.7	6.0094	0.6	8.6260	2.1	0.3761	2.0	0.96	2058.1	35.4	2299.3	19.0	2521.1	9.5	2521.1	9.5	81.6
05-Spot 40	230	94423	0.6	6.0034	0.5	11.1199	1.1	0.4844	0.9	0.86	2546.3	19.0	2533.2	9.8	2522.7	9.1	2522.7	9.1	100.9
05-Spot 71	261	352683	0.7	6.0006	0.6	11.0874	1.4	0.4827	1.2	0.88	2539.2	25.2	2530.5	12.7	2523.5	10.9	2523.5	10.9	100.6
-05-Spot 3	357	644090	1.0	6.0000	0.6	10.2232	1.4	0.4451	1.2	0.89	2373.3	24.6	2455.2	12.9	2523.7	10.6	2523.7	10.6	94.0
05-Spot 67	115	116542	3.0	5.9833	0.6	11.0547	1.3	0.4799	1.2	0.90	2527.0	24.1	2527.8	12.0	2528.4	9.5	2528.4	9.5	99.9
5-Spot 196	415	183926	1.7	5.9752	0.7	11.1613	1.1	0.4839	0.9	0.80	2544.2	18.4	2536.7	10.2	2530.6	10.9	2530.6	10.9	100.5
5-Spot 116	90	157011	0.5	5.9735	0.5	10.9185	0.9	0.4732	0.8	0.83	2497.8	16.1	2516.2	8.7	2531.1	8.8	2531.1	8.8	98.7
05-Spot 85	267	129831	1.3	5.9726	0.6	10.4331	1.9	0.4521	1.8	0.94	2404.7	35.6	2474.0	17.5	2531.4	10.8	2531.4	10.8	95.0
5-Spot 299	322	48686	0.6	5.9724	0.7	9.1516	2.0	0.3966	1.9	0.94	2153.3	34.8	2353.3	18.5	2531.4	11.4	2531.4	11.4	85.1
05-Spot 81	250	291964	0.5	5.9661	0.4	11.2485	1.0	0.4869	0.8	0.89	2557.4	17.8	2543.9	8.9	2533.2	7.4	2533.2	7.4	101.0
5-Spot 136	109	109265	0.6	5.9512	0.6	10.8986	1.2	0.4706	1.0	0.84	2486.3	20.1	2514.5	10.8	2537.4	10.5	2537.4	10.5	98.0
05-Spot 77	275	115772	1.4	5.9125	0.7	9.3531	1.4	0.4012	1.2	0.87	2174.8	22.5	2373.2	12.9	2548.3	11.6	2548.3	11.6	85.3
05-Spot 34	574	1089389	0.4	5.8819	0.6	10.0449	1.2	0.4287	1.0	0.85	2299.9	19.5	2438.9	11.0	2557.0	10.6	2557.0	10.6	89.9
5-Spot 151	386	147015	0.9	5.8814	0.7	9.4304	1.3	0.4024	1.1	0.86	2180.3	21.2	2380.8	12.2	2557.2	11.4	2557.2	11.4	85.3
5-Spot 225	410	370760	1.8	5.8777	0.7	9.7884	1.3	0.4175	1.1	0.84	2248.9	21.0	2415.1	12.1	2558.2	11.9	2558.2	11.9	87.9
5-Spot 159	313	92542	1.1	5.8753	0.6	9.7121	1.2	0.4140	1.0	0.85	2233.3	18.8	2407.8	10.8	2558.9	10.4	2558.9	10.4	87.3
05-Spot 14	128	256536	1.7	5.8744	0.8	9.3356	1.7	0.3979	1.5	0.89	2159.5	27.9	2371.5	15.6	2559.2	12.9	2559.2	12.9	84.4
5-Spot 303	128	288498	0.5	5.8743	0.6	11.3492	1.2	0.4837	1.0	0.86	2543.5	21.8	2552.3	11.3	2559.2	10.5	2559.2	10.5	99.4
5-Spot 262	69	78658	1.0	5.8683	0.7	12.0739	1.4	0.5141	1.2	0.86	2674.1	26.5	2610.2	13.1	2560.9	11.8	2560.9	11.8	104.4
5-Spot 121	332	216668	1.8	5.8676	0.6	10.5335	1.2	0.4485	1.1	0.88	2388.4	21.7	2482.9	11.5	2561.1	9.8	2561.1	9.8	93.3
5-Spot 142	408	342814	2.7	5.8554	0.4	10.5355	1.2	0.4476	1.1	0.94	2384.6	22.7	2483.0	11.3	2564.6	7.1	2564.6	7.1	93.0
5-Spot 152	351	1066745	1.6	5.8502	0.8	10.5180	1.3	0.4465	1.1	0.82	2379.5	21.2	2481.5	12.1	2566.1	12.6	2566.1	12.6	92.7
5-Spot 223	665	514614	2.0	5.8449	0.6	12.0718	1.1	0.5120	1.0	0.85	2665.0	21.0	2610.0	10.6	2567.6	10.0	2567.6	10.0	103.8
05-Spot 20	138	105134	1.3	5.8384	0.9	11.1057	1.4	0.4705	1.1	0.76	2485.6	22.3	2532.0	13.3	2569.5	15.5	2569.5	15.5	96.7
5-Spot 200	61	51595	1.2	5.8335	0.8	11.4548	1.3	0.4848	1.0	0.80	2548.3	21.4	2560.9	12.0	2570.9	13.0	2570.9	13.0	99.1
5-Spot 315	396	890227	2.1	5.8334	0.6	11.6598	1.7	0.4935	1.6	0.93	2585.9	33.6	2577.5	15.8	2570.9	10.0	2570.9	10.0	100.6
5-Spot 243	271	485779	1.4	5.8312	0.7	11.9007	1.3	0.5035	1.2	0.86	2628.9	25.0	2596.6	12.6	2571.5	11.5	2571.5	11.5	102.2
05-Spot 56	92	101807	0.5	5.8190	0.7	11.4531	1.2	0.4836	0.9	0.80	2542.8	19.7	2560.8	11.0	2575.0	11.8	2575.0	11.8	98.7
5-Spot 172	417	198418	3.2	5.8129	0.7	11.9328	1.3	0.5033	1.1	0.85	2627.9	23.1	2599.1	11.8	2576.8	11.2	2576.8	11.2	102.0
5-Spot 277	257	1949233	0.7	5.8031	0.7	10.3316	1.4	0.4350	1.1	0.84	2328.3	22.4	2464.9	12.6	2579.6	12.3	2579.6	12.3	90.3
5-Spot 285	416	931736	1.3	5.8023	0.5	11.7676	1.2	0.4954	1.1	0.90	2594.1	23.0	2586.1	11.2	2579.8	8.9	2579.8	8.9	100.6
05-Spot 42	207	94855	1.3	5.8003	0.8	11.4618	1.3	0.4824	1.0	0.80	2537.6	21.8	2561.5	12.1	2580.4	13.0	2580.4	13.0	98.3
5-Spot 310	745	120378	1.2	5.7997	0.7	9.6046	2.5	0.4042	2.4	0.96	2188.2	44.9	2397.6	23.1	2580.6	11.4	2580.6	11.4	84.8
5-Spot 127	338	651661	0.9	5.7984	0.6	10.3045	1.2	0.4335	1.1	0.89	2321.6	21.4	2462.5	11.4	2580.9	9.5	2580.9	9.5	90.0
5-Spot 268	43	49819	0.7	5.7792	0.6	11.6882	1.3	0.4901	1.1	0.87	2571.2	23.8	2579.8	12.1	2586.5	10.6	2586.5	10.6	99.4
5-Spot 105	204	88761	1.2	5.7666	0.6	11.6109	1.3	0.4858	1.2	0.88	2552.5	24.7	2573.6	12.5	2590.1	10.7	2590.1	10.7	98.5
5-Spot 233	222	112168	1.4	5.7443	0.6	9.7056	1.3	0.4045	1.1	0.88	2189.8	20.6	2407.2	11.7	2596.6	10.1	2596.6	10.1	84.3
5-Spot 248	92	73239	3.6	5.7159	0.6	11.6777	1.1	0.4843	0.9	0.81	2546.0	18.7	2578.9	10.2	2604.8	10.7	2604.8	10.7	97.7
5-Spot 102	234	12446279	1.7	5.7109	0.7	11.8724	1.2	0.4920	1.0	0.83	2579.2	21.2	2594.4	11.2	2606.3	11.2	2606.3	11.2	99.0
5-Spot 117	76	218331	0.7	5.7045	0.6	11.9121	1.1	0.4930	0.9	0.83	2583.8	20.1	2597.5	10.6	2608.2	10.5	2608.2	10.5	99.1
5-Spot 263	315	103142	1.6	5.6968	0.5	11.5114	1.1	0.4758	0.9	0.87	2509.1	19.7	2565.5	10.2	2610.4	9.0	2610.4	9.0	96.1
5-Spot 195	88	125740	1.2	5.6747	0.8	11.7881	1.5	0.4854	1.2	0.83	2550.6	25.5	2587.7	13.7	2616.9	13.7	2616.9	13.7	97.5
5-Spot 115	269	357499	6.5	5.6738	0.6	11.6583	1.0	0.4800	0.8	0.82	2527.1	17.2	2577.4	9.4	2617.1	9.4	2617.1	9.4	96.6
5-Spot 104	382	368539	1.6	5.6568	0.6	9.9124	1.6	0.4069	1.5	0.92	2200.5	27.9	2426.7	15.0	2622.1	10.4	2622.1	10.4	83.9
5-Spot 197	532	375700	5.7	5.6238	0.6	12.1738	1.1	0.4968	0.9	0.84	2599.8	19.0	2617.9	9.9	2631.9	9.6	2631.9	9.6	98.8
05-Spot 61	452	267149	1.7	5.6158	0.7	12.0296	1.4	0.4902	1.2	0.87	2571.4	26.2	2606.7	13.4	2634.2	11.8	2634.2	11.8	97.6
5-Spot 182	308	425885	1.4	5.6126	0.6	12.0861	1.1	0.4922	1.0	0.85	2580.2	20.6	2611.1	10.7	2635.2	9.9	2635.2	9.9	97.9
05-Spot 52	176	105472	1.1	5.6087	0.6	12.4863	1.2	0.5081	1.0	0.84	2648.7	22.0	2641.7	11.3	2636.3	10.6	2636.3	10.6	100.5
05-Spot 21	127	139890	0.8	5.6033	0.6	12.5761	1.4	0.5113	1.2	0.88	2662.2	26.1	2648.4	12.8	2637.9	10.7	2637.9	10.7	100.9
5-Spot 241	407	1899914	1.6	5.5965	0.7	11.3364	1.6	0.4603	1.5	0.91	2441.1	29.5	2551.2	14.9	2640.0	11.2	2640.0	11.2	92.5
5-Spot 183	352	224799	1.9	5.5665	0.6	12.7952	1.1	0.5168	0.9	0.85	2685.6	20.0	2664.7	10.1	2648.9	9.3	2648.9	9.3	101.4
5-Spot 280	113	888932	1.2	5.5154	0.7	12.5762	1.3	0.5033	1.1	0.84	2627.9	23.3	2648.4	12.1	2664.2	11.5	2664.2	11.5	98.6
5-Spot 257	90	79771	0.8	5.5137	0.6	12.5367	1.2	0.5016	1.0	0.86	2620.5	22.6	2645.5	11.4	2664.7	10.1	2664.7	10.1	98.3
5-Spot 122	39	56963	2.2	5.5122	0.7	12.7015	1.2	0.5080	0.9	0.80	2648.1	20.5	2657.8	11.0	2665.1	11.6	2665.1	11.6	99.4
5-Spot 199	157	511895	1.5	5.5071	0.7	12.8983	1.3	0.5154	1.1	0.84	2679.7	24.7	2672.3	12.6	2666.6	11.9	2666.6	11.9	100.5
5-Spot 158	29	87324	1.0	5.5034	0.8	12.8348	1.2	0.5125	0.9	0.75	2667.3	19.1	2667.6	11.0	2667.8	12.9	2667.8	12.9	100.0
5-Spot 160	60	56997	2.4	5.4939	0.6	13.0878	1.1	0.5217	0.9	0.82	2706.4	20.5	2686.0	10.7	2670.6	10.7	2670.6	10.7	101.3
05-Spot 24	189	212290	2.9	5.4879	0.5	13.2245	1.1	0.5266	0.9	0.88	2727.1	20.9	2695.8	10.1	2672.4	8.4	2672.4	8.4	102.0
5-Spot 245	78	77270	1.5	5.4874	0.7	12.9804	1.3	0.5168	1.1	0.85	2685.7	25.2	2678.2	12.7	2672.6	11.7	2672.6	11.7	100.5
5-Spot 169	30	21268	2.4	5.4854	0.6	12.4086	1.2	0.4939	1.0	0.87	2587.4	21.5	2635.8	10.9	2673.2	9.3	2673.2	9.3	96.8
5-Spot 175	64	93679	0.9	5.4774	0.5	12.6267	1.2	0.5018	1.1	0.91	2621.6	24.3	2652.2	11.7	2675.6	8.6	2675.6	8.6	98.0
5-Spot 164	139	618527	2.2	5.4700	0.7	13.0775	1.1	0.5190	0.9	0.79	2695.1	19.9	2685.3	10.8	2677.9	11.7	2677.9	11.7	100.6
5-Spot 246	99	121058	1.6	5.4679	0.7	13.4320	1.2	0.5329	1.0	0.82	2753.7	21.3	2710.5	10.9	2678.5	10.9	2678.5	10.9	102.8
5-Spot 272	34	61433	2.4	5.4669	0.9	12.4626	1.5	0.4944	1.2	0.81	2589.5	25.8	2639.9	14.0	2678.8	14.5	2678.8	14.5	96.7
5-Spot 145	16	12470	5.1	5.4564	0.9	13.1123	1.5	0.5191	1.2	0.80	2695.5	26.1	2687.8	14.0	2682.0	14.8	2682.0	14.8	100.5
5-Spot 201	287	215719	3.0	5.4544	1.9	12.7824	2.2	0.5059	1.1	0.49	2639.0	23.4	2663.7	20.9	2682.6	32.1	2682.6	32.1	98.4
5-Spot 218	151	108594	1.5	5.4500	0.8	11.4267	1.4	0.4519	1.2	0.84	2403.5	24.0	2558.6	13.2	2683.9	12.6	2683.9	12.6	89.6
-05-Spot 6	28	42259	2.7	5.4476	0.6	12.2363	1.1	0.4837	0.9	0.83	2543.2	19.6	2622.7	10.6	2684.6	10.5	2684.6	10.5	94.7
5-Spot 185	26	51801	3.6	5.4200	0.8	12.6525	1.2	0.4976	1.0	0.77	2603.4	20.5	2654.1	11.7	2693.0	13.2	2693.0	13.2	96.7
5-Spot 139	769	109946	1.1	5.4160	0.6	10.7723	1.3	0.4233	1.2	0.89	2275.5	22.5	2503.7	12.2	2694.3	9.7	2694.3	9.7	84.5
5-Spot 179	88	97558	2.7	5.4157	0.7	13.0038	1.3	0.5110	1.1	0.84	2660.8	23.6	2679.9	12.2	2694.3	11.6	2694.3	11.6	98.8
5-Spot 188	28	25753	2.9	5.4108	0.6	13.0037	1.1	0.5105	1.0	0.86	2658.9	20.9	2679.9	10.5	2695.8	9.3	2695.8	9.3	98.6
05-Spot 62	128	127134	1.5	5.3673	0.8	13.6952	1.7	0.5333	1.5	0.87	2755.5	33.7	2728.9	16.3	2709.2	14.0	2709.2	14.0	101.7
5-Spot 304	155	144763	2.0	5.1707	0.7	14.1533	1.0	0.5310	0.7	0.73	2745.7	15.8	2760.0	9.2	2770.6	10.9	2770.6	10.9	99.1
5-Spot 228	481	592738	1.6	5.1433	0.7	13.8386	1.9	0.5164	1.8	0.94	2684.1	40.0	2738.7	18.4	2779.2	10.9	2779.2	10.9	96.6
5-Spot 261	130	167923	1.5	5.0877	0.6	14.5707	1.3	0.5379	1.2	0.91	2774.6	27.2	2787.6	12.6	2797.0	9.1	2797.0	9.1	99.2
-05-Spot 5	96	84207	1.0	4.9567	0.7	15.2273	1.2	0.5476	1.0	0.83	2815.4	22.7	2829.6	11.5	2839.7	11.0	2839.7	11.0	99.1
5-Spot 205	216	543394	1.2	4.7939	0.5	14.1287	1.1	0.4915	1.0	0.88	2577.0	20.3	2758.4	10.4	2894.0	8.5	2894.0	8.5	89.0
05-Spot 44	201	395382	2.0	4.7731	0.5	16.6040	1.1	0.5750	1.0	0.87	2928.5	22.8	2912.2	10.6	2901.0	8.8	2901.0	8.8	100.9
5-Spot 301	114	118996	1.6	4.6882	0.6	16.9867	1.0	0.5778	0.9	0.82	2939.9	20.2	2934.1	10.0	2930.1	9.7	2930.1	9.7	100.3
05-Spot 94	114	71831	1.9	4.6874	0.7	16.9862	1.3	0.5777	1.1	0.84	2939.4	25.1	2934.1	12.1	2930.4	11.0	2930.4	11.0	100.3

5-Spot 251	185	32234257	3.8	4.6594	0.7	17.0322	1.1	0.5758	0.9	0.80	2931.7	20.9	2936.6	10.6	2940.0	10.7	2940.0	10.7	99.7
05-Spot 73	49	29530	1.4	4.5785	0.7	16.6243	1.5	0.5523	1.3	0.86	2834.6	29.2	2913.4	14.1	2968.3	12.0	2968.3	12.0	95.5
5-Spot 106	247	110392	1.4	3.9901	0.6	19.2454	1.2	0.5572	1.1	0.87	2855.0	24.7	3054.2	11.9	3188.0	9.6	3188.0	9.6	89.6
05-Spot 19	160	159401	1.0	3.9429	0.6	22.5962	1.1	0.6465	0.9	0.82	3214.4	22.6	3209.7	10.6	3206.8	9.9	3206.8	9.9	100.2
5-Spot 187	125	466333	0.7	3.9362	0.7	21.7421	1.1	0.6210	0.9	0.80	3113.8	22.6	3172.3	11.1	3209.5	10.9	3209.5	10.9	97.0
5-Spot 110	194	139233	1.4	3.8939	0.6	22.0034	1.3	0.6217	1.1	0.87	3116.6	28.2	3183.9	12.7	3226.5	10.2	3226.5	10.2	96.6

Table DTB17-11. U-Pb geochronologic analyses.																			
						Isotope ratios						Apparent ages (Ma)							
Analysis	U	206Pb	U/Th	206Pb*	±	207Pb*	±	206Pb*	±	error	206Pb*	±	207Pb*	±	206Pb*	±	Best age	±	Conc
	(ppm)	204Pb		207Pb*	(%)	235U*	(%)	238U	(%)	corr.	238U*	(Ma)	235U	(Ma)	207Pb*	(Ma)	(Ma)	(Ma)	(%)
1-Spot 178	1746	46888	2.6	16.3069	0.6	0.8148	1.2	0.0964	1.0	0.85	593.3	5.7	605.1	5.4	649.7	13.6	593.3	5.7	91.3
1-Spot 137	597	3109416	1.0	16.6629	0.8	0.8195	1.3	0.0991	1.0	0.80	609.0	6.0	607.7	5.8	603.1	16.5	609.0	6.0	101.0
1-Spot 129	1447	65220	14.9	16.3263	0.7	0.8552	1.2	0.1013	1.0	0.82	622.1	5.8	627.5	5.6	647.1	14.9	622.1	5.8	96.1
1-Spot 202	158	27243	2.0	16.1864	1.1	0.8723	1.8	0.1024	1.5	0.81	628.7	8.9	636.8	8.7	665.6	22.8	628.7	8.9	94.5
1-Spot 110	129	24181	2.8	16.2215	1.2	0.8830	1.8	0.1039	1.4	0.75	637.4	8.2	642.6	8.6	660.9	25.9	637.4	8.2	96.4
11-Spot 67	177	23776	1.7	15.8669	1.1	0.9032	1.8	0.1040	1.4	0.78	637.7	8.4	653.4	8.6	708.1	23.7	637.7	8.4	90.1
1-Spot 168	361	61370	2.9	16.1012	0.9	0.8957	1.2	0.1046	0.9	0.70	641.5	5.3	649.4	5.9	676.9	18.7	641.5	5.3	94.8
1-Spot 161	437	340174	5.3	16.0209	0.9	0.9071	1.3	0.1054	0.9	0.70	646.3	5.6	655.5	6.3	687.6	19.8	646.3	5.6	94.0
11-Spot 88	114	15643	0.8	16.4336	1.3	0.8845	1.8	0.1055	1.2	0.67	646.4	7.5	643.4	8.7	633.1	28.9	646.4	7.5	102.1
11-Spot 95	439	208003	7.6	16.0636	1.0	0.9051	1.6	0.1055	1.3	0.81	646.5	8.0	654.4	7.8	681.8	20.3	646.5	8.0	94.8
1-Spot 167	623	234642	0.9	16.0372	0.8	0.9085	1.3	0.1057	1.0	0.78	647.8	6.0	656.3	6.1	685.4	16.8	647.8	6.0	94.5
1-Spot 149	256	45614	4.5	15.6052	0.9	0.9340	1.7	0.1058	1.4	0.85	648.0	8.7	669.7	8.1	743.4	18.1	648.0	8.7	87.2
1-Spot 100	181	27166	5.6	15.7601	1.4	0.9264	1.8	0.1059	1.2	0.67	649.1	7.6	665.7	9.0	722.5	29.1	649.1	7.6	89.8
-11-Spot 1	240	62331	3.0	16.0218	0.8	0.9121	1.5	0.1060	1.3	0.85	649.7	7.8	658.2	7.2	687.4	16.5	649.7	7.8	94.5
1-Spot 194	230	70394	1.6	16.1873	1.1	0.9036	1.6	0.1061	1.2	0.76	650.2	7.6	653.6	7.8	665.5	22.6	650.2	7.6	97.7
1-Spot 270	1156	441091	2.5	16.0322	0.6	0.9130	1.2	0.1062	1.0	0.88	650.7	6.4	658.6	5.7	686.1	12.1	650.7	6.4	94.8
-11-Spot 2	1250	293584	1.7	16.2787	0.8	0.8998	1.5	0.1063	1.3	0.84	651.1	7.9	651.6	7.3	653.4	17.6	651.1	7.9	99.6
1-Spot 248	214	61433	2.6	16.0958	1.0	0.9102	1.8	0.1063	1.5	0.83	651.2	9.4	657.2	8.8	677.6	21.5	651.2	9.4	96.1
1-Spot 156	304	51416	3.0	16.0475	0.9	0.9135	1.6	0.1064	1.3	0.81	651.6	8.0	658.9	7.8	684.0	20.1	651.6	8.0	95.3
1-Spot 180	312	371379	2.3	16.0773	0.9	0.9120	1.8	0.1064	1.6	0.87	651.8	9.9	658.1	8.9	680.0	19.3	651.8	9.9	95.8
1-Spot 144	227	48227	2.0	16.0146	0.9	0.9158	1.5	0.1064	1.3	0.82	651.9	7.9	660.2	7.5	688.4	18.8	651.9	7.9	94.7
1-Spot 224	530	147874	4.1	16.1546	1.0	0.9081	1.6	0.1064	1.2	0.79	652.1	7.6	656.0	7.6	669.8	20.8	652.1	7.6	97.4
1-Spot 118	141	10492	0.9	16.1191	1.0	0.9103	1.7	0.1065	1.4	0.81	652.2	8.7	657.2	8.4	674.5	21.6	652.2	8.7	96.7
1-Spot 274	237	42162	1.7	16.0069	0.9	0.9173	1.5	0.1065	1.1	0.77	652.6	7.0	661.0	7.1	689.4	19.7	652.6	7.0	94.7
1-Spot 235	265	74552	2.8	16.0103	1.0	0.9175	1.8	0.1066	1.5	0.83	652.8	9.3	661.0	8.7	688.9	21.2	652.8	9.3	94.8
11-Spot 86	159	29149	2.7	16.0873	0.8	0.9131	1.4	0.1066	1.1	0.81	652.9	7.1	658.7	6.9	678.7	17.9	652.9	7.1	96.2
1-Spot 198	268	183341	4.9	15.9658	0.8	0.9211	1.6	0.1067	1.4	0.86	653.6	8.4	663.0	7.6	694.9	17.1	653.6	8.4	94.1
1-Spot 268	75	13724	2.5	16.5036	1.5	0.8928	1.9	0.1069	1.1	0.60	654.8	7.0	647.9	8.9	623.9	32.0	654.8	7.0	105.0
1-Spot 124	592	72524	1.5	16.0270	0.7	0.9197	1.3	0.1070	1.1	0.84	655.0	6.8	662.2	6.3	686.7	14.8	655.0	6.8	95.4
11-Spot 44	208	632289	1.9	15.9043	0.9	0.9274	1.7	0.1070	1.4	0.82	655.4	8.5	666.3	8.1	703.1	19.9	655.4	8.5	93.2
1-Spot 302	247	756738	2.3	16.1981	0.9	0.9107	1.6	0.1070	1.4	0.82	655.5	8.5	657.4	8.0	664.1	20.0	655.5	8.5	98.7
1-Spot 282	140	21365	3.0	16.1448	0.9	0.9143	1.4	0.1071	1.1	0.77	655.9	6.8	659.4	6.8	671.1	19.2	655.9	6.8	97.7
1-Spot 293	111	8626	2.1	16.2893	1.3	0.9063	1.7	0.1071	1.2	0.69	656.0	7.5	655.1	8.4	652.0	27.1	656.0	7.5	100.6
1-Spot 214	270	58409	2.6	16.1833	1.1	0.9129	1.8	0.1072	1.4	0.79	656.4	8.8	658.6	8.6	666.0	23.2	656.4	8.8	98.6
1-Spot 209	79	307797	2.0	15.6345	1.3	0.9455	1.8	0.1073	1.3	0.71	656.8	8.1	675.8	9.0	739.4	27.4	656.8	8.1	88.8
11-Spot 71	125	38543	2.2	16.0521	1.0	0.9209	1.8	0.1073	1.6	0.85	656.8	9.8	662.9	9.0	683.4	21.0	656.8	9.8	96.1
11-Spot 56	632	68236	4.8	16.2646	0.8	0.9095	1.4	0.1073	1.1	0.81	657.2	7.1	656.8	6.7	655.2	17.5	657.2	7.1	100.3
1-Spot 238	731	1293516	4.1	16.1138	0.7	0.9189	1.3	0.1074	1.1	0.83	657.8	6.6	661.8	6.2	675.2	15.4	657.8	6.6	97.4
1-Spot 221	181	210295	2.4	16.2658	1.0	0.9105	1.6	0.1075	1.2	0.77	658.0	7.6	657.3	7.6	655.1	21.4	658.0	7.6	100.4
1-Spot 218	96	87652	3.1	15.5441	1.2	0.9528	1.7	0.1075	1.2	0.70	658.0	7.6	679.5	8.6	751.7	26.3	658.0	7.6	87.5
1-Spot 186	211	58013	2.1	15.9929	1.0	0.9261	1.6	0.1075	1.3	0.79	658.0	8.2	665.6	8.0	691.3	21.3	658.0	8.2	95.2
11-Spot 16	531	114759	0.9	16.2742	1.0	0.9105	1.5	0.1075	1.1	0.75	658.3	6.9	657.3	7.1	654.0	21.0	658.3	6.9	100.7
1-Spot 241	602	6074288	3.3	16.1021	0.7	0.9204	1.2	0.1075	1.0	0.81	658.4	6.0	662.6	5.8	676.7	14.7	658.4	6.0	97.3
11-Spot 32	402	87654	1.6	15.8934	0.8	0.9330	1.2	0.1076	0.9	0.73	658.8	5.6	669.2	6.0	704.6	17.8	658.8	5.6	93.5
-11-Spot 6	383	121464	3.3	16.1259	0.7	0.9198	1.2	0.1076	1.0	0.83	658.9	6.1	662.3	5.7	673.6	14.0	658.9	6.1	97.8
1-Spot 229	211	62575	2.5	15.9125	0.8	0.9322	1.5	0.1076	1.3	0.85	659.0	8.0	668.8	7.3	702.0	17.0	659.0	8.0	93.9
1-Spot 151	216	28990	1.6	15.9426	1.1	0.9314	1.6	0.1077	1.2	0.73	659.6	7.5	668.4	8.1	698.0	24.1	659.6	7.5	94.5
1-Spot 153	859	76418	3.0	16.2264	0.7	0.9153	1.3	0.1078	1.1	0.84	659.7	6.8	659.8	6.3	660.3	15.0	659.7	6.8	99.9
1-Spot 247	243	84376	0.7	15.9934	0.8	0.9287	1.3	0.1078	1.0	0.78	659.8	6.5	666.9	6.5	691.2	17.7	659.8	6.5	95.5
-11-Spot 7	145	330899	2.5	15.9980	1.2	0.9286	1.7	0.1078	1.2	0.69	659.9	7.4	666.9	8.3	690.6	26.4	659.9	7.4	95.6
1-Spot 206	243	43584	1.7	16.2456	1.0	0.9146	1.6	0.1078	1.2	0.78	660.0	7.8	659.5	7.8	657.7	21.5	660.0	7.8	100.3
1-Spot 292	145	119725	1.7	16.0741	0.8	0.9244	1.3	0.1078	1.0	0.76	660.0	6.0	664.7	6.2	680.5	17.8	660.0	6.0	97.0
11-Spot 96	455	60956	2.8	16.1788	0.9	0.9186	1.4	0.1078	1.1	0.78	660.2	6.7	661.6	6.7	666.6	18.4	660.2	6.7	99.0
1-Spot 308	647	201484	3.3	16.0175	0.6	0.9279	1.2	0.1078	1.1	0.89	660.2	6.9	666.5	6.0	688.0	11.9	660.2	6.9	96.0
11-Spot 58	154	69082	2.2	15.9380	0.8	0.9329	1.8	0.1079	1.6	0.90	660.5	10.0	669.2	8.7	698.6	16.9	660.5	10.0	94.5
11-Spot 40	666	63332	2.8	15.9761	0.9	0.9314	1.5	0.1080	1.3	0.82	660.9	7.9	668.4	7.6	693.5	19.0	660.9	7.9	95.3
1-Spot 135	250	1383842	2.6	16.3286	0.8	0.9117	1.4	0.1080	1.1	0.81	661.2	6.9	658.0	6.6	646.8	17.0	661.2	6.9	102.2
1-Spot 245	159	35264	3.0	16.1321	1.1	0.9230	1.5	0.1080	1.1	0.71	661.3	6.6	663.9	7.3	672.8	22.8	661.3	6.6	98.3
1-Spot 195	283	698127	4.1	16.1143	0.9	0.9243	1.6	0.1081	1.4	0.84	661.5	8.6	664.6	8.0	675.1	19.0	661.5	8.6	98.0
1-Spot 212	166	32500	2.4	15.9692	0.8	0.9331	1.4	0.1081	1.1	0.81	661.8	7.2	669.3	6.9	694.5	17.8	661.8	7.2	95.3
11-Spot 63	451	34016	3.4	16.1753	0.9	0.9212	1.4	0.1081	1.1	0.78	661.8	7.1	663.0	7.0	667.0	19.1	661.8	7.1	99.2
1-Spot 131	558	95223	1.6	16.2741	0.5	0.9157	1.0	0.1081	0.9	0.87	661.8	5.5	660.1	4.9	654.0	10.6	661.8	5.5	101.2
1-Spot 200	122	21953	2.7	16.0727	1.2	0.9275	1.9	0.1082	1.5	0.76	662.1	9.1	666.3	9.3	680.6	26.4	662.1	9.1	97.3
-11-Spot 4	175	31433	2.4	15.9483	1.0	0.9349	1.9	0.1082	1.6	0.84	662.2	9.9	670.2	9.1	697.2	21.3	662.2	9.9	95.0
11-Spot 54	291	35153	2.0	15.9768	0.9	0.9338	1.7	0.1083	1.4	0.82	662.6	8.7	669.6	8.2	693.4	20.2	662.6	8.7	95.6
11-Spot 79	371	60182	1.9	16.1066	1.0	0.9265	1.8	0.1083	1.5	0.82	662.7	9.5	665.8	8.9	676.1	22.1	662.7	9.5	98.0
1-Spot 244	126	71795	2.6	15.7133	1.2	0.9507	2.0	0.1084	1.5	0.77	663.4	9.6	678.5	9.7	728.8	26.3	663.4	9.6	91.0
11-Spot 39	281	48289	2.0	16.0034	0.8	0.9336	1.5	0.1084	1.3	0.83	663.5	7.9	669.5	7.4	689.9	17.9	663.5	7.9	96.2
1-Spot 190	234	6640695	1.7	16.0474	0.8	0.9314	1.5	0.1084	1.2	0.81	663.7	7.5	668.4	7.1	684.0	18.1	663.7	7.5	97.0
11-Spot 98	165	120760	2.7	16.0303	0.9	0.9327	1.5	0.1085	1.2	0.81	663.9	7.4	669.0	7.1	686.3	18.4	663.9	7.4	96.7
1-Spot 106	1181	162182	3.6	16.1783	0.8	0.9258	1.3	0.1087	1.0	0.78	665.0	6.5	665.4	6.4	666.7	17.7	665.0	6.5	99.8
1-Spot 134	413	67161	3.9	16.3643	0.7	0.9159	1.3	0.1087	1.1	0.84	665.5	6.7	660.2	6.1	642.1	14.6	665.5	6.7	103.6
1-Spot 163	146	22416	1.5	16.1578	0.7	0.9278	1.4	0.1088	1.2	0.86	665.6	7.7	666.5	7.0	669.4	15.9	665.6	7.7	99.4
11-Spot 94	204	30072	2.9	15.3337	1.5	0.9779	2.1	0.1088	1.5	0.70	665.8	9.3	692.5	10.6	780.4	31.8	665.8	9.3	85.3
1-Spot 205	726	1393468	2.1	16.2618	0.7	0.9223	1.2	0.1088	1.0	0.83	665.9	6.5	663.6	6.0	655.6	14.7	665.9	6.5	101.6
11-Spot 57	203	48090	2.8	16.0966	1.1	0.9318	1.8	0.1088	1.4	0.80	666.0	8.9	668.6	8.7	677.5	22.8	666.0	8.9	98.3
1-Spot 207	243	350200	2.7	16.2090	1.0	0.9255	1.7	0.1088	1.4	0.83	666.1	9.0	665.3	8.4	662.6	20.5	666.1	9.0	100.5
1-Spot 304	135	71891	1.9	15.9402	0.9	0.9422	1.5	0.1090	1.3	0.83	666.8	8.0	674.0	7.5	698.3	18.3	666.8	8.0	95.5
1-Spot 220	351	67665	3.3	16.1486	0.8	0.9305	1.3	0.1090	1.0	0.79	667.1	6.7	667.9	6.5	670.6	17.3	667.1	6.7	99.5
-11-Spot 5	339	60653	2.4	16.2268	0.8	0.9261	1.5	0.1090	1.3	0.85	667.2	7.9	665.6	7.2	660.2	16.6	667.2	7.9	101.1
1-Spot 184	393	144054	1.9	16.2389	0.8	0.9263	1.4	0.1091	1.1	0.82	667.8	7.2	665.7	6.8	658.6	16.8	667.8	7.2	101.4
1-Spot 191	162	631321	1.9	15.8733	0.8	0.9477	1.4	0.1092	1.1	0.79	667.8	7.0	676.9	6.9	707.3	18.0	667.8	7.0	94.4

1-Spot 269	259	32543	1.2	16.3285	0.9	0.9229	1.3	0.1093	1.0	0.77	668.9	6.5	663.9	6.5	646.9	18.4	668.9	6.5	103.4
11-Spot 35	254	29991	2.1	16.2537	1.1	0.9272	1.7	0.1093	1.3	0.76	669.0	8.1	666.2	8.1	656.7	22.9	669.0	8.1	101.9
1-Spot 271	261	106744	3.3	16.0336	1.1	0.9403	1.7	0.1094	1.3	0.75	669.2	8.0	673.0	8.3	685.9	24.0	669.2	8.0	97.6
11-Spot 21	110	34745	2.2	15.6353	0.9	0.9649	1.5	0.1095	1.2	0.81	669.6	7.9	685.8	7.6	739.3	19.2	669.6	7.9	90.6
1-Spot 276	440	187073	2.7	16.2692	0.9	0.9292	1.5	0.1097	1.2	0.81	670.9	7.8	667.2	7.4	654.7	19.2	670.9	7.8	102.5
11-Spot 26	524	196996	2.0	16.0847	0.7	0.9401	1.5	0.1097	1.4	0.89	671.1	8.7	672.9	7.5	679.0	14.6	671.1	8.7	98.8
1-Spot 233	316	36349	2.2	16.0218	0.9	0.9442	1.3	0.1098	1.0	0.75	671.3	6.4	675.1	6.6	687.4	19.1	671.3	6.4	97.7
1-Spot 105	269	29490	2.3	16.1928	0.8	0.9343	1.5	0.1098	1.3	0.84	671.4	8.3	669.9	7.6	664.7	18.0	671.4	8.3	101.0
11-Spot 27	297	61397	4.1	15.9026	0.9	0.9523	1.4	0.1099	1.1	0.78	672.0	7.2	679.3	7.1	703.3	18.9	672.0	7.2	95.6
1-Spot 263	123	58977	2.4	16.2302	0.9	0.9360	1.4	0.1102	1.0	0.73	674.1	6.5	670.8	6.8	659.8	20.2	674.1	6.5	102.2
1-Spot 115	157	23709	1.4	16.3472	1.0	0.9295	1.7	0.1103	1.3	0.78	674.2	8.4	667.4	8.2	644.4	22.5	674.2	8.4	104.6
1-Spot 114	107	18605	0.8	16.0305	1.3	0.9481	1.8	0.1103	1.2	0.65	674.4	7.4	677.1	8.8	686.3	28.8	674.4	7.4	98.3
11-Spot 76	105	33481	1.4	16.0613	1.2	0.9492	1.7	0.1106	1.2	0.70	676.4	7.7	677.7	8.5	682.1	26.1	676.4	7.7	99.2
1-Spot 309	199	63394	3.5	16.1106	0.9	0.9471	1.3	0.1107	0.9	0.73	676.9	6.0	676.6	6.4	675.6	19.0	676.9	6.0	100.2
11-Spot 20	1054	281988	2.8	15.7558	0.9	0.9690	1.6	0.1108	1.3	0.81	677.2	8.4	687.9	8.0	723.0	20.0	677.2	8.4	93.7
-11-Spot 3	97	47943	1.8	15.9727	1.0	0.9562	1.4	0.1108	1.0	0.69	677.5	6.4	681.3	7.1	694.0	21.9	677.5	6.4	97.6
11-Spot 33	418	37329	2.9	16.0097	0.7	0.9542	1.5	0.1108	1.3	0.89	677.6	8.5	680.3	7.3	689.1	14.2	677.6	8.5	98.3
11-Spot 66	178	21780	2.2	16.0120	1.1	0.9540	1.7	0.1108	1.3	0.75	677.6	8.0	680.2	8.2	688.7	23.3	677.6	8.0	98.4
1-Spot 112	455	25749	1.6	15.5630	0.7	0.9868	1.0	0.1114	0.8	0.74	681.1	5.0	697.1	5.3	749.1	15.0	681.1	5.0	90.9
1-Spot 228	483	49113	3.9	16.1752	0.9	0.9504	1.5	0.1115	1.2	0.80	681.7	7.8	678.3	7.5	667.0	19.3	681.7	7.8	102.2
11-Spot 28	276	99425	6.3	16.0434	0.8	0.9626	1.8	0.1121	1.6	0.89	684.7	10.2	684.6	8.8	684.6	17.6	684.7	10.2	100.0
11-Spot 68	95	36261	2.0	15.9735	1.0	0.9677	1.6	0.1122	1.2	0.75	685.2	7.7	687.3	7.9	693.9	22.3	685.2	7.7	98.8
1-Spot 249	102	8428	1.5	15.2858	2.3	1.0117	2.8	0.1122	1.5	0.55	685.6	9.9	709.7	14.1	786.9	48.4	685.6	9.9	87.1
1-Spot 272	43	11884	2.1	15.9035	1.6	0.9734	1.9	0.1123	0.9	0.50	686.2	6.2	690.2	9.4	703.2	34.5	686.2	6.2	97.6
11-Spot 53	141	13114	2.4	16.0684	1.0	0.9636	1.7	0.1123	1.4	0.80	686.3	9.1	685.2	8.7	681.2	22.4	686.3	9.1	100.8
1-Spot 187	94	1912098	2.8	16.0463	1.0	0.9747	1.4	0.1135	1.0	0.70	692.9	6.6	690.9	7.2	684.2	22.0	692.9	6.6	101.3
11-Spot 84	120	46836	2.5	15.7708	1.3	0.9923	2.0	0.1135	1.5	0.76	693.3	9.9	699.9	10.0	721.0	27.0	693.3	9.9	96.2
1-Spot 181	255	151446	2.2	15.5304	1.1	1.0099	1.5	0.1138	1.0	0.65	694.8	6.5	708.8	7.7	753.5	24.1	694.8	6.5	92.2
1-Spot 231	813	85569	2.3	15.9284	0.7	0.9913	1.0	0.1146	0.8	0.75	699.3	5.0	699.4	5.1	699.9	14.3	699.3	5.0	99.9
1-Spot 111	287	52304	2.7	15.7612	1.0	1.0044	1.5	0.1149	1.1	0.76	700.9	7.4	706.0	7.5	722.3	20.2	700.9	7.4	97.0
11-Spot 34	330	88556	2.5	15.8684	1.1	0.9977	1.6	0.1149	1.2	0.75	701.0	8.0	702.6	8.2	707.9	22.7	701.0	8.0	99.0
1-Spot 138	623	77591	2.3	16.0745	0.8	0.9849	1.4	0.1149	1.2	0.82	701.0	7.8	696.1	7.2	680.4	17.5	701.0	7.8	103.0
1-Spot 306	226	39844	2.4	15.9443	0.6	0.9938	1.3	0.1150	1.2	0.89	701.6	7.8	700.7	6.7	697.8	12.6	701.6	7.8	100.5
11-Spot 18	330	82886	5.0	16.1573	1.0	0.9814	1.6	0.1151	1.3	0.79	702.0	8.6	694.3	8.3	669.4	21.6	702.0	8.6	104.9
1-Spot 277	43	30887	0.4	15.0514	1.4	1.0551	1.7	0.1152	1.1	0.61	703.0	7.2	731.4	9.1	819.4	28.8	703.0	7.2	85.8
11-Spot 45	246	832478	2.2	15.9251	1.1	1.0006	1.6	0.1156	1.2	0.73	705.3	7.8	704.1	8.1	700.4	23.2	705.3	7.8	100.7
1-Spot 237	380	184464	2.7	15.8170	0.8	1.0075	1.3	0.1156	1.1	0.82	705.3	7.1	707.6	6.7	714.8	16.1	705.3	7.1	98.7
1-Spot 188	299	68559	2.0	15.8777	0.9	1.0042	1.2	0.1157	0.9	0.70	705.7	5.7	705.9	6.3	706.7	18.8	705.7	5.7	99.9
1-Spot 101	94	24236	2.4	15.7869	1.1	1.0131	1.7	0.1160	1.3	0.76	707.7	8.5	710.4	8.6	718.8	23.1	707.7	8.5	98.5
1-Spot 305	66	17106	2.3	15.7017	1.4	1.0203	2.0	0.1162	1.4	0.72	708.9	9.6	714.1	10.2	730.4	29.2	708.9	9.6	97.1
1-Spot 227	144	91517	2.0	11.6803	0.9	2.6881	1.4	0.2278	1.2	0.80	1323.1	13.8	1325.2	10.7	1328.6	16.8	1328.6	16.8	99.6
1-Spot 179	227	81915	0.6	11.4551	0.8	2.7205	1.4	0.2261	1.2	0.83	1314.1	13.8	1334.1	10.4	1366.2	15.0	1366.2	15.0	96.2
11-Spot 15	113	42814	1.2	11.3776	0.8	2.9948	1.5	0.2472	1.2	0.83	1424.2	15.8	1406.3	11.3	1379.3	15.9	1379.3	15.9	103.3
11-Spot 59	39	10245	1.2	11.3583	1.4	2.8640	2.0	0.2360	1.4	0.70	1366.0	17.2	1372.5	15.1	1382.5	27.7	1382.5	27.7	98.8
11-Spot 52	139	6002342	1.0	11.2940	0.8	2.9338	1.8	0.2404	1.6	0.90	1388.9	20.0	1390.7	13.5	1393.4	15.0	1393.4	15.0	99.7
1-Spot 213	59	54878	1.6	11.2669	1.1	2.9402	1.6	0.2404	1.2	0.75	1388.6	15.4	1392.3	12.5	1398.0	20.9	1398.0	20.9	99.3
1-Spot 232	117	34669	1.0	11.2614	0.8	2.7920	1.5	0.2281	1.2	0.84	1324.7	14.9	1353.4	11.1	1399.0	15.7	1399.0	15.7	94.7
1-Spot 255	121	55450	1.5	11.2019	0.7	3.0790	1.2	0.2503	0.9	0.80	1439.8	12.1	1427.5	9.0	1409.1	13.4	1409.1	13.4	102.2
1-Spot 240	100	33176	1.3	11.1902	1.0	3.1568	1.5	0.2563	1.1	0.75	1470.9	14.6	1446.7	11.5	1411.1	19.0	1411.1	19.0	104.2
1-Spot 216	170	913893	1.4	11.1880	0.8	2.9736	1.4	0.2414	1.1	0.80	1393.9	13.9	1400.9	10.5	1411.5	15.9	1411.5	15.9	98.8
1-Spot 147	267	93572	3.0	11.1655	0.7	3.1165	1.3	0.2525	1.1	0.83	1451.3	14.4	1436.8	10.2	1415.3	14.0	1415.3	14.0	102.5
1-Spot 250	269	160534	1.7	11.1523	0.9	3.1360	1.7	0.2538	1.4	0.85	1457.9	18.6	1441.6	12.9	1417.6	16.6	1417.6	16.6	102.8
1-Spot 164	184	74115	3.6	11.1080	1.0	3.1423	1.5	0.2533	1.2	0.78	1455.3	15.7	1443.1	11.9	1425.2	18.3	1425.2	18.3	102.1
1-Spot 201	316	54188	1.7	11.0934	0.8	3.0502	1.2	0.2455	0.9	0.77	1415.3	11.7	1420.3	9.1	1427.7	14.5	1427.7	14.5	99.1
11-Spot 90	207	137455	2.4	11.0602	0.8	3.0613	1.4	0.2457	1.1	0.81	1416.1	14.3	1423.1	10.6	1433.4	15.5	1433.4	15.5	98.8
11-Spot 60	211	172994	2.0	11.0572	0.8	3.1262	1.5	0.2508	1.3	0.86	1442.7	16.6	1439.2	11.5	1434.0	14.6	1434.0	14.6	100.6
1-Spot 123	113	173331	2.8	11.0542	0.8	3.2480	1.5	0.2605	1.3	0.83	1492.5	16.9	1468.7	11.8	1434.5	16.0	1434.5	16.0	104.0
1-Spot 133	184	79292	2.0	11.0265	0.7	3.0981	1.4	0.2479	1.2	0.88	1427.5	15.6	1432.2	10.7	1439.3	12.8	1439.3	12.8	99.2
11-Spot 61	275	140084	2.4	11.0248	0.6	3.1135	1.6	0.2491	1.4	0.92	1433.6	18.6	1436.0	12.0	1439.6	11.3	1439.6	11.3	99.6
11-Spot 30	275	62125	2.8	11.0238	0.8	3.1383	1.4	0.2510	1.1	0.82	1443.8	14.5	1442.1	10.5	1439.7	14.8	1439.7	14.8	100.3
1-Spot 219	89	40723	1.7	11.0101	0.8	3.1392	1.4	0.2508	1.1	0.83	1442.5	14.8	1442.4	10.6	1442.1	14.7	1442.1	14.7	100.0
11-Spot 42	201	91328	0.9	10.9831	0.9	3.2407	4.1	0.2583	4.0	0.98	1480.9	52.4	1467.0	31.5	1446.8	17.1	1446.8	17.1	102.4
1-Spot 136	495	170135	1.3	10.9805	0.8	2.9999	1.5	0.2390	1.2	0.85	1381.6	15.4	1407.6	11.1	1447.2	14.7	1447.2	14.7	95.5
1-Spot 116	152	132216	2.5	10.9527	0.6	3.0512	1.0	0.2425	0.8	0.82	1399.6	10.6	1420.5	7.9	1452.1	11.2	1452.1	11.2	96.4
1-Spot 297	168	1315501	1.6	10.9429	0.9	3.2372	1.5	0.2570	1.2	0.80	1474.6	16.4	1466.1	12.0	1453.8	17.5	1453.8	17.5	101.4
11-Spot 36	184	209883	1.9	10.9339	0.7	3.1584	1.4	0.2506	1.3	0.89	1441.4	16.7	1447.1	11.2	1455.3	12.5	1455.3	12.5	99.0
11-Spot 50	180	103512	2.6	10.9184	1.1	3.1312	1.4	0.2481	1.0	0.67	1428.5	12.4	1440.4	11.1	1458.0	20.5	1458.0	20.5	98.0
1-Spot 258	931	190960	1.0	10.9028	0.6	3.2267	1.4	0.2553	1.3	0.91	1465.5	16.5	1463.6	10.8	1460.7	11.2	1460.7	11.2	100.3
1-Spot 141	70	104689	4.8	10.8963	0.9	3.2263	1.7	0.2551	1.4	0.82	1464.6	17.8	1463.5	12.8	1461.9	18.0	1461.9	18.0	100.2
1-Spot 126	120	49289	1.6	10.8802	0.8	2.8310	2.0	0.2235	1.8	0.91	1300.3	21.5	1363.8	15.1	1464.7	16.1	1464.7	16.1	88.8
1-Spot 146	60	213721	1.7	10.8779	0.9	3.1908	1.4	0.2518	1.0	0.74	1448.0	13.1	1454.9	10.5	1465.1	17.2	1465.1	17.2	98.8
1-Spot 142	247	213015	1.2	10.8598	0.9	3.1303	1.6	0.2467	1.4	0.83	1421.2	17.4	1440.2	12.6	1468.3	17.2	1468.3	17.2	96.8
1-Spot 119	195	537371	3.8	10.8577	0.8	3.0825	1.4	0.2428	1.2	0.82	1401.4	14.8	1428.3	10.9	1468.6	15.3	1468.6	15.3	95.4
11-Spot 22	120	137808	2.6	10.8159	0.8	3.2166	1.4	0.2524	1.2	0.85	1451.0	16.0	1461.2	11.2	1475.9	14.5	1475.9	14.5	98.3
1-Spot 294	317	168161	2.8	10.7127	0.6	3.3332	1.2	0.2591	1.0	0.87	1485.2	13.8	1488.9	9.3	1494.1	11.0	1494.1	11.0	99.4
1-Spot 192	156	441487	3.1	10.5602	0.8	3.3990	1.3	0.2604	1.0	0.81	1492.1	13.9	1504.2	10.2	1521.2	14.5	1521.2	14.5	98.1
1-Spot 197	119	154817	1.8	10.1362	0.6	3.7729	1.2	0.2775	1.0	0.85	1578.7	14.4	1587.0	9.7	1598.0	11.8	1598.0	11.8	98.8
11-Spot 38	115	35422	1.9	9.9922	0.9	3.9714	1.7	0.2879	1.4	0.84	1631.2	20.7	1628.4	13.9	1624.7	17.5	1624.7	17.5	100.4
1-Spot 264	190	50331	1.2	9.9710	0.7	3.5723	1.3	0.2585	1.1	0.82	1481.9	14.1	1543.4	10.2	1628.7	13.5	1628.7	13.5	91.0
11-Spot 89	71	28915	1.7	9.9562	0.8	3.8522	1.3	0.2783	1.0	0.76	1582.7	13.8	1603.7	10.4	1631.4	15.6	1631.4	15.6	97.0
1-Spot 298	224	33900	2.1	9.9260	0.8	3.8987	1.4	0.2808	1.2	0.84	1595.3	16.5	1613.4	11.3	1637.1	14.1	1637.1	14.1	97.5
1-Spot 120	690	450306	3.2	9.8985	0.8	4.2692	1.4	0.3066	1.2	0.81	1724.1	17.5	1687.4	11.7	1642.2	15.4	1642.2	15.4	105.0
1-Spot 290	645	242637	2.6	9.8425	0.7	4.1574	1.4	0.2969	1.2	0.86	1675.9	18.0	1665.7	11.5	1652.7	13.2	1652.7	13.2	101.4
11-Spot 78	140	50972	2.6	9.8239	0.9	3.9841	1.7	0.2840	1.4	0.84	1611.4	19.8	1631.0	13.5	1656.2	16.9	1656.2	16.9	97.3
11-Spot 80	318	80818	2.8	9.8036	0.8	4.1162	1.4	0.2928	1.2	0.82	1655.5	16.8	1657.5	11.5	1660.1	15.1	1660.1	15.1	99.7
1-Spot 226	391	36452	2.4	9.7587	1.0	3.7130	2.3	0.2629	2.1	0.91	1504.7	28.0	1574.2	18.3	1668.6	17.6	1668.6	17.6	90.2
1-Spot 296	149	31992	3.5	9.7398	0.8	4.3536	1.5	0.3077	1.2	0.84	1729.3	18.9	1703.6	12.3	1672.1	15.1	1672.1	15.1	103.4
1-Spot 128	305	144411	2.3	9.7373	0.6	3.5422	2.7	0.2503	2.6	0.97	1439.9	33.7	1536.7	21.3	1672.6	11.7	1672.6	11.7	86.1
1-Spot 242	173	75811	1.7	9.7206	0.7	4.2226	1.3	0.2978	1.1	0.82	1680.5	15.6	1678.4	10.5	1675.8	13.4	1675.8	13.4	100.3
1-Spot 172	85	22190	1.5	9.7056	0.8	4.2478	1.5	0.2991	1.3	0.84	1687.0	18.7	1683.3	12.3	1678.7	15.0	1678.7	15.0	100.5
1-Spot 239	226	107345	1.2	9.7054	0.8	4.3572	1.2	0.3068	0.9	0.76	1725.1	14.4	1704.3	10.3	1678.7	15.0	1678.7	15.0	102.8
11-Spot 99	447	156726	3.7	9.7046	0.8	4.3187	1.4	0.3041	1.2	0.84	1711.6	17.9	1696.9	11.7	1678.8	14.3	1678.8	14.3	102.0
1-Spot 300	378	70963	2.9	9.7018	0.8	4.2803	1.5	0.3013	1.3	0.85	1697.8	18.8	1689.6	12.2	1679.4	14.5	1679.4	14.5	101.1
1-Spot 215	231	183143	1.5	9.6967	0.8	4.2913	1.8	0.3019	1.6	0.89	1700.9	23.5	1691.7	14.5	1680.3	14.7	1680.3	14.7	101.2
1-Spot 310	262	157631	1.8	9.6953	0.7	4.2688	1.3	0.3003	1.1	0.84	1692.8	16.7	1687.4	11.0	1680.6	13.2	1680.6	13.2	100.7
11-Spot 62	579	179591	1.8	9.6864	0.9	4.2678	1.6	0.3000	1.4	0.85	1691.1	20.8	1687.2	13.5	1682.3	15.8	1682.3	15.8	100.5

1-Spot 299	337	165791	3.5	9.6830	0.9	4.2519	1.5	0.2987	1.2	0.82	1685.0	18.4	1684.1	12.5	1683.0	16.0	1683.0	16.0	100.1
1-Spot 176	78	17400	1.7	9.6788	0.8	4.4075	1.4	0.3095	1.1	0.81	1738.4	16.8	1713.7	11.3	1683.8	14.7	1683.8	14.7	103.2
1-Spot 303	122	46671	3.2	9.6759	0.8	4.3414	1.4	0.3048	1.2	0.85	1715.0	18.1	1701.3	11.7	1684.3	13.9	1684.3	13.9	101.8
1-Spot 251	64	62809	1.6	9.6703	0.8	4.3375	1.4	0.3043	1.1	0.82	1712.8	16.8	1700.5	11.2	1685.4	14.4	1685.4	14.4	101.6
1-Spot 175	199	119464	3.0	9.6658	0.7	4.2003	1.3	0.2946	1.1	0.82	1664.4	15.4	1674.1	10.5	1686.2	13.5	1686.2	13.5	98.7
1-Spot 193	282	101454	1.2	9.6613	0.7	4.3671	1.2	0.3061	0.9	0.80	1721.7	13.9	1706.1	9.5	1687.1	12.8	1687.1	12.8	102.0
1-Spot 159	108	27234	3.0	9.6597	0.8	4.2653	1.4	0.2990	1.2	0.84	1686.1	17.7	1686.7	11.7	1687.4	14.1	1687.4	14.1	99.9
1-Spot 196	254	1266388	5.2	9.6501	0.6	3.8468	1.1	0.2694	1.0	0.83	1537.5	13.1	1602.6	9.3	1689.2	11.7	1689.2	11.7	91.0
1-Spot 311	302	43436	3.5	9.6498	0.7	4.1799	1.3	0.2927	1.1	0.85	1654.8	16.6	1670.1	11.0	1689.3	13.2	1689.3	13.2	98.0
1-Spot 210	129	62868	3.4	9.6495	0.7	4.4091	1.2	0.3087	1.0	0.81	1734.3	15.4	1714.1	10.3	1689.3	13.4	1689.3	13.4	102.7
1-Spot 243	163	161697	2.8	9.6493	0.7	4.2600	1.4	0.2983	1.2	0.85	1682.7	17.6	1685.7	11.4	1689.4	13.4	1689.4	13.4	99.6
1-Spot 155	339	230663	3.1	9.6477	0.7	4.3364	1.5	0.3036	1.3	0.90	1708.9	19.9	1700.3	12.2	1689.7	12.2	1689.7	12.2	101.1
1-Spot 169	60	30297	2.6	9.6400	0.9	4.4648	1.6	0.3123	1.3	0.80	1752.0	19.5	1724.5	13.1	1691.2	17.3	1691.2	17.3	103.6
1-Spot 307	136	82802	0.7	9.6357	0.8	4.1338	1.3	0.2890	1.1	0.80	1636.6	15.5	1661.0	11.0	1692.0	14.8	1692.0	14.8	96.7
1-Spot 171	121	41907	2.4	9.6322	0.7	4.4012	1.3	0.3076	1.1	0.83	1728.9	16.0	1712.6	10.6	1692.7	13.3	1692.7	13.3	102.1
1-Spot 283	412	391355	4.3	9.6292	0.7	4.4304	1.5	0.3095	1.4	0.89	1738.4	20.8	1718.0	12.7	1693.2	12.8	1693.2	12.8	102.7
1-Spot 122	196	99224	3.2	9.6277	0.9	4.4753	1.7	0.3126	1.4	0.84	1753.7	22.0	1726.4	14.2	1693.5	17.2	1693.5	17.2	103.6
1-Spot 108	227	131136	1.9	9.6242	0.7	4.3480	1.4	0.3036	1.2	0.88	1709.3	18.5	1702.5	11.5	1694.2	12.0	1694.2	12.0	100.9
11-Spot 72	180	75984	3.8	9.6088	0.7	4.2069	1.5	0.2933	1.3	0.88	1658.0	19.0	1675.4	12.1	1697.1	13.0	1697.1	13.0	97.7
1-Spot 284	274	62011	3.4	9.6071	0.8	4.0025	1.4	0.2790	1.1	0.82	1586.4	15.6	1634.7	11.0	1697.5	14.3	1697.5	14.3	93.5
1-Spot 157	142	140976	4.2	9.6061	0.5	4.3294	1.1	0.3018	1.0	0.89	1700.0	14.9	1699.0	9.3	1697.7	9.6	1697.7	9.6	100.1
1-Spot 104	284	45630	4.8	9.5995	0.8	4.4155	1.4	0.3076	1.1	0.82	1728.7	16.9	1715.3	11.3	1698.9	14.4	1698.9	14.4	101.7
1-Spot 125	225	73052	3.6	9.5779	0.8	4.3669	1.5	0.3035	1.2	0.84	1708.5	18.7	1706.1	12.2	1703.1	14.7	1703.1	14.7	100.3
1-Spot 291	101	104895	3.0	9.5692	0.8	4.5107	1.3	0.3132	1.1	0.82	1756.4	16.6	1732.9	10.9	1704.7	13.8	1704.7	13.8	103.0
1-Spot 177	248	126467	3.2	9.5682	0.7	4.3164	1.2	0.2997	1.0	0.83	1689.7	14.5	1696.5	9.7	1704.9	12.2	1704.9	12.2	99.1
11-Spot 65	307	335698	3.7	9.5627	0.8	4.3191	1.3	0.2997	1.0	0.79	1689.7	15.3	1697.0	10.8	1706.0	14.8	1706.0	14.8	99.0
11-Spot 25	110	52190	2.5	9.5538	0.8	4.3244	1.4	0.2998	1.2	0.83	1690.2	17.2	1698.0	11.4	1707.7	14.2	1707.7	14.2	99.0
11-Spot 47	372	151161	4.8	9.5500	0.8	4.3618	1.6	0.3022	1.4	0.87	1702.4	21.3	1705.1	13.5	1708.5	14.8	1708.5	14.8	99.6
1-Spot 182	377	339203	6.2	9.5416	0.8	4.4955	1.7	0.3112	1.5	0.89	1746.8	22.5	1730.1	13.8	1710.1	14.0	1710.1	14.0	102.1
11-Spot 14	854	594782	3.0	9.5414	0.8	4.1318	1.8	0.2860	1.6	0.89	1621.7	22.4	1660.6	14.4	1710.1	15.0	1710.1	15.0	94.8
1-Spot 173	88	37809	2.3	9.5395	0.7	4.3737	1.2	0.3027	0.9	0.77	1704.9	13.7	1707.4	9.7	1710.5	13.7	1710.5	13.7	99.7
11-Spot 24	182	176607	2.1	9.5239	0.8	4.2450	1.5	0.2933	1.2	0.84	1658.2	18.0	1682.8	12.0	1713.5	14.4	1713.5	14.4	96.8
1-Spot 280	166	53011	2.5	9.5172	0.8	4.3509	1.4	0.3005	1.2	0.84	1693.5	17.4	1703.1	11.5	1714.8	13.8	1714.8	13.8	98.8
1-Spot 259	158	57709	2.9	9.5156	0.7	4.5195	1.3	0.3120	1.1	0.85	1750.8	16.8	1734.6	10.7	1715.1	12.4	1715.1	12.4	102.1
1-Spot 185	251	66726	3.7	9.5143	0.7	4.2590	1.5	0.2940	1.3	0.88	1661.5	19.7	1685.5	12.6	1715.3	13.4	1715.3	13.4	96.9
1-Spot 286	111	84857	2.2	9.5120	0.6	4.3736	1.4	0.3019	1.3	0.89	1700.5	18.8	1707.4	11.7	1715.8	11.6	1715.8	11.6	99.1
1-Spot 174	122	58747	2.3	9.5113	0.8	4.3975	1.3	0.3035	1.0	0.78	1708.6	14.8	1711.9	10.5	1715.9	14.7	1715.9	14.7	99.6
11-Spot 75	121	55883	3.3	9.5099	0.7	4.5057	1.6	0.3109	1.4	0.88	1745.2	21.0	1732.0	13.0	1716.2	13.6	1716.2	13.6	101.7
1-Spot 160	196	62829	3.5	9.5085	0.7	4.4477	1.3	0.3069	1.1	0.85	1725.2	17.1	1721.3	11.1	1716.5	13.1	1716.5	13.1	100.5
1-Spot 113	270	222028	3.5	9.5012	0.8	4.4009	1.6	0.3034	1.3	0.85	1708.1	19.9	1712.5	12.9	1717.9	15.0	1717.9	15.0	99.4
1-Spot 253	196	315271	1.9	9.4994	0.9	4.4137	1.4	0.3042	1.1	0.78	1712.2	16.8	1714.9	11.9	1718.2	16.6	1718.2	16.6	99.6
1-Spot 273	113	53921	1.7	9.4984	0.9	4.4102	1.4	0.3039	1.0	0.75	1710.8	15.3	1714.3	11.3	1718.4	16.7	1718.4	16.7	99.6
1-Spot 230	306	353774	4.2	9.4859	0.9	4.4179	1.6	0.3041	1.3	0.83	1711.5	19.5	1715.7	13.0	1720.8	16.3	1720.8	16.3	99.5
11-Spot 97	209	56025	2.3	9.4719	0.7	4.5584	1.4	0.3133	1.2	0.84	1756.8	18.0	1741.7	11.5	1723.5	13.7	1723.5	13.7	101.9
11-Spot 41	146	192613	3.8	9.4704	0.8	4.3119	1.4	0.2963	1.2	0.83	1672.9	17.0	1695.6	11.4	1723.8	14.2	1723.8	14.2	97.0
1-Spot 285	155	44933	3.7	9.4571	0.8	4.3670	1.4	0.2997	1.2	0.84	1689.6	18.0	1706.1	12.0	1726.4	14.5	1726.4	14.5	97.9
1-Spot 139	236	130982	10.4	9.4325	0.8	4.5557	1.1	0.3118	0.8	0.74	1749.5	12.9	1741.2	9.5	1731.2	14.0	1731.2	14.0	101.1
11-Spot 74	157	404909	1.8	9.4192	0.9	4.5152	1.7	0.3086	1.4	0.83	1733.8	21.8	1733.8	14.3	1733.8	17.4	1733.8	17.4	100.0
11-Spot 11	582	207098	5.8	9.4190	0.7	4.6831	1.4	0.3201	1.2	0.86	1790.0	19.1	1764.2	11.9	1733.8	13.5	1733.8	13.5	103.2
1-Spot 158	299	78886	1.9	9.4144	0.7	4.2306	1.4	0.2890	1.2	0.85	1636.5	17.5	1680.0	11.7	1734.7	13.7	1734.7	13.7	94.3
1-Spot 121	201	291557	3.8	9.3926	0.7	4.6254	1.4	0.3152	1.2	0.85	1766.4	18.3	1753.9	11.7	1739.0	13.5	1739.0	13.5	101.6
11-Spot 93	466	106061	2.4	9.3741	0.8	4.5302	1.5	0.3081	1.3	0.85	1731.5	19.2	1736.5	12.5	1742.6	14.7	1742.6	14.7	99.4
11-Spot 55	116	115678	4.7	9.3701	0.8	4.3967	1.5	0.2989	1.3	0.85	1686.0	19.0	1711.7	12.4	1743.4	14.3	1743.4	14.3	96.7
1-Spot 152	411	165372	2.6	9.3642	0.7	4.5540	1.1	0.3094	0.9	0.78	1737.9	13.0	1740.9	9.1	1744.5	12.4	1744.5	12.4	99.6
11-Spot 77	310	142333	1.9	9.3615	0.8	4.4656	1.3	0.3033	1.1	0.81	1707.8	16.1	1724.6	11.1	1745.0	14.5	1745.0	14.5	97.9
1-Spot 166	275	289768	2.4	9.3588	0.7	4.6646	1.3	0.3168	1.1	0.86	1773.9	17.5	1760.9	11.1	1745.6	12.5	1745.6	12.5	101.6
1-Spot 103	367	133682	3.6	9.3168	0.7	4.6620	1.3	0.3152	1.2	0.86	1766.0	18.0	1760.4	11.3	1753.8	12.5	1753.8	12.5	100.7
11-Spot 37	347	108947	3.9	9.2938	0.8	4.7069	1.4	0.3174	1.2	0.83	1777.1	18.2	1768.5	11.8	1758.3	14.4	1758.3	14.4	101.1
1-Spot 295	266	108348	7.0	9.2919	0.6	4.7342	1.4	0.3192	1.2	0.90	1785.7	19.2	1773.3	11.5	1758.7	10.8	1758.7	10.8	101.5
11-Spot 46	252	294403	2.6	9.2649	0.8	4.6883	1.6	0.3152	1.3	0.85	1766.1	20.5	1765.2	13.1	1764.0	15.1	1764.0	15.1	100.1
1-Spot 127	182	64159	4.6	9.2546	1.1	4.6591	1.7	0.3129	1.3	0.79	1754.8	20.6	1759.9	14.3	1766.1	19.3	1766.1	19.3	99.4
1-Spot 130	243	241345	7.0	9.2443	0.8	4.7687	1.3	0.3199	1.0	0.79	1789.1	16.0	1779.4	10.9	1768.1	14.6	1768.1	14.6	101.2
1-Spot 312	276	209676	2.9	9.2392	0.8	4.6651	1.3	0.3127	1.1	0.81	1754.2	16.7	1761.0	11.2	1769.1	14.2	1769.1	14.2	99.2
1-Spot 143	311	431293	6.7	9.2361	0.6	4.6883	1.2	0.3142	1.0	0.87	1761.3	15.8	1765.2	9.9	1769.7	10.5	1769.7	10.5	99.5
11-Spot 85	168	75970	5.7	9.2359	0.9	4.8044	1.4	0.3220	1.0	0.74	1799.3	16.1	1785.7	11.6	1769.7	17.0	1769.7	17.0	101.7
11-Spot 64	52	1183366	10.2	9.2112	1.1	4.5722	1.8	0.3056	1.5	0.80	1718.9	22.2	1744.2	15.2	1774.6	19.9	1774.6	19.9	96.9
1-Spot 278	115	132900	4.2	9.2075	0.7	4.8152	1.5	0.3217	1.3	0.87	1798.0	20.3	1787.6	12.5	1775.4	13.6	1775.4	13.6	101.3
11-Spot 51	219	50471	3.5	9.2070	1.0	4.8195	1.4	0.3220	1.0	0.71	1799.3	15.7	1788.3	11.8	1775.5	18.0	1775.5	18.0	101.3
1-Spot 208	237	74718	4.7	9.2061	0.7	4.7012	1.1	0.3140	0.9	0.78	1760.5	13.5	1767.5	9.3	1775.7	12.6	1775.7	12.6	99.1
11-Spot 87	303	63854	5.7	9.2008	0.9	4.7744	1.5	0.3187	1.2	0.81	1783.6	19.0	1780.4	12.7	1776.7	16.4	1776.7	16.4	100.4
1-Spot 222	244	164620	1.4	9.1968	0.8	4.6714	1.6	0.3117	1.4	0.86	1749.2	20.7	1762.1	13.2	1777.5	14.7	1777.5	14.7	98.4
1-Spot 154	374	77032	2.8	9.1859	0.6	4.8076	1.2	0.3204	1.0	0.87	1791.8	16.4	1786.2	10.1	1779.7	10.7	1779.7	10.7	100.7
11-Spot 82	290	284337	3.2	9.1789	0.6	4.7724	1.3	0.3178	1.1	0.87	1779.2	17.4	1780.1	10.8	1781.0	11.4	1781.0	11.4	99.9
1-Spot 217	347	18518868	5.1	9.1645	0.6	4.7395	1.4	0.3152	1.3	0.89	1766.0	19.4	1774.3	11.9	1783.9	11.8	1783.9	11.8	99.0
1-Spot 199	384	3601373	4.6	9.1644	0.8	4.8147	1.4	0.3202	1.1	0.81	1790.5	17.7	1787.5	11.8	1783.9	15.1	1783.9	15.1	100.4
11-Spot 23	237	76879	2.9	9.1625	0.8	4.4999	1.4	0.2992	1.1	0.83	1687.1	16.8	1730.9	11.3	1784.3	13.9	1784.3	13.9	94.6
1-Spot 211	183	36644	2.7	9.1341	0.7	4.8235	1.4	0.3197	1.2	0.86	1788.2	18.9	1789.0	11.8	1790.0	13.0	1790.0	13.0	99.9
1-Spot 183	136	216085	5.2	9.1169	0.7	4.9804	1.0	0.3295	0.8	0.74	1835.8	12.3	1816.0	8.9	1793.4	12.9	1793.4	12.9	102.4
1-Spot 267	161	206383	2.9	9.1105	0.7	4.8912	1.3	0.3233	1.1	0.82	1806.0	16.6	1800.7	10.8	1794.7	13.2	1794.7	13.2	100.6
1-Spot 279	400	420252	4.5	9.0963	0.6	4.8791	1.0	0.3220	0.9	0.84	1799.6	13.6	1798.7	8.7	1797.5	10.1	1797.5	10.1	100.1
1-Spot 260	224	68365	4.8	9.0714	0.8	4.9204	1.3	0.3239	1.0	0.80	1808.6	16.1	1805.8	10.9	1802.5	14.2	1802.5	14.2	100.3
11-Spot 19	212	132307	3.9	9.0365	0.9	4.7785	1.6	0.3133	1.3	0.84	1757.0	20.3	1781.1	13.3	1809.5	15.7	1809.5	15.7	97.1
11-Spot 91	357	171665	2.5	8.9821	0.8	4.9197	1.3	0.3206	1.0	0.75	1792.8	14.9	1805.6	10.6	1820.5	15.1	1820.5	15.1	98.5
1-Spot 314	524	1547262	1.9	8.9486	0.6	5.1761	1.3	0.3361	1.1	0.86	1867.8	17.7	1848.7	10.8	1827.2	11.6	1827.2	11.6	102.2
1-Spot 150	89	23515	3.3	8.8739	0.8	5.3124	1.2	0.3421	0.9	0.74	1896.5	15.0	1870.9	10.5	1842.4	15.0	1842.4	15.0	102.9
1-Spot 132	359	89506	2.0	8.2398	0.7	5.9523	1.4	0.3559	1.2	0.85	1962.6	20.2	1968.9	12.3	1975.6	13.3	1975.6	13.3	99.3
1-Spot 165	231	398786	1.6	8.2349	0.7	6.0106	1.4	0.3591	1.1	0.84	1978.1	19.4	1977.4	11.8	1976.6	12.9	1976.6	12.9	100.1
1-Spot 102	134	50262	1.3	6.6530	0.7	9.0548	1.4	0.4371	1.2	0.87	2337.7	24.3	2343.6	13.0	2348.7	11.7	2348.7	11.7	99.5
11-Spot 12	180	34928	3.5	6.2250	0.7	10.3528	1.4	0.4676	1.2	0.86	2473.1	25.4	2466.8	13.3	2461.7	12.5	2461.7	12.5	100.5
11-Spot 69	289	73205	3.3	6.2205	0.8	10.2338	1.7	0.4619	1.5	0.87	2447.9	30.1	2456.1	15.6	2462.9	13.9	2462.9	13.9	99.4
1-Spot 148	259	113031	2.8	6.2040	0.7	10.2775	1.2	0.4626	1.0	0.82	2451.2	20.6	2460.1	11.4	2467.4	12.0	2467.4	12.0	99.3
11-Spot 13	258	317006	3.1	6.1817	0.9	10.3219	1.4	0.4630	1.1	0.78	2452.7	21.7	2464.1	12.6	2473.5	14.4	2473.5	14.4	99.2
11-Spot 43	301	90443	2.9	6.1743	0.9	10.5304	1.8	0.4718	1.6	0.86	2491.3	32.4	2482.6	17.0	2475.5	16.0	2475.5	16.0	100.6
1-Spot 109	197	184396	1.1	6.1004	0.9	9.7310	1.5	0.4307	1.2	0.82	2309.0	23.5	2409.6	13.6	2495.8	14.3	2495.8	14.3	92.5
11-Spot 31	72	443582	1.5	6.0692	1.0	10.9163	1.6	0.4807	1.2	0.78	2530.4	26.1	2516.0	14.8	2504.4	16.6	2504.4	16.6	101.0
11-Spot 70	108	95720	3.7	6.0692	0.9	11.1707	1.6	0.4919	1.3	0.82	2579.0	27.5	2537.5	14.7	2504.4	15.1	2504.4	15.1	103.0

1-Spot 145	314	405601	2.0	6.0103	0.9	11.1608	1.4	0.4867	1.0	0.77	2556.5	22.1	2536.6	12.7	2520.8	14.5	2520.8	14.5	101.4
1-Spot 223	247	3652041	2.2	5.9699	0.9	11.2324	1.7	0.4865	1.5	0.86	2555.7	31.2	2542.6	16.1	2532.1	14.9	2532.1	14.9	100.9
1-Spot 289	237	501239	1.4	5.9410	0.8	11.1696	1.4	0.4815	1.2	0.81	2533.7	24.7	2537.4	13.5	2540.3	14.1	2540.3	14.1	99.7
1-Spot 107	139	67611	1.9	5.8434	0.9	11.4398	1.5	0.4850	1.2	0.78	2549.1	24.8	2559.7	14.1	2568.0	15.7	2568.0	15.7	99.3
1-Spot 203	36	29272	0.4	5.7611	1.0	11.8439	1.8	0.4951	1.4	0.81	2592.7	30.8	2592.1	16.6	2591.7	17.3	2591.7	17.3	100.0
11-Spot 29	290	2606166	2.3	5.7283	0.7	11.9619	1.8	0.4972	1.6	0.92	2601.7	34.4	2601.4	16.5	2601.2	11.8	2601.2	11.8	100.0
11-Spot 49	234	814076	1.6	5.7221	0.9	11.7244	1.6	0.4868	1.4	0.84	2556.8	28.8	2582.7	15.1	2603.0	14.4	2603.0	14.4	98.2
1-Spot 246	65	54958	1.5	5.6348	0.8	12.4000	1.6	0.5070	1.3	0.86	2643.7	29.0	2635.2	14.7	2628.6	13.4	2628.6	13.4	100.6
1-Spot 140	175	97594	1.4	5.5911	0.7	12.1423	1.5	0.4926	1.3	0.87	2581.9	27.9	2615.5	14.1	2641.6	12.2	2641.6	12.2	97.7
1-Spot 288	202	68568	1.4	5.4745	0.8	12.7601	1.6	0.5069	1.4	0.88	2643.2	31.4	2662.1	15.4	2676.5	12.7	2676.5	12.7	98.8
11-Spot 73	168	154113	1.7	5.4539	0.8	13.0477	1.5	0.5163	1.3	0.86	2683.6	29.3	2683.1	14.6	2682.7	12.9	2682.7	12.9	100.0
1-Spot 170	81	61051	0.9	5.4337	0.7	13.2912	1.3	0.5240	1.1	0.85	2716.2	24.2	2700.6	12.2	2688.9	11.4	2688.9	11.4	101.0
11-Spot 81	46	63581	0.9	5.3785	0.9	13.7450	1.4	0.5364	1.0	0.74	2768.4	22.7	2732.3	12.9	2705.7	15.3	2705.7	15.3	102.3
1-Spot 236	155	3194443	0.9	5.3744	0.7	13.6747	1.3	0.5333	1.1	0.83	2755.2	25.1	2727.4	12.8	2707.0	12.3	2707.0	12.3	101.8
1-Spot 266	259	84590	5.2	5.3103	0.8	14.0284	1.3	0.5405	1.0	0.78	2785.6	23.1	2751.6	12.3	2726.8	13.3	2726.8	13.3	102.2
1-Spot 281	53	98040	2.2	5.3091	0.8	13.8183	1.4	0.5323	1.1	0.82	2751.1	25.1	2737.3	12.9	2727.1	12.9	2727.1	12.9	100.9
1-Spot 262	167	128697	1.3	5.2091	0.6	14.2246	1.2	0.5376	1.1	0.87	2773.6	24.3	2764.8	11.7	2758.4	9.9	2758.4	9.9	100.6
11-Spot 48	130	201593	2.8	5.1159	1.0	14.8587	1.5	0.5516	1.1	0.75	2831.6	26.2	2806.2	14.4	2788.0	16.2	2788.0	16.2	101.6
1-Spot 301	189	986002	2.2	4.9571	0.5	15.2701	1.3	0.5492	1.2	0.91	2822.0	26.9	2832.2	12.4	2839.5	8.9	2839.5	8.9	99.4
1-Spot 204	79	75901	2.9	4.6906	0.7	17.8145	1.4	0.6063	1.2	0.87	3055.2	29.1	2979.8	13.2	2929.3	11.0	2929.3	11.0	104.3
1-Spot 315	214	123366	7.2	3.8723	0.8	22.4310	1.3	0.6302	1.0	0.76	3150.5	24.5	3202.6	12.6	3235.3	13.3	3235.3	13.3	97.4

Table DTB17-14. U-Pb geochronologic analyses.																			
						Isotope ratios						Apparent ages (Ma)							
Analysis	U	206Pb	U/Th	206Pb*	±	207Pb*	±	206Pb*	±	error	206Pb*	±	207Pb*	±	206Pb*	±	Best age	±	Conc
	(ppm)	204Pb		207Pb*	(%)	235U*	(%)	238U	(%)	corr.	238U*	(Ma)	235U	(Ma)	207Pb*	(Ma)	(Ma)	(Ma)	(%)
4-Spot 279	255	9289	1.7	17.0486	1.3	0.6911	1.7	0.0855	1.1	0.66	528.8	5.6	533.5	6.9	553.4	27.4	528.8	5.6	95.6
4-Spot 155	476	34710	2.0	13.3013	0.7	1.8928	1.2	0.1827	1.0	0.82	1081.6	9.5	1078.6	7.8	1072.5	13.5	1072.5	13.5	100.8
14-Spot 53	326	110487	1.4	13.1903	0.9	1.9143	1.5	0.1832	1.3	0.83	1084.5	12.5	1086.1	10.1	1089.3	17.0	1089.3	17.0	99.6
14-Spot 78	198	29621	2.1	13.1176	0.9	1.9402	1.6	0.1847	1.4	0.85	1092.4	14.0	1095.1	10.9	1100.4	17.0	1100.4	17.0	99.3
4-Spot 164	73	7842	1.4	13.0668	1.1	1.9847	1.5	0.1882	1.1	0.72	1111.5	11.3	1110.3	10.5	1108.1	21.6	1108.1	21.6	100.3
14-Spot 96	269	67725	1.3	12.9575	1.0	2.0018	1.5	0.1882	1.1	0.74	1111.6	11.1	1116.1	9.9	1124.8	19.6	1124.8	19.6	98.8
4-Spot 222	179	11920	2.9	12.9418	1.0	2.0142	1.4	0.1891	0.9	0.67	1116.7	9.6	1120.3	9.6	1127.3	20.9	1127.3	20.9	99.1
4-Spot 127	271	20092	3.5	12.8846	0.8	2.0454	1.4	0.1912	1.1	0.81	1128.0	11.6	1130.8	9.4	1136.1	15.9	1136.1	15.9	99.3
14-Spot 21	107	6732	4.1	12.8587	1.2	2.0886	1.7	0.1949	1.2	0.69	1147.7	12.4	1145.1	11.8	1140.1	24.8	1140.1	24.8	100.7
4-Spot 268	52	9303	3.6	12.5573	1.1	2.0908	1.6	0.1905	1.2	0.73	1124.1	12.4	1145.8	11.3	1187.1	22.1	1187.1	22.1	94.7
4-Spot 105	63	7627	1.0	12.5380	1.2	2.1383	1.6	0.1945	1.1	0.69	1145.8	11.6	1161.3	11.1	1190.1	23.0	1190.1	23.0	96.3
14-Spot 84	147	265110	1.4	12.3879	1.1	2.0691	1.5	0.1860	1.0	0.66	1099.6	10.0	1138.6	10.2	1213.8	21.9	1213.8	21.9	90.6
4-Spot 186	138	79800	1.5	11.9130	1.0	2.4708	1.5	0.2136	1.1	0.76	1247.8	12.6	1263.5	10.5	1290.3	18.5	1290.3	18.5	96.7
4-Spot 295	189	22274	1.1	11.6129	0.8	2.4025	1.7	0.2024	1.5	0.88	1188.4	16.6	1243.3	12.5	1339.8	16.0	1339.8	16.0	88.7
4-Spot 223	336	52079	1.8	11.4964	0.7	2.7795	1.4	0.2319	1.2	0.87	1344.2	14.9	1350.0	10.5	1359.3	13.1	1359.3	13.1	98.9
-14-Spot 3	366	102222	1.5	11.4730	0.7	2.9248	1.2	0.2435	1.0	0.82	1404.8	12.3	1388.4	9.0	1363.2	13.3	1363.2	13.3	103.0
4-Spot 309	181	31166	1.3	11.3871	1.0	2.8539	1.4	0.2358	1.0	0.72	1364.8	12.6	1369.8	10.7	1377.7	19.0	1377.7	19.0	99.1
14-Spot 36	219	152806	3.0	11.3521	0.7	2.8294	1.4	0.2331	1.1	0.84	1350.5	13.9	1363.4	10.1	1383.6	14.0	1383.6	14.0	97.6
14-Spot 90	233	20864	0.9	11.3228	0.8	2.8052	1.7	0.2305	1.5	0.90	1336.9	18.2	1356.9	12.6	1388.6	14.4	1388.6	14.4	96.3
4-Spot 130	217	11989	1.7	11.2406	0.9	3.0487	1.6	0.2487	1.3	0.82	1431.5	16.6	1419.9	12.0	1402.5	17.0	1402.5	17.0	102.1
4-Spot 146	449	33717	3.6	11.1675	0.8	3.0429	1.2	0.2466	0.9	0.76	1420.7	11.9	1418.5	9.4	1415.0	15.2	1415.0	15.2	100.4
4-Spot 298	239	55747	2.0	11.1386	0.7	2.8247	1.2	0.2283	1.0	0.82	1325.5	11.6	1362.1	8.9	1420.0	13.2	1420.0	13.2	93.3
14-Spot 70	220	30620	1.1	11.1171	0.8	3.0728	1.4	0.2479	1.2	0.84	1427.5	15.6	1425.9	11.0	1423.6	14.8	1423.6	14.8	100.3
4-Spot 150	47	4847	3.7	11.0916	1.3	3.1170	1.7	0.2509	1.2	0.68	1442.9	15.0	1436.9	13.2	1428.0	24.2	1428.0	24.2	101.0
4-Spot 178	245	16404	1.6	11.0669	0.6	3.1361	1.0	0.2518	0.8	0.81	1447.9	10.3	1441.6	7.5	1432.3	10.9	1432.3	10.9	101.1
4-Spot 107	203	29500	1.3	11.0665	0.9	3.0777	1.6	0.2471	1.3	0.82	1423.6	16.4	1427.1	12.0	1432.4	17.0	1432.4	17.0	99.4
4-Spot 313	65	15450	2.3	11.0402	1.2	3.0266	1.8	0.2424	1.3	0.72	1399.4	16.2	1414.4	13.6	1436.9	23.5	1436.9	23.5	97.4
14-Spot 37	102	27133	1.8	11.0226	1.1	3.1021	1.8	0.2481	1.4	0.77	1428.7	17.6	1433.2	13.6	1439.9	21.4	1439.9	21.4	99.2
14-Spot 83	424	42911	1.7	11.0043	0.7	3.1543	1.5	0.2519	1.3	0.86	1448.0	16.3	1446.0	11.3	1443.1	14.2	1443.1	14.2	100.3
4-Spot 270	154	37004	1.4	10.9742	0.6	3.1435	1.3	0.2503	1.2	0.88	1440.1	14.9	1443.4	10.1	1448.3	11.7	1448.3	11.7	99.4
4-Spot 304	79	13850	3.1	10.9596	0.9	3.0536	1.4	0.2428	1.0	0.76	1401.4	13.1	1421.1	10.4	1450.9	16.8	1450.9	16.8	96.6
4-Spot 293	147	30565	1.6	10.8522	0.9	3.1444	1.4	0.2476	1.2	0.80	1426.1	14.8	1443.6	11.1	1469.6	16.3	1469.6	16.3	97.0
14-Spot 19	69	35350	3.8	10.7658	1.0	3.1880	1.7	0.2490	1.5	0.83	1433.5	18.7	1454.3	13.5	1484.7	18.4	1484.7	18.4	96.5
14-Spot 97	68	178208	5.3	10.7598	1.2	3.1831	1.7	0.2485	1.3	0.74	1430.8	16.2	1453.1	13.3	1485.8	22.0	1485.8	22.0	96.3
4-Spot 184	252	27854	1.3	10.1081	0.9	3.8575	1.2	0.2829	0.8	0.67	1606.1	11.1	1604.8	9.4	1603.2	16.1	1603.2	16.1	100.2
4-Spot 158	111	28712	1.5	9.8864	1.0	4.1114	1.4	0.2949	1.0	0.72	1666.1	14.9	1656.6	11.5	1644.5	18.1	1644.5	18.1	101.3
4-Spot 300	104	11716	3.8	9.8012	0.8	4.1677	1.3	0.2964	1.0	0.75	1673.4	14.2	1667.7	10.5	1660.5	15.6	1660.5	15.6	100.8
14-Spot 34	171	61074	1.3	9.7490	0.7	4.2181	1.4	0.2984	1.2	0.86	1683.3	17.2	1677.5	11.1	1670.4	13.0	1670.4	13.0	100.8
4-Spot 165	129	8272	2.5	9.7484	0.9	4.2528	1.4	0.3008	1.1	0.78	1695.3	16.2	1684.3	11.4	1670.5	16.0	1670.5	16.0	101.5
14-Spot 99	289	365253	2.6	9.6994	0.7	4.1533	1.6	0.2923	1.4	0.90	1653.0	20.5	1664.9	12.7	1679.8	12.2	1679.8	12.2	98.4
4-Spot 180	381	80001	2.7	9.6756	0.8	4.3788	1.2	0.3074	0.9	0.77	1728.0	14.2	1708.4	10.0	1684.4	14.3	1684.4	14.3	102.6
4-Spot 314	1608	38849	14.2	9.6702	0.8	4.0785	1.7	0.2862	1.5	0.90	1622.3	21.8	1650.0	13.9	1685.4	14.0	1685.4	14.0	96.3
4-Spot 162	125	24324	1.1	9.6449	0.9	4.2345	1.3	0.2963	0.9	0.71	1673.1	13.9	1680.7	10.9	1690.2	17.2	1690.2	17.2	99.0
4-Spot 160	600	1818766	4.1	9.6189	0.7	4.4369	1.1	0.3097	0.8	0.76	1739.0	12.3	1719.2	8.8	1695.2	12.6	1695.2	12.6	102.6
14-Spot 43	303	32171	2.5	9.6050	0.9	4.4494	1.4	0.3101	1.1	0.79	1741.1	17.3	1721.6	11.9	1697.9	16.2	1697.9	16.2	102.5
4-Spot 134	103	5721	1.4	9.5870	0.8	4.5797	1.5	0.3186	1.3	0.83	1782.7	19.5	1745.6	12.5	1701.3	15.3	1701.3	15.3	104.8
14-Spot 40	416	226577	5.6	9.5703	0.7	4.4285	1.4	0.3075	1.2	0.87	1728.5	18.0	1717.7	11.4	1704.5	12.6	1704.5	12.6	101.4
4-Spot 163	63	10470	2.6	9.5695	1.0	4.1426	1.4	0.2876	1.0	0.73	1629.7	14.6	1662.7	11.4	1704.7	17.7	1704.7	17.7	95.6
4-Spot 116	1774	16671	2.0	9.5259	0.6	3.6660	2.5	0.2534	2.4	0.97	1455.9	31.6	1564.0	20.0	1713.1	11.7	1713.1	11.7	85.0
4-Spot 106	134	55125	0.7	9.5186	0.8	4.2705	1.4	0.2949	1.1	0.81	1666.2	16.2	1687.7	11.3	1714.5	14.8	1714.5	14.8	97.2
4-Spot 136	218	108525	4.0	9.4954	1.1	4.2845	1.9	0.2952	1.5	0.80	1667.4	21.9	1690.4	15.3	1719.0	20.6	1719.0	20.6	97.0
4-Spot 119	702	99645	2.6	9.4895	0.9	4.5087	1.6	0.3104	1.3	0.83	1742.9	20.5	1732.6	13.5	1720.1	16.8	1720.1	16.8	101.3
4-Spot 272	723	27843	1.2	9.4874	0.7	3.6566	2.3	0.2517	2.2	0.96	1447.3	28.6	1562.0	18.4	1720.5	12.0	1720.5	12.0	84.1
4-Spot 202	1295	33451	1.3	9.4784	0.7	4.4734	1.5	0.3077	1.3	0.89	1729.1	19.9	1726.0	12.3	1722.3	12.4	1722.3	12.4	100.4
14-Spot 71	710	107245	5.8	9.4554	0.6	4.3805	1.6	0.3005	1.5	0.94	1694.0	22.2	1708.7	13.2	1726.8	10.3	1726.8	10.3	98.1
14-Spot 63	121	328090	1.8	9.4427	1.1	4.5822	1.8	0.3140	1.4	0.78	1760.1	21.4	1746.0	14.8	1729.2	20.2	1729.2	20.2	101.8
4-Spot 276	65	19049	2.0	9.4365	1.0	4.4314	1.5	0.3034	1.1	0.73	1708.2	16.1	1718.2	12.2	1730.4	18.5	1730.4	18.5	98.7
4-Spot 141	394	45377	3.3	9.4077	0.7	4.6133	1.5	0.3149	1.3	0.88	1764.8	20.1	1751.7	12.3	1736.0	12.6	1736.0	12.6	101.7
4-Spot 198	1198	298496	10.5	9.4063	0.6	4.7095	1.0	0.3214	0.8	0.80	1796.7	12.9	1768.9	8.7	1736.3	11.4	1736.3	11.4	103.5
4-Spot 101	321	6708	2.4	9.4047	1.5	4.2445	1.9	0.2896	1.2	0.61	1639.7	17.0	1682.7	15.8	1736.6	28.0	1736.6	28.0	94.4
4-Spot 231	1107	113159	2.4	9.3987	0.8	4.6276	1.2	0.3156	0.9	0.74	1768.1	14.1	1754.3	10.2	1737.8	15.1	1737.8	15.1	101.7
4-Spot 228	127	7729	0.8	9.3868	0.9	4.6186	1.3	0.3146	1.0	0.76	1763.2	15.3	1752.6	10.9	1740.1	15.6	1740.1	15.6	101.3
4-Spot 156	618	189136	1.4	9.3862	0.6	4.6955	1.2	0.3198	1.0	0.85	1788.7	16.2	1766.4	10.2	1740.2	11.7	1740.2	11.7	102.8
4-Spot 100	837	78376	3.1	9.3812	0.6	4.4276	1.4	0.3014	1.2	0.90	1698.1	18.6	1717.5	11.5	1741.2	11.3	1741.2	11.3	97.5
4-Spot 201	547	86408	2.7	9.3714	0.7	4.7515	1.3	0.3231	1.1	0.83	1804.8	17.1	1776.4	11.0	1743.1	13.3	1743.1	13.3	103.5
4-Spot 278	885	3328131	5.8	9.3670	0.7	4.6876	1.2	0.3186	1.0	0.82	1782.9	15.6	1765.0	10.2	1744.0	12.9	1744.0	12.9	102.2

4-Spot 285	799	320530	8.1	9.3640	0.6	4.6830	1.1	0.3182	1.0	0.86	1780.8	14.9	1764.2	9.4	1744.5	10.5	1744.5	10.5	102.1
14-Spot 18	565	117254	3.2	9.3628	0.7	4.6882	1.3	0.3185	1.1	0.85	1782.4	17.7	1765.1	11.2	1744.8	12.9	1744.8	12.9	102.2
14-Spot 93	664	38758	1.1	9.3584	0.7	4.6960	1.4	0.3189	1.3	0.89	1784.2	19.7	1766.5	11.9	1745.7	11.9	1745.7	11.9	102.2
4-Spot 122	583	136741	2.4	9.3559	0.7	4.7046	1.4	0.3194	1.2	0.84	1786.7	18.1	1768.1	11.5	1746.1	13.6	1746.1	13.6	102.3
4-Spot 289	180	780114	1.4	9.3544	1.0	3.6935	4.1	0.2507	3.9	0.97	1442.1	50.8	1570.0	32.5	1746.4	19.1	1746.4	19.1	82.6
4-Spot 291	515	38115	3.3	9.3527	0.7	4.6324	1.1	0.3144	0.8	0.77	1762.1	13.0	1755.1	9.1	1746.8	12.8	1746.8	12.8	100.9
4-Spot 188	1195	65396	2.8	9.3512	0.8	4.4992	1.4	0.3053	1.1	0.80	1717.4	17.0	1730.8	11.7	1747.1	15.3	1747.1	15.3	98.3
-14-Spot 9	559	63040	2.2	9.3487	0.8	4.5933	1.6	0.3116	1.4	0.86	1748.4	21.1	1748.0	13.4	1747.6	14.9	1747.6	14.9	100.1
4-Spot 288	606	332744	4.0	9.3437	0.8	4.6619	1.3	0.3161	1.1	0.82	1770.5	16.6	1760.4	11.0	1748.5	13.9	1748.5	13.9	101.3
4-Spot 182	572	91162	2.8	9.3426	0.7	4.7611	1.3	0.3227	1.1	0.84	1803.1	17.0	1778.1	10.8	1748.8	12.8	1748.8	12.8	103.1
14-Spot 28	2167	172290	9.0	9.3388	1.0	4.7768	1.6	0.3237	1.2	0.77	1807.7	19.0	1780.8	13.2	1749.5	18.5	1749.5	18.5	103.3
4-Spot 121	305	60713	1.2	9.3261	0.8	4.4153	1.4	0.2988	1.2	0.83	1685.2	17.2	1715.2	11.6	1752.0	14.4	1752.0	14.4	96.2
4-Spot 151	995	504363	1.8	9.3214	0.6	4.6936	1.2	0.3174	1.1	0.85	1777.2	16.4	1766.1	10.4	1752.9	11.8	1752.9	11.8	101.4
4-Spot 211	1129	336906	8.6	9.3205	0.7	4.7045	1.3	0.3182	1.1	0.84	1780.7	16.7	1768.0	10.8	1753.1	12.9	1753.1	12.9	101.6
4-Spot 264	754	601380	2.9	9.3072	0.7	4.7011	1.2	0.3175	1.0	0.82	1777.4	15.4	1767.4	10.2	1755.7	12.8	1755.7	12.8	101.2
14-Spot 92	435	75848	1.7	9.3036	0.7	4.7267	1.3	0.3191	1.1	0.84	1785.2	17.4	1772.0	11.1	1756.4	13.0	1756.4	13.0	101.6
14-Spot 20	575	98193	1.5	9.3009	0.7	4.6659	1.2	0.3149	0.9	0.81	1764.7	14.4	1761.1	9.6	1756.9	12.4	1756.9	12.4	100.4
14-Spot 64	367	82069	2.5	9.2991	0.8	4.7131	1.6	0.3180	1.4	0.85	1780.0	21.3	1769.6	13.5	1757.3	15.3	1757.3	15.3	101.3
4-Spot 299	304	119028	1.2	9.2969	0.6	4.6066	1.2	0.3107	1.1	0.88	1744.4	16.1	1750.5	10.0	1757.7	10.2	1757.7	10.2	99.2
14-Spot 94	366	56530	3.1	9.2865	0.7	4.7468	1.5	0.3198	1.3	0.87	1789.0	20.2	1775.5	12.5	1759.8	13.4	1759.8	13.4	101.7
14-Spot 26	452	1998484	1.8	9.2803	0.7	4.8630	1.4	0.3275	1.2	0.85	1826.0	18.4	1795.9	11.5	1761.0	13.0	1761.0	13.0	103.7
4-Spot 245	476	31982	2.9	9.2790	0.8	4.5427	1.3	0.3058	1.0	0.79	1720.2	15.2	1738.8	10.7	1761.2	14.5	1761.2	14.5	97.7
14-Spot 62	472	49228	3.0	9.2782	0.7	4.6532	1.6	0.3133	1.4	0.89	1756.7	21.1	1758.9	13.0	1761.4	13.2	1761.4	13.2	99.7
14-Spot 32	565	48082	1.6	9.2779	0.6	4.7566	1.3	0.3202	1.1	0.86	1790.8	16.8	1777.3	10.5	1761.5	11.9	1761.5	11.9	101.7
4-Spot 195	271	31054	1.4	9.2772	0.8	4.6640	1.8	0.3140	1.6	0.89	1760.1	24.4	1760.8	14.9	1761.6	14.7	1761.6	14.7	99.9
14-Spot 27	461	3357	1.5	9.2753	1.7	4.2597	2.1	0.2867	1.2	0.58	1624.9	17.3	1685.6	17.1	1762.0	30.9	1762.0	30.9	92.2
4-Spot 235	858	944566	3.1	9.2727	0.9	4.7950	1.3	0.3226	1.0	0.77	1802.5	16.2	1784.0	11.3	1762.5	15.7	1762.5	15.7	102.3
14-Spot 11	358	138514	1.6	9.2710	0.8	4.4886	1.6	0.3019	1.4	0.88	1700.9	20.7	1728.9	13.1	1762.8	13.8	1762.8	13.8	96.5
-14-Spot 2	790	94793	2.8	9.2703	0.8	4.7090	1.3	0.3167	1.0	0.79	1773.8	15.5	1768.8	10.6	1763.0	14.1	1763.0	14.1	100.6
14-Spot 85	450	58175	1.2	9.2702	0.7	4.7171	1.5	0.3173	1.3	0.90	1776.5	20.7	1770.3	12.4	1763.0	11.9	1763.0	11.9	100.8
4-Spot 204	480	327591	3.2	9.2689	0.7	4.6510	1.3	0.3128	1.1	0.86	1754.5	16.8	1758.5	10.7	1763.2	12.0	1763.2	12.0	99.5
14-Spot 58	532	39252	2.8	9.2664	0.7	4.7105	1.5	0.3167	1.3	0.87	1773.7	19.7	1769.1	12.3	1763.7	13.3	1763.7	13.3	100.6
4-Spot 120	390	67770	2.4	9.2610	0.8	4.6295	1.5	0.3111	1.3	0.86	1746.0	19.7	1754.6	12.5	1764.8	14.1	1764.8	14.1	98.9
14-Spot 76	413	275869	1.5	9.2466	0.8	4.6921	1.6	0.3148	1.4	0.87	1764.3	21.1	1765.8	13.2	1767.6	14.3	1767.6	14.3	99.8
4-Spot 196	403	60407	2.6	9.2465	0.7	4.8205	1.2	0.3234	1.0	0.84	1806.4	16.3	1788.5	10.4	1767.7	12.3	1767.7	12.3	102.2
4-Spot 217	122	137661	2.0	9.2444	0.8	4.7501	1.4	0.3186	1.2	0.82	1783.0	18.2	1776.1	12.0	1768.1	15.0	1768.1	15.0	100.8
4-Spot 225	307	64782	2.5	9.2434	0.7	4.8668	1.3	0.3264	1.1	0.84	1821.0	17.9	1796.5	11.3	1768.3	13.4	1768.3	13.4	103.0
4-Spot 283	208	30613	1.5	9.2419	0.7	4.6229	1.5	0.3100	1.3	0.88	1740.7	19.6	1753.4	12.2	1768.6	12.7	1768.6	12.7	98.4
4-Spot 172	465	38776	1.1	9.2403	0.6	4.7168	1.3	0.3162	1.2	0.88	1771.4	18.0	1770.2	11.1	1768.9	11.6	1768.9	11.6	100.1
4-Spot 206	164	21740	0.8	9.2398	0.9	4.7762	1.3	0.3202	1.0	0.75	1790.8	15.8	1780.7	11.3	1769.0	16.2	1769.0	16.2	101.2
4-Spot 215	350	51633	1.8	9.2317	0.6	4.7053	1.3	0.3152	1.2	0.90	1766.1	18.7	1768.2	11.2	1770.6	10.6	1770.6	10.6	99.7
14-Spot 91	294	51635	1.4	9.2294	0.8	4.8013	1.5	0.3215	1.2	0.83	1797.2	19.1	1785.1	12.4	1771.0	15.1	1771.0	15.1	101.5
4-Spot 244	441	80953	1.5	9.2264	0.8	4.7104	1.2	0.3153	1.0	0.78	1766.9	14.8	1769.1	10.3	1771.6	14.2	1771.6	14.2	99.7
4-Spot 192	2240	8352	1.3	9.2258	1.3	3.7831	2.2	0.2532	1.8	0.82	1455.2	23.9	1589.2	18.0	1771.7	23.5	1771.7	23.5	82.1
4-Spot 227	478	171605	2.3	9.2245	0.7	4.7451	1.5	0.3176	1.3	0.89	1778.0	20.8	1775.2	12.6	1772.0	12.6	1772.0	12.6	100.3
4-Spot 191	302	32675	1.3	9.2243	0.6	4.8590	1.1	0.3252	0.9	0.81	1815.1	13.5	1795.2	8.9	1772.1	11.3	1772.1	11.3	102.4
14-Spot 67	165	95842	0.8	9.2232	0.8	4.6634	1.3	0.3121	1.1	0.82	1750.9	16.6	1760.7	11.1	1772.3	14.0	1772.3	14.0	98.8
4-Spot 137	778	62854	2.8	9.2217	0.8	4.8712	1.5	0.3259	1.3	0.86	1818.7	21.0	1797.3	12.9	1772.6	14.1	1772.6	14.1	102.6
4-Spot 301	288	541113	1.3	9.2206	0.7	4.6644	1.3	0.3121	1.1	0.87	1750.8	17.4	1760.9	10.9	1772.8	11.9	1772.8	11.9	98.8
4-Spot 255	317	155703	0.8	9.2202	0.6	4.7218	1.4	0.3159	1.2	0.89	1769.6	18.8	1771.1	11.4	1772.9	11.0	1772.9	11.0	99.8
-14-Spot 7	193	30505	0.8	9.2200	0.8	4.7074	1.4	0.3149	1.2	0.83	1764.9	18.1	1768.5	11.7	1772.9	14.1	1772.9	14.1	99.5
4-Spot 126	717	158786	2.3	9.2187	0.8	4.5213	1.3	0.3024	1.1	0.81	1703.4	16.2	1734.9	11.1	1773.2	14.1	1773.2	14.1	96.1
4-Spot 111	251	34421	1.3	9.2186	0.7	4.7059	1.2	0.3148	1.0	0.84	1764.1	16.0	1768.3	10.3	1773.2	12.0	1773.2	12.0	99.5
4-Spot 226	301	21455	3.6	9.2172	0.8	4.7548	1.3	0.3180	1.0	0.77	1779.9	15.0	1777.0	10.5	1773.4	14.6	1773.4	14.6	100.4
4-Spot 233	460	30042	1.5	9.2166	0.6	4.8358	1.2	0.3234	1.0	0.88	1806.3	16.0	1791.1	9.8	1773.6	10.2	1773.6	10.2	101.8
4-Spot 185	224	31684	2.0	9.2139	0.7	4.6537	1.2	0.3111	1.0	0.83	1746.2	15.8	1758.9	10.4	1774.1	12.8	1774.1	12.8	98.4
14-Spot 59	273	175143	3.3	9.2129	0.7	4.7659	1.5	0.3186	1.3	0.87	1782.8	20.0	1778.9	12.3	1774.3	13.2	1774.3	13.2	100.5
4-Spot 140	542	80993	1.9	9.2054	0.8	4.6944	1.7	0.3135	1.6	0.90	1758.2	24.2	1766.2	14.6	1775.8	14.0	1775.8	14.0	99.0
4-Spot 238	447	1152668	5.4	9.1972	0.8	4.6474	1.2	0.3101	0.9	0.75	1741.4	14.2	1757.8	10.4	1777.4	15.2	1777.4	15.2	98.0
4-Spot 262	340	37877	2.8	9.1878	0.8	4.7091	1.3	0.3139	1.0	0.79	1760.0	15.4	1768.9	10.6	1779.3	14.1	1779.3	14.1	98.9
14-Spot 75	135	18022	1.2	9.1756	0.8	4.9975	1.4	0.3327	1.2	0.83	1851.5	18.6	1818.9	11.8	1781.7	14.1	1781.7	14.1	103.9
4-Spot 260	301	502777	2.8	9.1597	0.8	4.7135	1.5	0.3133	1.2	0.82	1756.8	18.3	1769.6	12.2	1784.9	15.2	1784.9	15.2	98.4
4-Spot 250	447	90474	1.8	9.1578	0.6	4.6707	1.0	0.3104	0.8	0.79	1742.4	12.6	1762.0	8.7	1785.2	11.5	1785.2	11.5	97.6
4-Spot 282	318	437586	1.2	9.1574	0.7	4.7544	1.2	0.3159	1.0	0.83	1769.7	15.7	1776.9	10.3	1785.3	12.4	1785.3	12.4	99.1
14-Spot 60	1374	123560	1.3	9.1399	0.7	4.9594	1.2	0.3289	1.0	0.80	1833.0	15.3	1812.4	10.2	1788.8	13.2	1788.8	13.2	102.5
4-Spot 177	466	41128	2.3	9.1389	0.5	4.8038	1.2	0.3185	1.1	0.90	1782.6	17.2	1785.6	10.3	1789.0	9.6	1789.0	9.6	99.6
4-Spot 294	163	37116	1.2	9.1365	0.6	4.6926	1.1	0.3111	0.9	0.82	1746.1	13.6	1765.9	9.1	1789.5	11.5	1789.5	11.5	97.6
4-Spot 297	176	115239	2.0	9.1253	0.8	4.6435	1.2	0.3075	0.9	0.76	1728.2	13.5	1757.1	9.8	1791.7	13.8	1791.7	13.8	96.5
14-Spot 82	160	160911	1.3	9.1249	0.8	4.9035	1.5	0.3247	1.3	0.84	1812.4	20.0	1802.9	12.7	1791.8	15.0	1791.8	15.0	101.2
4-Spot 239	287	186636	2.2	9.1234	0.9	4.7383	1.5	0.3137	1.2	0.81	1758.7	19.2	1774.0	12.8	1792.1	16.3	1792.1	16.3	98.1
4-Spot 237	207	43862	3.0	9.1185	0.7	4.4628	1.3	0.2953	1.1	0.83	1667.8	15.8	1724.1	10.7	1793.1	12.9	1793.1	12.9	93.0
4-Spot 216	389	142663	4.3	9.1177	0.6	4.7581	1.3	0.3148	1.2	0.90	1764.2	18.4	1777.5	11.2	1793.2	10.8	1793.2	10.8	98.4
4-Spot 210	657	300562	2.0	9.1043	0.7	4.8391	1.3	0.3197	1.1	0.82	1788.1	16.9	1791.7	11.1	1795.9	13.5	1795.9	13.5	99.6
4-Spot 271	195	25921	1.4	9.0897	0.8	4.6825	1.2	0.3088	0.9	0.74	1734.9	13.8	1764.1	10.2	1798.8	14.9	1798.8	14.9	96.4
4-Spot 234	46	3484	1.1	9.0799	0.8	4.9009	1.4	0.3229	1.1	0.80	1803.8	17.7	1802.4	11.8	1800.8	15.2	1800.8	15.2	100.2
4-Spot 305	88	13477	3.0	9.0796	0.8	4.8541	1.5	0.3198	1.2	0.84	1788.7	19.3	1794.3	12.4	1800.9	14.4	1800.9	14.4	99.3
14-Spot 65	648	883896	4.4	9.0745	0.7	5.0249	1.3	0.3309	1.1	0.86	1842.5	17.9	1823.5	11.0	1801.9	12.0	1801.9	12.0	102.3
4-Spot 302	191	221075	2.7	9.0744	0.7	4.8869	1.0	0.3218	0.8	0.76	1798.3	12.3	1800.0	8.7	1801.9	12.1	1801.9	12.1	99.8
4-Spot 258	375	34464	2.1	9.0638	0.8	5.0801	1.4	0.3341	1.2	0.83	1858.2	19.2	1832.8	12.1	1804.0	14.4	1804.0	14.4	103.0
4-Spot 265	366	31028	1.9	9.0295	0.8	4.8516	1.2	0.3179	0.9	0.76	1779.3	14.7	1793.9	10.4	1810.9	14.5	1810.9	14.5	98.3
4-Spot 115	256	44020	2.2	9.0223	0.8	5.1159	1.4	0.3349	1.1	0.81	1862.2	18.4	1838.8	12.0	1812.4	15.1	1812.4	15.1	102.7
4-Spot 199	72	12990	1.7	9.0129	1.0	4.9111	1.6	0.3212	1.2	0.76	1795.4	18.7	1804.2	13.2	1814.3	18.5	1814.3	18.5	99.0
4-Spot 131	392	149613	2.2	9.0055	0.7	5.1119	1.3	0.3340	1.1	0.82	1857.8	17.0	1838.1	10.9	1815.8	13.5	1815.8	13.5	102.3
4-Spot 117	282	40015	4.1	9.0042	0.6	5.0044	1.1	0.3270	0.9	0.85	1823.6	15.0	1820.1	9.4	1816.0	10.5	1816.0	10.5	100.4
4-Spot 266	63	69474	2.1	8.9889	0.9	4.9030	1.5	0.3198	1.1	0.76	1788.7	17.4	1802.8	12.3	1819.1	17.2	1819.1	17.2	98.3
4-Spot 267	225	15100	3.1	8.9857	0.6	4.8994	1.5	0.3194	1.3	0.90	1787.0	20.5	1802.2	12.3	1819.8	11.5	1819.8	11.5	98.2
14-Spot 16	561	161831	5.3	8.9831	0.7	4.9624	1.4	0.3235	1.2	0.87	1806.6	19.2	1812.9	11.9	1820.3	12.7	1820.3	12.7	99.2
14-Spot 57	314	47246	1.0	8.9626	0.8	5.1114	1.7	0.3324	1.5	0.88	1850.0	24.5	1838.0	14.7	1824.4	15.1	1824.4	15.1	101.4
4-Spot 249	296	83024	2.1	8.9598	0.7	4.9559	1.4	0.3222	1.2	0.88	1800.4	19.2	1811.8	11.7	1825.0	11.9	1825.0	11.9	98.7
4-Spot 148	61	3999	2.4	8.9503	1.2	4.8401	1.9	0.3143	1.5	0.79	1762.0	22.7	1791.9	15.8	1826.9	21.0	1826.9	21.0	96.4
14-Spot 95	258	104033	1.9	8.9441	0.9	5.1990	1.5	0.3374	1.2	0.80	1874.2	19.9	1852.5	13.1	1828.2	16.7	1828.2	16.7	102.5
4-Spot 253	226	33247	2.7	8.9429	0.7	4.9894	1.1	0.3238	0.9	0.79	1808.0	13.6	1817.5	9.2	1828.4	12.2	1828.4	12.2	98.9
4-Spot 124	536	101071	1.3	8.9321	0.7	5.1100	1.4	0.3312	1.2	0.85	1844.1	19.5	1837.8	12.1	1830.6	13.5	1830.6	13.5	100.7
14-Spot 51	167	22648	3.1	8.9309	0.9	5.1735	1.7	0.3352	1.4	0.86	1863.8	22.9	1848.3	14.1	1830.8	15.6	1830.8	15.6	101.8
4-Spot 263	105	171413	2.0	8.9285	0.8	4.8279	1.2	0.3128	0.9	0.74	1754.3	13.4	1789.8	9.9	1831.3	14.2	1831.3	14.2	95.8
4-Spot 152	242	38128	1.6	8.9234	0.7	4.9721	1.4	0.3219	1.2	0.87	1799.1	19.0	1814.6	11.8	1832.4	12.7	1832.4	12.7	98.2

14-Spot 24	246	35152	3.2	8.9157	0.8	5.3329	1.3	0.3450	1.0	0.81	1910.6	17.4	1874.1	11.1	1833.9	13.9	1833.9	13.9	104.2
4-Spot 169	259	18972	1.7	8.9013	0.7	5.0916	1.3	0.3288	1.1	0.83	1832.8	17.6	1834.7	11.3	1836.9	13.6	1836.9	13.6	99.8
4-Spot 138	76	12935	2.2	8.8998	1.0	5.0684	1.5	0.3273	1.1	0.73	1825.3	17.3	1830.8	12.7	1837.2	18.5	1837.2	18.5	99.4
4-Spot 242	82	48168	2.4	8.8977	0.7	4.7782	1.2	0.3085	1.0	0.81	1733.2	14.8	1781.1	10.1	1837.6	12.8	1837.6	12.8	94.3
4-Spot 224	97	49025	1.2	8.8901	0.9	5.0124	1.5	0.3233	1.2	0.80	1806.0	18.8	1821.4	12.6	1839.1	16.0	1839.1	16.0	98.2
4-Spot 135	142	189272	4.1	8.8776	0.8	5.1409	1.3	0.3312	1.1	0.81	1844.0	16.9	1842.9	11.0	1841.7	13.6	1841.7	13.6	100.1
4-Spot 104	125	24586	4.6	8.8551	0.8	5.2285	1.2	0.3359	0.9	0.75	1867.1	15.1	1857.3	10.6	1846.3	14.8	1846.3	14.8	101.1
14-Spot 45	67	12976	1.4	8.7687	1.0	5.3642	1.6	0.3413	1.3	0.80	1892.9	21.1	1879.2	13.7	1864.0	17.2	1864.0	17.2	101.5
4-Spot 306	181	31795	3.3	8.7520	0.8	5.2330	1.4	0.3323	1.1	0.79	1849.6	17.5	1858.0	11.7	1867.4	15.0	1867.4	15.0	99.0
4-Spot 161	292	300060	1.4	8.7308	0.8	5.5129	1.2	0.3492	1.0	0.78	1931.0	15.9	1902.6	10.5	1871.8	13.9	1871.8	13.9	103.2
4-Spot 207	408	37927	1.8	8.7009	0.9	5.1113	1.4	0.3227	1.1	0.79	1802.9	17.1	1838.0	11.7	1878.0	15.3	1878.0	15.3	96.0
4-Spot 269	310	89599	3.2	8.4565	0.6	5.3713	1.2	0.3296	1.0	0.84	1836.4	15.5	1880.3	9.9	1929.2	11.2	1929.2	11.2	95.2
4-Spot 248	206	43840	0.9	8.1663	0.9	5.8584	1.4	0.3471	1.0	0.77	1920.9	17.3	1955.1	11.8	1991.5	15.5	1991.5	15.5	96.5
4-Spot 208	232	46399	1.0	7.5876	0.7	6.8671	1.3	0.3781	1.1	0.85	2067.2	20.0	2094.4	11.8	2121.2	12.1	2121.2	12.1	97.5
4-Spot 311	1058	138099	11.5	7.4661	0.7	7.0939	1.4	0.3843	1.1	0.84	2096.3	20.4	2123.3	12.1	2149.5	12.9	2149.5	12.9	97.5
4-Spot 167	386	54831	2.1	7.0270	0.6	6.8144	1.1	0.3474	0.9	0.83	1922.4	15.5	2087.6	9.9	2254.7	10.8	2254.7	10.8	85.3
4-Spot 147	111	153343	2.4	6.9961	0.8	7.7954	1.6	0.3957	1.4	0.86	2149.3	25.1	2207.7	14.4	2262.3	14.0	2262.3	14.0	95.0
14-Spot 79	494	20840	2.0	6.9483	0.7	6.6261	1.3	0.3341	1.1	0.84	1858.0	17.7	2062.8	11.6	2274.2	12.5	2274.2	12.5	81.7
4-Spot 243	879	95275	9.2	6.8108	2.8	7.9642	3.1	0.3936	1.2	0.40	2139.4	22.6	2227.0	27.7	2308.5	48.1	2308.5	48.1	92.7
14-Spot 66	562	101523	1.6	6.6710	0.7	8.9500	1.2	0.4332	1.0	0.84	2320.2	19.8	2332.9	11.0	2344.1	11.2	2344.1	11.2	99.0
4-Spot 209	359	78938	3.8	6.6214	0.8	8.7707	1.4	0.4214	1.1	0.84	2266.7	22.0	2314.5	12.5	2356.8	12.9	2356.8	12.9	96.2
14-Spot 74	399	464665	2.5	6.5628	0.8	9.0909	1.4	0.4329	1.2	0.84	2318.8	23.6	2347.2	13.3	2372.0	13.6	2372.0	13.6	97.8
14-Spot 10	361	44226	3.3	6.4936	0.6	9.5632	1.4	0.4506	1.2	0.88	2397.9	23.8	2393.6	12.4	2390.0	11.0	2390.0	11.0	100.3
4-Spot 113	312	52778	2.7	6.4678	0.6	9.4914	1.2	0.4454	1.1	0.88	2374.9	21.1	2386.7	11.1	2396.8	10.0	2396.8	10.0	99.1
4-Spot 157	884	67284	2.2	6.4578	0.8	10.0981	1.5	0.4732	1.2	0.84	2497.4	25.7	2443.8	13.6	2399.5	13.4	2399.5	13.4	104.1
14-Spot 23	508	314963	2.9	6.4549	0.6	9.4415	1.3	0.4422	1.1	0.88	2360.5	22.3	2381.9	11.8	2400.2	10.4	2400.2	10.4	98.3
14-Spot 12	1032	133431	2.6	6.4438	0.8	9.6480	1.3	0.4511	1.1	0.82	2400.1	21.6	2401.8	12.1	2403.1	12.8	2403.1	12.8	99.9
14-Spot 86	1027	176913	2.8	6.4388	0.8	9.7439	1.6	0.4552	1.3	0.84	2418.4	26.6	2410.9	14.4	2404.5	14.2	2404.5	14.2	100.6
4-Spot 133	230	52943	2.6	6.4266	0.7	9.3827	1.4	0.4375	1.2	0.86	2339.5	23.6	2376.1	12.8	2407.7	12.2	2407.7	12.2	97.2
4-Spot 236	256	37063	3.1	6.4097	0.8	9.7030	1.4	0.4513	1.2	0.83	2400.9	23.2	2407.0	12.8	2412.2	13.0	2412.2	13.0	99.5
14-Spot 73	488	140777	1.9	6.3858	0.8	9.6582	1.6	0.4475	1.4	0.87	2384.2	27.0	2402.7	14.4	2418.5	13.3	2418.5	13.3	98.6
4-Spot 118	199	54145	2.5	6.3792	0.7	10.0654	1.5	0.4659	1.3	0.89	2465.5	27.4	2440.8	13.8	2420.3	11.5	2420.3	11.5	101.9
4-Spot 240	240	156039	2.9	6.3653	0.9	9.5047	1.5	0.4390	1.2	0.80	2346.1	23.5	2388.0	13.7	2424.0	15.1	2424.0	15.1	96.8
14-Spot 15	347	242477	2.5	6.3578	0.7	9.6815	1.2	0.4466	1.0	0.80	2380.2	19.3	2404.9	11.2	2426.0	12.3	2426.0	12.3	98.1
4-Spot 315	926	306480	1.8	6.3392	0.9	10.2641	1.4	0.4721	1.1	0.79	2492.8	23.4	2458.9	13.3	2430.9	15.0	2430.9	15.0	102.5
4-Spot 132	406	121554	2.1	6.3288	0.7	10.1999	1.2	0.4684	1.0	0.81	2476.5	19.8	2453.1	10.9	2433.7	11.6	2433.7	11.6	101.8
4-Spot 232	865	314671	2.4	6.3281	0.6	10.2057	1.2	0.4686	1.1	0.88	2477.4	22.4	2453.6	11.4	2433.9	9.8	2433.9	9.8	101.8
-14-Spot 8	361	60165	2.0	6.3239	0.6	9.7642	1.2	0.4480	1.1	0.88	2386.5	21.4	2412.8	11.2	2435.0	9.7	2435.0	9.7	98.0
14-Spot 54	320	254391	2.1	6.3122	0.7	10.3077	1.4	0.4721	1.2	0.85	2492.7	23.8	2462.8	12.5	2438.2	11.9	2438.2	11.9	102.2
-14-Spot 5	351	619735	1.8	6.3114	0.6	9.9649	1.1	0.4563	1.0	0.85	2423.4	19.5	2431.5	10.4	2438.4	10.0	2438.4	10.0	99.4
14-Spot 13	370	176887	1.2	6.3088	0.7	10.0770	1.6	0.4613	1.5	0.91	2445.2	29.6	2441.9	14.7	2439.1	11.0	2439.1	11.0	100.3
4-Spot 143	375	233472	2.2	6.3012	1.0	10.1648	1.4	0.4647	1.0	0.69	2460.5	19.9	2449.9	13.1	2441.1	17.4	2441.1	17.4	100.8
14-Spot 47	333	263539	0.9	6.3009	1.0	9.8760	1.6	0.4515	1.2	0.78	2402.0	24.9	2423.3	14.7	2441.2	16.8	2441.2	16.8	98.4
4-Spot 149	406	94532	2.4	6.2974	0.7	9.9961	1.3	0.4568	1.1	0.84	2425.2	22.1	2434.4	12.0	2442.1	12.0	2442.1	12.0	99.3
4-Spot 213	581	515995	2.6	6.2967	0.7	10.0231	1.3	0.4579	1.1	0.85	2430.4	22.2	2436.9	11.9	2442.3	11.5	2442.3	11.5	99.5
4-Spot 275	349	42084	2.3	6.2961	0.8	10.1497	1.5	0.4637	1.3	0.84	2455.8	25.6	2448.5	13.9	2442.5	13.9	2442.5	13.9	100.5
4-Spot 123	482	244062	2.5	6.2946	0.8	10.3767	1.3	0.4739	1.0	0.78	2500.8	21.1	2469.0	12.0	2442.9	13.6	2442.9	13.6	102.4
4-Spot 173	407	77033	2.6	6.2890	0.6	10.1341	1.3	0.4624	1.1	0.89	2450.3	23.0	2447.1	11.8	2444.4	10.0	2444.4	10.0	100.2
14-Spot 61	386	58993	1.7	6.2875	0.6	10.2843	1.5	0.4692	1.4	0.93	2480.0	29.2	2460.7	14.1	2444.8	9.4	2444.8	9.4	101.4
-14-Spot 4	446	100703	2.3	6.2855	0.8	10.3043	1.3	0.4699	1.0	0.77	2483.3	20.4	2462.5	11.8	2445.3	13.8	2445.3	13.8	101.6
14-Spot 42	348	55402	2.3	6.2819	1.0	10.1549	1.6	0.4629	1.2	0.78	2452.2	25.4	2449.0	14.8	2446.3	17.0	2446.3	17.0	100.2
4-Spot 241	645	64338	2.2	6.2815	0.8	10.2958	1.3	0.4693	1.0	0.80	2480.3	21.2	2461.7	11.9	2446.4	12.9	2446.4	12.9	101.4
4-Spot 259	430	45895	2.4	6.2795	0.7	10.0236	1.1	0.4567	0.9	0.79	2425.0	17.8	2437.0	10.3	2447.0	11.5	2447.0	11.5	99.1
14-Spot 17	307	72821	2.2	6.2789	0.7	10.2107	1.2	0.4652	0.9	0.79	2462.4	19.4	2454.0	11.1	2447.1	12.6	2447.1	12.6	100.6
4-Spot 109	318	58100	2.3	6.2772	0.7	9.8083	1.5	0.4467	1.3	0.88	2380.7	26.0	2416.9	13.7	2447.6	12.0	2447.6	12.0	97.3
4-Spot 230	696	97273	2.4	6.2763	0.7	10.1534	1.5	0.4624	1.4	0.89	2450.1	27.6	2448.8	14.0	2447.8	11.5	2447.8	11.5	100.1
4-Spot 179	208	155489	1.6	6.2694	0.7	10.5132	1.3	0.4782	1.2	0.87	2519.6	24.0	2481.1	12.3	2449.7	11.0	2449.7	11.0	102.9
4-Spot 292	251	431298	2.7	6.2671	0.7	9.8302	1.2	0.4470	1.0	0.82	2381.9	19.7	2419.0	11.1	2450.3	11.7	2450.3	11.7	97.2
14-Spot 30	454	601262	2.5	6.2658	0.8	9.8345	1.4	0.4471	1.2	0.84	2382.4	23.6	2419.4	13.0	2450.6	13.2	2450.6	13.2	97.2
4-Spot 194	481	37303	1.9	6.2617	0.6	10.0918	1.0	0.4585	0.9	0.84	2433.0	17.8	2443.2	9.7	2451.7	9.5	2451.7	9.5	99.2
4-Spot 171	281	352446	2.7	6.2606	0.7	10.3033	1.2	0.4680	1.0	0.81	2474.9	19.6	2462.4	10.9	2452.1	11.7	2452.1	11.7	100.9
4-Spot 114	259	38292	2.4	6.2597	0.6	10.0449	1.1	0.4562	1.0	0.86	2422.9	19.3	2438.9	10.3	2452.3	9.8	2452.3	9.8	98.8
4-Spot 168	332	40319	1.8	6.2555	0.9	10.5320	1.3	0.4780	1.0	0.74	2518.7	19.9	2482.7	11.9	2453.4	14.6	2453.4	14.6	102.7
4-Spot 166	385	314617	1.9	6.2502	0.7	10.1675	1.1	0.4611	0.9	0.76	2444.4	17.6	2450.1	10.6	2454.9	12.7	2454.9	12.7	99.6
4-Spot 102	548	137941	1.8	6.2479	0.7	9.7357	1.4	0.4414	1.1	0.85	2356.7	22.6	2410.1	12.5	2455.5	12.2	2455.5	12.2	96.0
4-Spot 203	238	69704	2.0	6.2469	0.7	9.8961	1.3	0.4486	1.1	0.84	2388.8	22.1	2425.1	12.2	2455.8	12.0	2455.8	12.0	97.3
4-Spot 112	349	83825	1.7	6.2448	0.8	10.1844	1.5	0.4615	1.2	0.85	2446.1	25.3	2451.7	13.5	2456.3	13.0	2456.3	13.0	99.6
4-Spot 251	371	457132	2.4	6.2425	0.8	9.9566	1.1	0.4510	0.8	0.72	2399.6	16.0	2430.8	10.2	2456.9	13.0	2456.9	13.0	97.7
4-Spot 247	277	171205	2.6	6.2394	0.6	10.1524	1.0	0.4596	0.9	0.82	2437.9	17.4	2448.8	9.6	2457.8	9.9	2457.8	9.9	99.2
14-Spot 38	350	51663	1.9	6.2308	0.9	10.2737	1.4	0.4645	1.1	0.79	2459.3	23.0	2459.7	13.1	2460.1	14.6	2460.1	14.6	100.0
4-Spot 310	151	90226	2.6	6.2302	0.7	9.9314	1.3	0.4490	1.1	0.85	2390.6	22.5	2428.4	12.2	2460.3	11.7	2460.3	11.7	97.2
4-Spot 200	351	906389	2.1	6.2242	0.7	10.3994	1.3	0.4697	1.0	0.82	2482.0	21.5	2471.0	11.8	2461.9	12.4	2461.9	12.4	100.8
4-Spot 183	313	312631	2.5	6.2200	0.7	10.2602	1.2	0.4631	0.9	0.79	2453.0	18.8	2458.5	10.7	2463.1	11.9	2463.1	11.9	99.6
4-Spot 308	527	82329	2.2	6.2135	0.6	10.2445	1.3	0.4619	1.2	0.89	2447.8	24.5	2457.1	12.5	2464.8	10.4	2464.8	10.4	99.3
4-Spot 296	245	46938	2.3	6.2115	0.8	10.0044	1.4	0.4509	1.2	0.84	2399.2	23.6	2435.2	12.9	2465.4	12.7	2465.4	12.7	97.3
4-Spot 145	347	942779	2.7	6.2085	0.8	10.4984	1.4	0.4729	1.2	0.84	2496.4	25.1	2479.8	13.4	2466.2	13.2	2466.2	13.2	101.2
14-Spot 56	243	320324	2.1	6.2080	0.7	10.2307	1.8	0.4608	1.7	0.91	2443.2	34.0	2455.9	16.9	2466.3	12.5	2466.3	12.5	99.1
4-Spot 290	247	50596	2.3	6.1793	0.7	10.1690	1.3	0.4559	1.1	0.85	2421.6	22.0	2450.3	11.9	2474.1	11.5	2474.1	11.5	97.9
4-Spot 189	198	220729	3.0	6.1639	0.6	10.2939	1.1	0.4604	1.0	0.85	2441.3	19.7	2461.6	10.6	2478.3	10.1	2478.3	10.1	98.5
4-Spot 219	184	121886	1.0	6.1209	0.9	10.7911	1.3	0.4793	1.0	0.76	2524.0	21.0	2505.3	12.2	2490.1	14.4	2490.1	14.4	101.4
4-Spot 254	214	5462350	2.4	6.1145	0.7	10.5641	1.2	0.4687	1.0	0.83	2477.8	19.6	2485.6	10.7	2491.9	11.0	2491.9	11.0	99.4
14-Spot 87	304	36273	0.5	6.0900	0.7	10.0446	1.5	0.4439	1.3	0.87	2367.9	25.5	2438.9	13.7	2498.7	12.4	2498.7	12.4	94.8
14-Spot 50	1012	29509	1.1	6.0830	0.8	9.2956	1.3	0.4103	1.1	0.81	2216.2	20.1	2367.6	12.1	2500.6	13.0	2500.6	13.0	88.6
4-Spot 205	553	189257	0.7	6.0412	0.6	11.2885	1.6	0.4948	1.5	0.92	2591.5	31.5	2547.3	14.9	2512.2	10.5	2512.2	10.5	103.2
4-Spot 307	967	40125	1.6	6.0381	0.7	10.0937	1.2	0.4422	1.0	0.82	2360.6	20.0	2443.4	11.5	2513.1	12.0	2513.1	12.0	93.9
4-Spot 103	674	55315	1.5	6.0298	0.8	9.6231	1.4	0.4210	1.1	0.80	2265.1	21.1	2399.4	12.6	2515.4	13.8	2515.4	13.8	90.1
4-Spot 252	554	53881	1.0	6.0220	0.4	10.8897	1.0	0.4758	0.9	0.89	2509.0	18.0	2513.8	9.0	2517.6	7.5	2517.6	7.5	99.7
14-Spot 69	163	21082	1.4	6.0123	0.8	11.4895	1.3	0.5012	1.1	0.82	2619.0	23.4	2563.7	12.4	2520.3	12.9	2520.3	12.9	103.9
14-Spot 80	268	77063	1.2	6.0020	0.8	11.2223	1.3	0.4887	1.0	0.78	2565.2	22.0	2541.8	12.4	2523.1	14.1	2523.1	14.1	101.7
4-Spot 144	173	32312	1.9	5.9851	0.8	11.0572	1.6	0.4802	1.3	0.85	2528.1	27.9	2528.0	14.6	2527.9	13.9	2527.9	13.9	100.0
4-Spot 257	175	46062	0.6	5.9850	0.6	10.7279	1.1	0.4659	0.9	0.81	2465.5	17.6	2499.8	9.8	2527.9	10.5	2527.9	10.5	97.5
4-Spot 110	332	42236	1.5	5.9599	0.7	11.1128	1.2	0.4806	0.9	0.78	2529.7	19.0	2532.6	10.9	2534.9	12.3	2534.9	12.3	99.8
4-Spot 176	738	83708	0.6	5.9420	0.7	11.5227	1.3	0.4968	1.1	0.83	2600.0	23.5	2566.4	12.3	2540.0	12.2	2540.0	12.2	102.4
14-Spot 52	209	31206	0.9	5.9393	0.7	11.2369	1.6	0.4843	1.4	0.90	2545.8	30.3	2543.0	15.0	2540.8	12.0	2540.8	12.0	100.2
4-Spot 221	167	234357	0.4	5.9170	0.7	10.9065	1.4	0.4682	1.2	0.86	2475.9	24.3	2515.2	12.8	2547.1	11.8	2547.1	11.8	97.2
4-Spot 154	1727	84485	5.7	5.8904	0.5	10.9564	1.3	0.4683	1.1	0.91	2476.0	23.5	2519.4	11.6	2554.6	8.5	2554.6	8.5	96.9

4-Spot 256	187	94594	1.3	5.8527	0.6	11.1857	1.0	0.4750	0.9	0.84	2505.5	18.3	2538.7	9.8	2565.4	9.5	2565.4	9.5	97.7
4-Spot 286	265	43322	1.1	5.8438	0.6	11.2495	1.3	0.4770	1.2	0.87	2514.2	24.1	2544.0	12.4	2567.9	10.8	2567.9	10.8	97.9
14-Spot 72	1013	137114	2.9	5.8403	0.6	10.9634	1.6	0.4646	1.4	0.91	2459.8	29.2	2520.0	14.6	2568.9	10.7	2568.9	10.7	95.8
4-Spot 139	334	104763	1.1	5.8381	0.7	11.8189	1.6	0.5007	1.4	0.88	2616.6	29.7	2590.2	14.7	2569.5	12.5	2569.5	12.5	101.8
-14-Spot 1	1661	37564	7.5	5.8277	0.6	10.3898	2.4	0.4393	2.3	0.97	2347.7	46.2	2470.1	22.5	2572.5	10.0	2572.5	10.0	91.3
14-Spot 14	380	30088	0.9	5.8132	0.8	11.8404	1.6	0.4994	1.4	0.86	2611.3	29.2	2591.9	14.8	2576.7	13.6	2576.7	13.6	101.3
4-Spot 142	195	31104	1.2	5.8099	0.9	11.4830	1.6	0.4841	1.3	0.82	2545.0	27.7	2563.2	14.9	2577.6	15.1	2577.6	15.1	98.7
14-Spot 46	748	878378	3.1	5.7953	0.8	12.2836	1.5	0.5165	1.3	0.86	2684.4	28.9	2626.3	14.3	2581.8	12.8	2581.8	12.8	104.0
4-Spot 303	195	33346	1.2	5.7768	0.7	11.7134	1.2	0.4910	1.0	0.81	2574.9	21.0	2581.8	11.4	2587.2	11.8	2587.2	11.8	99.5
4-Spot 281	808	58123	6.9	5.7487	0.7	9.8826	1.4	0.4122	1.2	0.88	2225.1	23.4	2423.9	13.0	2595.3	11.0	2595.3	11.0	85.7
4-Spot 197	135	113768	1.0	5.7479	0.8	12.5835	1.2	0.5248	0.9	0.78	2719.5	20.6	2649.0	11.2	2595.5	12.5	2595.5	12.5	104.8
-14-Spot 6	378	159853	0.6	5.7300	0.8	12.0039	1.4	0.4991	1.2	0.82	2609.8	24.9	2604.7	13.3	2600.7	13.7	2600.7	13.7	100.3
4-Spot 277	396	43396	1.5	5.7196	0.7	11.6505	1.2	0.4835	1.0	0.81	2542.5	20.5	2576.7	11.3	2603.8	11.7	2603.8	11.7	97.6
14-Spot 77	594	46498	2.7	5.6683	0.8	11.3371	1.7	0.4663	1.5	0.89	2467.2	31.6	2551.3	16.3	2618.8	13.4	2618.8	13.4	94.2
4-Spot 280	502	100931	1.2	5.6502	0.7	11.3657	1.4	0.4660	1.2	0.85	2465.8	23.8	2553.6	12.7	2624.1	12.0	2624.1	12.0	94.0
14-Spot 98	105	66969	2.8	5.5329	0.8	12.9637	1.3	0.5204	1.1	0.82	2701.0	24.5	2677.0	12.7	2658.9	12.7	2658.9	12.7	101.6
4-Spot 261	482	73150	4.0	5.5185	0.8	12.7981	1.3	0.5125	1.0	0.80	2667.1	22.9	2664.9	12.3	2663.2	13.0	2663.2	13.0	100.1
14-Spot 81	189	23903	1.4	5.5117	0.8	12.2400	1.3	0.4895	1.1	0.82	2568.5	23.4	2623.0	12.6	2665.3	12.8	2665.3	12.8	96.4
4-Spot 229	183	255624	2.0	5.4748	0.7	13.0886	1.4	0.5199	1.2	0.84	2698.9	25.4	2686.1	12.9	2676.4	12.2	2676.4	12.2	100.8
4-Spot 108	399	115921	1.4	5.4226	0.6	13.3184	1.3	0.5240	1.2	0.88	2716.2	26.1	2702.5	12.6	2692.2	10.5	2692.2	10.5	100.9
14-Spot 49	341	279009	1.5	5.4095	0.9	13.4699	1.6	0.5287	1.3	0.84	2736.0	29.8	2713.2	15.1	2696.2	14.4	2696.2	14.4	101.5
14-Spot 55	48	13290	2.9	5.4039	0.8	13.2651	1.7	0.5201	1.5	0.87	2699.7	32.2	2698.7	15.9	2697.9	13.7	2697.9	13.7	100.1
4-Spot 246	42	20601	2.1	5.3945	0.8	12.5793	1.3	0.4924	1.0	0.78	2580.9	21.0	2648.7	12.0	2700.8	13.2	2700.8	13.2	95.6
14-Spot 48	1011	1378693	3.7	5.3943	0.8	13.7881	1.5	0.5397	1.3	0.87	2782.0	29.8	2735.3	14.4	2700.9	12.4	2700.9	12.4	103.0
14-Spot 68	242	78595	1.6	5.3906	0.8	13.0837	1.4	0.5117	1.1	0.82	2664.1	24.7	2685.7	13.0	2702.0	12.9	2702.0	12.9	98.6
4-Spot 181	159	29112	1.6	5.3726	0.7	13.6967	1.3	0.5339	1.1	0.87	2758.0	25.5	2729.0	12.4	2707.5	10.8	2707.5	10.8	101.9
4-Spot 220	49	15665	2.9	5.3537	1.0	13.0546	1.5	0.5071	1.1	0.76	2644.3	24.8	2683.6	14.1	2713.3	15.9	2713.3	15.9	97.5
4-Spot 128	293	37907	0.9	5.3013	0.8	13.6839	1.4	0.5264	1.1	0.79	2726.1	24.2	2728.1	12.9	2729.5	13.7	2729.5	13.7	99.9
4-Spot 175	501	253671	1.4	5.2877	0.7	14.4286	1.1	0.5536	0.9	0.78	2840.0	19.9	2778.3	10.5	2733.8	11.3	2733.8	11.3	103.9
4-Spot 153	188	51350	1.2	5.2404	0.7	14.0737	1.1	0.5351	0.9	0.79	2763.0	20.3	2754.7	10.8	2748.6	11.4	2748.6	11.4	100.5
4-Spot 218	231	302776	1.2	5.1682	0.8	14.1873	1.3	0.5320	1.0	0.80	2749.9	23.2	2762.3	12.3	2771.3	12.8	2771.3	12.8	99.2
14-Spot 44	160	50822	1.5	5.1077	0.7	14.8197	1.2	0.5492	1.0	0.84	2821.9	24.0	2803.7	11.9	2790.6	11.1	2790.6	11.1	101.1
14-Spot 35	981	173652	2.7	5.1004	0.8	14.9829	1.7	0.5545	1.5	0.87	2843.8	33.9	2814.2	16.2	2793.0	13.8	2793.0	13.8	101.8
4-Spot 284	107	32531	1.4	5.0680	0.9	14.4453	1.3	0.5312	1.0	0.74	2746.5	21.7	2779.4	12.4	2803.4	14.2	2803.4	14.2	98.0
14-Spot 29	350	26600	2.6	5.0638	0.8	15.7090	1.5	0.5772	1.3	0.83	2937.2	29.8	2859.3	14.4	2804.8	13.6	2804.8	13.6	104.7
4-Spot 274	677	22098104	1.2	5.0218	0.6	14.8620	1.2	0.5415	1.0	0.85	2789.9	23.2	2806.4	11.5	2818.4	10.5	2818.4	10.5	99.0
4-Spot 214	324	256504	1.6	4.9736	0.7	15.0416	1.2	0.5428	1.0	0.84	2795.2	23.7	2817.9	11.9	2834.1	11.2	2834.1	11.2	98.6
14-Spot 89	229	38558	1.3	4.9569	0.5	15.1522	1.4	0.5450	1.2	0.92	2804.2	28.4	2824.9	12.9	2839.6	8.7	2839.6	8.7	98.8
4-Spot 190	213	43050	2.7	3.8806	0.6	21.8154	1.1	0.6143	0.9	0.86	3087.0	22.9	3175.5	10.5	3232.0	8.7	3232.0	8.7	95.5
14-Spot 88	112	125444	1.1	3.8102	0.9	24.3118	1.4	0.6721	1.1	0.78	3314.1	28.1	3281.0	13.5	3260.8	13.6	3260.8	13.6	101.6

Table DTB17-17. U-Pb geochronologic analyses.

						Isotope ratios						Apparent ages (Ma)							
Analysis	U	206Pb	U/Th	206Pb*	±	207Pb*	±	206Pb*	±	error	206Pb*	±	207Pb*	±	206Pb*	±	Best age	±	Conc
	(ppm)	204Pb		207Pb*	(%)	235U*	(%)	238U	(%)	corr.	238U*	(Ma)	235U	(Ma)	207Pb*	(Ma)	(Ma)	(Ma)	(%)
7-Spot 29	192	63796	1.7	13.0965	0.8	1.9710	1.5	0.1873	1.3	0.87	1106.7	13.7	1105.6	10.4	1103.6	15.2	1103.6	15.2	100.3
7-Spot 66	340	134136	0.7	9.8838	0.5	4.1045	1.2	0.2944	1.0	0.89	1663.3	15.2	1655.2	9.5	1645.0	10.1	1645.0	10.1	101.1
7-Spot 38	158	108020	2.8	9.7189	0.6	4.3589	1.1	0.3074	0.9	0.83	1727.8	13.5	1704.6	8.9	1676.1	11.1	1676.1	11.1	103.1
7-Spot 46	107	1163262	3.7	9.6955	0.6	4.3178	1.3	0.3038	1.2	0.89	1709.9	17.8	1696.8	11.0	1680.6	11.4	1680.6	11.4	101.7
7-Spot 30	276	75934	1.5	9.6895	0.7	4.4144	1.3	0.3104	1.2	0.87	1742.5	17.8	1715.0	11.1	1681.7	12.2	1681.7	12.2	103.6
-Spot 103	422	166028	0.9	9.6260	0.5	4.4318	1.2	0.3095	1.1	0.91	1738.4	17.2	1718.3	10.3	1693.9	9.6	1693.9	9.6	102.6
7-Spot 56	381	169039	2.8	9.5980	0.6	4.2371	1.5	0.2951	1.4	0.92	1666.9	20.2	1681.2	12.3	1699.2	10.7	1699.2	10.7	98.1
7-Spot 54	113	131758	3.3	9.5834	0.6	4.3343	1.3	0.3014	1.1	0.89	1698.2	17.1	1699.9	10.6	1702.0	10.8	1702.0	10.8	99.8
7-Spot 12	183	374257	2.9	9.5831	0.4	4.4081	1.1	0.3065	1.0	0.92	1723.5	15.5	1713.9	9.2	1702.1	7.9	1702.1	7.9	101.3
7-Spot 69	201	104785	1.6	9.5692	0.8	4.3691	1.5	0.3034	1.3	0.87	1707.9	20.2	1706.5	12.7	1704.8	13.8	1704.8	13.8	100.2
7-Spot 47	173	549241	1.9	9.5433	0.6	4.3893	1.3	0.3039	1.1	0.88	1710.8	17.0	1710.3	10.6	1709.7	11.0	1709.7	11.0	100.1
7-Spot 97	438	60807	2.0	9.5369	0.6	4.0225	1.3	0.2783	1.1	0.90	1583.0	15.9	1638.8	10.3	1711.0	10.3	1711.0	10.3	92.5
7-Spot 27	267	80230	6.6	9.5252	0.5	4.5711	1.1	0.3159	0.9	0.88	1769.8	14.6	1744.0	8.9	1713.2	9.1	1713.2	9.1	103.3
7-Spot 63	268	317519	2.5	9.5092	0.6	4.6475	1.2	0.3207	1.1	0.88	1793.0	16.5	1757.8	10.0	1716.3	10.5	1716.3	10.5	104.5
7-Spot 58	291	136054	2.2	9.4986	0.7	4.5867	1.3	0.3161	1.1	0.85	1770.7	17.5	1746.9	11.1	1718.4	13.0	1718.4	13.0	103.0
-17-Spot 5	211	198961	2.1	9.4340	0.7	4.6271	1.2	0.3167	1.0	0.83	1773.7	14.9	1754.2	9.7	1730.9	11.9	1730.9	11.9	102.5
7-Spot 84	456	559906	1.0	9.4106	0.6	4.6301	0.9	0.3162	0.7	0.79	1770.9	11.0	1754.7	7.5	1735.5	10.2	1735.5	10.2	102.0
-Spot 105	299	191407	2.3	9.4048	0.7	4.7462	1.4	0.3239	1.2	0.86	1808.7	18.8	1775.4	11.6	1736.6	13.0	1736.6	13.0	104.2
7-Spot 61	287	333454	3.6	9.4020	0.6	4.6357	1.2	0.3162	1.1	0.87	1771.4	16.7	1755.7	10.3	1737.1	11.1	1737.1	11.1	102.0
-Spot 108	430	314632	1.1	9.3928	0.7	4.6220	1.3	0.3150	1.1	0.82	1765.3	16.6	1753.3	10.9	1738.9	13.6	1738.9	13.6	101.5
-17-Spot 9	316	336536	1.7	9.3810	0.8	4.7360	1.8	0.3224	1.6	0.91	1801.3	25.4	1773.6	15.0	1741.2	13.7	1741.2	13.7	103.4
7-Spot 95	379	204020	5.5	9.3743	0.7	4.5885	1.3	0.3121	1.1	0.84	1751.0	17.1	1747.2	11.0	1742.5	13.0	1742.5	13.0	100.5
-Spot 107	279	329575	2.8	9.3740	0.8	4.6563	1.4	0.3167	1.2	0.84	1773.6	18.2	1759.4	11.7	1742.6	14.0	1742.6	14.0	101.8
7-Spot 87	267	19226970	3.4	9.3519	0.6	4.8002	1.0	0.3257	0.9	0.83	1817.6	13.7	1784.9	8.7	1746.9	10.5	1746.9	10.5	104.0
-Spot 102	653	198268	4.1	9.3506	0.8	3.5883	1.6	0.2435	1.3	0.85	1404.6	16.6	1546.9	12.3	1747.2	14.9	1747.2	14.9	80.4
7-Spot 50	134	123727	2.1	9.3449	0.8	4.7702	1.5	0.3234	1.2	0.84	1806.5	19.3	1779.7	12.2	1748.3	14.3	1748.3	14.3	103.3
7-Spot 67	228	310604	1.6	9.3449	0.7	4.6370	1.4	0.3144	1.3	0.89	1762.4	19.8	1756.0	12.1	1748.3	12.4	1748.3	12.4	100.8
7-Spot 28	520	139427	1.4	9.3039	0.8	4.5978	1.3	0.3104	1.0	0.78	1742.6	14.9	1748.9	10.5	1756.3	14.5	1756.3	14.5	99.2
-17-Spot 7	509	96298	1.2	9.2992	0.6	4.3932	1.2	0.2964	1.0	0.88	1673.6	15.4	1711.1	9.8	1757.3	10.4	1757.3	10.4	95.2
7-Spot 57	238	79313	3.1	9.2971	0.7	4.7161	1.3	0.3181	1.1	0.84	1780.7	16.5	1770.1	10.7	1757.7	12.8	1757.7	12.8	101.3
-17-Spot 8	115	74929	1.8	9.2828	0.6	4.8721	1.1	0.3282	1.0	0.86	1829.5	15.4	1797.4	9.5	1760.5	10.5	1760.5	10.5	103.9
7-Spot 42	169	70631	2.8	9.2814	0.6	4.6224	1.3	0.3113	1.2	0.88	1747.1	17.7	1753.3	10.9	1760.8	11.2	1760.8	11.2	99.2
7-Spot 60	297	474630	1.3	9.2660	0.6	4.6042	1.3	0.3096	1.2	0.90	1738.5	17.7	1750.0	10.8	1763.8	10.6	1763.8	10.6	98.6
7-Spot 86	723	140966	5.8	9.2513	0.6	3.9040	1.3	0.2621	1.1	0.89	1500.4	14.9	1614.5	10.2	1766.7	10.6	1766.7	10.6	84.9
7-Spot 62	162	157240	3.5	9.2250	0.7	4.7817	1.3	0.3201	1.1	0.85	1790.0	17.4	1781.7	10.9	1771.9	12.4	1771.9	12.4	101.0
7-Spot 49	110	780466	2.3	9.2234	0.5	4.7990	1.0	0.3212	0.9	0.86	1795.4	13.8	1784.7	8.6	1772.2	9.5	1772.2	9.5	101.3
-Spot 100	227	76994	3.0	9.2183	0.7	4.4248	1.7	0.2960	1.5	0.91	1671.2	22.2	1717.0	13.8	1773.2	12.7	1773.2	12.7	94.2
-Spot 106	84	72694	2.8	9.2076	0.7	4.9058	1.3	0.3278	1.1	0.83	1827.5	17.0	1803.3	10.8	1775.4	12.9	1775.4	12.9	102.9
7-Spot 80	162	4713941	3.3	9.2070	0.6	4.7937	1.2	0.3202	1.0	0.85	1790.9	16.3	1783.8	10.3	1775.5	11.6	1775.5	11.6	100.9
-Spot 101	155	104401	2.3	9.2000	0.8	4.6573	1.5	0.3109	1.3	0.85	1745.1	19.5	1759.6	12.6	1776.9	14.4	1776.9	14.4	98.2
7-Spot 35	112	107161	0.8	9.1855	0.9	4.8191	1.4	0.3212	1.2	0.81	1795.5	18.3	1788.2	12.2	1779.7	15.5	1779.7	15.5	100.9
7-Spot 41	141	1817736	2.6	9.1774	0.6	4.7404	1.1	0.3157	0.9	0.84	1768.5	14.1	1774.4	9.2	1781.3	10.9	1781.3	10.9	99.3
7-Spot 64	466	102015	1.2	9.1726	0.8	4.5118	1.6	0.3003	1.3	0.86	1692.7	19.8	1733.2	12.9	1782.3	14.5	1782.3	14.5	95.0
7-Spot 45	95	192458	2.2	9.1646	0.5	4.7066	1.2	0.3130	1.1	0.91	1755.3	17.3	1768.4	10.4	1783.9	9.2	1783.9	9.2	98.4
-Spot 109	73	214234	1.3	9.1511	0.7	4.8513	1.3	0.3221	1.1	0.86	1800.1	17.3	1793.8	10.8	1786.6	12.1	1786.6	12.1	100.8
7-Spot 52	96	72830	0.7	9.1263	0.6	4.7720	1.1	0.3160	0.9	0.84	1770.1	14.0	1780.0	9.0	1791.5	10.6	1791.5	10.6	98.8
7-Spot 20	341	720291	2.4	9.1108	0.8	5.1191	1.4	0.3384	1.1	0.80	1879.0	18.0	1839.3	11.8	1794.6	15.3	1794.6	15.3	104.7
7-Spot 44	41	20669	1.1	9.0755	0.9	4.9630	1.5	0.3268	1.2	0.82	1822.9	19.3	1813.0	12.6	1801.7	15.5	1801.7	15.5	101.2

7 -Spot 92	84	76821	1.9	9.0722	0.6	4.9677	1.0	0.3270	0.8	0.78	1823.8	12.9	1813.8	8.8	1802.3	11.8	1802.3	11.8	101.2
7 -Spot 85	340	449955	6.3	9.0279	0.7	4.9035	1.1	0.3212	0.9	0.82	1795.6	14.6	1802.9	9.6	1811.2	12.0	1811.2	12.0	99.1
7 -Spot 18	209	123314	3.9	9.0233	0.8	5.1461	1.3	0.3369	1.1	0.82	1871.8	17.9	1843.7	11.4	1812.2	13.7	1812.2	13.7	103.3
7 -Spot 11	112	359419	3.2	9.0148	0.5	5.1002	1.0	0.3336	0.9	0.86	1855.8	14.0	1836.1	8.6	1813.9	9.5	1813.9	9.5	102.3
7 -Spot 23	49	16618	2.6	8.9861	0.7	5.0114	1.2	0.3268	1.0	0.83	1822.6	16.3	1821.2	10.5	1819.7	12.5	1819.7	12.5	100.2
7 -Spot 21	126	936910	1.3	8.9734	0.6	5.1379	1.1	0.3345	0.9	0.82	1860.3	14.6	1842.4	9.4	1822.2	11.3	1822.2	11.3	102.1
7 -Spot 99	42	178998	3.4	8.9340	0.6	5.2238	1.0	0.3386	0.8	0.77	1880.1	12.3	1856.5	8.3	1830.2	11.2	1830.2	11.2	102.7
7 -Spot 88	168	69782	2.7	8.8793	0.4	5.2687	1.0	0.3394	0.9	0.89	1884.0	14.6	1863.8	8.6	1841.3	8.1	1841.3	8.1	102.3
7 -Spot 59	73	90759	1.4	8.8748	0.7	5.2739	1.1	0.3396	0.9	0.82	1884.8	15.3	1864.7	9.8	1842.2	11.9	1842.2	11.9	102.3
7 -Spot 82	61	66050	3.3	8.8466	0.7	5.2350	1.4	0.3360	1.2	0.86	1867.6	20.0	1858.3	12.2	1848.0	13.1	1848.0	13.1	101.1
7 -Spot 22	40	64180	1.9	8.8274	0.7	5.2429	1.3	0.3358	1.1	0.83	1866.5	17.9	1859.6	11.3	1852.0	13.4	1852.0	13.4	100.8
7 -Spot 93	641	72535	1.1	8.7862	0.5	4.4215	1.0	0.2819	0.9	0.88	1600.8	12.8	1716.4	8.5	1860.4	8.9	1860.4	8.9	86.0
7 -Spot 90	62	78408	2.9	8.7810	0.6	5.3133	1.4	0.3385	1.3	0.90	1879.6	20.4	1871.0	11.9	1861.5	11.2	1861.5	11.2	101.0
7 -Spot 71	167	113445	1.2	8.7730	0.6	5.1645	1.1	0.3287	0.9	0.82	1832.3	14.8	1846.8	9.6	1863.1	11.7	1863.1	11.7	98.3
7 -Spot 40	25	69440	4.3	8.6960	0.8	5.5704	1.4	0.3515	1.2	0.83	1941.6	19.7	1911.5	12.2	1879.0	14.4	1879.0	14.4	103.3
17 -Spot 1	12	14099	2.0	8.6841	0.8	5.4253	1.3	0.3418	1.0	0.77	1895.6	16.0	1888.9	10.9	1881.5	14.7	1881.5	14.7	100.7
7 -Spot 15	78	50571	1.1	8.5698	0.6	5.6832	1.1	0.3534	1.0	0.87	1950.7	16.2	1928.8	9.6	1905.3	9.9	1905.3	9.9	102.4
7 -Spot 83	339	8663	1.8	8.3153	2.1	5.1701	2.4	0.3119	1.1	0.48	1750.2	17.6	1847.7	20.4	1959.3	37.7	1959.3	37.7	89.3
7 -Spot 34	185	28093	2.5	6.9546	0.7	8.0796	1.6	0.4077	1.4	0.90	2204.4	26.1	2240.0	14.1	2272.6	11.9	2272.6	11.9	97.0
7 -Spot 19	293	241304	2.7	6.5156	0.6	9.9221	1.5	0.4691	1.4	0.92	2479.5	27.9	2427.6	13.5	2384.3	9.5	2384.3	9.5	104.0
7 -Spot 81	244	222311	2.5	6.4546	0.7	10.1347	1.1	0.4746	0.8	0.77	2503.9	16.9	2447.1	9.7	2400.3	11.3	2400.3	11.3	104.3
7 -Spot 98	98	340377	2.7	6.4537	0.8	9.3940	1.3	0.4399	1.0	0.80	2350.2	20.6	2377.2	12.0	2400.5	13.4	2400.5	13.4	97.9
7 -Spot 48	167	65742	2.1	6.3391	0.5	10.1456	1.2	0.4666	1.1	0.90	2468.9	22.5	2448.1	11.3	2430.9	9.1	2430.9	9.1	101.6
7 -Spot 77	110	266626	3.0	6.3213	0.6	9.9735	1.3	0.4574	1.2	0.90	2428.3	23.6	2432.3	11.9	2435.7	9.4	2435.7	9.4	99.7
7 -Spot 94	307	172064	2.9	6.2676	0.7	9.8157	1.4	0.4464	1.1	0.84	2379.2	22.7	2417.6	12.5	2450.1	12.5	2450.1	12.5	97.1
-Spot 110	130	296955	2.8	6.2554	0.8	10.2343	1.3	0.4645	1.1	0.82	2459.5	22.1	2456.2	12.2	2453.5	12.8	2453.5	12.8	100.2
7 -Spot 55	124	135917	2.9	6.1645	0.7	10.4063	1.5	0.4655	1.3	0.87	2463.6	26.8	2471.6	13.9	2478.2	12.4	2478.2	12.4	99.4
7 -Spot 65	203	2536367	2.3	6.0629	0.6	9.6629	1.3	0.4251	1.1	0.88	2283.5	21.8	2403.2	11.8	2506.2	10.2	2506.2	10.2	91.1
17 -Spot 6	218	357767	1.9	6.0124	0.8	10.2582	1.8	0.4475	1.6	0.90	2384.2	32.6	2458.3	16.8	2520.2	13.2	2520.2	13.2	94.6
7 -Spot 89	116	41310	0.8	5.8346	1.3	10.1475	4.4	0.4296	4.2	0.95	2303.9	80.9	2448.3	40.5	2570.5	21.8	2570.5	21.8	89.6
7 -Spot 53	150	85038	2.3	5.6966	0.7	11.3338	1.2	0.4685	1.0	0.83	2476.8	20.7	2551.0	11.3	2610.5	11.3	2610.5	11.3	94.9
7 -Spot 25	53	43895	1.6	5.6321	0.7	12.6397	1.2	0.5165	0.9	0.79	2684.4	20.2	2653.2	10.9	2629.4	11.7	2629.4	11.7	102.1
7 -Spot 31	428	291581	14.8	5.5839	0.5	11.7731	0.9	0.4770	0.8	0.83	2514.2	16.0	2586.5	8.7	2643.7	8.8	2643.7	8.8	95.1
7 -Spot 73	519	83037	2.1	5.3702	0.5	12.6416	1.0	0.4926	0.9	0.87	2581.9	18.4	2653.3	9.4	2708.3	8.1	2708.3	8.1	95.3
7 -Spot 14	90	100305	1.8	5.3562	0.6	13.9549	1.0	0.5423	0.8	0.80	2793.2	18.5	2746.7	9.7	2712.6	10.2	2712.6	10.2	103.0
17 -Spot 3	179	270741	1.4	5.3542	0.5	12.6573	1.1	0.4917	1.0	0.89	2578.1	21.3	2654.5	10.6	2713.2	8.6	2713.2	8.6	95.0
17 -Spot 4	113	71126	1.4	5.1440	0.6	14.1325	1.3	0.5275	1.1	0.89	2730.8	25.4	2758.6	12.2	2779.0	9.6	2779.0	9.6	98.3
7 -Spot 13	38	1646113	1.8	4.6470	0.4	18.1882	1.1	0.6133	1.0	0.93	3083.1	25.6	2999.7	10.8	2944.3	6.5	2944.3	6.5	104.7
7 -Spot 51	32	77367	1.5	4.5483	0.6	18.1961	1.4	0.6005	1.3	0.90	3031.9	30.3	3000.2	13.4	2979.0	9.8	2979.0	9.8	101.8
7 -Spot 36	123	166672	1.6	4.2953	0.5	20.2506	1.0	0.6311	0.8	0.84	3154.0	21.0	3103.4	9.7	3070.8	8.7	3070.8	8.7	102.7
7 -Spot 74	77	370807	1.3	3.9860	0.6	23.4844	1.2	0.6792	1.1	0.88	3341.3	27.8	3247.2	11.8	3189.6	9.1	3189.6	9.1	104.8
7 -Spot 68	86	129084	1.3	3.9812	0.6	23.2499	1.3	0.6716	1.2	0.88	3312.1	29.9	3237.5	12.7	3191.5	9.7	3191.5	9.7	103.8
7 -Spot 78	279	891167	1.6	3.8410	0.5	22.7452	1.1	0.6339	1.0	0.87	3165.0	23.8	3216.1	10.6	3248.1	8.5	3248.1	8.5	97.4
7 -Spot 79	115	13083	2.8	3.8333	0.6	21.1512	1.3	0.5883	1.2	0.89	2982.5	27.6	3145.5	12.6	3251.3	9.2	3251.3	9.2	91.7

Table DTB17-18. U-Pb geochronologic analyses.

						Isotope ratios						Apparent ages (Ma)							
Analysis	U	206Pb	U/Th	206Pb*	±	207Pb*	±	206Pb*	±	error	206Pb*	±	207Pb*	±	206Pb*	±	Best age	±	Conc
	(ppm)	204Pb		207Pb*	(%)	235U*	(%)	238U	(%)	corr.	238U*	(Ma)	235U	(Ma)	207Pb*	(Ma)	(Ma)	(Ma)	(%)
8 -Spot 66	587	60278	3.9	14.1246	0.7	1.2308	1.5	0.1261	1.3	0.88	765.8	9.6	814.7	8.5	950.7	14.7	765.8	9.6	80.5
8 -Spot 95	220	40850	6.7	13.7961	0.8	1.6906	1.3	0.1692	1.1	0.81	1007.9	10.2	1005.0	8.6	998.7	16.1	998.7	16.1	100.9
8 -Spot 92	194	38933	1.5	13.7158	0.9	1.7182	1.5	0.1710	1.3	0.81	1017.6	11.8	1015.3	9.9	1010.5	18.1	1010.5	18.1	100.7
8 -Spot 46	112	226764	1.8	13.5146	0.7	1.7827	1.6	0.1748	1.4	0.88	1038.6	13.3	1039.2	10.2	1040.4	14.9	1040.4	14.9	99.8
8 -Spot 13	45	9555	1.5	13.4078	1.1	1.7613	1.5	0.1713	1.0	0.69	1019.5	9.9	1031.3	9.9	1056.4	22.4	1056.4	22.4	96.5
8 -Spot 67	125	46346	1.2	13.3435	0.8	1.8290	1.4	0.1771	1.2	0.81	1051.0	11.4	1055.9	9.5	1066.1	16.9	1066.1	16.9	98.6
8 -Spot 10	207	217253	1.6	13.2703	0.6	1.8522	1.4	0.1783	1.3	0.90	1057.9	12.3	1064.2	9.3	1077.1	12.3	1077.1	12.3	98.2
8 -Spot 38	150	92054	2.2	13.2664	0.6	1.8805	1.3	0.1810	1.2	0.88	1072.5	11.5	1074.2	8.7	1077.7	12.4	1077.7	12.4	99.5
8 -Spot 54	217	1077988	3.0	13.2223	0.6	1.8445	1.3	0.1770	1.1	0.88	1050.3	10.8	1061.5	8.3	1084.4	12.0	1084.4	12.0	96.9
8 -Spot 22	92	33911	2.0	13.1335	0.7	1.8494	1.5	0.1762	1.3	0.88	1046.4	12.5	1063.2	9.7	1097.9	14.1	1097.9	14.1	95.3
8 -Spot 74	185	54430	1.5	13.0951	0.8	1.9419	1.2	0.1845	0.9	0.72	1091.6	8.6	1095.7	8.0	1103.8	16.8	1103.8	16.8	98.9
8 -Spot 59	36	91919	1.5	13.0582	1.0	1.8813	1.4	0.1783	1.0	0.73	1057.4	10.2	1074.5	9.5	1109.4	19.7	1109.4	19.7	95.3
8 -Spot 11	175	28529	77.8	13.0417	0.9	1.9115	1.5	0.1809	1.2	0.78	1071.8	11.7	1085.1	10.1	1111.9	19.0	1111.9	19.0	96.4
-Spot 113	308	521576	2.9	12.8446	0.6	2.0712	1.3	0.1930	1.2	0.89	1137.8	12.3	1139.3	9.0	1142.3	11.8	1142.3	11.8	99.6
18 -Spot 2	92	18704	3.0	12.8247	0.8	1.9727	1.4	0.1836	1.2	0.85	1086.4	12.1	1106.2	9.7	1145.3	15.3	1145.3	15.3	94.9
8 -Spot 85	209	137304	2.7	12.8139	0.7	1.8311	1.2	0.1702	1.0	0.80	1013.5	9.2	1056.7	8.1	1147.0	14.6	1147.0	14.6	88.4
8 -Spot 12	143	44395	3.0	12.7895	0.6	2.1789	1.4	0.2022	1.3	0.90	1187.1	13.7	1174.3	9.8	1150.8	12.0	1150.8	12.0	103.2
8 -Spot 34	215	104590	1.7	12.7714	0.7	2.0443	1.2	0.1894	1.1	0.85	1118.3	10.9	1130.4	8.5	1153.6	13.0	1153.6	13.0	96.9
8 -Spot 91	35	10634	2.5	12.7690	0.8	2.1564	1.2	0.1998	0.9	0.72	1174.2	9.3	1167.1	8.3	1154.0	16.4	1154.0	16.4	101.7
8 -Spot 71	226	292384	1.8	12.7438	0.8	1.9802	1.7	0.1831	1.5	0.88	1083.9	15.0	1108.8	11.5	1157.9	15.8	1157.9	15.8	93.6
8 -Spot 50	246	37835	3.7	12.7386	0.8	2.1021	1.3	0.1943	1.0	0.80	1144.6	11.0	1149.5	9.0	1158.7	15.7	1158.7	15.7	98.8
18 -Spot 7	396	108436	2.0	12.6837	0.8	1.9909	1.6	0.1832	1.3	0.85	1084.6	13.1	1112.4	10.5	1167.3	16.5	1167.3	16.5	92.9
8 -Spot 36	374	45051	0.8	12.6459	0.7	2.1599	1.5	0.1982	1.3	0.88	1165.6	13.8	1168.2	10.2	1173.2	13.5	1173.2	13.5	99.3
18 -Spot 3	206	65135	2.2	12.6029	0.9	2.1827	1.5	0.1996	1.3	0.83	1173.2	13.7	1175.6	10.8	1180.0	17.2	1180.0	17.2	99.4
8 -Spot 96	34	20510	2.3	12.5928	1.3	2.1223	2.0	0.1939	1.5	0.75	1142.6	15.5	1156.1	13.7	1181.5	26.1	1181.5	26.1	96.7
8 -Spot 58	49	36015	1.9	12.5927	0.9	2.2908	1.6	0.2093	1.3	0.81	1225.2	14.5	1209.5	11.4	1181.6	18.6	1181.6	18.6	103.7
8 -Spot 76	66	62129	1.7	12.5881	1.0	2.2025	1.4	0.2012	1.0	0.73	1181.6	11.2	1181.8	10.0	1182.3	19.3	1182.3	19.3	99.9
8 -Spot 60	237	576087	5.2	12.5828	0.7	2.1571	1.3	0.1969	1.1	0.83	1158.9	11.7	1167.3	9.2	1183.1	14.6	1183.1	14.6	98.0
-Spot 120	70	46688	1.6	12.5821	0.9	2.1378	1.3	0.1952	0.9	0.71	1149.3	9.8	1161.1	9.0	1183.2	18.2	1183.2	18.2	97.1
8 -Spot 49	198	364290	1.1	12.5721	0.7	2.1643	1.2	0.1974	1.0	0.82	1161.5	10.5	1169.6	8.3	1184.8	13.3	1184.8	13.3	98.0
18 -Spot 1	110	38454	1.4	12.5551	0.7	2.1586	1.3	0.1966	1.1	0.83	1157.3	11.2	1167.8	8.8	1187.5	14.1	1187.5	14.1	97.5
8 -Spot 17	141	261599	3.5	12.5485	0.8	2.1335	1.4	0.1943	1.1	0.82	1144.4	11.8	1159.7	9.5	1188.5	15.7	1188.5	15.7	96.3
-Spot 118	166	75774	13.5	12.5407	0.9	2.1497	1.5	0.1956	1.2	0.78	1151.7	12.3	1165.0	10.4	1189.7	18.6	1189.7	18.6	96.8
8 -Spot 87	83	21561	2.4	12.4995	0.8	2.1933	1.4	0.1989	1.1	0.82	1169.5	11.9	1178.9	9.5	1196.2	15.2	1196.2	15.2	97.8
-Spot 109	127	150610	2.2	12.4931	0.8	2.1913	1.4	0.1986	1.1	0.82	1168.0	11.9	1178.3	9.5	1197.2	15.5	1197.2	15.5	97.6
8 -Spot 33	114	354573	1.9	12.4912	0.8	2.1581	1.5	0.1956	1.2	0.82	1151.6	12.7	1167.7	10.1	1197.5	16.3	1197.5	16.3	96.2
18 -Spot 4	472	184573	3.5	12.4609	0.7	2.3602	1.3	0.2134	1.1	0.84	1246.9	12.8	1230.6	9.6	1202.3	14.5	1202.3	14.5	103.7
8 -Spot 25	176	101536	2.3	12.4499	0.8	2.1972	1.5	0.1985	1.2	0.83	1167.2	13.3	1180.2	10.5	1204.1	16.4	1204.1	16.4	96.9
8 -Spot 39	68	36552	1.8	12.3644	0.9	2.1338	1.3	0.1914	0.9	0.71	1129.1	9.3	1159.8	8.8	1217.6	17.6	1217.6	17.6	92.7
8 -Spot 88	250	23534	2.0	12.2102	0.8	2.2604	1.1	0.2003	0.8	0.71	1176.7	8.7	1200.0	8.0	1242.2	15.9	1242.2	15.9	94.7
8 -Spot 70	131	66599	2.4	12.2079	0.8	2.3911	1.6	0.2118	1.4	0.88	1238.4	15.9	1239.9	11.5	1242.6	15.1	1242.6	15.1	99.7
8 -Spot 51	235	75917	2.0	11.6776	0.7	2.6255	1.3	0.2225	1.0	0.84	1294.9	12.3	1307.8	9.2	1329.1	13.4	1329.1	13.4	97.4
8 -Spot 65	197	57355	1.8	11.6376	0.6	2.7752	1.1	0.2343	0.9	0.83	1357.2	10.7	1348.9	7.9	1335.7	11.2	1335.7	11.2	101.6
8 -Spot 63	296	126503	1.8	11.6174	0.4	2.7388	1.0	0.2309	0.9	0.90	1339.0	10.7	1339.0	7.3	1339.1	8.1	1339.1	8.1	100.0

-Spot 103	273	84815	1.8	11.6035	0.7	2.5976	1.2	0.2187	1.0	0.84	1275.0	11.8	1300.0	9.0	1341.4	12.9	1341.4	12.9	95.1
8 -Spot 24	393	590274	2.3	11.5039	0.8	2.8125	1.4	0.2348	1.2	0.82	1359.4	14.4	1358.9	10.8	1358.0	16.0	1358.0	16.0	100.1
8 -Spot 83	74	14423	2.6	11.4969	0.8	2.8828	1.3	0.2405	1.0	0.78	1389.2	12.3	1377.4	9.5	1359.2	15.4	1359.2	15.4	102.2
-Spot 102	350	74318	3.0	11.4811	0.7	2.7967	1.2	0.2330	0.9	0.78	1350.1	11.3	1354.7	8.9	1361.8	14.4	1361.8	14.4	99.1
8 -Spot 68	616	280479	1.8	11.1803	0.9	3.0207	1.7	0.2450	1.4	0.85	1412.9	18.3	1412.9	12.9	1412.8	16.8	1412.8	16.8	100.0
-18 -Spot 9	121	66876	2.0	11.1474	0.8	3.1202	1.5	0.2524	1.3	0.85	1450.7	16.3	1437.7	11.3	1418.4	14.7	1418.4	14.7	102.3
8 -Spot 47	312	52957	1.3	11.1437	0.6	3.1009	1.3	0.2507	1.1	0.89	1442.2	14.6	1432.9	9.7	1419.1	10.8	1419.1	10.8	101.6
8 -Spot 78	41	31140	1.8	11.1235	1.0	2.8382	1.5	0.2291	1.2	0.76	1329.6	14.1	1365.7	11.6	1422.5	19.2	1422.5	19.2	93.5
8 -Spot 89	249	53940	1.8	11.1178	0.7	2.9646	1.3	0.2391	1.1	0.84	1382.3	13.3	1398.6	9.7	1423.5	13.3	1423.5	13.3	97.1
8 -Spot 55	159	148149	2.1	11.0655	0.7	3.0285	1.5	0.2432	1.4	0.89	1403.1	17.0	1414.8	11.6	1432.5	13.2	1432.5	13.2	97.9
8 -Spot 80	287	73552	0.7	11.0568	0.7	3.1178	1.2	0.2501	1.0	0.81	1439.2	12.9	1437.1	9.5	1434.0	13.8	1434.0	13.8	100.4
8 -Spot 19	149	61208	4.1	11.0276	0.9	3.2022	1.8	0.2562	1.5	0.87	1470.5	20.1	1457.7	13.6	1439.1	16.6	1439.1	16.6	102.2
8 -Spot 44	217	59055	2.5	11.0060	0.5	3.1379	1.4	0.2506	1.3	0.92	1441.5	16.7	1442.0	10.8	1442.8	10.3	1442.8	10.3	99.9
8 -Spot 14	117	149025	2.2	10.9775	0.8	3.1697	1.3	0.2525	1.1	0.82	1451.2	14.1	1449.8	10.2	1447.8	14.4	1447.8	14.4	100.2
-Spot 116	433	148320	2.1	10.9757	0.7	3.1869	1.4	0.2538	1.2	0.87	1458.0	15.9	1454.0	10.9	1448.1	13.4	1448.1	13.4	100.7
8 -Spot 42	296	67380	2.5	10.9512	0.7	3.1454	1.2	0.2499	0.9	0.80	1438.2	12.2	1443.9	9.1	1452.3	13.4	1452.3	13.4	99.0
-Spot 107	163	149986	1.8	10.9110	0.8	3.2049	1.3	0.2537	1.0	0.78	1457.7	13.2	1458.3	10.1	1459.3	15.5	1459.3	15.5	99.9
8 -Spot 84	423	68120	2.7	10.9046	0.7	3.1758	1.2	0.2513	1.0	0.81	1445.0	12.6	1451.3	9.3	1460.4	13.5	1460.4	13.5	98.9
8 -Spot 56	190	94392	2.3	10.8071	0.7	3.2237	1.3	0.2528	1.1	0.86	1452.8	14.9	1462.9	10.3	1477.5	12.7	1477.5	12.7	98.3
8 -Spot 61	371	74064	2.6	10.7962	0.6	3.1796	1.2	0.2491	1.0	0.86	1433.7	13.3	1452.2	9.4	1479.4	11.9	1479.4	11.9	96.9
8 -Spot 57	271	75231	2.2	10.7774	0.6	3.2182	1.2	0.2517	1.0	0.84	1447.0	13.0	1461.5	9.2	1482.7	12.2	1482.7	12.2	97.6
8 -Spot 40	49	21797	2.6	10.7555	0.9	3.2757	1.4	0.2556	1.1	0.75	1467.5	14.1	1475.3	11.1	1486.6	17.8	1486.6	17.8	98.7
-Spot 117	134	27152	1.9	10.7453	0.6	3.1755	1.2	0.2476	1.0	0.83	1426.0	12.4	1451.2	9.0	1488.3	12.2	1488.3	12.2	95.8
8 -Spot 26	77	33306	2.5	10.7285	0.9	3.3867	1.5	0.2636	1.2	0.81	1508.4	16.3	1501.3	11.8	1491.3	16.8	1491.3	16.8	101.1
8 -Spot 97	71	29734	1.8	10.5947	1.0	3.4559	1.5	0.2657	1.1	0.72	1518.8	14.4	1517.2	11.6	1515.0	19.2	1515.0	19.2	100.2
8 -Spot 41	150	32530	2.2	10.3054	0.7	3.6662	1.3	0.2741	1.1	0.86	1561.8	15.3	1564.0	10.2	1567.1	12.2	1567.1	12.2	99.7
8 -Spot 35	254	60042	1.7	10.2574	0.5	3.7447	1.2	0.2787	1.1	0.90	1584.8	15.7	1581.0	9.9	1575.8	10.0	1575.8	10.0	100.6
8 -Spot 93	443	2057198	5.8	10.0719	0.5	3.8805	1.1	0.2836	0.9	0.86	1609.4	13.3	1609.6	8.7	1609.9	10.1	1609.9	10.1	100.0
8 -Spot 29	585	3235842	3.5	10.0348	0.9	3.4792	1.5	0.2533	1.2	0.81	1455.6	15.6	1522.5	11.7	1616.8	16.2	1616.8	16.2	90.0
8 -Spot 98	190	35354	2.3	9.9182	0.6	3.6309	1.4	0.2613	1.3	0.90	1496.5	16.9	1556.3	11.3	1638.5	11.7	1638.5	11.7	91.3
-Spot 108	249	292854	1.8	9.7917	0.7	4.2762	1.2	0.3038	1.0	0.82	1710.2	14.7	1688.8	9.8	1662.3	12.4	1662.3	12.4	102.9
8 -Spot 28	264	60122	2.9	9.7889	0.6	4.2404	1.4	0.3012	1.2	0.89	1697.2	18.5	1681.9	11.4	1662.8	11.5	1662.8	11.5	102.1
8 -Spot 99	134	76909	1.0	9.6948	0.8	4.1694	1.6	0.2933	1.4	0.86	1657.9	19.8	1668.0	12.9	1680.7	14.9	1680.7	14.9	98.6
-Spot 112	494	52970	1.9	9.6348	0.7	3.6979	1.5	0.2585	1.3	0.88	1482.2	16.8	1570.9	11.6	1692.2	12.9	1692.2	12.9	87.6
8 -Spot 21	310	3673510	2.5	9.5931	0.8	4.3382	1.6	0.3020	1.4	0.88	1701.0	21.6	1700.7	13.5	1700.2	14.3	1700.2	14.3	100.1
8 -Spot 72	627	161690	2.4	9.5613	0.8	4.2457	1.5	0.2945	1.3	0.85	1664.2	19.3	1682.9	12.7	1706.3	14.9	1706.3	14.9	97.5
8 -Spot 30	553	413835	3.6	9.4650	0.7	4.4744	1.6	0.3073	1.4	0.90	1727.3	21.8	1726.2	13.2	1724.9	12.5	1724.9	12.5	100.1
8 -Spot 90	352	131768	0.8	9.4092	0.9	4.2220	1.5	0.2882	1.2	0.79	1632.7	16.7	1678.3	12.0	1735.7	16.5	1735.7	16.5	94.1
8 -Spot 86	260	826804	2.0	9.3630	0.7	4.5228	1.5	0.3073	1.3	0.87	1727.2	19.8	1735.2	12.5	1744.7	13.7	1744.7	13.7	99.0
8 -Spot 37	229	360174	1.2	9.3627	0.8	4.2782	1.2	0.2906	1.0	0.79	1644.7	14.2	1689.2	10.3	1744.8	14.1	1744.8	14.1	94.3
-Spot 115	203	72671	1.8	9.3527	0.6	4.4410	1.0	0.3014	0.8	0.82	1698.1	12.0	1720.0	8.1	1746.8	10.2	1746.8	10.2	97.2
8 -Spot 23	293	317144	2.4	9.3107	0.6	4.6237	1.3	0.3124	1.1	0.87	1752.3	17.6	1753.6	11.0	1755.0	11.8	1755.0	11.8	99.8
8 -Spot 75	202	343083	1.8	9.2796	0.6	4.5504	1.0	0.3064	0.9	0.82	1722.9	12.9	1740.2	8.7	1761.1	11.0	1761.1	11.0	97.8
8 -Spot 94	389	405545	3.7	9.2625	0.7	4.7651	1.4	0.3203	1.2	0.87	1791.0	19.4	1778.8	11.9	1764.5	12.7	1764.5	12.7	101.5
-Spot 105	275	464363	4.9	9.1389	0.7	4.7795	1.1	0.3169	0.9	0.80	1774.7	14.2	1781.3	9.6	1789.0	12.4	1789.0	12.4	99.2
8 -Spot 32	431	110453	2.2	9.0705	0.8	4.7888	1.7	0.3152	1.5	0.88	1766.1	22.5	1782.9	14.0	1802.7	14.5	1802.7	14.5	98.0
8 -Spot 15	249	45480	2.8	8.8549	0.7	4.5041	1.5	0.2894	1.3	0.89	1638.5	19.0	1731.7	12.2	1846.3	12.0	1846.3	12.0	88.7
8 -Spot 62	222	297227	4.6	8.7955	0.7	5.3440	1.2	0.3410	1.0	0.82	1891.7	15.9	1875.9	10.1	1858.5	12.1	1858.5	12.1	101.8
8 -Spot 53	165	67110	1.2	8.4011	0.8	5.7287	1.4	0.3492	1.1	0.82	1930.8	18.6	1935.7	11.7	1941.0	13.7	1941.0	13.7	99.5
8 -Spot 27	193	28248478	3.1	6.1466	0.7	10.6052	1.3	0.4730	1.1	0.85	2496.6	23.7	2489.2	12.5	2483.1	11.9	2483.1	11.9	100.5
8 -Spot 52	420	8623027	3.0	5.8263	0.6	11.8571	1.3	0.5013	1.2	0.88	2619.2	25.5	2593.2	12.6	2572.9	10.5	2572.9	10.5	101.8
-Spot 101	215	253983	1.4	5.6969	0.5	12.5906	1.1	0.5204	1.0	0.89	2701.0	22.1	2649.5	10.6	2610.4	8.4	2610.4	8.4	103.5
-Spot 111	216	85154	1.3	5.6123	0.6	12.7559	1.3	0.5194	1.1	0.87	2696.8	25.0	2661.8	12.3	2635.3	10.7	2635.3	10.7	102.3
8 -Spot 64	610	46106	1.6	5.5761	0.6	10.5164	1.2	0.4255	1.1	0.87	2285.3	20.3	2481.4	11.3	2646.0	9.9	2646.0	9.9	86.4
8 -Spot 16	51	72308	1.1	5.4904	0.8	13.0080	1.3	0.5182	1.1	0.81	2691.6	24.0	2680.2	12.7	2671.7	13.1	2671.7	13.1	100.7
8 -Spot 20	36	36280	3.7	5.4443	0.9	12.7171	1.5	0.5024	1.2	0.79	2623.9	25.0	2658.9	13.9	2685.6	15.0	2685.6	15.0	97.7
8 -Spot 45	8	21309	0.8	5.3928	1.0	12.8255	2.3	0.5018	2.0	0.90	2621.7	43.5	2666.9	21.2	2701.3	16.4	2701.3	16.4	97.1
-18 -Spot 8	124	72139	2.1	5.3922	0.7	13.3408	1.2	0.5220	0.9	0.81	2707.5	21.0	2704.1	11.1	2701.5	11.5	2701.5	11.5	100.2
-Spot 104	48	348209	1.5	5.3672	0.6	13.6938	1.3	0.5333	1.1	0.86	2755.3	24.3	2728.8	11.9	2709.2	10.6	2709.2	10.6	101.7
8 -Spot 69	16	12127	3.2	5.3653	0.8	12.8116	1.4	0.4987	1.1	0.81	2608.4	24.1	2665.9	13.1	2709.8	13.5	2709.8	13.5	96.3
8 -Spot 18	54	25970374	1.3	5.3584	0.7	13.2678	1.4	0.5159	1.2	0.87	2681.6	26.5	2698.9	13.1	2711.9	11.1	2711.9	11.1	98.9
-Spot 119	131	191671	1.9	5.3311	0.7	11.1371	1.5	0.4308	1.3	0.88	2309.3	25.3	2534.7	13.7	2720.3	11.3	2720.3	11.3	84.9
-Spot 106	211	137543	1.3	5.2444	0.7	14.5513	1.4	0.5537	1.2	0.85	2840.6	26.9	2786.4	13.1	2747.3	12.0	2747.3	12.0	103.4
8 -Spot 73	152	90469	1.1	4.9893	0.6	15.3424	1.4	0.5554	1.2	0.89	2847.7	28.1	2836.7	13.1	2829.0	10.2	2829.0	10.2	100.7
-Spot 100	128	72585	2.1	4.4400	0.7	18.4556	1.4	0.5946	1.2	0.87	3007.9	29.8	3013.8	13.7	3017.7	11.2	3017.7	11.2	99.7
8 -Spot 48	184	198110	2.0	4.1217	0.7	20.3793	1.3	0.6095	1.1	0.85	3067.9	26.7	3109.5	12.5	3136.5	11.0	3136.5	11.0	97.8

Table DTB17-19. U-Pb geochronologic analyses.

						Isotope ratios						Apparent ages (Ma)							
Analysis	U	206Pb	U/Th	206Pb*	±	207Pb*	±	206Pb*	±	error	206Pb*	±	207Pb*	±	206Pb*	±	Best age	±	Conc
	(ppm)	204Pb		207Pb*	(%)	235U*	(%)	238U	(%)	corr.	238U*	(Ma)	235U	(Ma)	207Pb*	(Ma)	(Ma)	(Ma)	(%)
-Spot 52	3466	2949	1.7	8.4232	4.9	0.6085	5.1	0.0372	1.5	0.29	235.4	3.5	482.6	19.5	1936.2	86.9	235.4	3.5	NA
-Spot 60	201	213348	3.2	16.0118	0.7	0.9162	1.3	0.1064	1.1	0.83	652.1	6.5	660.4	6.2	688.7	15.3	652.1	6.5	94.7
-Spot 31	137	79060	2.0	16.2409	0.9	0.9159	1.4	0.1079	1.2	0.81	660.7	7.3	660.2	7.0	658.4	18.2	660.7	7.3	100.4
-Spot 117	38	14993	2.5	14.0350	1.2	1.5432	1.8	0.1572	1.3	0.75	941.0	11.6	947.8	10.9	963.7	24.0	963.7	24.0	97.6
-Spot 14	73	22119	5.1	13.6943	0.9	1.6205	1.6	0.1610	1.3	0.84	962.4	11.7	978.2	9.8	1013.7	17.4	1013.7	17.4	94.9
-Spot 34	56	61312	2.2	13.5871	0.9	1.7542	1.5	0.1729	1.1	0.77	1028.3	10.7	1028.7	9.4	1029.6	18.6	1029.6	18.6	99.9
-Spot 21	15	7529	1.0	13.4952	1.4	1.8230	1.9	0.1785	1.4	0.71	1058.8	13.4	1053.8	12.7	1043.3	27.7	1043.3	27.7	101.5
-Spot 35	339	105462	1.4	13.4860	1.0	1.6104	1.8	0.1576	1.5	0.84	943.3	13.4	974.3	11.4	1044.7	20.1	1044.7	20.1	90.3
-Spot 115	85	55123	3.7	13.4270	0.9	1.7888	1.7	0.1743	1.4	0.82	1035.6	12.9	1041.4	10.8	1053.6	19.1	1053.6	19.1	98.3
-Spot 37	70	46517	3.6	13.4211	1.0	1.9121	1.6	0.1862	1.2	0.76	1100.8	12.0	1085.3	10.3	1054.4	20.2	1054.4	20.2	104.4
-Spot 106	144	100875	3.0	13.3492	0.8	1.8549	1.4	0.1797	1.1	0.83	1065.2	11.1	1065.2	9.0	1065.3	15.1	1065.3	15.1	100.0
-Spot 72	193	72683	4.1	13.3182	0.7	1.7495	1.3	0.1691	1.1	0.86	1007.0	10.6	1027.0	8.6	1069.9	13.8	1069.9	13.8	94.1
-Spot 43	126	60409	7.8	13.1465	1.0	1.8666	1.7	0.1781	1.4	0.83	1056.3	13.8	1069.3	11.3	1095.9	19.2	1095.9	19.2	96.4
-Spot 93	36	4374	2.7	12.8941	1.1	2.0350	1.7	0.1904	1.4	0.78	1123.5	14.0	1127.3	11.8	1134.6	21.5	1134.6	21.5	99.0
-Spot 48	112	195758	3.1	12.8941	0.9	1.9857	1.5	0.1858	1.2	0.79	1098.5	11.7	1110.7	9.9	1134.6	18.0	1134.6	18.0	96.8
-Spot 120	66	32296	2.7	12.8876	0.8	2.1409	1.5	0.2002	1.3	0.87	1176.4	14.0	1162.1	10.4	1135.7	15.0	1135.7	15.0	103.6
-Spot 87	350	177803	1.4	12.8786	0.6	2.0666	1.2	0.1931	1.1	0.87	1138.2	11.1	1137.8	8.4	1137.0	12.0	1137.0	12.0	100.1
-Spot 107	70	24366	2.7	12.8305	0.9	2.0458	1.5	0.1905	1.2	0.80	1123.8	12.4	1130.9	10.3	1144.5	18.1	1144.5	18.1	98.2
-Spot 17	298	99375	2.7	12.8173	0.6	1.9232	1.3	0.1789	1.2	0.89	1060.7	11.6	1089.2	8.9	1146.5	12.0	1146.5	12.0	92.5
-Spot 102	198	122827	3.6	12.7724	0.8	2.1024	1.6	0.1948	1.4	0.87	1147.6	14.4	1149.6	10.8	1153.4	15.5	1153.4	15.5	99.5
-Spot 29	180	131297	6.0	12.7080	0.8	2.0246	1.3	0.1867	1.0	0.80	1103.4	10.4	1123.8	8.8	1163.5	15.4	1163.5	15.4	94.8
-Spot 71	104	64706	3.0	12.6749	0.8	2.1064	1.6	0.1937	1.4	0.88	1141.5	14.8	1150.9	11.1	1168.7	15.1	1168.7	15.1	97.7

-Spot 99	163	83928	2.8	12.6655	0.9	2.1569	1.6	0.1982	1.3	0.82	1165.7	13.8	1167.3	10.9	1170.2	17.7	1170.2	17.7	99.6
-Spot 24	116	386044	3.9	12.6430	0.6	2.0873	1.4	0.1915	1.2	0.88	1129.4	12.5	1144.6	9.4	1173.7	12.8	1173.7	12.8	96.2
-Spot 26	100	67526	5.2	12.6218	1.0	2.1004	1.6	0.1924	1.2	0.76	1134.1	12.8	1148.9	11.1	1177.0	20.8	1177.0	20.8	96.4
-Spot 62	150	45918	2.6	12.4897	0.8	2.2135	1.5	0.2006	1.3	0.86	1178.5	14.1	1185.3	10.6	1197.8	15.2	1197.8	15.2	98.4
-Spot 88	91	93289	3.3	12.2764	0.9	2.1410	1.6	0.1907	1.4	0.84	1125.2	14.2	1162.1	11.3	1231.7	17.3	1231.7	17.3	91.4
-Spot 109	377	343237	4.1	12.0987	0.8	2.5161	1.2	0.2209	0.9	0.76	1286.5	10.6	1276.7	8.7	1260.2	15.2	1260.2	15.2	102.1
-Spot 105	99	1105209	2.5	12.0001	0.7	2.4538	1.4	0.2137	1.2	0.87	1248.2	14.0	1258.5	10.2	1276.2	13.6	1276.2	13.6	97.8
-Spot 12	174	94507	1.8	11.7436	0.6	2.6106	1.1	0.2224	0.9	0.85	1294.8	10.9	1303.6	8.0	1318.2	11.2	1318.2	11.2	98.2
-Spot 111	139	59780	4.4	11.6298	0.6	2.7074	1.3	0.2285	1.1	0.87	1326.4	13.3	1330.5	9.5	1337.0	12.1	1337.0	12.1	99.2
-Spot 16	908	673224	3.2	11.4987	0.5	2.5470	1.2	0.2125	1.0	0.90	1242.1	11.8	1285.6	8.4	1358.9	9.7	1358.9	9.7	91.4
-Spot 91	47	3867	2.3	11.4311	0.9	2.7426	1.2	0.2275	0.7	0.58	1321.2	8.0	1340.1	8.6	1370.3	18.1	1370.3	18.1	96.4
-Spot 79	116	251969	1.2	11.4079	0.8	2.8814	1.4	0.2385	1.1	0.82	1378.9	13.8	1377.0	10.2	1374.2	15.0	1374.2	15.0	100.3
-Spot 113	166	226025	2.5	11.3975	0.7	2.8319	1.3	0.2342	1.1	0.82	1356.5	13.1	1364.0	9.8	1375.9	14.3	1375.9	14.3	98.6
-Spot 15	57	101133	4.7	11.3943	0.9	2.7308	1.5	0.2258	1.2	0.81	1312.3	14.7	1336.9	11.3	1376.5	17.0	1376.5	17.0	95.3
-Spot 73	75	74339	3.2	11.3791	0.9	2.8015	1.5	0.2313	1.3	0.83	1341.3	15.3	1355.9	11.4	1379.0	16.5	1379.0	16.5	97.3
-Spot 92	249	79448	3.3	11.3565	0.6	2.9636	1.1	0.2442	0.9	0.86	1408.5	11.9	1398.3	8.3	1382.8	10.8	1382.8	10.8	101.9
-Spot 57	48	17131	2.2	11.3134	0.9	2.7837	1.7	0.2285	1.4	0.84	1326.7	16.6	1351.2	12.3	1390.1	17.2	1390.1	17.2	95.4
-Spot 110	101	68431	3.2	11.3107	0.8	2.8487	1.5	0.2338	1.3	0.83	1354.3	15.3	1368.5	11.3	1390.6	15.9	1390.6	15.9	97.4
-Spot 67	370	104826	3.3	11.1731	0.7	2.4310	1.6	0.1971	1.4	0.90	1159.6	15.0	1251.8	11.4	1414.0	13.5	1414.0	13.5	82.0
-Spot 119	458	69145	0.8	11.1340	0.6	2.3879	1.4	0.1929	1.3	0.90	1137.1	13.6	1239.0	10.4	1420.7	11.9	1420.7	11.9	80.0
-Spot 4	139	99120	2.4	11.0641	0.7	3.0992	1.5	0.2488	1.3	0.89	1432.3	17.2	1432.5	11.5	1432.8	13.0	1432.8	13.0	100.0
-Spot 114	130	64876	4.0	11.0400	0.7	3.0785	1.2	0.2466	1.0	0.82	1420.9	12.6	1427.4	9.2	1436.9	13.3	1436.9	13.3	98.9
-Spot 61	325	2035922	2.5	11.0392	0.5	3.1875	1.4	0.2553	1.3	0.93	1465.8	16.6	1454.1	10.5	1437.1	9.3	1437.1	9.3	102.0
-Spot 25	304	1646463	4.1	10.9439	1.0	3.0858	1.6	0.2450	1.3	0.81	1412.8	16.7	1429.2	12.5	1453.6	18.1	1453.6	18.1	97.2
-Spot 64	182	93273	1.9	10.9051	0.6	2.8501	1.3	0.2255	1.1	0.86	1310.9	12.9	1368.8	9.5	1460.3	12.0	1460.3	12.0	89.8
-Spot 82	99	288836	2.8	10.9037	0.7	3.0767	1.2	0.2434	1.0	0.82	1404.4	12.4	1426.9	9.1	1460.6	12.9	1460.6	12.9	96.2
-Spot 33	158	961232	2.2	10.8349	0.9	3.1821	1.5	0.2502	1.3	0.83	1439.3	16.4	1452.8	11.8	1472.6	16.2	1472.6	16.2	97.7
-Spot 30	73	2753626	1.9	10.0628	0.8	3.8153	1.5	0.2786	1.2	0.84	1584.2	17.3	1596.0	11.9	1611.6	15.1	1611.6	15.1	98.3
-Spot 22	404	384724	4.5	9.9605	0.6	4.0066	1.3	0.2896	1.2	0.88	1639.3	17.1	1635.5	10.9	1630.6	11.7	1630.6	11.7	100.5
-Spot 112	455	384352	8.5	9.9422	0.7	4.0661	1.2	0.2933	1.0	0.82	1658.1	14.9	1647.5	10.1	1634.0	13.2	1634.0	13.2	101.5
-Spot 47	66	45049	1.0	9.7152	0.7	4.1384	1.2	0.2917	1.0	0.83	1650.1	14.3	1661.9	9.6	1676.8	12.1	1676.8	12.1	98.4
-Spot 70	196	267854	4.6	9.6327	0.7	4.3182	1.6	0.3018	1.4	0.89	1700.3	21.2	1696.8	13.1	1692.6	13.4	1692.6	13.4	100.5
-Spot 13	58	29176	3.3	9.6041	3.1	3.6496	3.5	0.2543	1.6	0.46	1460.7	21.4	1560.4	28.3	1698.1	58.0	1698.1	58.0	86.0
-Spot 51	100	877764	1.2	9.5120	0.8	4.3109	1.4	0.2975	1.1	0.81	1679.0	16.7	1695.4	11.4	1715.8	14.8	1715.8	14.8	97.9
-Spot 98	189	293264	1.4	9.4083	0.6	4.4270	1.2	0.3022	1.0	0.85	1702.3	14.9	1717.4	9.7	1735.9	11.3	1735.9	11.3	98.1
-Spot 103	299	189466	1.4	9.3896	0.6	4.6561	1.2	0.3172	1.1	0.88	1776.1	17.0	1759.4	10.3	1739.5	10.6	1739.5	10.6	102.1
-Spot 100	97	70877	1.9	9.3556	0.6	4.4369	1.0	0.3012	0.8	0.79	1697.2	11.9	1719.2	8.4	1746.2	11.4	1746.2	11.4	97.2
-Spot 3	140	412791	1.5	9.2828	0.5	4.7026	1.2	0.3167	1.1	0.89	1773.8	16.4	1767.7	9.9	1760.5	9.8	1760.5	9.8	100.8
-Spot 27	172	141170	4.4	9.2671	0.9	4.3427	1.5	0.2920	1.2	0.79	1651.6	16.8	1701.5	12.0	1763.6	16.3	1763.6	16.3	93.6
-Spot 7	106	481861	1.3	9.2561	0.6	4.7430	1.2	0.3185	1.1	0.87	1782.6	16.7	1774.9	10.4	1765.8	11.3	1765.8	11.3	101.0
-Spot 18	107	401645	1.6	9.2508	0.6	4.7060	1.1	0.3159	0.9	0.83	1769.6	14.4	1768.3	9.4	1766.8	11.5	1766.8	11.5	100.2
-Spot 77	147	156375	2.6	9.2313	0.6	4.4108	1.0	0.2954	0.8	0.83	1668.7	12.3	1714.4	8.4	1770.7	10.3	1770.7	10.3	94.2
-Spot 44	118	102975	1.8	9.1999	0.6	4.6454	1.2	0.3101	1.1	0.86	1741.2	16.2	1757.5	10.3	1776.9	11.5	1776.9	11.5	98.0
-Spot 50	258	188376	2.9	9.1485	0.6	4.9060	1.2	0.3257	1.0	0.85	1817.3	16.5	1803.3	10.3	1787.1	11.5	1787.1	11.5	101.7
-Spot 54	103	450299	1.5	9.0582	0.8	4.8207	1.2	0.3168	1.0	0.79	1774.3	15.2	1788.5	10.4	1805.1	13.8	1805.1	13.8	98.3
-Spot 23	58	84430	4.4	8.6563	0.9	5.1224	1.5	0.3217	1.2	0.81	1798.2	19.5	1839.8	13.0	1887.2	16.0	1887.2	16.0	95.3
-Spot 20	159	94319	1.7	6.0903	0.8	10.7622	1.4	0.4756	1.2	0.85	2508.0	24.9	2502.8	13.2	2498.6	12.6	2498.6	12.6	100.4
-Spot 45	255	316871	1.2	6.0789	0.7	11.2104	1.4	0.4945	1.2	0.87	2590.0	26.1	2540.8	13.1	2501.7	11.8	2501.7	11.8	103.5
-Spot 81	144	916455	1.2	5.9736	0.9	10.8635	1.5	0.4709	1.3	0.83	2487.3	26.4	2511.5	14.3	2531.1	14.4	2531.1	14.4	98.3
-Spot 58	332	302899	1.8	5.9210	0.7	11.1942	1.8	0.4809	1.6	0.91	2531.3	33.6	2539.4	16.5	2545.9	12.4	2545.9	12.4	99.4
-Spot 1	333	1462639	3.8	5.8863	0.7	10.8958	1.6	0.4654	1.4	0.89	2463.2	29.6	2514.3	15.1	2555.8	12.2	2555.8	12.2	96.4
-Spot 74	550	162112	5.5	5.8805	0.7	8.8085	1.3	0.3758	1.1	0.82	2056.8	18.7	2318.4	11.7	2557.4	12.2	2557.4	12.2	80.4
-Spot 36	268	1355569	1.6	5.8788	0.8	11.8492	1.6	0.5054	1.4	0.87	2637.1	29.8	2592.6	14.8	2557.9	13.0	2557.9	13.0	103.1
-Spot 80	125	119256	1.4	5.8771	0.6	9.4007	2.5	0.4009	2.4	0.97	2173.1	44.2	2377.9	22.5	2558.4	9.2	2558.4	9.2	84.9
-Spot 59	302	192178	1.2	5.8474	0.7	10.3408	1.5	0.4387	1.4	0.90	2345.0	27.1	2465.8	14.1	2566.9	10.9	2566.9	10.9	91.4
-Spot 94	405	94922	3.0	5.8451	1.0	9.5659	1.8	0.4057	1.4	0.81	2195.2	26.6	2393.9	16.2	2567.5	17.3	2567.5	17.3	85.5
-Spot 104	112	361367	1.8	5.7558	0.5	12.4695	1.1	0.5208	1.0	0.88	2702.4	21.7	2640.4	10.5	2593.2	8.9	2593.2	8.9	104.2
-Spot 46	317	1466822	1.1	5.7266	0.6	12.1751	1.3	0.5059	1.2	0.90	2639.1	25.9	2618.0	12.5	2601.7	9.8	2601.7	9.8	101.4
-Spot 101	276	165643	2.2	5.6919	0.6	10.4176	1.3	0.4302	1.1	0.88	2306.8	21.7	2472.6	11.8	2611.8	10.3	2611.8	10.3	88.3
-Spot 118	328	527034	1.7	5.6112	0.9	12.4838	1.5	0.5083	1.2	0.82	2649.2	26.2	2641.5	13.9	2635.6	14.2	2635.6	14.2	100.5
-Spot 85	197	427315	2.6	5.6106	0.7	12.6581	1.2	0.5153	1.0	0.83	2679.2	21.8	2654.6	11.2	2635.8	11.0	2635.8	11.0	101.6
-Spot 96	141	159865	1.8	5.5913	0.7	12.6717	1.2	0.5141	1.0	0.83	2674.0	22.0	2655.6	11.4	2641.5	11.1	2641.5	11.1	101.2
-Spot 11	292	674606	3.0	5.5833	0.7	12.8069	1.1	0.5188	0.9	0.81	2694.2	19.9	2665.5	10.5	2643.9	10.9	2643.9	10.9	101.9
-Spot 41	133	78112	1.6	5.5369	0.6	11.3845	1.3	0.4574	1.2	0.89	2427.9	23.9	2555.2	12.4	2657.7	9.8	2657.7	9.8	91.4
-Spot 32	174	534670	2.0	5.5274	0.7	12.6266	1.4	0.5064	1.2	0.87	2641.2	26.9	2652.2	13.4	2660.6	11.6	2660.6	11.6	99.3
-Spot 86	77	581185	4.0	5.5262	0.7	12.3496	1.0	0.4952	0.8	0.76	2593.1	16.9	2631.4	9.8	2660.9	11.1	2660.9	11.1	97.4
-Spot 97	82	72543	3.1	5.5250	0.8	12.5216	1.6	0.5020	1.4	0.87	2622.3	29.2	2644.4	14.6	2661.3	12.7	2661.3	12.7	98.5
-Spot 69	204	1646565	1.5	5.4878	0.8	12.3465	1.7	0.4916	1.5	0.88	2577.7	31.7	2631.1	15.9	2672.5	13.1	2672.5	13.1	96.5
-Spot 66	21	45436	4.6	5.4871	0.8	12.9133	1.8	0.5141	1.6	0.89	2674.2	34.5	2673.3	16.7	2672.7	13.5	2672.7	13.5	100.1
-Spot 19	26	42139	1.9	5.4416	0.8	12.4821	1.4	0.4928	1.2	0.83	2582.9	25.1	2641.4	13.4	2686.5	13.3	2686.5	13.3	96.1
-Spot 10	160	126764	1.1	5.2911	0.4	14.0351	1.0	0.5388	1.0	0.93	2778.5	21.7	2752.1	9.8	2732.7	6.4	2732.7	6.4	101.7
-Spot 56	42	69863	1.1	5.2852	0.6	13.3243	1.6	0.5110	1.4	0.91	2660.8	31.0	2702.9	14.7	2734.6	10.6	2734.6	10.6	97.3
-Spot 28	303	429327	1.9	5.2734	0.8	12.3001	1.5	0.4706	1.3	0.85	2486.3	25.9	2627.6	13.8	2738.2	12.6	2738.2	12.6	90.8
-Spot 83	114	105371	1.5	4.9511	0.7	15.5523	1.3	0.5587	1.1	0.83	2861.3	24.5	2849.7	12.3	2841.5	11.8	2841.5	11.8	100.7
-Spot 78	48	73484	1.8	4.7911	0.6	14.9282	1.2	0.5190	1.1	0.88	2694.8	23.2	2810.7	11.4	2894.9	9.1	2894.9	9.1	93.1
-Spot 5	49	133407	2.0	4.7195	0.6	16.5129	1.2	0.5655	1.0	0.83	2889.2	22.5	2907.0	11.1	2919.3	10.5	2919.3	10.5	99.0
-Spot 89	46	247876	2.2	4.0785	0.7	21.4953	1.4	0.6361	1.2	0.85	3173.7	29.6	3161.2	13.5	3153.3	11.8	3153.3	11.8	100.6

Appendix F: Hf data tables

Table F.1 - DTB17 Bayhorse Detrital Zircon Hf isotopic data.										
Sample	(^{176}Yb + ^{176}Lu) / ^{176}Hf (%)	Volts Hf	^{176}Hf/^{177}Hf	± (1σ)	^{176}Lu/^{177}Hf	^{176}Hf/^{177}Hf (T)	E-Hf (0)	E-Hf (0) ± (1σ)	E-Hf (T)	U-Pb Zircon Age (Ma)
LINKDTB17-11_SPOT137	38.06952775	2.41839374	0.282812519	2.2416E-05	0.001984915	0.282789821	0.973133443	0.792675386	13.77597235	609
LINKDTB17-11_SPOT129	9.855387233	5.668366658	0.282496412	1.6928E-05	0.000598145	0.282489425	-10.20519381	0.598614925	3.433186684	622.1
LINKDTB17-11_SPOT194	21.12910766	3.598879627	0.28244854	2.3483E-05	0.001196248	0.28243393	-11.8980846	0.830430918	2.099833199	650.2
LINKDTB17-11_SPOT270	93.0281918	2.221715812	0.282635636	4.4744E-05	0.005504623	0.282568355	-5.281892873	1.58226272	6.871598804	650.7
LINKDTB17-11_SPOT2	74.97356864	2.516378029	0.282462288	3.0962E-05	0.003793635	0.282415891	-11.41191701	1.09490179	1.481246438	651.1
LINKDTB17-11_SPOT248	11.02904595	3.695779483	0.282457418	1.9937E-05	0.000662133	0.282449318	-11.58415149	0.705026838	2.667286634	651.2
LINKDTB17-11_SPOT156	10.31515204	4.176040903	0.282460038	1.8134E-05	0.000611185	0.282452557	-11.49150101	0.64126649	2.790975957	651.6
LINKDTB17-11_SPOT153	16.70587742	4.152644128	0.28247862	1.7919E-05	0.000959904	0.282466724	-10.83437564	0.633647695	3.474926024	659.7
LINKDTB17-11_SPOT247	51.91931064	3.920920127	0.282454322	2.1537E-05	0.002671633	0.282421208	-11.6936292	0.761613261	1.865222362	659.8
LINKDTB17-11_SPOT206	23.08677145	3.194550263	0.282441111	2.4331E-05	0.001370563	0.282424118	-12.16080772	0.86040646	1.972779046	660
LINKDTB17-11_SPOT57	12.77059767	3.49743353	0.282538618	1.8198E-05	0.00074767	0.282529264	-8.712681778	0.643539662	5.831529042	666
LINKDTB17-11_SPOT207	10.25442411	3.504750783	0.282504957	2.3809E-05	0.000652064	0.282496797	-9.903030039	0.841938797	4.683979229	666.1
LINKDTB17-11_SPOT304	49.19436595	3.12586336	0.282459205	2.3989E-05	0.001470209	0.282440787	-11.52095929	0.848311546	2.716119399	666.8
LINKDTB17-11_SPOT26	24.72408354	3.397940105	0.282443011	2.05E-05	0.001330145	0.28242624	-12.0936143	0.724938976	2.297673487	671.1
LINKDTB17-11_SPOT233	20.34191415	3.345184642	0.282436015	1.8451E-05	0.001110331	0.282422011	-12.34101649	0.652458806	2.152405205	671.3
LINKDTB17-11_SPOT105	15.24476537	3.442809049	0.282427258	2.3437E-05	0.00082173	0.282416892	-12.65068665	0.828783481	1.973373043	671.4
LINKDTB17-11_SLOT28	6.670358387	4.568702929	0.28257215	2.3356E-05	0.001201092	0.282556697	-7.526925306	0.825944709	7.224117565	684.7
LINKDTB17-11_SLOT68	10.97176882	2.686448677	0.282489469	1.9394E-05	0.000679362	0.282480722	-10.45072997	0.685808459	4.544592166	685.2
LINKDTB17-11_SLOT249	10.50270627	3.268097922	0.282436484	2.0927E-05	0.000624909	0.282428434	-12.32441863	0.7400434	2.701698927	685.6
LINKDTB17-11_SLOT34	17.91052302	5.158708354	0.282546396	1.7646E-05	0.001029575	0.282532833	-8.437633828	0.624003163	6.746029651	701
LINKDTB17-11_SLOT138	27.35692588	3.542448017	0.282563174	1.3453E-05	0.001410427	0.282544594	-7.844318232	0.475732471	7.162575342	701
LINKDTB17-11_SLOT306	15.98739685	4.408849433	0.282527131	1.5432E-05	0.000985876	0.282514132	-9.118914295	0.545717551	6.097189235	701.6
LINKDTB17-14_SLOT279	36.27702346	3.185671432	0.282801852	2.406E-05	0.001952136	0.282782484	0.595927826	0.850839511	11.71347907	528.8
LINKDTB17-14_SLOT3	7.236489244	3.732879353	0.282094976	1.6218E-05	0.000537727	0.282081115	-24.40101436	0.573496382	5.754898684	1363.2
LINKDTB17-14_SLOT309	9.614300319	3.550348746	0.282045117	1.86E-05	0.000583161	0.282029922	-26.16417054	0.657742891	4.270187218	1377.7
LINKDTB17-14_SLOT36	10.01514378	4.23971297	0.282155999	1.626E-05	0.000625279	0.282139637	-22.24308043	0.574981305	8.296847836	1383.6
LINKDTB17-14_SLOT90	17.96533187	3.277992462	0.282167954	2.5155E-05	0.001274783	0.282134473	-21.82030814	0.889555276	8.227968112	1388.6
LINKDTB1705-SPOT238	24.90857906	3.675976895	0.282403106	2.4341E-05	0.001386509	0.282386018	-13.50474896	0.860744413	0.535754678	656.1
LINKDTB1705-SPOT141	8.772252017	4.712936372	0.282439095	1.8183E-05	0.000519561	0.282432655	-12.23208243	0.643007255	2.27063353	659.8
LINKDTB1705-SPOT120	12.95001433	4.452092355	0.28237868	1.5108E-05	0.000772969	0.282369072	-14.36850127	0.534254975	0.061581336	661.7
LINKDTB1705-SPOT70	7.872594562	3.863563675	0.282421658	2.1182E-05	0.000466646	0.282415845	-12.84869133	0.749043149	1.749548648	663.1
LINKDTB1705-SPOT289	10.24525129	4.818570673	0.282350019	2.1507E-05	0.000589418	0.282343198	-15.38204057	0.760526566	-1.87527537	616.3
LINKDTB1705-SPOT294	27.98476755	3.933285373	0.282444031	2.3263E-05	0.001503974	0.28242641	-12.05752188	0.822631099	1.242198142	623.9
LINKDTB1705-SPOT138	7.142454	3.468020893	0.282397831	1.9776E-05	0.000395057	0.282392842	-13.69128219	0.699332846	1.139611185	672.2
LINKDTB1705-SPOT239	13.44723166	4.384905899	0.282444689	1.7733E-05	0.000795827	0.282434578	-12.03425893	0.627081367	2.707758948	676.2
LINKDTB1705-SPOT17	11.47342189	4.721925233	0.281973123	1.5309E-05	0.00071837	0.281954619	-28.71003997	0.541360974	1.245122034	1362.2
LINKDTB1705-SPOT16	12.00280811	4.57408854	0.282157707	2.0283E-05	0.000727401	0.282138902	-22.18266764	0.71726932	7.893794032	1367.1
LINKDTB1705-SPOT49	12.60771992	3.601615355	0.282124841	2.0154E-05	0.000742531	0.282105595	-23.34489981	0.712692881	6.792292324	1370.6
LINKDTB1705-SPOT250	16.34248974	4.225123534	0.282192788	2.0814E-05	0.000999528	0.282166818	-20.94212086	0.736050944	9.03937275	1373.9
LINKDTB1705-SPOT265	16.10100017	3.793766568	0.282186184	2.2794E-05	0.000986815	0.282160464	-21.17567893	0.806049415	8.90996895	1378.1
LINKDTB1705-SPOT235	21.18229909	4.891511571	0.282180009	1.8034E-05	0.001255697	0.282147168	-21.39403873	0.637741373	8.545741783	1382.8
LINKDTB1705-SPOT281	10.08082208	4.550876212	0.282139298	1.9212E-05	0.000662642	0.282121756	-22.8336694	0.679369475	8.025992594	1399.5
LINKDTB1705-SPOT244	26.76298016	5.290884017	0.28237031	2.2848E-05	0.001609798	0.282350479	-14.66450399	0.807975333	-0.72958419	655.8
LINKDTB1704-SPOT4	74.58953281	2.873995296	0.282550801	2.851E-05	0.00383248	0.282506731	-8.281886657	1.008192511	3.82795655	612.4
LINKDTB1704-SPOT101	15.02259887	2.930072998	0.282336474	1.8533E-05	0.000864044	0.28232577	-15.86101461	0.655377678	-1.52143548	659.5
LINKDTB1704-SPOT254	9.791110746	3.332794722	0.282038374	1.9165E-05	0.000571012	0.282023756	-26.40260799	0.677728099	3.507998711	1353.9
LINKDTB1704-SPOT306	18.1134898	3.761892548	0.282198537	1.9875E-05	0.000989532	0.282173054	-20.73882134	0.702829464	8.986404158	1361.9
LINKDTB1704-SPOT114	10.44499904	4.134166761	0.282108077	1.5192E-05	0.000626218	0.282091824	-23.9377384	0.537216934	6.34491277	1372.4
LINKDTB1704-SPOT291	19.30565463	4.392048828	0.282162808	2.2646E-05	0.001173045	0.282132333	-22.00231427	0.800829297	7.811563626	1373.7
LINKDTB1704-SPOT206	13.11309935	4.431740997	0.282146255	1.512E-05	0.000802282	0.282125399	-22.58766196	0.534675533	7.586140321	1374.6
LINKDTB1704-SPOT163	14.30101973	3.822064805	0.282228346	2.5177E-05	0.00086315	0.282205805	-19.68472352	0.890313451	10.5800161	1380.8
LINKDTB1704-SPOT204	11.22400157	4.116486977	0.282236478	1.8602E-05	0.000675309	0.282218812	-19.39714833	0.657798196	11.09401516	1383.1
LINKDTB1704-SPOT159	12.0067799	3.701812477	0.282174205	1.8742E-05	0.00080156	0.282153193	-21.59927324	0.662756853	8.832573696	1386
LINKDTB1704-SPOT232	10.23533297	3.93761494	0.281932023	1.2641E-05	0.000610896	0.281915939	-30.16345315	0.447005865	0.551231205	1391.9

Geologic Map of the Bayhorse Anticline, Custer County, Idaho

Daniel T. Brennan, David M. Pearson, Paul K. Link
2018

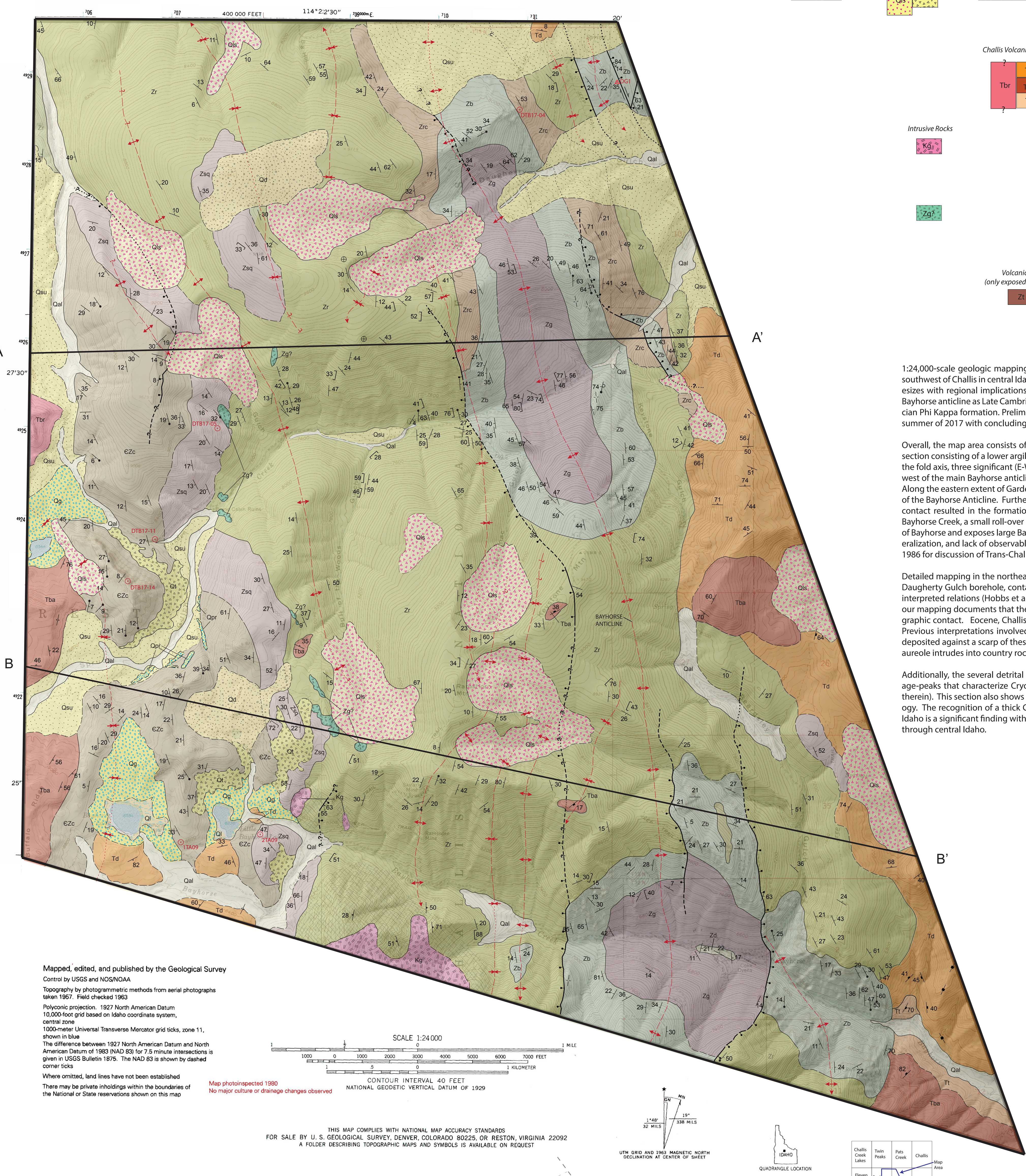

CORRELATION OF MAP UNITS

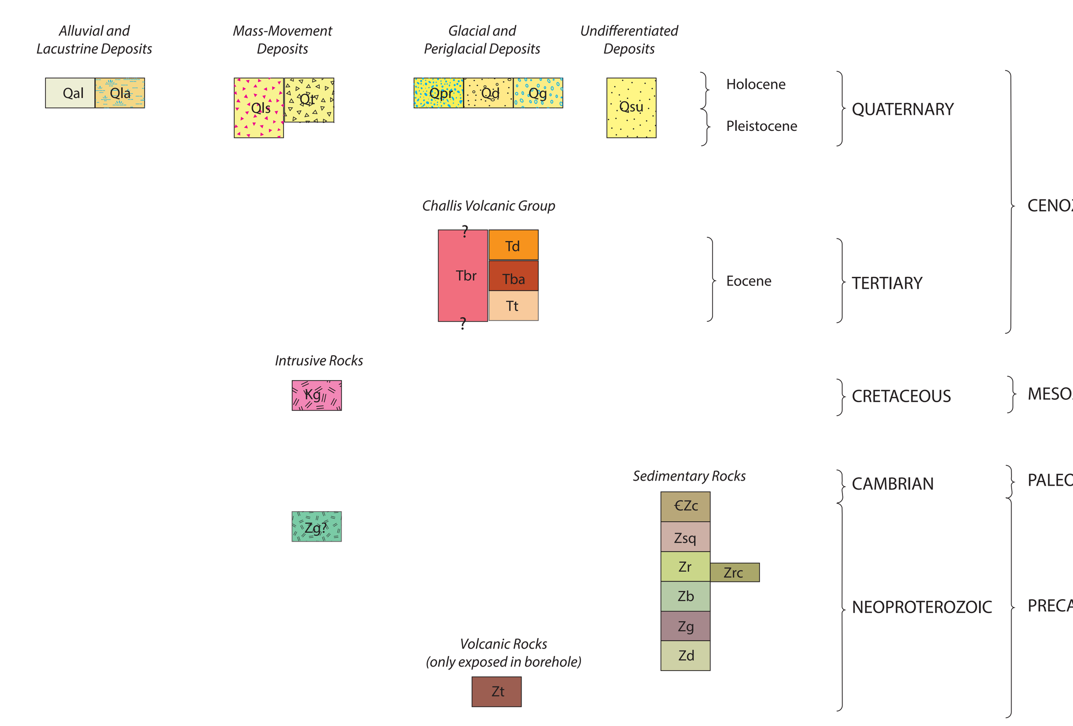

INTRODUCTION

1:24,000-scale geologic mapping and structural analysis of a region within the Bayhorse and Bayhorse Lake 7.5-minute quadrangles southwest of Challis in central Idaho refined 1:62,500-scale geologic mapping from Hobbs et al., (1991) and tested several crucial hypothesizes with regional implications. Previous mapping (Hobbs et al., 1991; Fisher et al., 1992; Krohe, 2016) designated the rocks of the Bayhorse anticline as Late Cambrian to Middle Ordovician in age, due in part to a miscorrelation with outcrops to the south of the Ordovician Phi Kappa formation. Preliminary field evaluation during fall 2016, was followed by a major field season during the late spring and summer of 2017 with concluding fieldwork during fall 2018.

Overall, the map area consists of north to south trending anticline of a slightly metamorphosed yet intact >2.5 km thick stratigraphic section consisting of a lower argillaceous and dolomitic sequence that is overlain by quartzite. Trending approximately perpendicular to the fold axis, three significant (E-W) drainages have incised, exposing stratigraphically lower units. Several smaller amplitude folds exist west of the main Bayhorse anticline. A series of relatively N-S to NW-SE striking faults, with primarily normal offset, cross cut this fabric. Along the eastern extent of Garden Creek, a shallowly east dipping normal fault duplicates steeper dipping strata along the eastern limb of the Bayhorse Anticline. Further west, along Garden Creek, a west-dipping normal fault along the Ramshorn Slate/Bayhorse Dolomite contact resulted in the formation of a roll-over anticline within the Ramshorn Slate, this fault can be traced to the south where in Bayhorse Creek, a small roll-over anticline is also present. Another east-dipping fault runs approximately north-south through the town of Bayhorse and exposes large Bayhorse Dolomite cliffs to the east that are also folded into a gentle anticline. Syn-kinematic fluorite mineralization, and lack of observable offset on Quaternary features suggest that these faults are Eocene, Trans-Challis in age (see Bennett, 1986 for discussion of Trans-Challis fault system).

Detailed mapping in the northeast of the map area documented continuity in surface geology adjacent to and within strata where the Daugherty Gulch borehole, containing a ca. 667 Ma subsurface tuff (Lund et al., 2010; Isakson, 2017) was drilled. Instead of previously interpreted relations (Hobbs et al., 1991) that involve a major thrust fault between the Clayton Mine Quartzite and the Ramshorn Slate, our mapping documents that the stratigraphically higher quartzites lie above the slate with an approximately 250 m gradational stratigraphic contact. Eocene, Challis Volcanic Group, extrusive lavas and tuffs cover the older sedimentary sequence to the east and west. Previous interpretations involved normal faults along the edges of the Bayhorse anticline and potentially these volcanic rocks were deposited against a scarp of these inferred faults (Hobbs and Hays, 1990). A Cretaceous aged granitic stock with a recognizable contact aureole intrudes into country rock in the southern extent of the field area.

Additionally, the several detrital zircon samples analyzed from key stratigraphic intervals show similarity to regional trends in detrital age-peaks that characterize Cryogenian to earliest Cambrian strata along the Cordilleran margin (Yonkee et al., 2014 and references therein). This section also shows a similarity to the Neoproterozoic stratigraphy of southeast Idaho in respects to thicknesses and lithology. The recognition of a thick Cryogenian to early Cambrian, relatively intact stratigraphic section west of the Lemhi Arch in central Idaho is a significant finding with implications for the rate and geometry of Neoproterozoic rift development and related sedimentation through central Idaho.

SYMBOLS

Contact: dashed where approximately located, dotted where concealed.

Normal fault: ball and bar on downthrown side; dashed where approximately located; dotted where concealed.

Reactivated (?) right-lateral strike-slip fault: bar and ball on downthrown side; dashed were approximately located; dotted where concealed.

57 48 Lineation on inclined fault surface. Tick shows fault dip value and direction; arrow shows bearing and plunge of lineation

Anticline axial trace: dashed where approximately located; dotted where concealed.

Syncline axial trace: dashed where approximately located; dotted where concealed.

2 Strike and dip of bedding.

Strike of vertical bedding.

52 Strike and dip of bedding where sedimentary structures show bedding to be upright.

17 Strike and dip of bedding where sedimentary structures show bedding to be overturned.

89 Strike and dip of primary foliation.

Strike of vertical primary foliation.

9 Strike and dip of secondary (metamorphic) foliation.

78 Strike and dip of joint.

Strike of vertical joint.

Strike and dip of cleavage

Extent of contact metamorphism

A Location and sample number used for detrital zircon analysis (see Fig. 1)

DG1 Location of borehole containing Tuff of Daugherty Gulch.

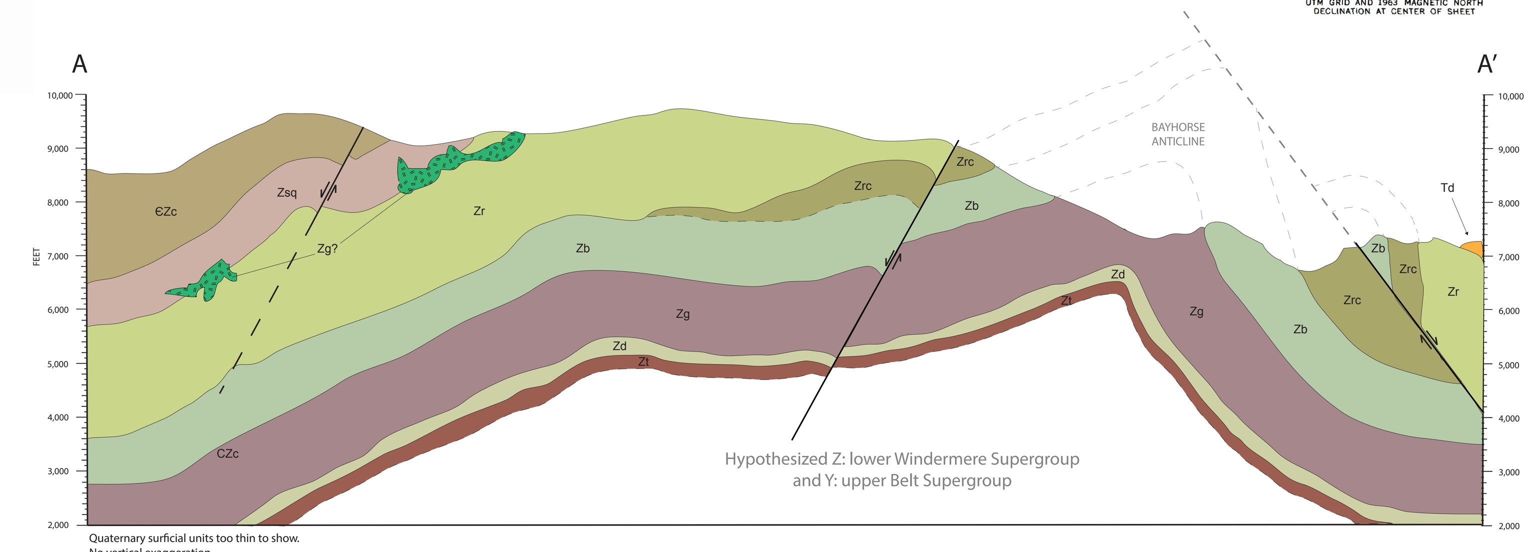

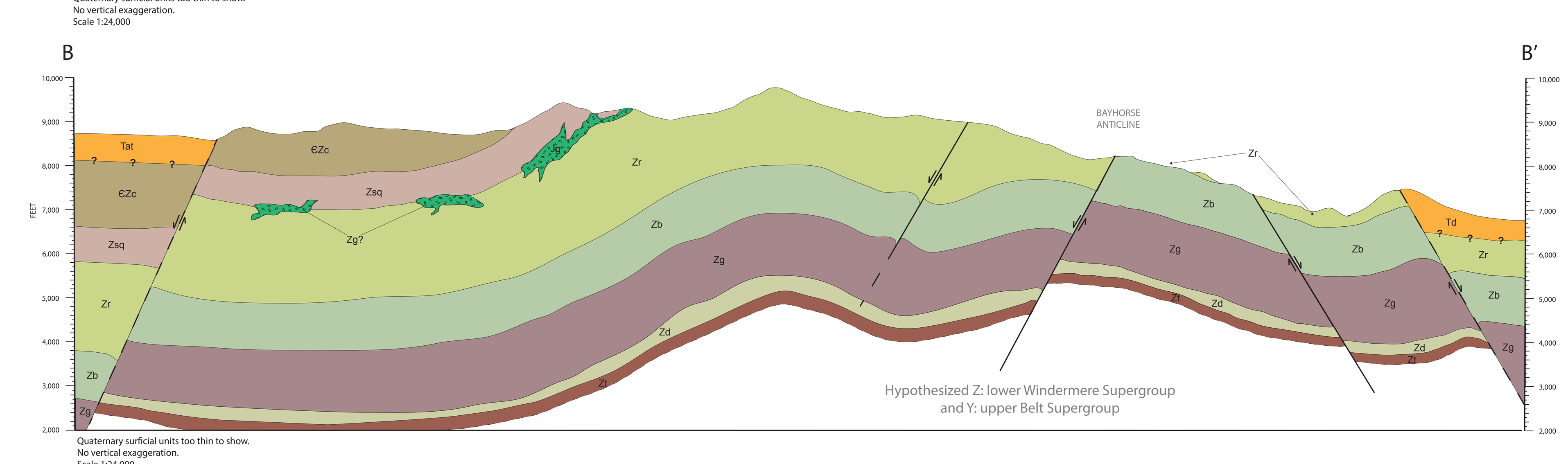

DESCRIPTION OF MAP UNITS

In the following unit descriptions we use the metric system for sizes of mineral or clast constituents of rock units and also for small-scale features of outcrops. Unit thickness and distance are listed in metric units. Grain size classification of unconsolidated and consolidated sediment is based on the Wentworth scale (Lane, 1947). Intrusive rocks are classified according to IUGS nomenclature using normalized values of modal quartz (Q), alkali feldspar (A), and plagioclase (P) on a ternary diagram (Streckeisen, 1976). Volcanic rocks are classified by total alkalis versus silica chemical composition according to IUGS recommendations (LeMaitre, 1984).

SEDIMENTARY DEPOSITS

Qal **Alluvium (Quaternary)**- Silt, sand, pebbles, and cobbles associated with drainage systems of Daugherty Gulch, Garden Creek, and Bayhorse Creek. May include terrace deposits along Garden Creek. Clasts are generally rounded and show crude stratification, sorting, and imbrication.

Qsu **Surficial Undivided (Quaternary)**- Unconsolidated, deposits of variable grain size and sorting. Contains mixed deposits of colluvium, solifluction, avalanche and alluvial processes.

Qls **Landslide (Quaternary)**- Angular to subangular and poorly sorted, silt to boulder sized debris. Formed by slope failure and characterized by a hummocky surface, with the main scarp commonly identifiable. Vegetated soil overburden is often present near the toe of the landslide. Common in cleaved Ramshorn Slate.

Qt **Talus (Quaternary)**- Locally derived loose masses of angular rock cobbles and boulders, that mantles slopes of moderate angle. Primarily restricted to slopes below cliffs of Ramshorn Slate or Clayton Mine Quartzite.

Qla **Lacustrine (Quaternary)**- Very well sorted unlithified sediment, with thinly laminated beds of silts and clays. Located in seasonally inundated low-lying areas surrounding Bayhorse and Little Bayhorse Lake.

Qpr **Protalus Rampart (Quaternary)**- Locally-derived, distinct ramparts of unsorted angular cobbles and boulders that accumulated at the toe of Clayton Mine Quartzite cliffs and talus fields.

Qd **Diamicton (Quaternary)**- Unsorted terrigenous sediment, ranging in size from clay to boulders in an organic-rich soil matrix. Often poorly drained.

Qg **Glacial (Pleistocene)**- Unsorted to poorly sorted cobbles, gravel, boulders in a clayey matrix, often poorly drained with thick soil accumulation. Located near and above Bayhorse and Little Bayhorse Lake. Calibrated ^{14}C basal date (ca. 14 ka) from Bayhorse Lake core (Finney and Shapley, personal comm.) suggests glacial features are Pinedale in age.

CHALLIS VOLCANIC GROUP

Td **Tertiary Dacite (Eocene)**- Orange to light gray sometimes altered to teal or bright red, dacite lava. Contains variable phenocrysts assemblages but is primarily (< 20%) plagioclase (~5 mm) and (< 7%) hornblende (~2 mm) in an aphanitic groundmass. Full thickness is not exposed but estimated to be less than 600 m (Hobbs and Hays, 1991). Potassium-argon age is 49.3 ± 1.4 Ma (Armstrong, 1975). Locally overlies some thin flows of basalt.

Tba **Potassium-rich Basalt and Andesite (Eocene)**- Orange to very dark gray/black when fresh, basalt lava. ~3% (< 2mm) bottle green olivine in a dark aphanitic groundmass. Occurs as a discrete local accumulation along the western margin of the mapping area. Likely less than 150 m thick. Potassium-argon age is 50.3 ± 1.5 Ma (Armstrong, 1975).

Tt **Lithic Tuff (Eocene)**-Light orange to greenish beige, un-welded, matrix supported, volcanic lithic tuff. Contains angular volcanic clasts ranging in size from fine pebbles to small cobbles. Surrounded by an aphanitic (ashy?), matrix. Appears to be volcanic in origin but may be reworked by sedimentary processes.

Tbr **Buster Lake Breccia (Eocene)**- Reddish-orange and brown weathering, well cemented pumiceous breccia. Contains pumaceous lava fragments (<5 cm) as well as greyish-purple (mafic?) fragments.

INTRUSIVE ROCKS

Kg **Juliette Stock (Cretaceous)**- Gray to pink, equigranular moderately coarse-grained, granite to quartz monzonite, with secondary muscovite. K-Ar age of biotite from main stock is 98.1 ± 3.3 Ma (McIntyre et al., 1976), U-Pb age of zircon from main stock is 96.9 ± 0.8 Ma (Krohe, 2016), falling within the magmatic age range of the Atlanta lobe of the Idaho Batholith. Where in contact with the Ramshorn Slate, mica- and andalusite-rich contact aureoles are present.

Zg? **Gabbro (Neoproterozoic?)**- Grayish green, amphibole, clinopyroxene (augite?) gabbro that consistently intrudes as 10 to 100-meter scale sill-like bodies near the stratigraphic contact between Ramshorn Slate and Interbedded siltite and quartzite. Contains phenocrysts of amphibole, plagioclase, and clinopyroxene and accessory pyrite generally < 2 mm in length in a fine-grained groundmass showing chlorite and epidote alteration. Potentially shows an inflation/bedding shift above the gabbro suggesting shallow laccolithic intrusion. Fission track date from an immediately adjacent quartzite reveals an annealing age of 140.1 ± 17.4 Ma (R.A. Zimmerman, written commun., 1983 in Hobbs et al., 1991). We interpret the fission track age to likely reflect annealing due to burial and the Gabbro is older. Our attempts to separate baddeleyite and zircon for U-Pb analysis were not successful. Mafic sills within a correlative stratigraphic interval in southeast Idaho, are undated but generally considered to record waning stages of Neoproterozoic rift related igneous activity (Crittenden, 1988; Yonkee et al., 2014), making a Neoproterozoic age more likely. A relation to the 650-665 Ma plutonism ~100 km to the north at Big Creek is alluring but unproven.

WINDERMERE SUPERGROUP

€Zc **Clayton Mine Quartzite (Neoproterozoic to Cambrian)-** Over 800 m of dominantly quartzitic rocks that are heterogeneous in color, degree of sorting, and bedding. Formation ranges from orange, well-sorted, medium-grained quartz sandstone with variable feldspar content to reddish purple, matrix supported pebble conglomerate, to clean quartz arenite. Lower Clayton Mine is dominantly tightly quartz-cemented, medium to thick tabular cross stratified, feldspathic arenite with distinct thin, shiny green silt interlaminations on top of bedding planes. Locally small (<2 cm in diameter) reduction spots are abundant. The unit is interpreted to record variable fluvial and shallow marine deposition and likely contains one or more undocumented unconformities. The upper contact is covered by Tertiary volcanic rocks and/or faulted.

Zsq **Interbedded Siltite and Quartzite (Neoproterozoic)**- Approximately 250-meter thick unit showing cyclically interbedded mudstone and sandstone consistent with a gradational contact between Ramshorn Slate and Clayton Mine Quartzite. Primarily medium to coarse grained, subfeldspathic arenite with finer beds containing more detrital feldspar and muscovite. Quartzite is interbedded with meter scale (3-4 m), thick laminated siltstone. One distinct bed of orange to fresh gray, locally oolitic, dolomite with laminations of distinct scattered subangular coarse quartz sand to fine pebbles is present.

Zr **Ramshorn Slate (Neoproterozoic)**- Approximately 650 meter thick unit of medium gray to blueish gray to olive green to reddish brown, fine-grained, medium-laminated to fine bedded, slate with a subtle sheen, showing localized foliation and crenulation. Often displays Leisegang banding. Where present, the Ramshorn Conglomerate overlies the Bayhorse Dolomite in a slight erosional unconformity, suggested by thinned Bayhorse Dolomite. Pervasively cleaved at high angles to bedding with lesser amounts of pencil cleavage. Breaks along cleavage except where slightly coarser grained to very fine sand. Often exhibits cyclic (~1cm) thick, normally-graded laminations indicative of fine-grained turbidite deposition with a noticeable lack of bioturbation. Flute cast swarms are abundant near contact with incised Ramshorn Conglomerate. Locally contact-metamorphosed to hornfels near the Juliette stock, with muscovite and andalusite visible. Chiastolite/andalusite is often weathered out, leaving lath-like depressions.

Zrc **Ramshorn Conglomerate (Neoproterozoic)**- Reddish pink, well rounded, poorly sorted, matrix supported, coarse to medium pebble in a fine sand matrix, vein quartz conglomerate with rare clasts of red jaspilite, and intrabasinal sandstone/siltstone pebbles. Laterally interfingers with reddish brown, coarse grained, well rounded, moderately sorted, quartz arenite and medium grey, fine bedded, slate with abundant flute cast swarms. Contains unusual, tight parallel wrinkle marks in mudstone facies interpreted as Kinneyia, which may represent a microbial biofilm. Depositied within a paleochannel that interfingers with Ramshorn Slate. Maximum thickness of approximately 200 meters.

Zb **Bayhorse Dolomite (Neoproterozoic)-** Approximately 375 meter thick unit consisting of gray to tan/orange, primarily dolo-micritic mudstone. Locally contains thin chert nodules, sometimes as localized (~3 cm) thick beds, dark gray silicified chert lithic (pisolite?) grainstone beds, and rare fine-grained sandy laminations that infrequently show cross-stratification. Stratigraphically lower portions show thin tabular bedding, stratigraphically higher levels show less defined bedding except for an interval of dark gray/brown laminated siltstone and argillite (~15 m) interval. Contains poorly defined stromatolitic bioherms, calcite veins (often as en echelon tension gashes), and localized cross laminations. Dolostone is heavily brecciated along faults and near the upper contact with Ramshorn Slate. Breccia clasts (< 20 cm in diameter) are commonly supported in a dark red or gray siliceous matrix. Fluorite mineralization is common where faulted and brecciated. Brecciated horizons are likely pipe breccias associated with Cenozoic volcanism or an irregular paleokarst surface. Overlies Garden Creek Phyllite in apparent ~10 m gradational contact.

Zg **Garden Creek Phyllite (Neoproterozoic)**- Dark gray to nearly black, slightly calcareous phyllite. Weathers to thin, smooth, flakes and chips, breaking often along irregular, wavy bedding planes. Otherwise, bedding is indistinct. Unit is poorly exposed except where deeply eroded by Garden and Bayhorse creeks. Exposures with southern aspect often do not sustain conifer growth. Overlies in apparent conformity the basal dolomite of Bayhorse Creek. Estimated thickness of approximately 500 meters.

Zd **Basal Dolomite of Bayhorse Creek (Neoproterozoic)**- Light to medium gray, weathers grayish orange to brown, thin to medium tabular bedded, sandy dolomicritic mudstone. A maximum of the upper 20 m is exposed along Bayhorse Creek near center of the Bayhorse anticline. True interpreted thickness is approximately 50 m in the Daugherty Gulch drill hole. Lower contact is thought to be in apparent depositional conformity with the 664 ± 7 (Lund et al., 2010) to 667.76 ± 0.22 (Isakson, 2017) Ma tuff of Daugherty Gulch.

Zt **Tuff of Daugherty Gulch (Neoproterozoic)**- 664 ± 7 Ma (SCHRIMP: Lund et al., 2010), 668 ± 0.8 (CA-TIMS: Isakson, 2017) Volcanic diamictite showing lower-greenschist-facies metamorphism. Contains ~50% clasts of rhyolite, lesser quartz and metasandstone (< 25 cm) in fine grained matrix. Shown only in cross-section.

REGIONAL CORRELATIONS

The stratigraphic patterns of Neoproterozoic rocks in northeastern Washington and southeastern Idaho exhibit remarkable similarities to the newly reassigned Neoproterozoic to Cambrian stratigraphy of the Bayhorse section. In southeast Idaho, the upper Scout Mountain Member of the Pocatello Formation contains a reworked fallout tuff bed, U-Pb SHRIMP dated to 667 ± 5 Ma (Fanning et al., 2004). This Cryogenian tuff is overlain by limestone and argillite of the upper member of the Pocatello Formation (Link et al., 1987), which in turn is overlain by micritic, oolitic, and sandy carbonate of the Blackrock Canyon limestone which contains poorly defined stromatolitic bioherms (Corsetti et al., 2007). Based on matching volcanic tuff ages and lithological similarity we correlate the Upper Scout Mountain Member to the to the 667 Ma tuff of Daugherty Gulch and the overlying basal Dolomite of Bayhorse Creek. At Bayhorse, this lower interval is overlain by the Garden Creek Phyllite and Bayhorse Dolomite which we suggest correlate to the Pocatello Formation, and the Blackrock Canyon Limestone. The Bayhorse Dolomite and Blackrock Canyon Limestone share similar oolitic and stromatolitic intervals. A karst surface has also been proposed for the upper contact of the Bayhorse Dolomite (Hobbs and Hays, 1990), and may represent a hiatus in deposition.

The Blackrock Canyon and the Bayhorse Dolomite are both overlain by fine grained units of the Papoose Creek/Kelly Canyon and Ramshorn Slate respectively. The Kelley Canyon Formation contains graded, fine grained beds, deposited from suspension and as distal turbidites (Yonkee et al., 2014), which are also observed in the Ramshorn Slate. Mafic igneous intrusions, as well as increasing quartzite content is noted in the upper Kelly Canyon (Crittenden, 1988; Yonkee et al., 2014) and may correlate with the similar interval in the upper Ramshorn Slate/siltite and quartzite of the Bayhorse section that contains gabbroic sills.

In southeastern Idaho, ~3.5 km of the Caddy Canyon Quartzite, Inkom Formation, Mutual Formation and Camelback Mountain Quartzites of the Brigham Group overlie the Papoose Creek/Kelly Canyon Formation. At Bayhorse, the ~1 km thick Clayton Mine Quartzite overlies the Ramshorn Slate. The stratigraphic position of the Clayton Mine, lying conformably above the Ramshorn Slate, suggests a correlation to the Caddy Canyon Quartzite. However, stratigraphically higher within the Clayton Mine Quartzite, a major shift is evident in the detrital zircon populations with the decreasing prevalence of Grenville grains and the transition to a significant ca. 1780 Ma peak. This same provenance shift is recognized within several other Lower and Middle Cambrian sandstones in southeast Idaho and southwest Montana. Based on these stratigraphic trends the upper Clayton Mine Quartzite may be Lower or Middle Cambrian in age.

The Bayhorse section also shows detrital zircon and lithologic similarities to metamorphosed Neoproterozoic and Cambrian stratigraphy found in central Idaho roof pendants (Lund et al., 2003; Ma et al., 2016; Stewart et al., 2017; Isakson 2017).

REFERENCES

Armstrong, R. L., 1975, The geochronometry of Idaho: Isochron/West, no. 14, p. 1-50
Bennett, E.H., 1986, Relationship of the trans-Challis fault system in central Idaho to Eocene and Basin and Range extensions: Geology, v. 14, p. 481.
Corsetti, F.A., Link, P.K., and Lorentz, N.J., 2007, δ13 C chemo stratigraphy of the Neoproterozoic succession near Pocatello, Idaho: Implications for glacial chronology and regional correlations, in Link, P.K., and Lewis, R.S., eds., Proterozoic Geology of Western North America and Siberia: SEPM (Society for Sedimentary Geology) Special Publication 86, p. 193–208.
Crittenden, M.D., Jr., 1988, Bedrock Geologic Map of the Promontory Mountains, Box Elder County, Utah: U.S. Geological Survey Open-File Report 88–646, scale 1:100,000
Fanning, C.M., and Link, P.K., 2004, U-Pb SHRIMP ages of Neoproterozoic (Sturtian) glaciogenic Pocatello Formation, southeastern Idaho: Geology, v. 32, p. 881–884, doi: 10.1130 /G20609.1.
Fisher, F.S., D.H. McIntyre, and K.M. Johnson, 1992, Geologic map of the Challis 1° x 2° quadrangle, Idaho: U.S. Geological Survey Miscellaneous Investigations Series Map I-1819, scale 1:250,000.
Hobbs, S.W., and W.H. Hays, 1990, Ordovician and older rocks in the Bayhorse area, Custer County, Idaho: U.S. Geological Survey Bulletin 1891, 40 p.
Hobbs, S.W, Hays, W. H., and Smith, R. K., 1968, The Kinnikinic Quartzite of central Idaho- Redefintion and subdivision: U.S. Geological Survey Bulletin 1254-J, p. J1-J22.
Hobbs, S.W., Hays, W.H., and McIntyre, D.H., 1991, Geologic map of the Bayhorse area, central Custer county, Idaho: U.S. Geological Survey Miscellaneous Investigations Series Map I-1882, scale 1:62,500.
Ingersoll, R.V., 1990. Actualistic sandstone petrofacies: discriminat- ing modern and ancient source rocks. Geology 18, 733–736.
Ingersoll, R.V., Kretchmer, A.G., Valles, P.K., 1993. The effect of sampling scale on actualistic sandstone petrofacies. Sedimentology 40, 937–953.
Isakson, V. H., 2017, Geochronology of the Tectonic, Stratigraphic and Magmatic evolution of Neoproterozoic to early Paleozoic, North American Cordillera and Cryogenian Glaciation: Boise State University PhD thesis, 477 p.
Jacob, T., 1990, Late Proterozoic(?) tuff near Challis, Idaho: Tobacco Root Geological Society, p. 97–106.
Krohe, N.J., 2016, Structural framework and detrital zircon provenance of the southern portion of the Clayton quadrangle, Custer County, Idaho: Idaho State University M.S. thesis, 108 p.
Lane, E.W., 1947, Report of the subcommittee on sediment terminology; Transactions of the American Geophysical Union, v. 28, no. 6, p. 936-938.
Le Maitre, R.W., 1984, A proposal by the IUGS Subcommission on the Systematics of Igneous Rocks for a chemical classification of valcanic rocks based on the total alkali silica (TAS) diagram: Australian Journal of Earth Sciences, v. 31, p. 243-255
Linde, G.M., Cashman, P.H., Trexler, J.H., and Dickinson, W.R., 2014, Stratigraphic trends in detrital zircon geochronology of upper Neoproterozoic and Cambrian strata, Osgood Mountains, Nevada, and elsewhere in the Cordilleran miogeocline: Evidence for early Cambrian uplift of the Transcontinental Arch: Geosphere, v. 10, p. 1402–1410, doi: 10 .1130 /GES01048 . 1.
Link, P.K., Jansen, S.T., Halimdihardja, P., Lande, A., Zahn, P., 1987, Stratigraphy of the Brigham Group (Late Proterozoic–Cambrian), Bannock, Portneuf, and Bear River Ranges, southeastern Idaho: Thirty-eighth Field Conference, Wyoming Geological Association Guidebook, pp. 133–148.
Link, P.K., Fanning, C.M., and Beranek, L.P., 2005, Reliability and longitudinal change of detrital-zircon age spectra in the Snake River system, Idaho and Wyoming: An example of reproducing the bumpy barcode: Sedimentary Geology, v. 182, p. 101–142, doi: 10.1016/j.sedgeo.2005.07.012.
Link, P.K., Todt, M.K., Pearson, D.M., and Thomas, R.C., 2017, 500–490 Ma detrital zircons in Upper Cambrian Worm Creek and correlative sandstones, Idaho, Montana, and Wyoming: Magmatism and tectonism within the passive margin: Lithosphere, v. 9, p. 1–17, doi: 10.1130/L671.1.
Lund, K., J.N. Aleinikoff, K.V. Evans, and C.M. Fanning, 2003, SHRIMP U-Pb geochronology of Neoproterozoic Windermere Supergroup, central Idaho: Implications for rifting of western Laurentia and synchroneity of Sturtian glacial deposits: Geological Society of America Bulletin, v. 115, p. 349-372.
Lund, K., Aleinikoff, J.N., Evans, K.V., duBray, E.A., Dewitt, E.H., and Unruh, D.M., 2010, SHRIMP U-Pb dating of recurrent Cryogenian and Late Cambrian–Early Ordovician alkalic mag- matism in central Idaho: Implications for Rodinian rift tectonics: Geological Society of America Bulletin, v. 122, p. 430–453
Lund, K., J.N. Aleinikoff, K.V. Evans, E.A. duBray, E.H. Dewitt, and D.M. Unruh, 2010, SHRIMP U-Pb dating of recurrent Cryogenian and Late Cambrian–Early Ordovician alkalic magmatism in central Idaho: Implications for Rodinian rift tectonics: Geological Society of America Bulletin, v. 122, no. 3/4, p. 430-453.
Ma, Chong, Bergeron, P., Foster, D.A., Dutrow, B.L., Mueller, P.A., and Allen, C., 2016, Detri -tal-zircon geochronology of the Sawtooth metamorphic complex, Idaho: Evidence for metamorphosed lower Paleozoic shelf strata within the Idaho batholith: Geosphere, v. 12, p. 1136–1153, doi: 10 .1130 /GES01201 .1.
Matthews, W., Guest, B., and Madronich, L., 2018, Latest Neoproterozoic to Cambrian detrital zircon facies of western Laurentia: Geosphere, v. 14, p. 243-264, doi: 10.1130/GE01544.1
McIntyre, D.H., and Hobbs, S.W., 1987, Geologic map of the Challis quadrangle, Custer County, Idaho: U.S. Geological Survey Quadrangle Map GQ-1599, scale 1:62,500.
Mitra, G., Yonkee, W.A., Gentry, D., 1984. Solution cleavage and its relationship to major structures in the Idaho–Utah–Wyoming thrust belt. Geology 12, 354–358.
Ross, C.P., 1937, Geology and ore deposits of the Bayhorse region, Custer County, Idaho: U.S. Geological Survey Bulletin 877, 161 p.
Stewart, D.E., Stewart, E.D., Lewis, R.S., Weppner, K.M., and Isakson, V.H., 2016, Geologic Map of the Stibnite Quadrangle, Valley County, Idaho: Idaho Geological Survey Geologic Map 51, scale 1:24,000
Streckeisen, A.L., 1976, To each plutonic rock its proper name: Earth-Science Reviews, v. 12, p. 1-33.
Weil, A.B., and Yonkee, W.A., 2012, Layer-parallel shortening across the Sevier fold-thrust belt and Laramide foreland of Wyoming: Spatial and temporal evolution of a complex geodynamic system: Earth and Planetary Science Letters, v. 357–358, p. 405–420, doi: 10.1016/j.epsl.2012.09.021.
Yonkee W.A., C.D. Dehler, P.K. Link, E.A. Balgord, J.A. Keeley, D.S. Hayes, M.L. Wells, C.M. Fanning, and S.M. Johnston, 2014, Tectono-stratigraphic framework of Neoproterozoic to Cambrian strata, west-central U.S.: Protracted rifting, glaciation, and

DISCUSSION

DETRITAL ZIRCON DATA

Quartzite samples for detrital zircon dating were collected from six localities within the mapping area. Individual U-Pb zircon ages were obtained using laser-ablation ICP-MS methods at University of Arizona Laserchron Center.

Four detrital zircon samples were collected from an E-W traverse along Garden Creek (DTB17-04, DTB17-05, DTB17-11, and DTB17-14). Additionally, two samples were collected from near Bayhorse Lake (2TA09 and 1TA09). The two stratigraphically lowest samples, just above the upper and lower Ramshorn Slate contacts show significant Grenville (1.0-1.3 Ga), ~1400 (Mid-continent Granite) Ma, ~1760, and ~2700 aged grains. Samples (DTB17-05 and (DTB17-11) collected right above and below the lower Clayton Mine Contact show unique ~650-665 Ma populations. The other Clayton Mine samples (1TA09 and DTB17-14) show minor Grenville (1.0-1.3) and ~1400 (Mid-continent Granite) population with a dominant ~1780 Ma peak.

Detrital zircon evidence from Neoproterozoic and Cambrian sandstones in Idaho as well as in the Roberts Mountains allochthon in central Nevada suggests that in Early Cambrian time, the Transcontinental Arch rose in the central United States cutting off the supply of Grenville aged (1.0-1.3 Ga) zircons to the western continental margin and resulting to a switch to more western Paleoproterozoic sources (Linde et al., 2014; Yonkee et al., 2014: Link et al., 2017). A significant concentration of detrital Grenville aged grains, therefore suggests a pre-early Cambrian depositional age.

DTB17-04 and 2TA09 show similar detrital zircon age populations as results from the Ediacaran lower Brigham Group (Yonkee et al., 2014) consistent with an Ediacaran age. DTB17-05 and DTB17-11 may record "signatures" of a first order sedimentary system, such a direct drainage off a specific mountain range, mixed with a third order sedimentary system such as large river and marine systems (Ingersol, 1990; Ingersoll et al., 1993; Link et al., 2005). 1TA09 and DTB17-14 show ages that are similar to detrital zircon ages from the upper Brigham Group such as the Camelback Quartzite which spans the Neoproterozoic to Cambrian boundary (Yonkee et al., 2014).

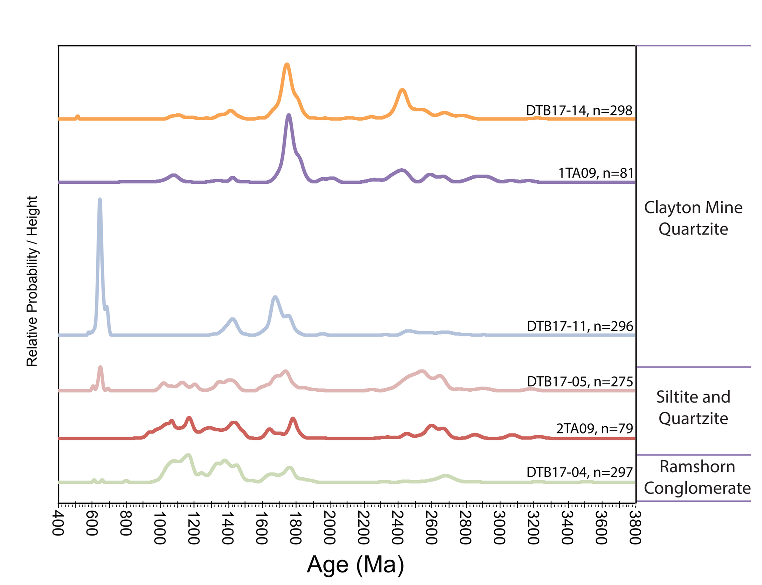

Figure 1. Normalized Age-probability plot of detrital zircon U-Pb analyses from the northern Bayhorse Anticline area.

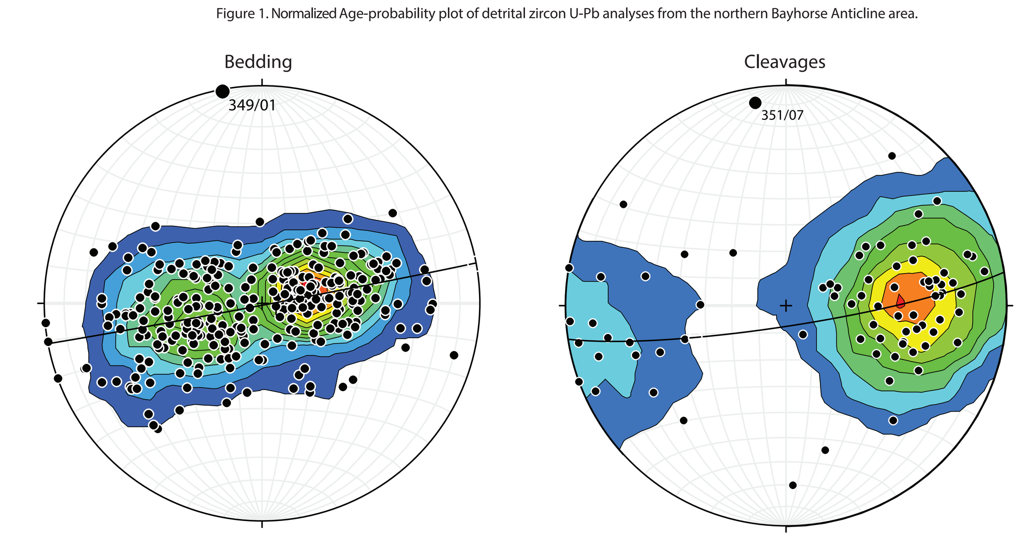

Figure 2. Stereonet diagrams of attitudes measured from the Bayhorse Anticline. The poles to the planes were plotted and a cylindrical best fit was applied. For bedding the fold axis was calculated to be 349/01, and for the cleavages it was calculated to be 351/07.

DAUGHERTY GULCH TUFF

Our field mapping documented continuity in surface geology from within strata where the Daugherty Gulch borehole, containing the 667 Ma subsurface tuff (Isakson, 2017) was drilled and the the north-trending Bayhorse anticline. The borehole was drilled into overburden but within ~50 to the west and southeast Bayhorse dolomite crops out. These outcrops show the pisolitic grainstone beds, and stromatolitic bioherms indicative of the Bayhorse Dolomite. Just west of Daugherty spring, a small paired syncline/anticline fold exists on the eastern limb of the regional Bayhorse anticline. Approximately, 500 m west of where the Daugherty borehole was drilled, a west dipping normal fault juxtaposes the Ramshorn Slate against the stratigraphically higher Bayhorse Dolomite, suggesting at most a couple 100 meters of offset. West of this fault, the borehole was drilled into the east dipping limb of this small anticline. The measured surficial bedding plane (44 to 17 E to SE) orientations are consistent with the attitudes described by Jacob (1990). Additionally, the thicknesses, lithology and gradational nature of stratigraphic contacts described by the borehole log (Jacob, 1990) are consistent with what is observed between correlative units when mapping. Thus, we infer stratigraphic continuum in the stratigraphy above this subsurface tuff.

STRUCTURAL ANALYSIS

Structural relations around large-scale folds constrain timing relations of internal strain (Weil and Yonkee, 2012). Pressure solution cleavage accommodates shortening through the dissolution of grains at the grain to grain contact boundary and reprecipitation in the pressure shadow, which results in pervasive fabrics that form in planes perpendicular to the principal shortening direction. When this cleavage fabric forms after folding, and the cleavage planes will parallel the axial plane of the fold.

In other instances, cleavage remains sub-perpendicular to bedding along fold limbs, indicating that cleavage formed early during layer parallel shortening and was subsequently tilted during large-scale folding and thrusting (Mitra and Yonkee, 1985). Stereonet analysis (fig. 2) shows that the cleavages in the Ramshorn Slate were folded around the same fold axis as the bedding, indicating that cleavage formed prior to significant folding. The formation of cleavage early in the deformational history of an area may be aided by elevated temperatures and pressures caused by increased overburden due to emplacement of earlier overriding thrust sheets (Mitra et al., 1984).

ACKNOWLEDGMENTS

The mapping and analyses presented here was funded by EdMap grant 16_1109 to David Pearson, Geological Society of America student research grant and Idaho State Geoscience Geslin grant to Daniel Brennan. The authors benefited greatly from time in the field and discussions on the general geology, structure, and stratigraphic correlations of central Idaho and the Bayhorse region with Reed Lewis and Dave "Bad Uncle" Stewart of the Idaho Geological Survey. Special thanks to Diana Boyack for assisting with cartography, undergraduate assistants: Braedon Warner and Kyle Miller, ISU's summer 2017 field camp and fall 2017 seminar classes. Also thank you to Bill and Nancy McKee for permission to access their land.